A MULTI BAND POWER OSCILLATION DAMPING CONTROLLER for INTERCONNECTED HYBRID AC MICRO-GRIDS SYSTEM

By

TAJRIN JAHAN RUMKY

Student ID: 15MEE016P

A thesis submitted in partial fulfilment of the requirements for the degree of

MASTER of SCIENCE in Electrical and Electronic Engineering

Department of Electrical and Electronic Engineering

CHITTAGONG UNIVERSITY OF ENGINEERING AND TECHNOLOGY

September 2024

Declaration

I hereby declare that the work contained in this thesis has not been previously submitted to meet requirements for an award at this or any other higher education institution. To the best of my knowledge and belief, the thesis contains no material previously published or written by another person except where due reference is cited. Furthermore, the Thesis complies with PLAGIARISM and ACADEMIC INTEGRITY regulation of CUET.

TAJRIN JAHAN RUMKY

15MEE016P

Department of Electrical and Electronics Engineering

Chittagong University of Engineering & Technology (CUET)

List of Publications

Conference

- **Tajrin Jahan Rumky**, Tofael Ahmed, Moudud Ahmed, and Saad Mekhilef, "Tri-Band Damping Controller for Low Frequency Oscillations in AC Microgrid System," in *2023 IEEE IAS Global Conference on Renewable Energy and Hydrogen Technologies (GlobConHT)*, 2023, pp. 1-6, https://doi.org/10.1109/GlobConHT56829.2023.10087513.
- **Tajrin Jahan Rumky**, Tofael Ahmed, Moudud Ahmed, Shameem Ahmad and M. M. Rahman "Performance of Microgrid Systems on Multiple Dynamic Loads Penetration," 10th International Conference on Power Systems, 2023 (ICPS 2023). https://doi.org/10.1109/ICPS60393.2023.10428691

Approval/Declaration by the Supervisor

This is to certify that Tajrin Jahan Rumky has carried out this research work under my supervision, and that she has fulfilled the relevant Academic Ordinance of the Chittagong University of Engineering and Technology, so that she is qualified to submit the following Thesis in the application for the degree of MASTER of SCIENCE in Electrical and Electronics Engineering. Furthermore, the Thesis complies with the PLAGIARISM and ACADEMIC INTEGRITY regulation of CUET.

DR. TOFAEL AHMED

Professor

Department of Electrical and Electronics Engineering

Chittagong University of Engineering & Technology

Acknowledgement

First and foremost, I thank Almighty Allah for giving me the strength and wisdom to finish my M.Sc. thesis.

Thank you to my supervisor, Prof. Dr. Tofael Ahmed, for his counselling, insight, passion, invaluable assistance, and support during the research program. My study has benefited from his expertise in electric power systems, power quality, and smart grids. He has been my inspiration and role model throughout this study program's challenges. I gained a lot from his demeanor and knowledge. He deserves credit for our lengthy discussions and meetings, which aided my research. My amazing, dynamic, and supportive superiors make me feel lucky. Your meticulousness helped me better my final report.

I thank the Department of Electrical and Electronic Engineering of CUET for helping me finish this dissertation.

I want to thank my life partner Dr. Minhaz Uddin for his patience. He endured my anxieties and shared my successes and failures. It was hard for me to reach this goal, but you understood and encouraged me.

Last but not least, I want to thank my parents and family. I'll always be grateful to my parents for their love and prayers. May Allah bless and forgive them. Ameen! Without their love, inspiration, and support, many of my dreams would never have come true. Finally, I want to thank my two champs, Ahbab and Arhab, who have provided me with endless joy.

Abstract

The increasing integration of renewable energy sources (RESs) with conventional energy sources units in a hybrid AC microgrid system has led to the emergence of power oscillation damping (POD) controller for damping low frequency oscillations (LFOs). A local microgrid has limited energy generation capacity and may need to resort to load shedding during a power shortage. Interconnected hybrid AC microgrid systems are essential for enhancing the reliability and stability of power supply by allowing mutual support during outages or power deficiencies. However, the integration of these subsystems often results in oscillatory modes that could compromise stability and operational efficacy. This thesis presents the design and implementation of a multi-band power oscillation damping (MB-POD) controller implemented for an interconnected hybrid AC microgrid system. The proposed MB-POD controller aims to mitigate LFOs across various frequency bands, enhancing the overall stability and reliability of the microgrid. LFOs are caused by integration of generation sources, variety of dynamic load scenarios, and load disturbances in any of the systems. These oscillations could take place locally or between microgrids. This study introduces an energy storage system (ESS)-based POD designed to mitigate such instabilities in an interconnected AC microgrid system. This study also elucidates the complex dynamics of power oscillation in an interconnected AC hybrid microgrid system, highlighting the deficiencies in conventional power oscillation damping methods. Utilizing advanced mathematical models and simulation techniques, we propose a novel approach to dampen the oscillatory modes effectively. Using the proposed multi-band damping controller as well as the extant single-band power oscillation damper (SB-POD), interconnected hybrid AC microgrid system is intended to operate in a MATLAB/Simulink environment. Using time-domain simulations the

proposed controller's performance is evaluated. Simulations and case studies elucidate the damper's efficacy in enhancing system stability while optimizing power flow and reducing the transient response time. The findings indicate substantial improvements in damping multiple oscillatory modes by improving the damping ratio from 9.1% and reducing oscillations by approximately 4-6%, making it a promising solution for modern power systems. MB-POD than SB-POD across various microgrids, thus paving the way for more resilient and adaptive interconnected hybrid AC microgrid system.

সারাংশ

একটি হাইব্রিড এসি মাইক্রোগ্রিড সিস্টেমে প্রচলিত শক্তির উৎস ইউনিটগুলির সাথে নবায়নযোগ্য শক্তির উৎসগুলির (RESs) ক্রমবর্ধমান একীকরণের ফলে পাওয়ার অসিলেশন ড্যাম্পিং (POD) কন্ট্রোলারের উদ্ভব ঘটেছে যা নিম্ন ফ্রিকোয়েন্সি অসিলেশনের (LFOs) ড্যাম্পিং করতে সাহায্য করে। একটি স্থানীয় মাইক্রোগ্রিডের শক্তি উৎপাদন ক্ষমতা সীমিত এবং শক্তি স্বল্পতার সময় লোড শেডিং করার প্রয়োজন হতে পারে। আন্তঃসংযুক্ত হাইব্রিড AC মাইক্রোগ্রিড সিস্টেমগুলি বিদ্যুতের সরবরাহের নির্ভরযোগ্যতা এবং স্থিতিশীলতা বাড়ানোর জন্য অপরিহার্য, কারণ এটি বিদ্যুৎ ঘাটতি বা আউটেজের সময় পারস্পরিক সহায়তা প্রদান করে। তবে, এই উপ-ব্যবস্থাগুলির সংহতকরণ প্রায়ই অসিলেটরি মোডগুলির উদ্ভব ঘটায় যা স্থিতিশীলতা এবং কার্যকারিতা বিঘ্নিত করতে পারে। এই থিসিসটি একটি মাল্টিব্যান্ড পাওয়ার অসিলেশন ড্যাম্পিং (MB-POD) কন্ট্রোলারের ডিজাইন এবং বাস্তবায়ন উপস্থাপন করে যা একটি আন্তঃসংযুক্ত হাইব্রিড AC মাইক্রোগ্রিড সিস্টেমের জন্য প্রয়োগ করা হয়েছে। প্রস্তাবিত MB-POD কন্ট্রোলারটি বিভিন্ন ফ্রিকোয়েন্সি ব্যান্ড জুড়ে LFOs কমানোর উদ্দেশ্যে তৈরি করা হয়েছে, যা মাইক্রোগ্রিডের সামগ্রিক স্থিতিশীলতা এবং নির্ভরযোগ্যতা উন্নত করে। LFOs ঘটে এই সংহতকরণের কারণে, বিভিন্ন ডায়নামিক লোড দৃশ্যকল্প এবং যে কোনও সিস্টেমে লোড বিঘ্নের কারণে। এই অসিলেশনগুলি স্থানীয় বা আন্তঃমাইক্রোগ্রিডগুলির মধ্যে হতে পারে। এই গবেষণাটি একটি শক্তি সঞ্চয় ব্যবস্থা (ESS)-ভিত্তিক POD পরিচয় করিয়ে দেয় যা একটি আন্তঃসংযুক্ত AC মাইক্রোগ্রিড সিস্টেমের এমন অস্থিতিশীলতা কমানোর জন্য ডিজাইন করা হয়েছে। এই গবেষণাটি একটি আন্তঃসংযুক্ত AC হাইব্রিড মাইক্রোগ্রিড সিস্টেমে পাওয়ার অসিলেশনের জটিল গতিবিদ্যা ব্যাখ্যা করে, প্রচলিত পাওয়ার অসিলেশন ড্যাম্পিং পদ্ধতির ঘাটতিগুলি তুলে ধরে। উন্নত গাণিতিক মডেল এবং সিমুলেশন কৌশলগুলি ব্যবহার করে, আমরা প্রস্তাবিত করেছি একটি নতুন পদ্ধতি যা অসিলেটরি মোডগুলি কার্যকরভাবে ড্যাম্পেন করতে সক্ষম। প্রস্তাবিত মাল্টিব্যান্ড ড্যাম্পিং কন্ট্রোলার ব্যবহার করে যেমন বর্তমান সিঙ্গেল-ব্যান্ড পাওয়ার অসিলেশন ড্যাম্পার (SB-POD), আন্তঃসংযুক্ত হাইব্রিড AC মাইক্রোগ্রিড সিস্টেমটি MATLAB/Simulink পরিবেশে পরিচালিত হবে। টাইম-ডোমেন সিমুলেশন ব্যবহার করে প্রস্তাবিত কন্ট্রোলারের কর্মক্ষমতা মূল্যায়ন করা হয়েছে। সিমুলেশন এবং কেস স্টাডিগুলি ড্যাম্পারের কার্যকারিতা বর্ণনা করে যা সিস্টেমের স্থিতিশীলতা উন্নত করতে, পাওয়ার ফ্লো অপ্টিমাইজ করতে এবং ট্রান্সিয়েন্ট প্রতিক্রিয়া সময় কমাতে সাহায্য করে। ফলাফলগুলি দেখায় যে একাধিক অসিলেটরি মোডের ড্যাম্পিংয়ে উল্লেখযোগ্য উন্নতি হয়েছে, ড্যাম্পিং রেশিও 9.1% উন্নত করে এবং প্রায় 4-6% অসিলেশন কমিয়ে দেয়, যা আধুনিক শক্তি ব্যবস্থার জন্য একটি প্রতিশ্রুতিবদ্ধ সমাধান। MB-POD সিস্টেমের মধ্যে বিভিন্ন মাইক্রোগ্রিড জুড়ে SB-POD থেকে বেশি কার্যকর, এভাবে আরও স্থিতিশীল এবং অভিযোজিত আন্তঃসংযুক্ত হাইব্রিড AC মাইক্রোগ্রিড সিস্টেমের পথ প্রশস্ত করে।

Table of Contents

List of Figures

List of Tables

Table No.	Table Caption	Page No.

Nomenclature

Symbols, Acronyms and Abbreviations

AC	Alternating Current
AC IMG	Alternating Current Interconnected Microgrid
BTB	Back-to-Back Converter
CPSS	Conventional Power System Stabilizer
CHP	Combined Heat and Plants
CIL	Constant impedance load
CPL	Constant Power Load
CCL	Constant Current Load
CT	Current Transformer
DFIG	Doubly-fed induction generator
DC IMG	Direct Current Interconnected Microgrid
DGs	Distributed Generations
ESS	Energy Storage System
FACTs	Flexible AC Transmission Systems
ISSs	Interconnecting Static Switches
IM	Induction Motor
IIDGs	Inverter-Interfaced Distributed Generator
IBDG	Induction-Based Distributed Generator
ICCL	Inner current control loop
LFOs	Low Frequency Oscillations
MG	Microgrid
IMG	Interconnected Microgrid
MB-PSS	Multi-Band Power System Stabilizer
MPPT	Maximum power point tracking
PSS	Power System Stabilizer
PLL	Phase locked loop
PV	Photovoltaic
PI	Proportional integral
POD	Power Oscillation Damper
RES	Renewable Energy Source

SoC	State of charge
SB-POD	Single-Band Power Oscillation Damper
SIDG	Synchronously Interfaced Distributed Generator
SCRs	Silicon Controlled Resistors
MB-POD	Multi-Band Power Oscillation Damper
TCL	Thermostatically Controlled Load
VSC	Voltage source converter
VST	Voltage Signal Transducer
VT	Voltage Transformer
WT	Wind Turbine

Chapter 1

INTRODUCTION

The background and motivation for the study that was carried out for this thesis are provided in this chapter. The thesis's main goals for study and contributions are emphasized and compiled. The thesis' organization has been introduced, including each chapter that comes after it.

1.1 BACKGROUND

Large synchronous generators, the backbone of traditional electrical power systems, are often located far from load centres. These power plants are linked together by long transmission lines so that they can produce electricity on demand. The current international emphasis on sustainability and decreasing emissions of greenhouse gases has resulted in a rapid expansion of a wide array of renewable energy resources and technology. As a result of their properties and scarcity, renewable energy sources (RESs) are typically integrated into the current electrical grid through the distribution network. This phenomenon has led to the use of the terms "distributed generation" (DG) to describe these assets [1]. The rapid industrial expansion and the decreasing availability of fossil fuels have led to the widespread adoption of these sustainable and efficient renewable energy alternatives. Microgrids, localized energy grids, have emerged as a solution to the technological, economic, and environmental challenges associated with traditional electricity infrastructure having renewable energy resources. These systems can generate, distribute, and regulate electricity flow using various energy sources like solar panels, wind turbines, diesel generators or natural gas, as well as energy storage systems (ESSs) are known as hybrid AC microgrid system [2].

This microgrid is recognized for their adaptability, intelligent functionalities, resilience, reliability, utilization of clean energy, efficiency, and economic viability. However, managing and integrating numerous dispersed generating units within a single microgrid poses challenges due to the unpredictability of DGs. Interconnecting multiple microgrids to form an interconnected microgrid system (IMGs) enables mutual assistance in the face of system outages or power deficiencies, enhancing the stability of power system and mitigating load shedding [3]. Interconnected microgrid can be classified into three types: Alternating Current Interconnected Microgrid (AC IMG), Direct Current Interconnected Microgrid (DC IMG), and AC-DC IMG [4]. AC IMGs are widely used as the primary form of IMGs, connecting DGs, ESSs, and loads to AC buses without modifying the existing power grid structure. DC interconnected microgrids rely on direct current for power distribution, reducing power loss and harmonic reduction issues. AC-DC interconnected microgrids combine both AC and DC distribution systems within the same network, providing flexibility and compatibility with a wide range of loads and generation sources.

The AC IMG system is considered more advantageous due to its simpler integration with existing electrical infrastructure [5]. However, it faces technological challenges in managing DGs due to low system inertia, demand, and generation uncertainty. These systems can cause low frequency oscillations (LFOs), which can cause stability issues due to diverse DGs, inverter control dynamics, load sharing, advanced protection schemes, and communication delays [6]. These issues may also occur in hybrid AC microgrids and AC IMGs.

1.1.1 Local Microgrids to Interconnected Microgrids Transition

These days, with the depletion of fossil fuel-based energy sources like coal, natural gas, and oil, as well as environmental concerns, there is a greater focus on power generation based on renewable energy [7]. Microgrids (MGs) consisting of many DGs have evolved in reaction to the drawbacks of micro-generation based on single-DG, including inadequate generating capacity, local voltage rise, emergency situations, and the propensity to surpass the thermal limits of certain lines and transformers [8]. But since an individual MG can only handle a few MVA of power, it won't be safe enough to meet its own needs. An IMG system is one of the most promising ideas to overcome the drawbacks of a local MG system, as shown by the development scheme of the evolution of MG structure in Fig. 1.1 [9]. This concept involves clustering and operating multiple different nearby MGs simultaneously to provide an integrated framework that offers increased flexibility, controlled power sharing, and effective power management [10]. This innovative infrastructure is spreading more extensively due to its improved resilience, flexibility, economic viability, dependable operation, and better handling of surplus and shortage power [11]. The configuration of the interconnected system is determined by the nature of power transmission (AC or DC) and connections at electrical boundaries, i.e., line and interface technology [12]. Based on line technologies, it takes three forms: fully AC networked MGs [13], fully DC networked MGs [14], and AC/DC networked MGs [15]. Interfaces can be based on various devices, including tie-line connections with static switches or circuit breakers, power transformers, and interlinking converters [16-19]. However, due to the complex structure of the networked MGs compared to a single MG, further studies are required on various structures based on line and interface technologies, coordinated control of individual MGs, and management of interconnection among MGs.

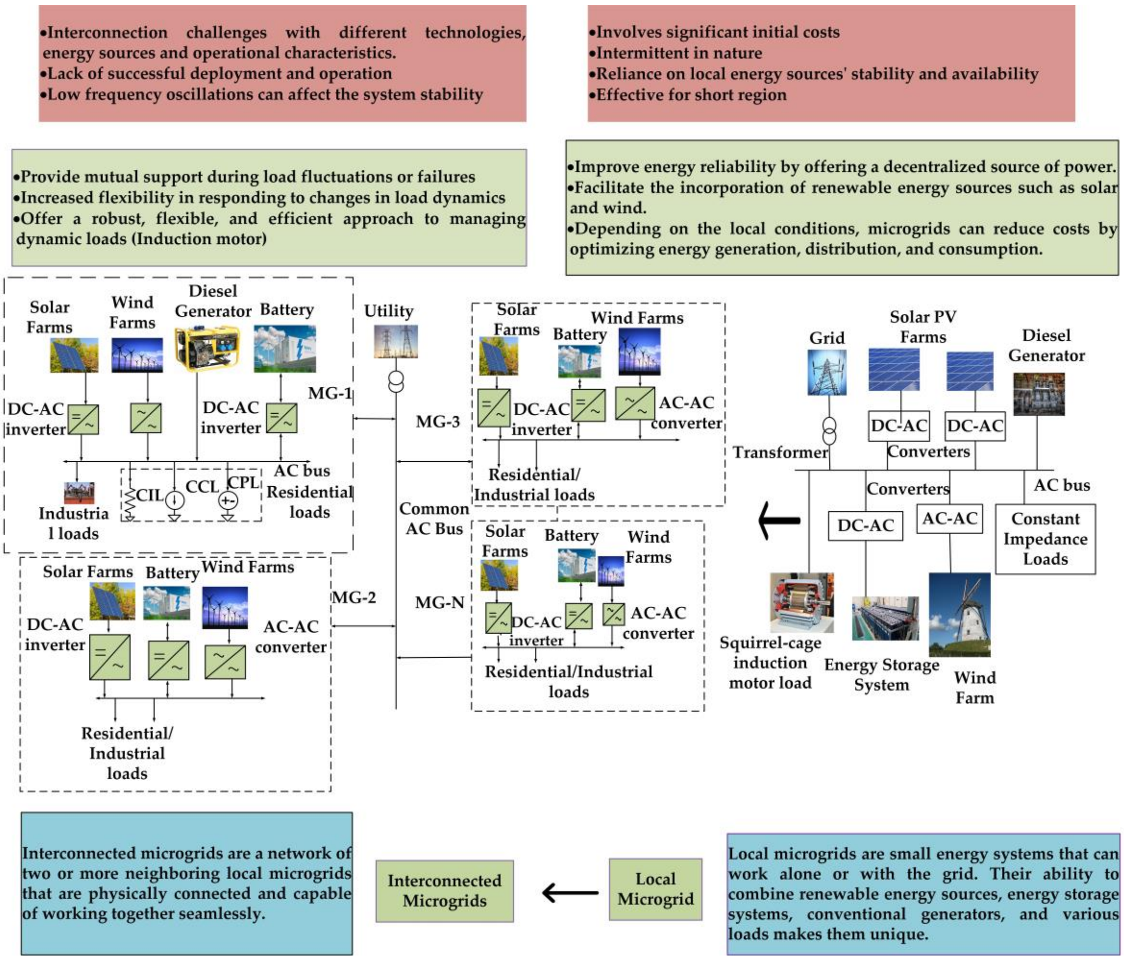

Fig. 1.1: An overview of the evolution of the local microgrid to interconnected microgrids infrastructure.

1.1.2 Control and Management System

The integrated MG system's stability, optimal performance, and operational viability are achieved using the control and management system, which is a collection of hardware and software associated with the power electronics converters and their controllers. The main duties of the control system are to regulate voltages and frequencies within predetermined ranges, supply adequate power, share and balance, switch between different operating modes (islanded and grid-connected), and provide efficient demand-side management [20]. A vital aspect of the control system is information sharing among MGs, which helps identify the optimal operating strategy to guarantee the dependability and efficiency of the system. The interconnected system can be controlled in a number of ways, including hierarchical [21], distributed [22], decentralized [23], and centralized [23]. Because the distributed and hierarchical control structures allow controllers at different levels to communicate and share information or control signals, they make it easier to create control systems at numerous control levels with distinct control responsibilities and aims.

Control of DGs at individual MGs, demand-supply management within each MG, and control for coordinated operation among IMGs are just a few of the control tasks that fall under the purview of an interconnected microgrid's control system [24, 25]. The DGs must be outfitted with appropriate power electronic interfaces, controls, and management to link and split inside a local MG to guarantee smooth functioning at the component level. In contrast, for flexible operation as a single aggregated framework in a networked MG system, every MG needs a dependable controller to link with other MG [26]. To achieve accurate power sharing, smooth transition and synchronization, frequency and voltage recovery, and adaptable power flow regulation, all control objectives must be met [27]. Above all, control system research must be done in addition to creating dependable and efficient control structures if optimal performance from the IMG system is to be achieved while also guaranteeing system stability.

1.2 CONTEXT

Electrical power systems must maintain stability throughout steady-state and transient circumstances. Large synchronous generators and flexible AC transmission systems (FACTS) equipment like STATCOMs and SVCs make up large traditional power systems. However, Inter-area low-frequency oscillations in interconnected power systems are significant obstacles to enhancing the dynamic performance of these systems, as they can either restrict the amount of power transferred across tie-lines or jeopardize the dynamic stability of the power systems [28]. Generators' substantial inertia allows such systems to stabilize around an operating point after small shocks. Due to the low-inertia nature of microgrids with distributed generation (DGs), even slight changes in system characteristics such as solar irradiation, wind speed, and loading conditions can lead to instability if not properly managed. Electromechanical oscillatory modes can also appear in microgrids, especially when multiple microgrids are interconnected or operating in tandem.

Microgrids are smaller, localized grids that can operate autonomously or in conjunction with the main grid. As stated earlier, they typically consist of DGs such as photovoltaic systems, wind turbines, batteries, and possibly small conventional generators. Large frequency fluctuations can arise because of the intermittent nature of RESs when the load frequency control capacity that is available is insufficient to correct for an imbalance between the amount of generation and the amount of demand. Interconnecting microgrids to create IMG systems can enhance reliability and security. LFOs may worsen when the system is operating in an interconnected state. Like the inter-area modes in major power systems, oscillations can arise when two or more microgrids interact with one another. These oscillations can be a result of the difference in frequency, phase, or power output among the interconnected microgrids [29]. Operating an interconnected power system with low inertia can be extremely challenging due to the unpredictability in both demand and generation. Although the inertia in a power system can partially mitigate disturbances caused by load changes or the intermittent nature of renewable energy sources (RESs), maintaining frequency deviations within acceptable limits remains difficult. This challenge arises because the fluctuations in load or the variability of RESs can still introduce significant disturbances. Many DGs in microgrids use inverters to convert DC to AC. The control strategies of these inverters, like droop control or virtual inertia, can introduce oscillatory behaviours. Proper coordination of these control strategies is essential to ensure stability [30]. Droop control is commonly used in microgrids to share loads among multiple DGs. Incorrect settings or uncoordinated droop curves can introduce oscillations [31]. Energy storage systems like batteries can act as dampers or introduce new oscillatory modes, depending on their control strategies. Their fast response can be leveraged to stabilize the microgrid [32]. Dynamic loads refer to those loads which change rapidly over time, such as motor starts, electronic drives, or fluctuating industrial processes. When these loads vary, they can introduce voltage and frequency fluctuations in the microgrid. If these fluctuations are not properly managed, they can lead to voltage collapse or frequency instability [33]. The mode of operation (islanded or grid-connected) can influence the oscillatory behaviours. In islanded mode, without the damping provided by the larger grid, certain oscillations might become more pronounced [34].

AC microgrid and AC IMG are predicted to experience oscillations due to their similarities to traditional power systems. AC microgrid and AC IMG may also face different stability difficulties than traditional power systems due to the diversity of DGs in IMG [7]. In-depth stability research is needed to characterize AC microgrid and AC IMG oscillations. The effect of DG control on low-frequency oscillations in AC IMG needs to be assessed. Stability studies are necessary to provide new controls for improving microgrid and IMG stability. It's essential to study and model the dynamics of an interconnected hybrid AC microgrid comprehensively, considering all the components and their interactions. Advanced tools, such as real-time digital simulator MATLAB/Simulink, can be used to emulate these behaviours and test various control strategies to ensure stability. As the energy landscape shifts towards more decentralized generation and the proliferation of microgrids, understanding and managing the electromechanical oscillatory modes in these systems will become increasingly important. Proper design, control coordination, and real-time monitoring will be crucial to ensure stable and reliable operations. The significant real-time energy management challenges, such as output power variation and voltage instability caused by the intermittent nature of DGs and inelastic loads in the system, can be mitigated by a reliable power supply or appropriate-size ESSs [29]. The fundamental task of the ESS and its control strategy is to achieve a balance between generation and demand, depending on the dispatchable power of each storage unit, while preserving voltage and frequency within reasonable limits in all operating modes [30]. A Power System Stabilizer (PSS) is a device added to generators' automatic voltage regulators to dampen low-frequency oscillations. It can be several types of PSSs such as the conventional power system stabilizer (CPSS), IEEE PSS2B, PSS3B, and PSS4B [31]. CPSS enhance microgrid stability and performance by mitigating power oscillations and improving dynamic response through excitation control of synchronous generators. They dampen low-frequency oscillations, maintaining voltage and frequency stability during transient disturbances. But CPSS are typically effective only within a specific range of frequencies and may not adequately address oscillations outside this range. A single-band power oscillation damping (SB-POD) controller based on CPSS is a modified controller can be used to dampen low frequency oscillations. Among them the multi-band Power system stabilizer (MB-PSS) is an advanced stabilizer that accommodates all global, inter-area, and local modes. It uses three pass filters to mitigate a broad spectrum of oscillations characterized by varying frequencies, enhancing damping performance in all modes. This PSS can be introduced as multi-band power oscillation damper (MB-POD), which can enhance stability, grid resilience, and integration of renewable resources in interconnected microgrid systems [32]. It can damp multiple oscillation modes simultaneously, ensuring system stability, particularly in systems with diverse sources and loads, such as solar, wind, and diesel generators. It can prevent and dampen oscillations that could destabilize individual microgrids or their interconnections, ensuring efficient resource utilization. It can operate in both grid-connected and islanded modes, reducing costs and complexity. In situations of rapid load changes or disturbances, a multi-band PSS can maintain transient stability. Integrating a multi-band PSS within the ESS can provide enhanced control and stabilization capabilities, counteracting oscillations brought about by renewables, optimizing energy utilization, and reducing reliance on mechanical solutions in islanded mode [33]. An overview of the context (statement of the problem) of this thesis is presented in Fig. 1.2.

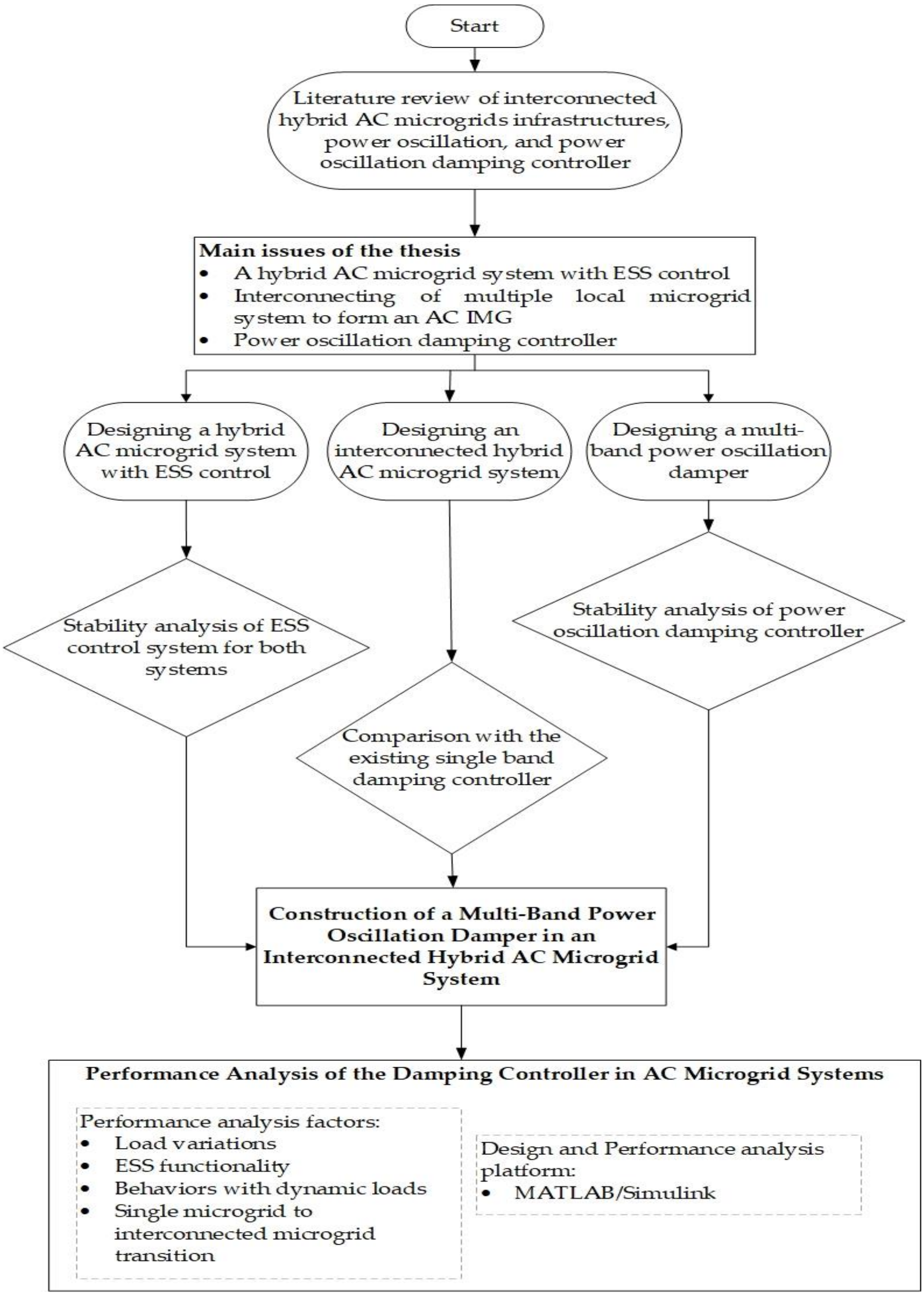

Fig. 1.2: An overview of the context of this thesis.

1.3 AIMS AND OBJECTIVES

The primary aim of this thesis is to develop and evaluate a multi-band power oscillation damper to enhance the stability and efficiency of an interconnected hybrid AC microgrid system by effectively damping low-frequency oscillations. This research seeks to address the critical challenges posed by these oscillations, thereby improving the integration of RESs and the overall operational reliability of microgrids. Designing this efficient power oscillation damper will be accomplished by implementing the following four objectives:

1.3.1 To develop a hybrid AC microgrid system with various DGs and an ESS.

- A comprehensive AC microgrid test system is designed and implemented incorporating various DGs such as solar, wind, and conventional generators (such as diesel), along with an ESS.
- Existing control approaches is applied to manage ESS dispatch effectively, ensuring optimal integration and operation within the microgrid.
- An inner current control loop and outer voltage-frequency $(V - f)$ control strategy is used in the ESS to determine the power output of the ESS.
- The existing control of ESS controller is approached to calculate the required active/reactive power adjustments to maintain stable voltage/frequency of the AC microgrid by comparing the voltage and frequency variances between the measured and reference values.

1.3.2 To design and implement an interconnected hybrid AC microgrid System

- The hybrid AC microgrid system is expanded to an interconnected hybrid AC microgrid configuration by establishing connections between multiple types of microgrids.
- The necessary control infrastructure is developed and integrated to facilitate coordinated operation and power sharing among the interconnected microgrids.
- The system is based on the interconnection of AC buses using interconnecting static switches (ISSs) in between the local microgrids to reduce conversion stages and challenges due to voltage and frequency controls and active and reactive power exchanges.
- To present an interconnection approach for three microgrids using a static switch and a power sharing strategy to provide uninterrupted power supply based on generation capacity.

1.3.3 To design an ESS-based multi-band power oscillation damper in an AC Microgrid system.

- A MB-POD is installed at the ESS to get responds more quickly than the other sources in the microgrid.
- A detailed analysis is conducted for the low-frequency oscillations occurring within the interconnected microgrid system under various operating conditions.
- The key factors contributing to LFOs is identified and assessed their impact on system stability and performance.
- To reduce the LFOs, the POD controller is designed to give the ESS controller an extra stabilizing input. A network disruption,

such as a shift in load, a DG outage, or a short circuit fault, could cause oscillations in voltage and frequency within the microgrid, which could then cause rotor speed oscillations at induction motor (IM) loads.

- The MB-POD is optimized for use with multiple microgrid systems to compare the performances of traditional single-band POD in terms of dampening purposes.
- This study compares the dynamic performance of multiple parallel small IMs with a large IM with the same power rating across various operating conditions. It uses eigenvalue analysis and non-linear dynamic simulations to account for model parameters and voltage/frequency transients across the IM terminals.

1.3.4 To analyse the performance and effectiveness of the multi-band power oscillation damper structure in ESS of an IMG system over a SB-POD based on various factors using MATLAB/Simulink.

- A multi-band power oscillation damper is developed specifically designed to mitigate LFOs in the interconnected microgrid system.
- The proposed controller is implemented in the test systems and evaluate its effectiveness in real-time damping of low-frequency oscillations through extensive simulations and testing.
- To verify the stability of the proposed damping controller, stability analyses are presented based on bode plots in the MATLAB/Simulink environment.
- The performance of the proposed damping controller structure is validated based on various factors such as load variations, source power variations or failures, ESS functionality, behaviours with

dynamic loads (small IMs and large IMs), and mode transition of microgrid systems over SB-POD using the MATLAB/Simulink simulation technique.

- To damp low frequency oscillations, an additional power oscillation damper (POD) is suggested for the ESS. This controller would supply a stabilizing signal proportionate to the frequency deviation, as the frequency deviation is proportional to the speed deviation.

1.4 SIGNIFICANCE OF THE OBJECTIVES

The objectives of this research focus on enhancing microgrid stability and efficiency through several key developments. Firstly, a hybrid AC microgrid system with diverse DGs and an ESS is developed to optimize energy management and ensure reliable operation. Secondly, the design of an interconnected hybrid AC microgrid system aims to improve power distribution flexibility and reliability through coordinated control strategies. Thirdly, an ESS-based MB-POD device is designed to quickly mitigate LFOs, enhancing system stability. Lastly, the performance of the MB-POD in an IMG system is analysed to validate its effectiveness in improving microgrid resilience under various conditions.

1.5 THESIS OUTLINE

This thesis is mainly focused on designing an interconnected MG system with a multi-band power oscillation damping controller in ESS. The modelling, implementation, and performance evaluation of the proposed controller are discussed in detail in the remaining chapters of this thesis. A brief overview of the contents of each chapter in designing the IMG and multi-band power oscillation damper is presented as follows:

Chapter 1 presents an overview of the research objectives and the significance of developing an ESS-based multi-band power oscillation damping controller in an interconnected hybrid AC microgrid system with an introduction of the specific objectives and research questions addressed in the study.

Chapter 2 introduces the structure of the IMGs with the power system stabilizer. This chapter also provides the details of the structure and configuration of the three power system stabilizer strategies.

Chapter 3 presents the development of an interconnected hybrid AC microgrid system by interconnecting local microgrids using ISSs, describes the interconnection approach for multiple microgrids using static switches and power sharing strategies. This chapter ventures into the heart of designing ESS-based power oscillation dampers, scrutinizing the criteria that dictate their effectiveness. The methodology section provides a systematic approach to the design process, supported by robust mathematical models and simulation techniques that act as the building blocks for developing efficient damping systems. Control strategies take centre stage, revealing the sophistication behind the algorithms that govern the ESS response to power disturbances.

Chapter 4 analyzes the performance and effectiveness of the MB-POD controller structure in a hybrid AC microgrid system with ESS and an interconnected system with one ESS based on various factors using MATLAB/Simulink, conducts stability analyses based on bode plots and pole-zero maps to verify the stability of the proposed damping controller, validates the performance of the damping controller structure under various factors such as load variations, dynamic loading of various sizes, and ESS functionality using MATLAB/Simulink simulation technique.

Chapter 5 evaluates the performance and efficacy of the MB-POD controller structure within an interconnected hybrid AC microgrid system equipped with an ESS. This assessment is conducted by examining various factors through

MATLAB/Simulink simulations. Stability analyses are performed using Bode plots and pole-zero maps to confirm the stability of the proposed damping controller. The chapter validates the performance of the damping controller structure under different conditions, including load variations, source power fluctuations, ESS functionality, and dynamic loads, utilizing MATLAB/Simulink simulation techniques.

Chapter 6 finally concludes this study by summarizing the key findings and contributions of the study, provides recommendations for future research directions and areas for further investigation, and concludes with a discussion on the significance of the research outcomes and their potential impact on the field of microgrid systems and energy storage control strategies.

Chapter 2

CHARACTERISTICS AND STRUCTURES OF INTERCONNECTED MICROGRID SYSTEMS AND POWER SYSTEM STABILIZERS

As the global energy landscape evolves towards more sustainable and decentralized energy solutions, interconnected microgrid systems have emerged as a pivotal component in modern power distribution networks. These microgrids, which can operate both autonomously and in conjunction with the main power grid, offer enhanced reliability, resilience, and efficiency. The integration of renewable energy sources, such as solar and wind, within these microgrids further underscores their importance in achieving environmental sustainability. However, the dynamic and intermittent nature of these renewable sources presents challenges in maintaining grid stability and power quality. Power system stabilizers play a crucial role in mitigating these challenges by enhancing the stability and reliability of the power system. This chapter delves into the characteristics and structures of interconnected microgrid systems and explores the critical role of power system stabilizers in ensuring their seamless and stable operation.

2.1 INTRODUCTION

The possibility of autonomous future electrical infrastructure, like MGs, has been raised by recent improvements in renewable-based distributed electrical generation systems and power electronics technology. These small, self-sufficient electrical system zones can facilitate the integration of DG, including renewable energy, and potentially increase effectiveness and dependability [34]. However, because of the nature of DGs and the difficulties in control and management, it is not practical to integrate DGs in bulk within a single MG. Consequently, a single MG system's power generating and distribution capabilities are restricted to a narrow geographic area, which limits safe load control, consistent power supply, and dependable operation [35]. To address the issues related to a local MG's resilience, one of the most promising approaches in the field of MG-based power systems is the networking of several MGs concept. The interconnected MG concept involves the interconnecting and simultaneous operation of multiple discrete MGs that are geographically close to each other. This creates an integrated framework that offers increased flexibility, regulated power sharing, and effective power management [10]. This innovative infrastructure is spreading more and more due to the variety of DGs, improved flexibility, resilience, economic optimality, dependable operation, control of system voltage and frequency during emergencies, supply of backup power for especially important loads, and improved management of power shortages and excess among MGs [11].

2.2 DISTRIBUTED GENERATIONS

DGs are small-scale units of local generation connected to the grid at distribution level [36]. They are an evolving aspect of the electricity sector and relate to a wide variety of energy sources and storage systems. This includes renewable generation such as solar panels, wind turbines, and small-scale hydroelectric generators. These resources are often variable, generating electricity only when the sun shines or the wind blows. These systems also generate electricity and thermal energy in a single, integrated system [37]. They are often used in industrial settings or large buildings like hospitals. RESs are not the only ones that may be used in distributed generation; synchronous generators and induction generators are additional examples [38]. "Synchronously interfaced distributed generations" typically refers to distributed generation sources that are connected to the grid through synchronous generators. Synchronous generators are in phase with the grid and operate at the same frequency.

Examples include small-scale hydroelectric generators, biomass power plants, or gas turbines that are directly connected to the grid. "Inverter interfaced distributed generations" refers to DG resources that use power electronics inverters to connect to the grid. This category includes solar PV systems, battery storage, and wind turbines with variable speed drives. These systems convert DC power to AC power matching the grid's voltage, frequency, and phase using inverters. While synchronous generators maintain grid stability through their inertia, utilities and grid operators are creating new techniques to control the stability and dependability of the grid as the share of inverter interfaced DGs rises. This includes advancements in smart grid technologies, such as advanced inverters that can provide grid support functions, and the use of energy storage systems to provide ancillary services such as frequency regulation and voltage support [39]. Technologies such as batteries (including electric vehicle batteries), flywheels, and pumped hydro storage allow excess energy to be stored and used at a later time [40]. This is particularly important for balancing supply and demand, especially with variable renewable sources. This is a method by which consumers reduce their electricity use at times of high demand in response to price signals or other incentives [41]. These include advanced metering infrastructure, smart inverters, and other technologies that enable two-way communication between the utility and its customers, allowing for more sophisticated energy management. These are localized grids that can disconnect from the traditional grid to operate autonomously and can help mitigate grid disturbances to strengthen grid resilience [42]. DGs can also be used to provide electricity in remote locations that are economically or geographically unable to be reconnected to the utility grid. These microgrid systems are formed when DGs are used to deliver electricity in these locations. The integration of DGs into the electrical grid represents a significant shift from the traditional model of centralized electricity generation, where a small number of large power plants generate most of the electricity and send it out over a network of transmission and distribution lines. DGs can help to improve the resilience of the power system, reduce transmission losses, and provide environmental benefits.

However, they also pose challenges for grid management and regulation due to their variable nature and the need for new infrastructure and market mechanisms to support their operation and integration.

2.3 MICROGRIDS

A microgrid is a localized group of electricity sources and loads that normally operates connected to and synchronous with the traditional centralized electrical grid (macrogrid) but can also disconnect to "island mode" — and function autonomously as physical and/or economic conditions dictate [43]. Microgrids can incorporate a variety of DGs such as solar panels, wind turbines (WTs), combined heat and power (CHP) plants, diesel generators, batteries, and other energy storage solutions, as well as several types of loads (dynamic load, constant impedance load, constant power load etc.) [2]. A hybrid AC microgrid structure has been illustrated in Fig. 2.1 [44]. Microgrids commonly use inverter interfaced distributed generators (IIDGs), induction based distributed generators (IBDGs), and synchronously interfaced distributed generators (SIDGs) for their generation [1]. To connect DC power sources to an AC microgrid, IIDGs use devices based on power electronics. IIDGs include things like fuel cells, PVs, and ESSs. Microgrids, including IIDGs, are covered in several studies [39]. DGs based on induction machines add new power sources to the microgrid system. Induction generators can be found in a variety of energy sources, including both fixed and variable speed WTs. IBDGs employ induction generators to integrate energy sources into the microgrid network. Fixed and variable speed WTs are illustrative instances of energy resources that integrate induction generators [45]. Diesel generators and micro-turbines are two examples of SIDGs that use traditional synchronous generators to transform mechanical energy from gas turbines into AC electricity [46]. Power for both stationary and moving loads can be supplied by a variety of energy producing options. Microgrids typically run appliances like induction motors, lights, computers, and thermostatically controlled loads (TCLs). It is difficult to build a system that can properly coordinate between the many energy resources to supply electricity to the various loads that make up a typical microgrid due to the diversity of components found in microgrids. Microgrids are energy management systems that optimize the performance of DGs. They can maintain operation independently from the main grid during outages, reducing energy losses and enhancing efficiency. Microgrids can be scaled to serve small communities or large industrial complexes, and their modular nature allows for flexibility in design and expansion [47]. Advanced energy management systems optimize power generation and distribution, minimizing energy costs and increasing reliability. Microgrids can provide power in areas not served by the main grid, ensure continuous power supply for critical military operations, and improve business resilience. They can also be the primary source of electricity for islands or remote locations. However, challenges such as low frequency oscillations, complex regulatory environments, and potential vulnerability to hacking and cyber-attacks necessitate robust security measures [48]. Consequently, the focus of this thesis is on illuminating and resolving some of the problems associated with the operation and control of microgrids.

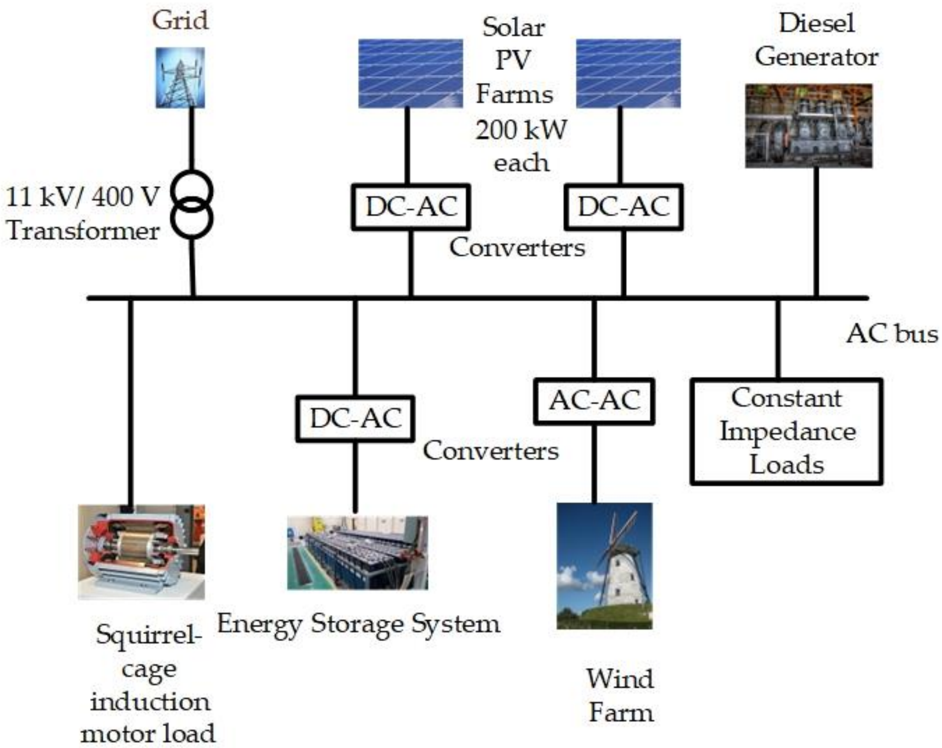

Fig. 2.1: A hybrid AC microgrid architecture.

2.4 INFRASTRUCTURE OF INTERCONNECTED MICROGRIDS

It is crucial to consider and investigate every potentiality of the interconnected MG architecture to create an interconnected MG-based electrical system that functions efficiently in accordance with present and future power grid requirements. Diverse MG cluster infrastructures are produced by the creation of numerous MG structure kinds, interlinking lines, devices, interlinking converter topologies, control strategies, and communication approaches to boost future smart grid developments. The rapid industrial expansion and decreasing fossil fuel reserves have led to the adoption of sustainable renewable energy alternatives. Microgrids, localized energy grids, have emerged as a solution to technological, economic, and environmental challenges. These systems can generate, distribute, and regulate electricity using renewable sources like solar panels, wind turbines, and natural gas. However, managing and integrating multiple dispersed generating units within a single microgrid poses challenges due to the unpredictable nature of RESs [49, 50]. The interconnection of multiple microgrids to create an IMG enables mutual assistance in the face of system outages or power deficiencies. The utilization of these IMGs has been found to enhance the stability of microgrids and mitigate the occurrence of load shedding [51, 52]. An IMG system has smaller DG units compared to a utility grid, are installed near electrical loads, and are dominated by renewable energy resources and inverter-based DG units. IMG systems operate at the medium-voltage level, unlike a utility grid which includes a HV transmission system, HV generation system, and MV distribution system.

In an IMG system, layout specifies how MGs are connected to one another. Various layouts such as series, parallel, and mixed connections exist, as depicted in Fig. 2.2, depending on the connection with the main grid and the connection with each MG.

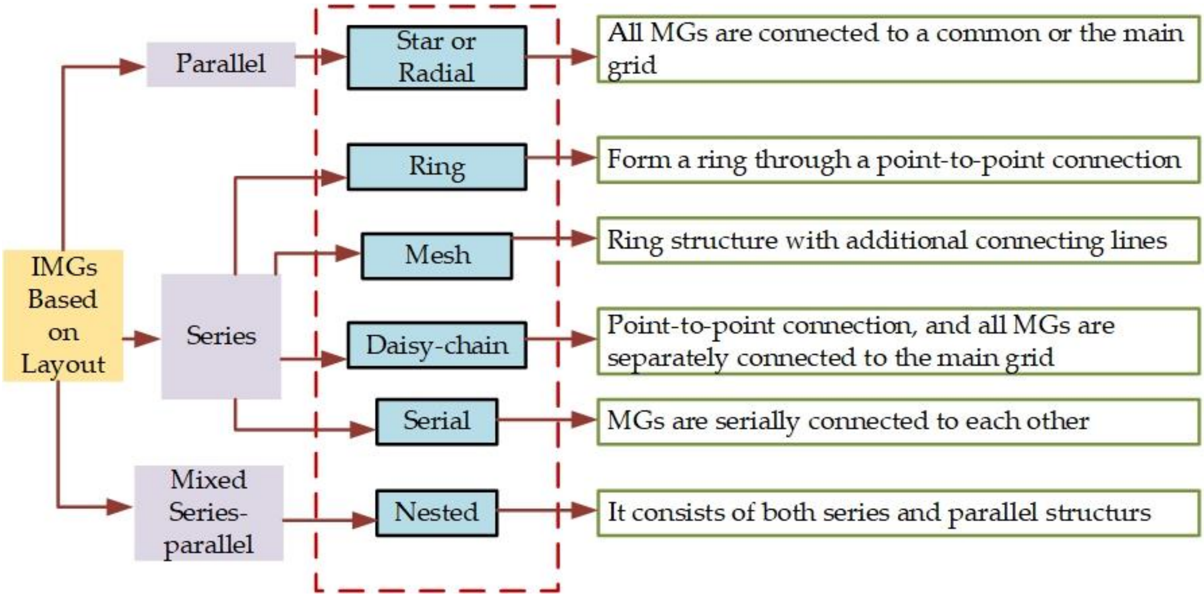

Fig. 2.2: Interconnected microgrid infrastructure based on layout.

Parallel-connected MGs refers to a framework in which all MGs are connected to a common node or to the main grid. In [53], a parallel-connected IMG system with an autonomous control technique is presented where both AC and DC MGs are connected to a common point through suitable interfaces. In a series-connected structure, MGs are connected to each other according to the point-to-point connection to develop IMGs and share power with adjacent MGs. A series-connected IMG system based on tie-line connections with various types of DGs and ESSs is used in [54] to explore the load frequency regulation of MGs in islanded mode. A mixed series-parallel structure is more feasible because it consists of both series and parallel structures and combines the benefits of both structures into a single structure [3]. In [55], a grid architecture model based on mixed series-parallel IMGs system is proposed to assist the system architect for the smart distribution network.

From Fig. 2.2, parallel types of IMGs can be classified into three types: AC IMGs, DC IMGs, and AC-DC IMGs. All the distributed generations in AC IMGs are linked to AC buses via converters. The DGs are connected to DC buses via converters in DC IMGs, which are normally coupled to DC loads, and the DC IMGs are connected to the external power grid via inverters [56]. Here are three types of interconnected microgrids based on their current types illustrated in Fig. 2.3:

2.4.1 AC Interconnected Microgrids:

Currently, AC IMGs are widely used as the primary form of IMGs which is illustrated in Fig. 2.3(a). These systems involve the connection of DGs, ESSs, and loads to AC buses. There is no need to modify the existing power grid structure to construct AC IMGs. These microgrids are designed to distribute AC power to connected loads. They can be composed of multiple AC generators, such as solar inverters, wind turbines, and diesel generators, all operating in parallel [57].

2.4.2 DC Interconnected Microgrids:

The loads, ESSs, and DGs in DC IMGs are all linked to DC buses by power converters visualized in Fig. 2.3(b). DC interconnected microgrids predominantly rely on direct current for power distribution so that the reactive power and eddy current losses that are taken up by the transmission lines don't matter. This greatly reduces the power loss. Also, DC IMGs don't have any issues with harmonic reduction or three-phase load mismatch. These microgrids are suitable for applications where DC loads or devices, such as LED lighting, computers, and battery storage systems, are prevalent. DC microgrids can be more energy-efficient for certain types of loads and are often used in data centers, telecom networks, and some off-grid applications like remote sensing stations [44].

2.4.3 AC-DC Interconnected Microgrids:

AC-DC interconnected microgrids combine both AC and DC distribution systems within the same network which is seen in Fig. 2.3(c). This approach allows for flexibility and compatibility with a wide range of loads and generation sources. AC-DC microgrids are versatile and can efficiently manage both traditional AC appliances and DC-powered devices. They are increasingly popular in modern buildings and industrial settings to accommodate diverse energy needs while optimizing energy use [58].

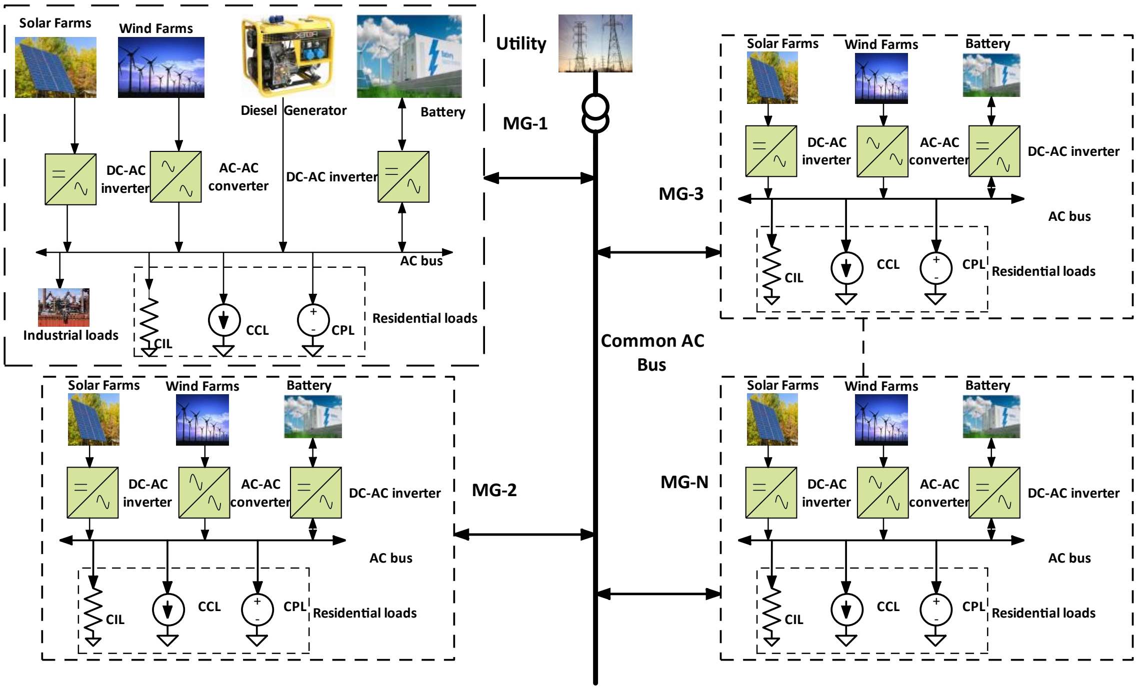

(a)

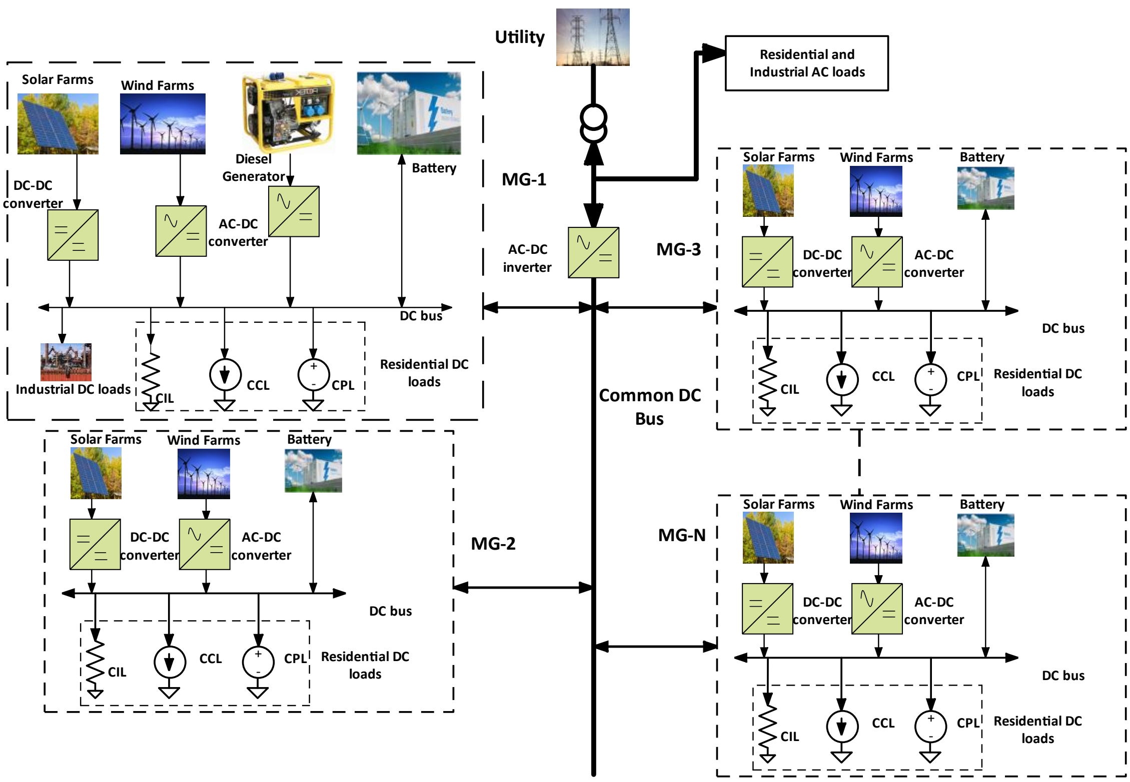

(b)

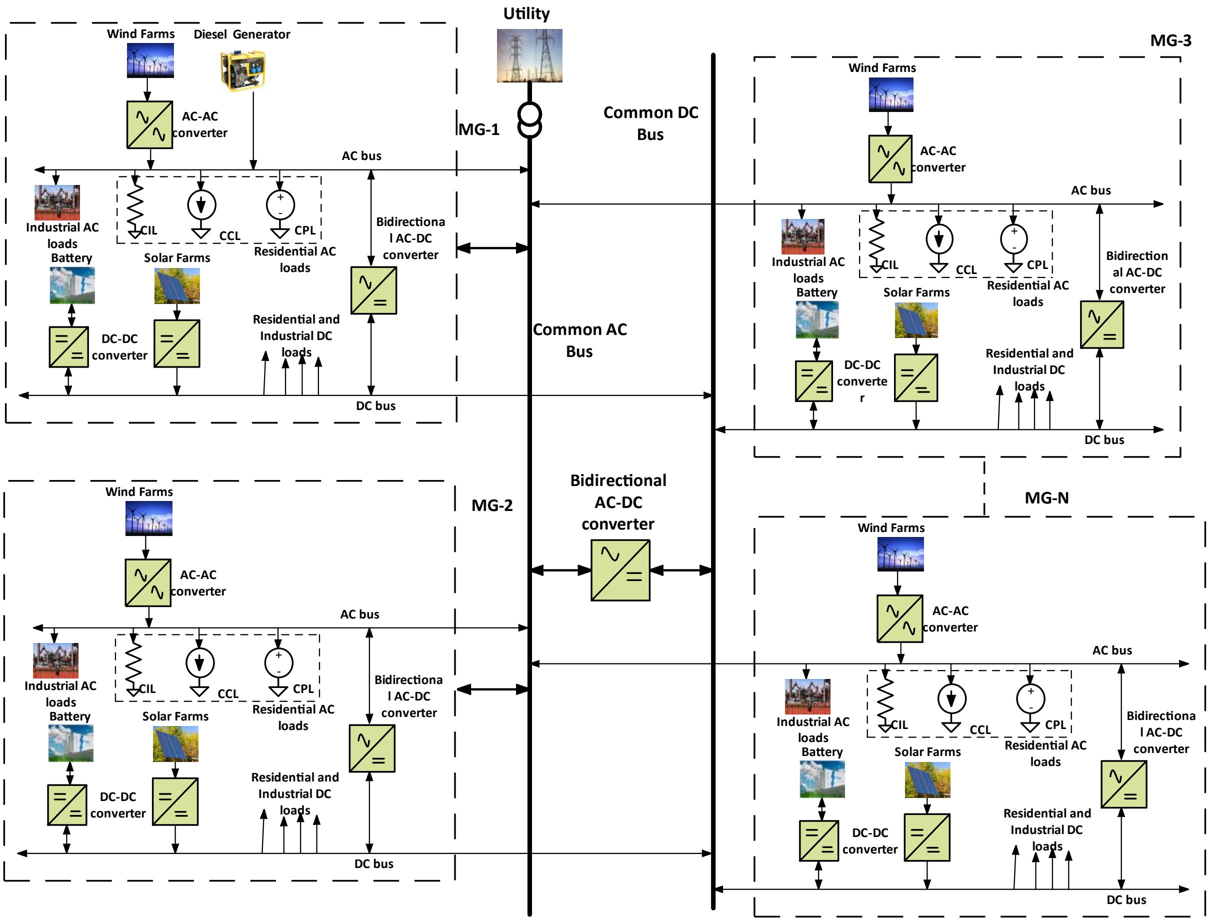

(c)

Fig. 2.3: Configuration of IMGs (a) AC IMG (b) DC IMG (c) AC-DC IMG [57, 59]

Among all the systems, the AC IMG system is deemed to be more advantageous compared to the others. The predominant electrical infrastructure in many regions is founded upon alternating current. Therefore, the process of integrating an AC IMG with the preexisting electrical grid and appliances is comparatively simpler as compared to the introduction of a DC or hybrid system. Nevertheless, despite the numerous advantages offered by AC IMGs, there are technological obstacles that occur in effectively managing the DGs that constitute these systems. Due to low system inertia, demand, and generation uncertainty, interconnected microgrid systems are sometimes challenging to operate and keep frequency variations, power oscillations and system voltages within limitations. AC Microgrids and AC IMGs are expected to oscillate causing LFOs [6]. LFOs in power systems are typically oscillations with a frequency ranging from 0.1 to 2 Hz [60]. These oscillations may occur locally or between microgrids. They may have distinct stability issues than standard power systems due to their diverse DGs, inverter control dynamics, load sharing, advanced protection schemes, and communication delays etc. Problems like LFOs may also occur in the AC microgrids and AC IMGs due to the dynamic performance of multiple induction machines instead of a single machine with the same rating under a wide range of operating conditions [61].

2.5 CHARACTERISTICS OF INTERCONNECED MICROGRIDS

The characteristics of an interconnected MG system depend entirely on the configuration and performance of the individual MGs within the network, i.e., the characteristics of individual MGs affect the ultimate performance, such as power quality, stability, and dynamics of the interconnected microgrid system.

2.5.1 Power System and Balance Stability

Inaccurate power sharing and balancing, loss of a generating unit, and the effects of different loads were the major causes of power system instability.

The voltage stability of the networked microgrid system is ensured by using distributed local control units to keep the AC and DC-link voltages within acceptable limits. Reactive power limitation, dynamic load interactions, and reactive power balancing issues are strongly associated with voltage instability in MGs. To address issues with DC bus voltage stability in the DC MG cluster, a hierarchical control approach is implemented in [62], with the sub-MG integration control located at the top, voltage compensation and droop coefficient adjustment control at the second layer, and droop control and voltage closed-loop regulation at the bottom. To reduce real power losses, voltage variations, and power generation expenses, a novel energy management framework for islanded MGs is developed in [63] that takes into account generation availability restrictions and voltage stability.

2.5.2 Control System Stability

The main causes of control system stability are insufficient management schemes and improper tuning of one or more device controllers. This stability is relevant to phase-locked loop (PLL), LCL filters, converter control loops, and electric equipment. Stability problems in MGs are intrinsically linked to the requirement for power conversion via power electronics interfaces to attain various voltage levels, which is essential for connecting ESSs, sources, and loads. The unique characteristics of the power-converter-dominated MG, such as its time-varying nature, nonlinearity, poor suppression of interference, low inertia, and multi-time scale, make it more difficult to maintain system stability. Due to difficulties with tuning, failure of inverter-based DGs, high harmonic-frequency fluctuations, and PLL synchronization, converters are vulnerable to small- and large-perturbation instabilities. To track the MG voltage reference for active load synchronization, a new technique is employed in place of the conventional PLL. This new approach avoids design complexity, poor accuracy, nonlinearity, tuning challenges, slow response, and detrimental effects on the PLL [64]. In order to improve system stability and respond to power changes, disturbances, and parameter modifications, a novel fuzzy logic-based online tuning technique for proportional-integral (PI) controllers is suggested in [65] for large MG systems. A novel harmonic droop controller is suggested in order to distribute the harmonic power across parallel islanded inverters that are regulated by the classical frequency droop approach and to lessen the voltage harmonic distortion [66].

2.5.3 Power Quality

Power quality is one of the significant characteristics of the MG-based power system, as the increasing penetration of nonlinear loads, renewable energy-based DGs with PQ challenges, and power electronic converter interfaces can result in distorted waveforms and increased energy costs. Therefore, novel power quality improvement strategies and analysis of power quality issues become essential in MG cluster systems due to the load sensitivity, higher utilization of RESs, and converter interfaces.

Different power quality improvement devices, such as the dynamic voltage restorer, static transfer switch, automatic voltage regulator, Static VAR compensator, distributed static compensator (D-STATCOM), and unified power quality controller have been developed to enhance the power quality indices such as voltage fluctuations, frequency deviations, and harmonic distortion of MGs [67]. Smart impedance, electrical springs, multifunctional DGs, and novel control methods are multi-functional power quality enhancement devices or systems that can perform multiple tasks simultaneously using the same hardware, which not only increases reliability and efficiency but also lowers costs [68]. Table 2.1 presents the allowed voltage characteristics, frequency variation range, and total harmonic distortion (THD) according to different countries and IEC and IEEE standards. adaptive control technique based on artificial neural networks and fuzzy logic is used in the inverter of each MG in a parallel DC IMG structure, and coupling VSC is proposed in [69] in order to improve the various power quality issues such as voltage unbalance, voltage sag/swell, frequency deviations, neutral current compensation, and THD.

Table 2.1: Standards for various power system characteristics [70].

Voltage							
Voltage sag			**Voltage swell**			**Voltage Unbalance**	
Country	**Limit**	**Time**	**Country**	**Limit**	**Time**	**Standard**	**Limit**
China, Denmark	20 %	0.625s, 0.5s	China, Japan, UK, Canada, and Romania	Not mandatory		IEEE	3%
Japan	20 %	1.0s	USA	120%	1.0s		
USA, Romania	15 %	0.6s	Denmark, Germany	120%	0.1s	IEC	2%
UK	15 %	0.14s	Spain	130%	0.25s		

THD						
	Voltage level	**Standards**	**Limit**		**Standards**	**Limit**
Voltage	(V >161) kV	IEC and IEEE 519	1.5%	Current	IEC 61000-3-2	5%
	(69 ≤ V ≤ 161) kV	IEC and IEEE 519	2.5%			
	(2.3 ≤ V ≤ 69) kV	IEC	5%			
	(1 ≤ V ≤ 69) kV	IEEE 519	5%		IEEE 1547	5%
	(V ≤ 1) kV	IEEE 519	8%			

2.5.4 Line and Interface Technologies

The nature of power transmission (AC or DC) and connections at electrical boundaries are determined by line and interface technology. Interfaces can be based on various devices, including tie-lines, power transformers, and converters. In the tie-line-based architecture, MGs involved in the network have same voltages and frequencies. Power transformers can be used for interconnecting only AC technologies of different voltages and not different phases and frequencies. In contrast, a combination of transformers and converters can be utilized in both AC and DC technologies with high levels of controllability in terms of frequency and voltage, effective power management, improved power quality, and flexibility [43, 44]. As demonstrated in Fig. 2.4, there are several forms of IMG infrastructure based on line and interface technologies.

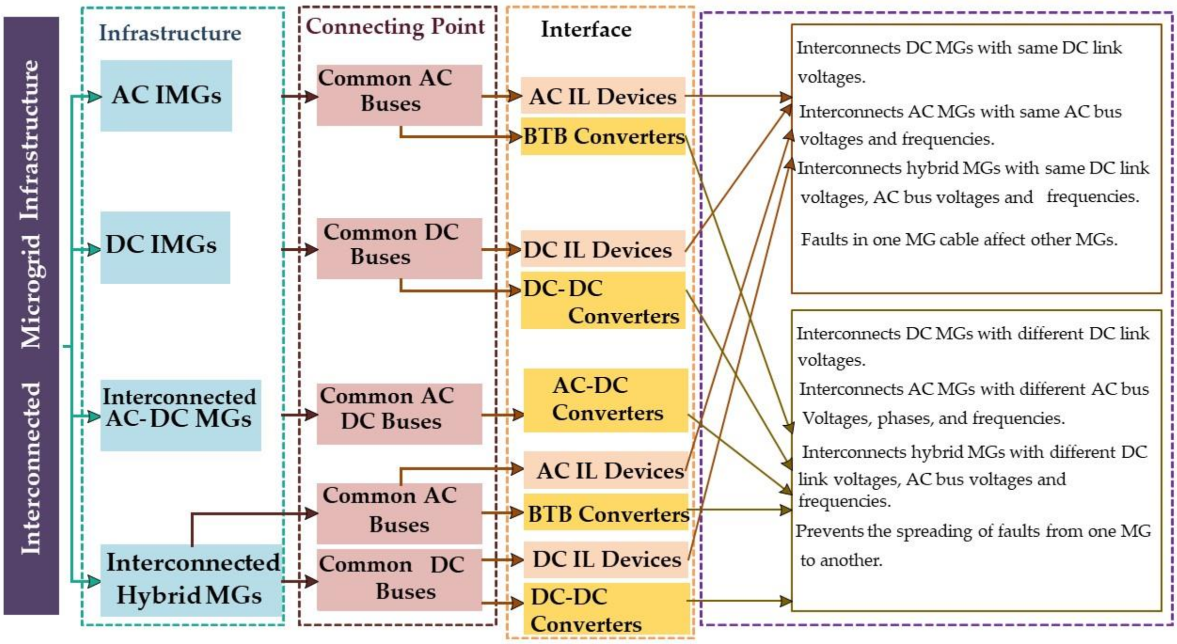

Fig. 2.4: An overview of the interconnected microgrid infrastructure based on line and interface technologies.

Interlinking devices in microgrids play a crucial role in enabling the connection and coordination of multiple microgrids within a larger power system. These devices facilitate the exchange of power, synchronization of voltage and frequency, and overall grid stability. Here are some common types of interlinking devices used in microgrids:

2.5.4.1 Static Switches

Static switches, also known as solid-state switches, are electronic devices that allow for the rapid and precise control of power flow between microgrids. These switches operate without mechanical parts, offering fast switching capabilities and enhanced reliability. Interconnecting static switch (ISS) is static electric device which designed to automatically transfer load for preferred power source to standby power source connected to its input in case of disruption in former and vice versa without any interruption of server room load. As name suggest it is fully static device without any electromechanically parts. Static Switch can transfer load within 1/4th of cycle time hence it ensures uninterrupted power to Datacentre load. Interconnecting static switch consists of antiparallel connected thyristor connected in each phase illustrated in Fig. 2.5 and Fig. 2.6. These thyristors are gate turn-off thyristor (GTO) which can turn on by gate signal and turn off by gate signal of negative polarity. By controlling switching on and off of these SCR, faster load transfer achieved. Total transfer time sum of time taken to detected disturbance in source and time taken to transfer load ion on other source.

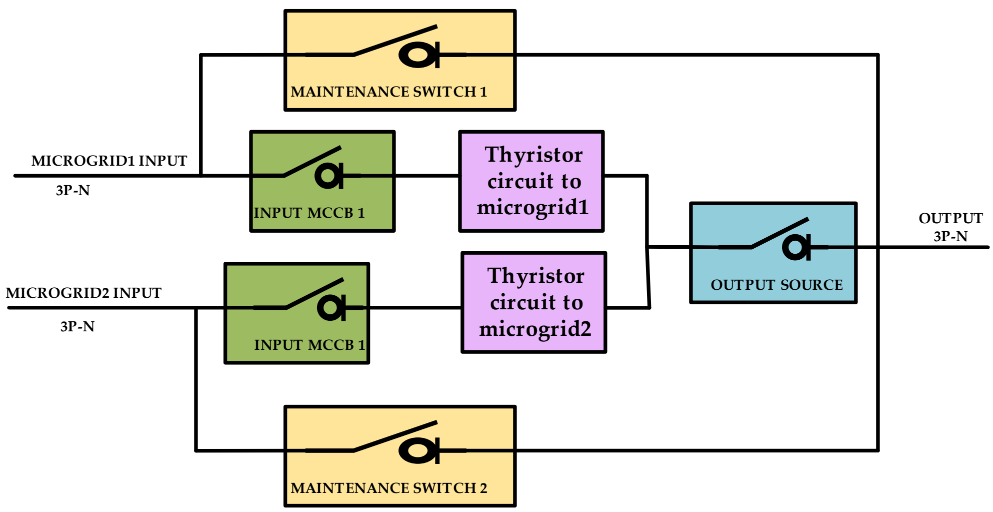

Fig. 2.5: Three-phase interconnecting static switch block diagram.

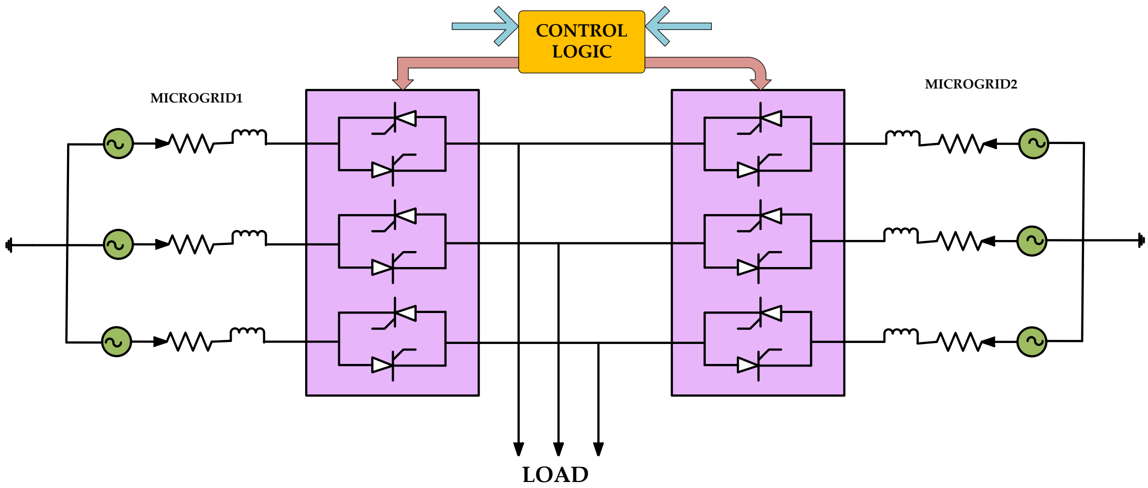

Fig. 2.6: Internal circuitry of an interconnecting static switch.

Interconnecting static switch-based interfaces, as shown in Fig. 2.7, are commonly used to interlink multiple AC MGs. Interconnecting static switches streamline connectivity between microgrids by eliminating multiple conversion stages, thereby reducing energy losses, increasing efficiency, and enhancing system performance [71]. These switches efficiently transport power between microgrids, minimizing energy loss and operational costs while enabling precise adjustment of voltage and frequency for reliable power transfer. Additionally, static switches facilitate bi-directional power flow, supporting load balancing, renewable energy sharing, and backup power supply, thereby improving system reliability. Their flexibility allows for easy addition or reconfiguration of microgrids, enhancing scalability and adaptability. By reducing grid congestion and stabilizing the grid, static switches contribute to improved grid reliability and facilitate integration of distributed energy resources. With rapid response times and high reliability requiring minimal maintenance, static switches ensure robust and resilient operation of interconnected microgrid systems.

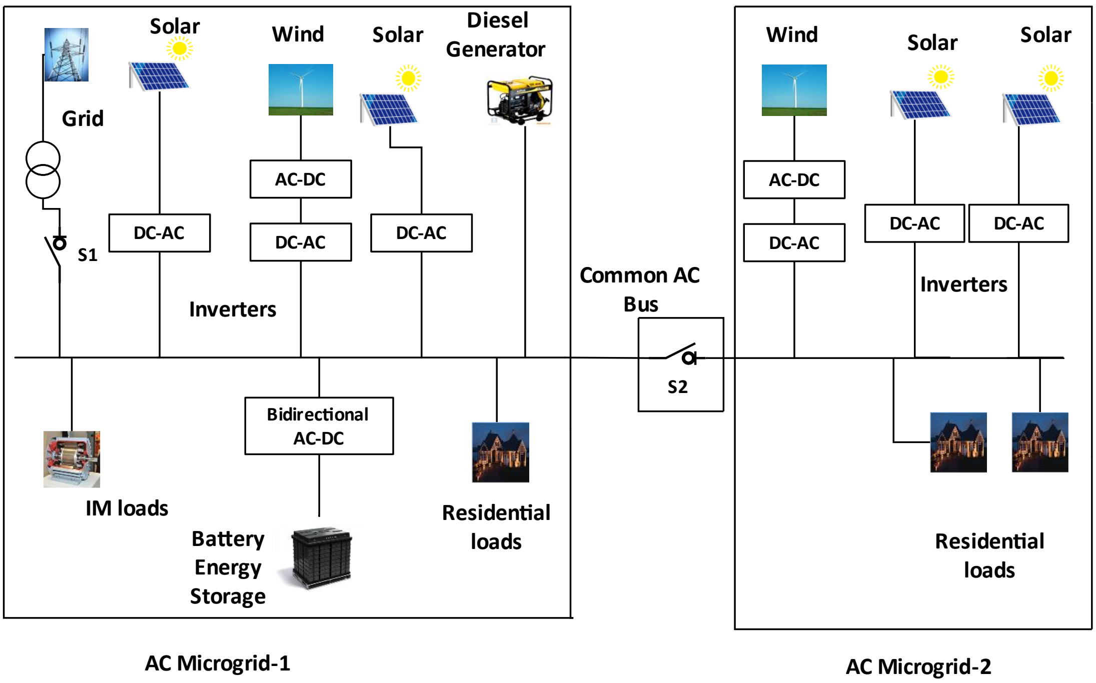

Fig. 2.7: Interconnection of AC MGs using AC interlinking device (circuit breaker or switch) and tie-line.

2.5.4.2 Synchronizers

Synchronizers are devices used to ensure that the voltage and frequency of interconnected microgrids are synchronized before connecting them. Synchronizers help prevent voltage and frequency mismatches, which can lead to instability or damage to the grid components.

2.5.4.3 Converters

Converters, such as inverters or rectifiers, are essential for converting DC power to AC power or vice versa, enabling compatibility between different microgrids with varying power sources and configurations.

2.5.4.4 Grid-Forming Inverters

Grid-forming inverters are specialized converters that can autonomously control the voltage and frequency of a microgrid, allowing it to operate independently or in coordination with other microgrids.

2.5.4.5 Interconnection Transformers

Interconnection transformers are used to match the voltage levels between interconnected microgrids, ensuring compatibility and efficient power transfer between systems operating at different voltage levels.

2.5.4.6 Microgrid Controllers

Microgrid controllers serve as the central intelligence of the microgrid system, coordinating the operation of various interlinking devices, optimizing power flow, and ensuring grid stability and reliability.

2.5.4.7 Communication Systems

Communication systems, such as supervisory control and data acquisition (SCADA) or distributed network protocol (DNP3), are essential for exchanging information and control commands between interconnected microgrids and the central control centre.

2.5.4.8 Protection Devices

Protection devices, including relays, circuit breakers, and surge arrestors, are critical for detecting and isolating faults within microgrids to prevent cascading failures and ensure system reliability.

These interlinking devices work together to establish a robust and resilient microgrid infrastructure, enabling efficient power sharing, fault tolerance, and grid stability in diverse operating conditions. The selection and integration of these devices depend on factors such as the size of the microgrid, the types of power sources, and the operational requirements of the system. Among them, the static switch holds paramount importance in modern power systems and microgrids due to its rapid switching capabilities, enhanced reliability, and efficient power control. Offering fast and precise control over power flow, static switches enable seamless response to dynamic changes in load demand, generation, and grid conditions. Their reliability, stemming from the absence of moving parts, ensures uninterrupted operation in critical applications. Moreover, static switches contribute to system efficiency by minimizing energy losses during operation. Their flexibility and scalability make them adaptable to diverse power system configurations, while their fault tolerance and grid resilience capabilities enhance system stability and reliability. Furthermore, static switches facilitate the integration of RESs, support voltage and frequency regulation, and enable grid interconnection and islanding operations, thus playing a crucial role in the advancement of sustainable and resilient microgrid systems.

2.5.5 Classification of Low-Frequency Oscillations in Conventional Power System

Low-frequency oscillations in power systems refer to oscillations of the electrical power system with frequencies ranging typically from 0.1 Hz to 2 Hz. These oscillations are a type of system-wide phenomenon that can affect large areas of the power grid [72]. Recent literature examines the damping of LFOs in power systems that incorporate ESS and renewables [52]. Power systems have relied on synchronous generators for nearly a century, but with renewable energy and system upgrades, power electronics-based generators may dominate. Battery energy storage systems in microgrids can help compensate for frequency fluctuations [53]. But the interconnection of two or more microgrids forms an interconnected microgrid system where the interactions between their controllers and load dynamics produce system oscillations that need to be considered for the best microgrid design because IMGs contain DGs that are fundamentally different from one another and have low inertia. These variations complicate the stability and functioning of interconnected microgrids. In addition, interconnected microgrids are large-scale power systems made up of multiple types of distributed generations, either converter-interfaced or synchronously interfaced, and load sources, each with their own unique structure and set of features. Systems in this configuration are extremely sensitive to frequency fluctuations caused by even small disruptions like load changes, dynamic load insertion, power sharing, structural changes in IMG systems, etc. According to [54], converter-interfaced microgrids are less reliable at low frequencies when induction motors are present. For conventional large, interconnected power systems, this phenomenon is known as electromechanical oscillations or LFOs; in IMG, oscillatory modes are defined in accordance with that outcome [55]. Table 2.2 outlines the frequency standards for different power systems, providing a comparative overview of the nominal operating frequencies and acceptable frequency ranges for various national and regional power grids. Depending on the frequency of the oscillations and the group of generators involved in the oscillations, conventional power system oscillations can be divided into two categories: local oscillations and inter-area oscillations [72].

2.5.5.1 Local Oscillations

In conventional power networks, synchronous generators are a key cause of oscillations. Local oscillations are the oscillations that occur when generators in a specific area oscillate against one other. Local oscillations often have frequencies in the 1-2 Hz range [72].

2.5.5.2 Inter-Area Oscillations

Inter-area oscillations are oscillations that occur when a group of generators in one region of a power system oscillate against another group of generators in another area. Inter-area oscillations typically have frequencies between 0.2-1 Hz [72].

2.5.6 Low-Frequency Oscillations in Interconnected Hybrid AC Microgrids

Low-frequency oscillations in microgrids are oscillatory phenomena that occur at frequencies typically ranging from 0.1 Hz to 2 Hz [73]. These oscillations are characterized by their relatively slow rate compared to high-frequency oscillations and can have significant impacts on the stability and performance of microgrid systems. These oscillations can be classified in four main categories [32, 61, 74, 75]:

2.5.6.1 Local Microgrid Oscillations (0.5 to 2 Hz)

Local microgrid oscillations are oscillations that occur within a single microgrid. These oscillations are typically confined to the boundaries of one microgrid and arise due to interactions between local generation sources, loads, and energy storage systems within that microgrid. It can happen due to local generator dynamics (e.g., synchronous and induction generators), load variations and disturbances, and control system interactions and tuning issues. The main characteristics of this type of oscillatory mode are confined to the components and devices within a single microgrid, potentially impacting the stability and performance of that microgrid. Examples include fluctuations resulting from the intermittent output of local RESs such as solar PV or wind turbines, as well as oscillations caused by local load changes or faults within the microgrid.

2.5.6.2 Inter-Microgrid Oscillations (0.1 Hz to 0.5 Hz)

Inter-microgrid oscillations arise when two or more interconnected microgrids engage in dynamic interactions during power exchanges. These oscillations are primarily driven by power flow interactions occurring across the interconnecting lines or tie points, leading to fluctuations in stability. Differences in control strategies and operational conditions between the interconnected microgrids further contribute to these oscillations, as each microgrid operates with its own parameters and protocols. Synchronization issues between the microgrids can exacerbate the situation, especially when power generation or demand varies significantly across the systems. These variations can create imbalances, resulting in oscillations that affect the overall performance and stability of the interconnected microgrids. To mitigate such issues, coordinated control strategies and improved synchronization techniques are necessary to ensure smooth power flow and system reliability. The main characteristics of this type of oscillatory mode are that it spans multiple microgrids, influencing the stability and power quality of the entire interconnected system. These oscillations typically occur at lower frequencies compared to local oscillations and can have a more widespread impact on system performance, as they involve the dynamic interactions across several microgrids rather than being confined to a single one. The lower frequency nature of these oscillations makes them more challenging to detect and control, which necessitates careful monitoring and coordinated management to maintain the overall stability and efficiency of the interconnected system. Examples of inter-microgrid oscillations include those caused by power transfer and load-sharing between microgrids during peak load conditions, where the dynamic exchange of power can lead to instability. Another example is the oscillations triggered by fluctuations in renewable energy generation, where variability in sources like solar or wind can cause imbalances between interconnected microgrids. Stability issues also arise when control systems and strategies between the microgrids are mismatched, leading to further disturbances in power flow and system reliability. These examples highlight the challenges in maintaining stable operations across interconnected microgrids, especially under varying load and generation conditions.

2.5.6.3 Local/Inter-Microgrid Oscillations (0.3 Hz to 1.5 Hz)

Local or inter-microgrid oscillations refer to disturbances that originate within a local microgrid but have the potential to propagate and impact interconnected microgrids, escalating from local disturbances to affect the broader network. These oscillations can be caused by local disturbances or faults that spread through interconnecting lines, or by the amplification of instabilities in local control systems, which then influence the interconnected network. Such oscillations typically start within a single microgrid but can extend to disrupt the stability of the entire system, necessitating coordinated control and mitigation strategies to prevent their escalation. Examples include a local generator fault or a sudden load change that causes oscillations spreading to neighbouring microgrids, or instabilities in local control systems resonating through interconnecting lines, affecting the performance of the overall network.

2.5.6.4 Intra-Microgrid Oscillations (0.2 Hz to 1 Hz)

Intra-microgrid oscillations are disturbances that occur within different segments or subsystems of a single microgrid, arising from interactions between various internal components. These oscillations can be caused by the interplay between different types of generation sources, such as renewable energy systems, conventional generators, and energy storage systems (ESS), as well as segment-specific disturbances, control system interactions, and load changes. Although confined within a single microgrid, these oscillations involve multiple subsystems and can significantly affect the overall stability and performance of the microgrid. Examples include oscillations between the renewable energy generation segment and the conventional generation segment within the microgrid, or fluctuations caused by interactions between different ESS and their control systems within the same microgrid.

The need for effective damping of such a wide range, almost two decades, of electromechanical oscillations motivated the concept of the MB-PSS. As its name reveals, the MB-PSS structure is based on multiple working bands. Three separate bands are used, respectively dedicated to the low-, intermediate-, and high-frequency modes of oscillations: the low band is typically associated with the power system global mode, the intermediate with the inter-area modes, and the high with the local modes. Each of the three bands is made of a differential bandpass filter, a gain, and a limiter. The outputs of the three bands are summed and passed through a final limiter producing the stabilizer output Vstab. This signal then modulates the set point of the generator voltage regulator so as to improve the damping of the electromechanical oscillations. To ensure robust damping, the MB-PSS should include a moderate phase advance at all frequencies of interest to compensate for the inherent lag between the field excitation and the electrical torque induced by the MB-PSS action [76]. This advanced controller is designed to target oscillations occurring at low, mid, and high frequencies, addressing a wider range of dynamic behaviours within the interconnected microgrid system. By incorporating multiple damping mechanisms tailored to different frequency ranges, the multi-band POD controller can effectively suppress oscillations across the entire frequency spectrum, thereby improving overall system stability and resilience.

Table 2.2: Frequency standards for various power systems [70].

Frequency							
Country	Nominal frequency	Frequency variation		Country	Nominal frequency	Frequency variation	
		Min.	Max.			Min.	Max.
China	50 Hz	49.5 Hz	50.2 Hz	Canada	60 Hz	59.4 Hz	60.6 Hz
UK	50 Hz	49.5 Hz	50.0 Hz	USA	60 Hz	58.5 Hz	61 Hz
Bangladesh	50 Hz	49.5 Hz	50.5Hz	West of Japan	60 Hz	58 Hz	61.8 Hz

2.5.7 Stability in Interconnected Power System

Power system stability is the ability of the power system to maintain balance under normal circumstances and to return equilibrium following disruptions [74]. Power system stability, particularly concerning low-frequency oscillations, is a critical consideration in both local hybrid AC microgrid and an interconnected hybrid AC microgrids systems. These oscillations can impact the reliable operation of these localized power distribution systems. In AC microgrids, which are small-scale localized power systems, low-frequency oscillations can occur due to variations in power generation and load demand. For example, if a sudden increase in load demand or a fluctuation in renewable energy generation (e.g., from solar panels or WTs) occurs, it can lead to low-frequency oscillations within the microgrid. To mitigate these oscillations, control strategies such as droop control, frequency regulation, power system stabilizers, and the use of energy storage systems are employed within the microgrid. These measures help maintain voltage and frequency stability [75]. AC interconnected microgrids involve the interconnection of multiple AC microgrids to enhance overall system reliability and efficiency. In such interconnected systems, low-frequency oscillations can propagate across microgrids. The coordination and control of multiple microgrids can be complex, and the presence of low-frequency oscillations in one microgrid can affect others. To address this, advanced control and communication systems are employed. These systems facilitate real-time monitoring and control of the interconnected microgrids, allowing operators to identify and dampen oscillations before they propagate [6]. Utilizing distributed control strategies, where controllers use local and neighboring information, can help in damping out low-frequency oscillations across an interconnected microgrid system. With the increased integration of inverter based DGs, there's a reduction in the system's natural inertia. Virtual inertia methods, provided by power electronics interfaces, can emulate the behavior of traditional synchronous generators, and improve frequency stability [43]. In both local hybrid AC microgrid and an interconnected hybrid AC microgrids, the key is to employ control mechanisms and monitoring systems that can detect and mitigate low-frequency oscillations to ensure stable and reliable power supply. These systems act as "stabilizers" for the microgrid networks, like how cruise control and steering adjustments in a vehicle help maintain a smooth and stable ride. The classification of power system stability is shown in Fig. 2.8. The key problem in sustaining the secure operation of an interconnected power system is its stability. Primarily, rotor-angle instability occurs during the transfer of power through a transmission line due to rotor-angle fluctuation between two generators caused by large perturbations at the load side. The fluctuations can be easily transferred to power, resulting in increased oscillations. Large fluctuations may lead to loss of synchronism between generators [24]. Therefore, it is essential to dampen power oscillations to make the system as efficient and stable as possible [22].

A stable operation of the IMG is difficult to achieve and maintain at all relevant operating points because of the extensive integration of MGs with various DGs, loads, interface technologies, control strategies, and both inter- and intra-system analysis. Although stability analysis of IMG follows a similar pattern to that of traditional power systems, the high penetration of RESs, higher unpredictability, higher feeder resistance to reactance (R/X) ratio, low system inertia, unbalanced three-phase loading, and constrained short-circuit capacity make stability analysis more challenging. Moreover, inter- and intra-MG oscillations and both AC and DC voltage stability have a great influence on the entire system's stability [52]. Thus, it is necessary to analyse various issues that lead to power system instability in order to mitigate those challenges. Stability analysis of a system involves five major steps, such as determining the physical reason for the instability, the disturbance's relative size, the physical elements engaged in the process, the duration of the instability, and the methodology used to evaluate or forecast the instability. The networked microgrid system's stability classification [77] is presented in Fig. 2.8. There are two primary categories of instability in the networked microgrid system: phenomena related to the components and control systems and phenomena related to the sharing and balancing of active and reactive power. Both types of instability can be short- or long-term phenomena; short-term stability problems last for a few seconds or less, but longer-term problems affect the system's long-term stability.

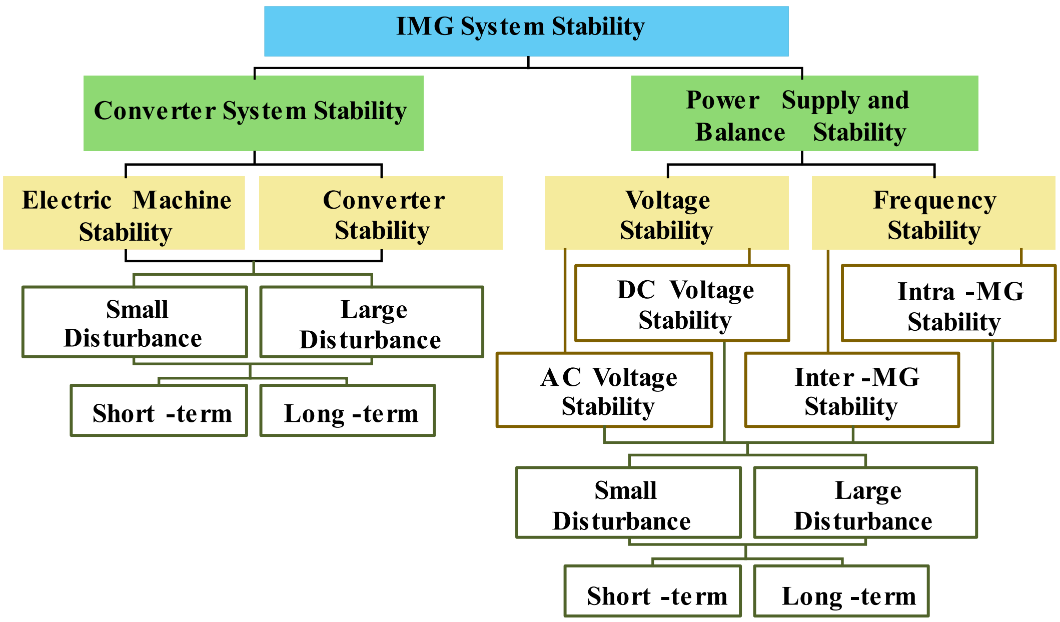

Fig. 2.8: Stability classification in the interconnected microgrid system.

The three main categories for discussing stability-related problems in an MG are voltage stability, transient stability, and small-signal stability. Sudden load changes, under-voltage load shedding, DG loss, MG faults, islanding, etc. are the causes of the numerous problems. The different difficulties are covered in depth below in Fig. 2.9.

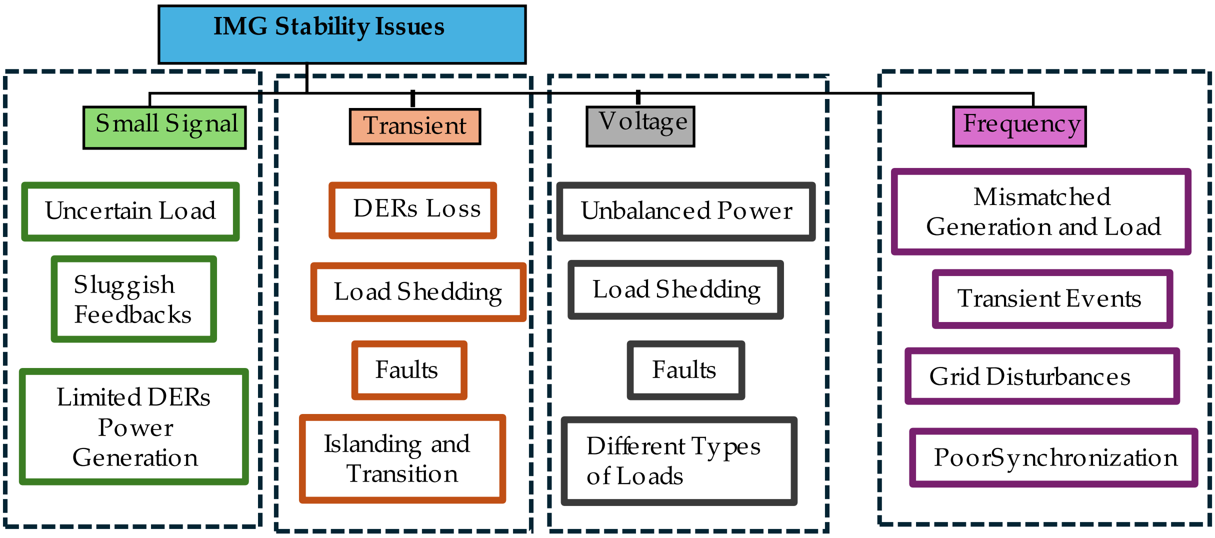

Fig. 2.9: Microgrid Stability Issues.

2.5.7.1 Small Signal Stability

It refers to the power system's ability to maintain synchronism in the face of minor, short-term interruptions. These oscillations occur at a highly frequent rate in the system due to the uncertain change in load and supply generation, i.e. small variations in power generation and load demand. Small signal stability can be caused by a variety of factors, including DG power limit constraints, slow feedback controllers, and unpredictable changes in load, particularly noncritical load, among others [78].

2.5.7.2 Transient Stability

It is described as a power system's ability to maintain synchronous operation in the face of significant transient disturbances. The most common reason for transient instability in the system includes MG islanding leading to fluctuation in various electrical parameters, loss in power generators in DGs leading to unbalanced power in the system, especially in the islanded mode of operation, a different type of electrical faults like line to ground or line to line faults, etc., addition or shedding of heavy loads in MG leading to instability, unbalanced real and reactive power [78, 79].

2.5.7.3 Voltage Stability

It can be characterized as MG's capacity, under the controller's guidance, to keep the voltages at their steady-state values during both normal and abnormal operating circumstances. These conditions include, but are not limited to, the system's actual and reactive power being out of balance, the presence of various load types (particularly inductive loads), significant load shedding during low voltage situations, etc. The whole tree topology of the several stability difficulties in the MG is shown in Fig. 2.9. It illustrates the several stability problems that the MG system is experiencing [78].

2.5.7.4 Frequency Stability

Frequency stability is a prime concern in a MG-based power system due to the high intermittent nature of RESs, low X/R ratios of MG cables, insufficient system response, and low system inertia. To improve an interconnected hybrid MG's frequency stability, an optimally resilient controller-based virtual inertia control is suggested in [80]. In [81], a specific structure-based controller is suggested to maintain the networked microgrid system's frequency stability. To maintain the frequency variation at a manageable level in the context of high load perturbations system uncertainties, and strong wind energy accessibility, an effective control approach is designed for a three-area power system [82].

2.6 CONTROL STRUCTURE OF INTERCONNECTED MICROGRIDS

The interconnected MG control system, a collection of software and hardware related to the power electronics converters and their controllers, is used to achieve the system's reliability, operational feasibility, optimal performance, and stability. Voltages and frequency regulations within specified ranges, proper power supply, sharing and balance, switching between different operating modes (on- and off-grid), and optimal demand-side management are the primary responsibilities of the IMG control system. Thus, to achieve optimal performance from the IMG system, research on the control system must be done in addition to developing reliable and effective control structures. In an IMG system, information sharing amongst MGs assists the control system in determining the best operating approach to ensure the system's reliable and effective performance. The networked MGs' assigned communication system is employed for information sharing amongst MGs. There are several control structures illustrated in Fig. 2.10 based on communication systems, such as hierarchical, distributed, decentralized, and centralized, for coordinating MGs in the IMG system.

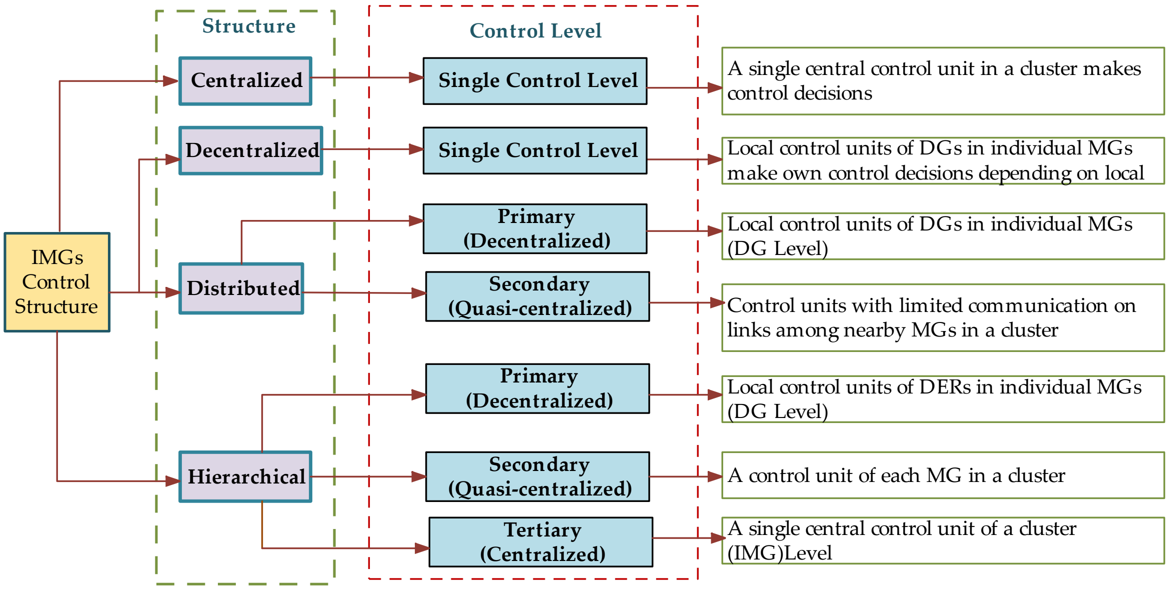

Fig. 2.10: Various control structure for IMGs system.

2.6.1 Hierarchical Control Structures

The hierarchical control structure, as illustrated in Fig. 2.11, facilitates the development of interconnected MG control at multiple control levels with different control responsibilities and targets by permitting controllers at various levels to communicate and exchange information or control signals. Therefore, in the hierarchical control of an interconnected MG, the operations of every MG in the interconnected microgrid are managed and synchronized through three separate control levels, as shown in Fig. 2.12. These layers are multiple local units from individual MGs in the first control level (primary), the central control unit of each MG in the second control level (secondary), and the central unit of the overall MG cluster system in the third control level (tertiary) [72]. A hierarchical control structure is proposed in [80] in order to accomplish control goals such precise power sharing, seamless transition and synchronization, recovery of frequency and voltage, and flexible regulation of power flow. Interconnected microgrid systems can adopt a hierarchical control structure consisting of primary, secondary, and tertiary control levels illustrated in Fig. 2.13 [83].

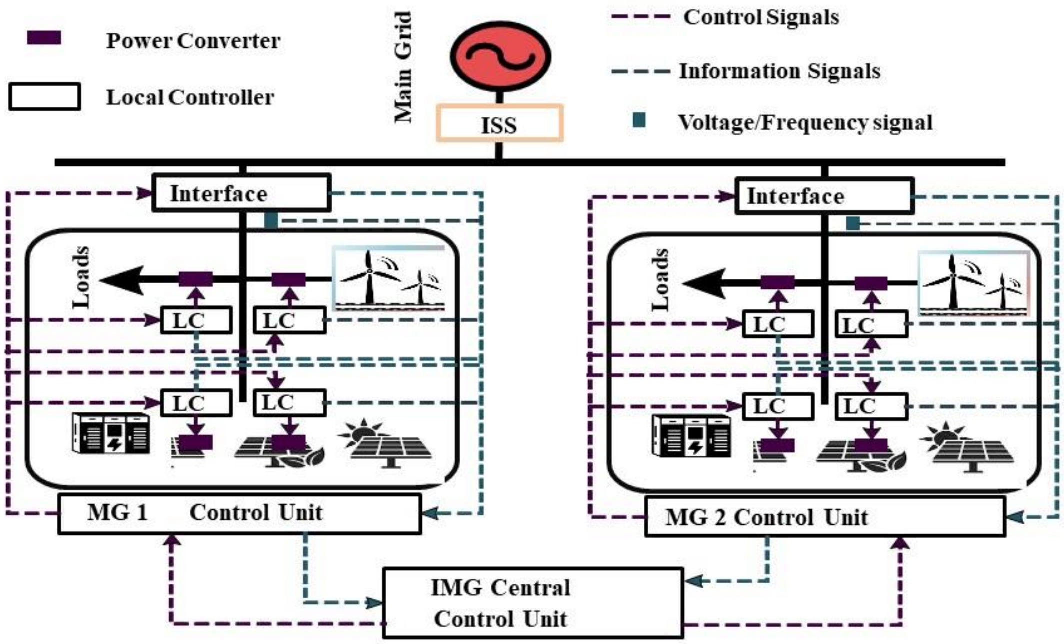

Fig. 2.11: Hierarchical Control Structure.

2.6.1.1 Primary Control:

It provides fast local responses to disturbances and operates in a decentralized manner. Droop control is a standard method employed at this level.

2.6.1.2 Secondary Control:

It restores the frequency and voltage magnitude to their nominal values after disturbances and corrects the deviations caused by the droop characteristics of primary control. This is typically a centralized or distributed control that acts on a slower timescale than primary control.

2.6.1.3 Tertiary Control:

It manages power exchanges with the main grid or between different microgrids, optimizing the overall system operation based on economic or other criteria.

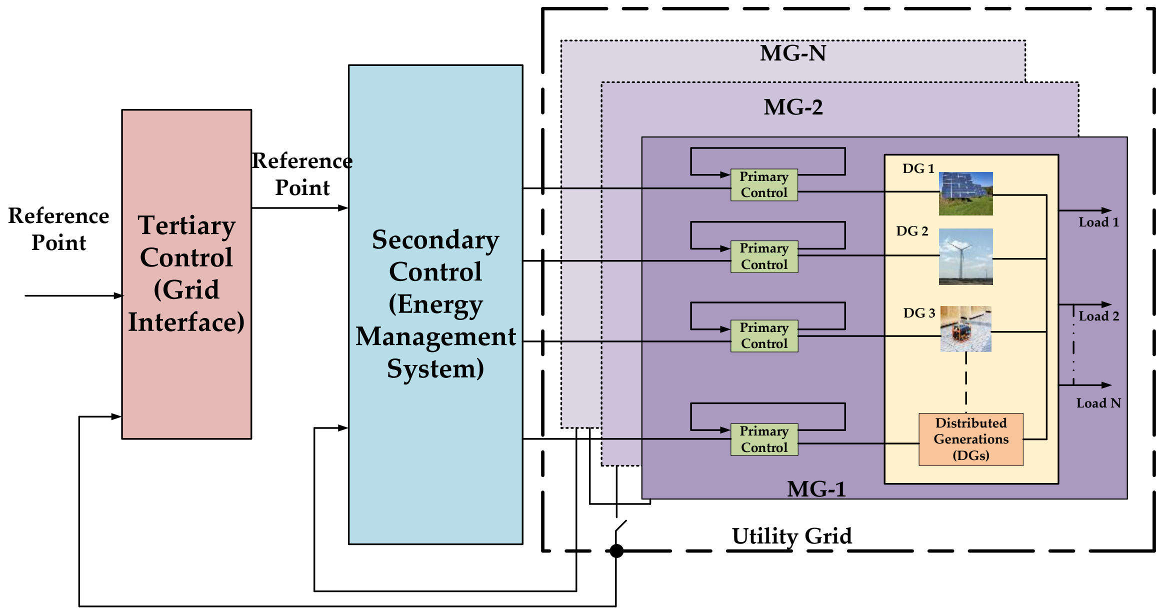

Fig. 2.12: A hierarchical control scheme for IMGs [83].

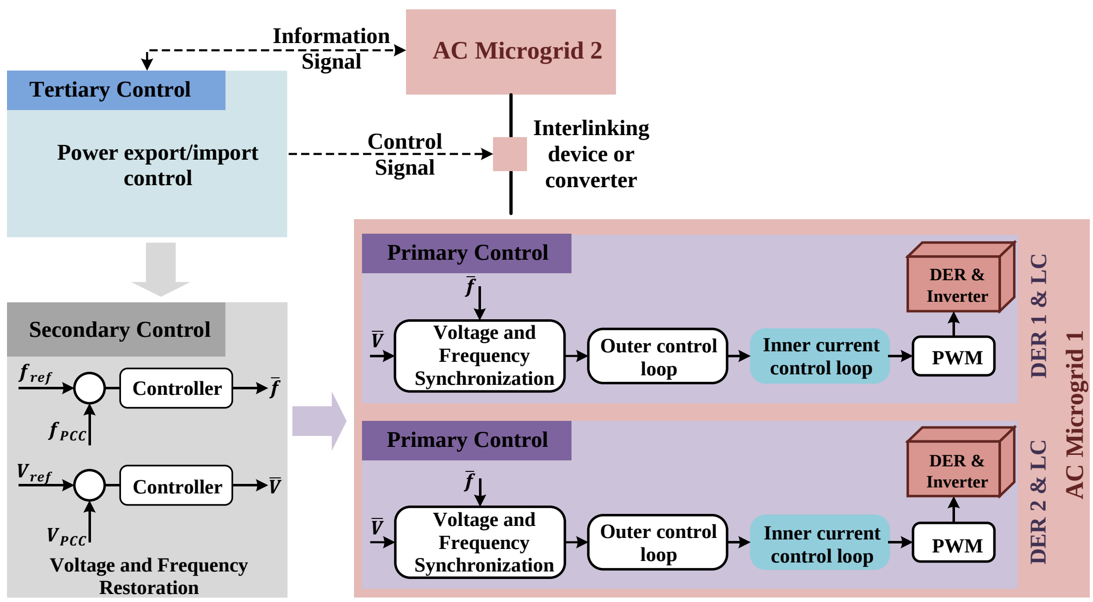

Fig. 2.13: Hierarchical control of AC IMG.

2.6.2 Centralized Control

In a centralized control structure (as shown in Fig. 2.14), a single central entity is responsible for collecting data from all of the MG's measurement units using a communication channel along with determining, verifying, and analysing the control operations of all MGs in the system in order to provide the necessary instructions for optimum management of DGs and loads [84]. Based on information collected from each MG's local unit, the central control unit manages and coordinates the operations of every MG that is a part of the MG cluster [85]. However, the entire cluster's operation, cost, and reliability are compromised by a single point of failure caused by the huge amounts of data handled and concentrated in a single area, higher bandwidth specifications, a lower expansion rate due to the centralized structure, reliance on a wide-band communication system, and restrictions on plug-and-play capabilities [86]. Furthermore, a two-way information exchange is necessary between the central control unit and each individual MG's local unit, as the central controller must receive data and provide signals to control all local units. In [87], a unique centralized/decentralized technique is proposed in which the reactive power in the AC IMG system is accurately shared before the communication link fault by using a centralized control technique that relies on the adaptive virtual impedance. In [88], a centralized control framework for managing and regulating power sharing in interconnected MGs is suggested.

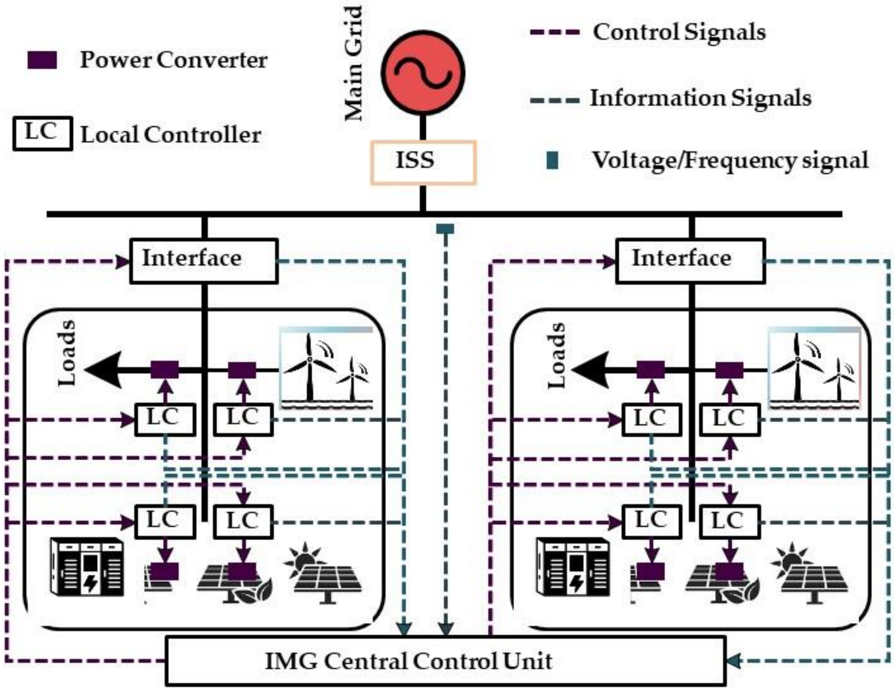

Fig. 2.14: Centralized control stricture.

2.6.3 Decentralized Control

In a decentralized control structure (as shown in Fig. 2.15), instead of a central controller, the local control units of each MG in a IMG is responsible for collecting local information, determining its own control activities, coordinating optimum operation without depending on information sharing with adjacent MGs, and making decisions based on information obtained from local specifications [86]. In decentralized control, a droop control approach is frequently employed so that each DG unit may independently regulate the voltage or frequency signal without assistance from the central controller. Because of the lack of communication links, this method is unable to ensure the cluster's suitable performance, and the increasing competition between individual MG units may compromise the cluster's overall effectiveness [84]. A decentralized self-optimizing power management strategy for interlinking converters in hybrid MG-based MG cluster is proposed in [89] reduce the overall voltage variation, expense, and geographical constraints. To improve the resilience and flexibility of interconnected MGs with mobile ESSs, a three-stage dynamic distributed control strategy based on rolling optimization is considered in [90].

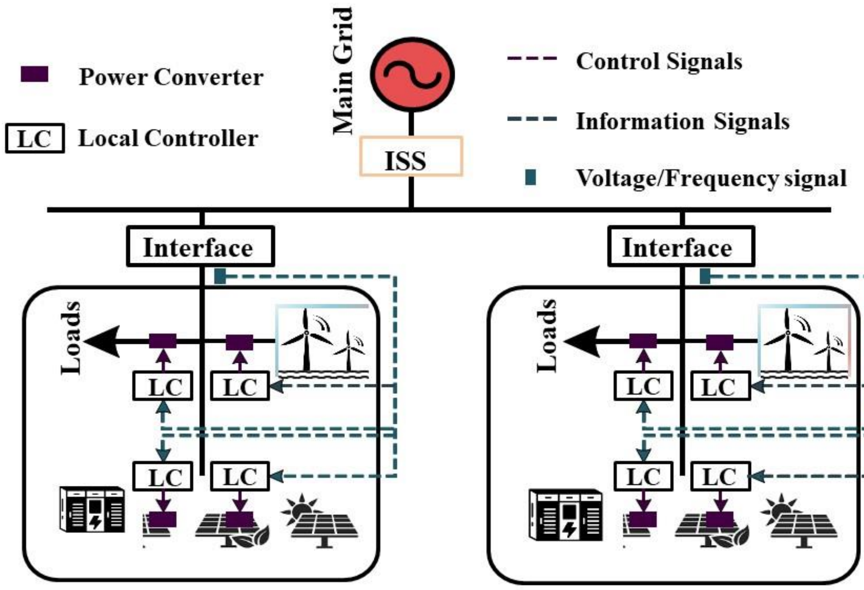

Fig. 2.15: Decentralized Control Structure.

2.6.4 Distributed Control

The distributed control structure, a two-level control structure, as shown in Fig. 2.16, is used in order to balance the advantages of centralized and decentralized controllers while coordinating the performance of local MG units. Each central unit or agent in control structure is responsible for collecting data from adjacent agents and from the local MG units to achieve optimum performance and power sharing across linked MGs [84]. Hence, the operation of each MG taking part in the MG network is managed and coordinated by several distributed central units, where each central unit consists of multiple local control units. For an AC IMG system operating in off-grid mode, a distributed control structure constructed with artificial neural networks is presented in [22] to achieve voltage harmonic suppression and frequency synchronization during load changes, controller startup and shutdown, and delays in communication. A distributed secondary control technique based on quantization inputs for DC IMG is developed in [91] to achieve voltage restoration, current sharing, and a reduction in communication burden.

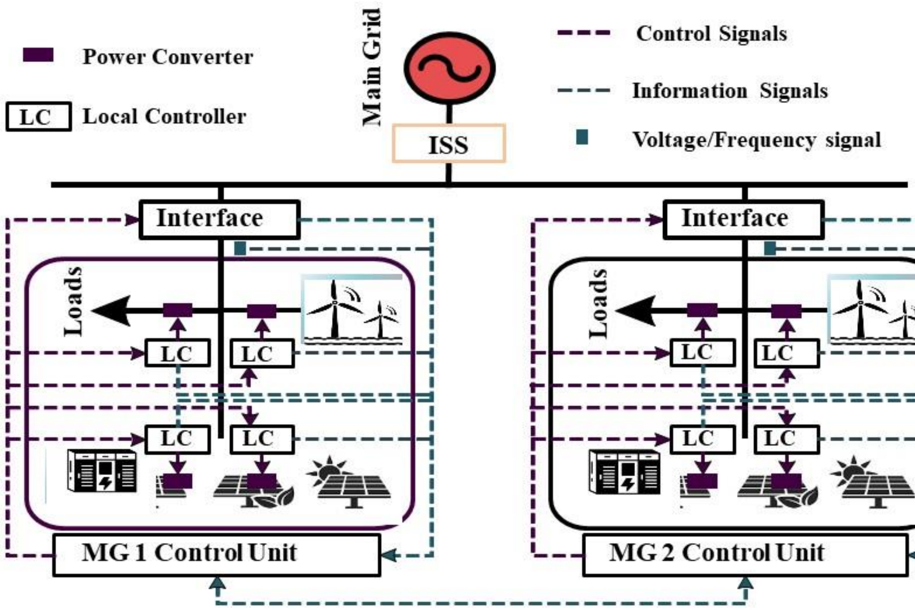

Fig. 2.16: Distributed control stricture.

Table 2.3 presents an overview of various literature based on four control structures along with their merits and demerits.

Table 2.3: An overview of the four control structures with advantages and disadvantages.

Control	Ref.	IMG type	Mode	Merits	Demerits
Centralized	[23]	DC IMG	IS	High precision; Flexibility in application; Reduced operation charge; High reliability in IS mode	Vulnerable to single-point failure; Lower Scalability, Higher bandwidth; Two-way communication; Computation burden
	[87]	AC IMG	GC/IS		
	[88]	DC IMG AC IMG	GC/IS		
Decentralized	[90]	AC IMG	GC/IS	Communication free; Higher expandability; Resiliency against failures in communication; Appropriate coordination of several autonomous units; Strong against single-point failures; High computation efficacy	Inadequate system efficiency due to the absence of communication; High operational cost; Low resiliency in IS mode; Costly point-to-point communication
	[89]	AC/DC IMG	IS		
	[92]	DC IMG	IS		
Distributed	[22]	AC IMG	IS	Restricted communication requirement; High scalability and flexibility; Offers cooperation among	Security concerns; Implementation complexity; Lower stability and speed; Communication lines among each nearby MGs
	[91]	DC IMG	IS		
	[93]	AC-DC IMG	IS		

				separate structures; Better reliability	
Hierarchical	[21]	DC IMG	GC/IS	Offers flexible control with multiple-system network; Cost effective; Easier to implement	Vulnerability to failure as a result of a strong connection between lower and higher control layers
	[94]	AC-DC IMG	GC/IS		
	[95]	AC IMG	GC/IS		

MG Microgrid IMG Interconnected Microgrid GC Grid-connected IS Islanded

2.7 POWER SYSTEM STABILIZERS

Power system stabilizers are crucial components in the dynamic stability control of electrical power systems. Their primary function is to enhance the damping of power system oscillations, which can be caused by various disturbances such as load changes, faults, and switching operations. Several factors driving power oscillations in electrical power systems are illustrated in Fig. 2.17. These oscillations, if not properly damped, can lead to system instability and even blackouts.

A PSS is typically added to the excitation system of a synchronous generator to provide damping torque in response to the speed variations of the machine. The device measures the generator's rotor speed or electrical power output and adjusts the excitation of the generator to apply the correct damping torque.

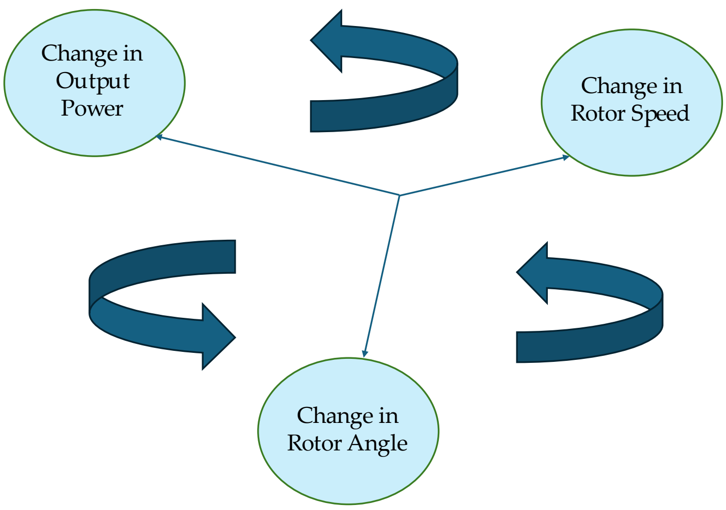

Fig. 2.17: Factors Driving Power Oscillations in Electrical Systems.

Power system stabilizer devices are responsible for providing a damping torque component to generators for reducing fluctuations in the system caused by small perturbations. It is a device added to the automatic voltage regulator of generators to enhance the damping of low-frequency oscillations in power systems. The typical PSSs, such as CPSS, PSS2B, and PSS3B, are designed with a single frequency band dedicated to transmitting the stabilizing signal. PSSs can be integrated into microgrid and interconnected microgrid environments to enhance system damping during low-frequency oscillations. They modulate the generator excitation to counteract the oscillatory motion [14].

2.7.1 Overview of Structures for Power System Stabilizers

Among the frequently utilized input signals to the PSS are shaft speed, electrical power, and terminal frequency. These signals have been used to create several PSS variants. The advantages and disadvantages of the various PSS structures are discussed in this section. An overview of PSSs' has been illustrated in Fig. 2.18.

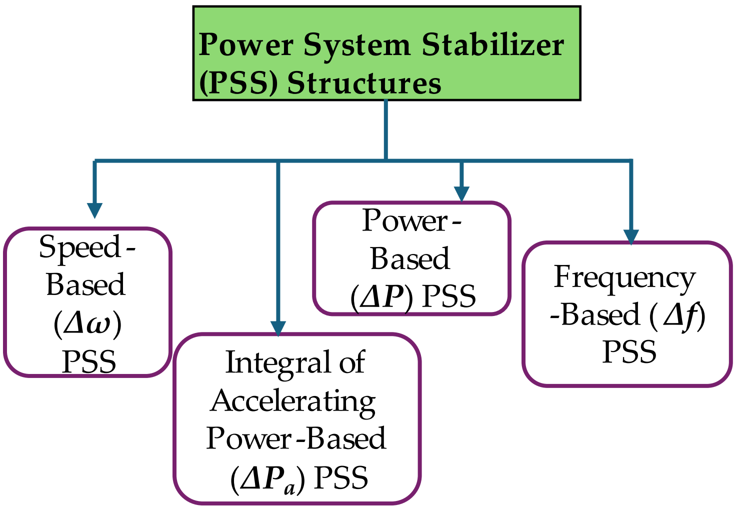

Fig. 2.18: An overview of Power System Stabilizer Structures.

2.7.1.1 Speed-Based ($\Delta\omega$) PSS

These stabilizers use shaft speed as a direct measurement. The speed signal measurement technique must incorporate run-out compensation to reduce noise from sources such as shaft run-out (lateral movement). Although many thermal units have employed stabilizers based on the direct measurement of shaft speed, this kind of stabilizer has a few drawbacks. The main drawback is that the stabilizing signal's torsional components must be attenuated using a torsional filter [96]. This filter places a maximum limit on the permitted stabilizer gain because it generates a phase lag at lower frequencies that destabilizes the "exciter mode". This is frequently overly restrictive and reduces the stabilizer's overall efficacy in the damping system.

2.7.1.2 Frequency-Based (Δf) PSS

In this case, the terminal voltage and current inputs are combined to provide a corrected frequency, or the terminal frequency signal is used directly. The frequency signal is more susceptible to oscillation modes involving broad areas than it is to modes involving single units, such as those within a power plant [97]. As a result, compared to using the speed input signal, larger damping contributions are obtained to these inter-area modes of oscillation. Torsional components are present in frequency signals that are monitored at the thermal unit terminals. Therefore, while using steam turbine units, torsional modes need to be filtered. The limits of frequency-based stabilizers are identical to those of speed-based systems in this regard. Changes in the configuration of the power system led to phase shifts in the ac voltage, which in turn induce huge frequency transients that constitute power system noise from heavy industrial loads like arc furnaces [98].

2.7.1.3 Power-Based (ΔP) PSS

Electrical power was thought to be an obvious choice for an input signal to early stabilizers because of how easy it was to measure and how it related to shaft speed. The rotor's equation of motion can be expressed as equation 2.1:

$$\frac{d}{dt}\Delta\widetilde{\omega_g} = \frac{1}{2H}\left(\Delta P_m - \Delta P_e\right) \tag{2.1}$$

Where,

H = Inertia constant,

ΔP_m = Change in mechanical power input;

ΔP_e = Change in electrical power input; and

$\Delta\widetilde{\omega_g}$ = Speed deviation.

This equation suggests that a signal proportional to shaft acceleration—that is, a signal that leads speed changes by 90°—can be obtained from a scaled electrical power measurement if mechanical power variations are disregarded. This idea served as the foundation for other early stabilizer designs [99]. The stabilizing signal obtained in this way might offer pure damping torque at precisely one electromechanical frequency when combined with both high-pass and low-pass filtering. There are two primary problems with this design. Firstly, because it can't be configured to offer a pure damping contribution at multiple frequencies, a compromise is needed for units impacted by both local and inter-area modes [100]. The second drawback is that each time there is a change in mechanical power, an undesirable stabilizer output is generated. The gain and output limits that can be used with these units are severely restricted as a result. Unless stabilizer gain is severely restricted, even moderate loading and unloading rates result in significant fluctuations in reactive power and terminal voltage. Though they are being quickly replaced by units based on the integral-of-accelerating power architecture, many power-based stabilizers are still in use.

2.7.1.4 Integral of Accelerating Power-Based (ΔPa) PSS

Stabilizers that gauge the generator's accelerating power were developed in response to the shortcomings of earlier stabilizer designs. Owing to the intricate structure and requirement for customization at every site, an indirect technique of determining the accelerating power was devised. We may demonstrate the working of this stabilizer shown in equation 2.2 by rewriting equation 2.1 in terms of the integral of power.

$$\Delta\widetilde{\omega_g} = \frac{1}{2H}\int(\Delta P_m - \Delta P_e)\partial t \qquad 2.2$$

The integral of mechanical power is related to shaft speed and electrical power. By adding signals proportional to shaft-speed change and integral of electrical power change, this stabilizer uses the relationship to replicate a signal corresponding to the integral of mechanical power change. This signal will have torsional oscillations on horizontal shaft units unless a filter is applied [101]. The derived integral of the mechanical power signal can be conditioned with a low pass filter to reduce torsional frequencies because changes in mechanical power are generally slow. Given shaft speed and electrical power measurements, the overall transfer function for calculating the integral of the accelerating power signal is as follows in equation 2.3:

$$\int\frac{\Delta P_a}{2H}\partial t \longrightarrow \frac{\Delta P_e}{2H} + G(s)\left[\frac{\Delta P_e(s)}{2H} + \Delta\widetilde{\omega_s}\right] \qquad 2.3$$

Where, G(s) is the transfer function of low-pass filter.

The primary benefit of this stabilizer is that it eliminates the requirement for a torsional filter in the signal's primary stabilizing path. As a result, the exciter mode stability issue is resolved, allowing for a larger stabilizer gain and improved system oscillation damping. This construction can be utilized with a corrected frequency signal or a traditional end-of-shaft speed measurement.

2.7.2 Classification of Power System Stabilizers

There are several types of power system stabilizers illustrated in the next section.

2.7.2.1 Conventional Power System Stabilizer

CPSS play a crucial role in enhancing the stability and performance of microgrids, which are decentralized energy systems comprising DGs like RESs, energy storage systems, and loads. PSS are designed to mitigate power oscillations and improve the dynamic response of microgrid systems by adjusting the excitation control of synchronous generators. By modulating the generator's excitation system, PSS can dampen low-frequency oscillations, enhance system stability, and maintain voltage and frequency within acceptable limits during transient disturbances. While conventional PSS have been primarily developed and deployed in large, interconnected power systems, their adaptation and integration into microgrids pose unique challenges due to the dynamic nature and varying operating conditions of these systems. Nevertheless, research and development efforts continue to focus on optimizing and customizing conventional PSS for microgrid applications to ensure reliable and resilient operation in diverse grid scenarios.

In a synchronous machine, to damp the oscillations of the rotor, by controlling its excitation, CPSS blocks can be used. The low frequency oscillations must be adequately damped in order to keep up the system stable. A simple structure of conventional PSS is shown in Fig. 2.19. The V_{stab} signal i.e. the output of the CPSS can be used as an extra input for the excitation system. In a PSS, mechanical speed deviation can be used as one of the inputs. The acceleration power (i.e P_m -P_e) where Pm is the mechanical power and Pe is the electrical power), can also be used as an input for PSS [102]. The model comprises of an output limiter, a LP filter, a gain, a washout HP filter, and a phase compensation system framework.

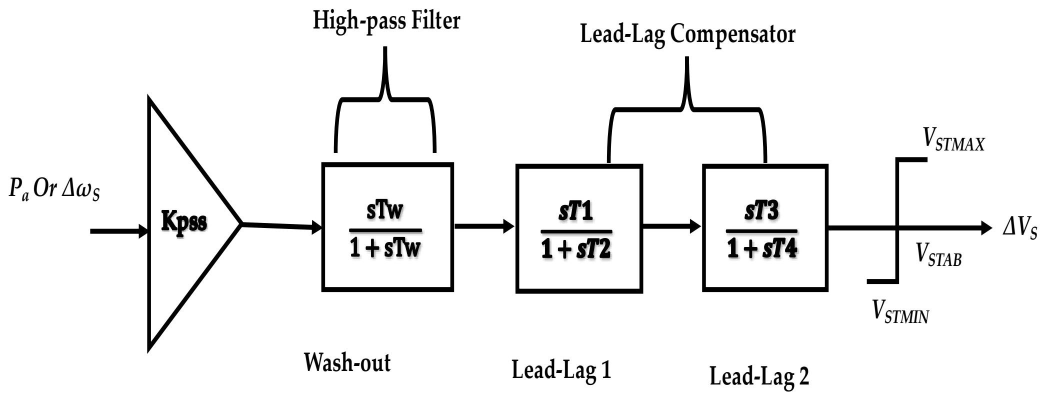

Fig. 2.19: Conventional power system stabilizer.

Table 2.4 presents the key parameters of the PSS utilized for assessing the performance of the CPSS, detailing the specific settings and characteristics essential for accurate verification and analysis.

Table 2.4: Parameters of the PSS for verifying the performance of the CPSS [103]

Parameter	Range of value
K_{pss}	1-50
T_W	10
T_1 - T_4	0.01-1.5
V_{STMAX}	0.1
V_{STMIN}	-0.1

The transfer function of the PSS of the ith machine is as follows in equation 2.4 [104]:

$$\Delta V_s = K_{pss} \frac{sTw}{1+sTw} \frac{sT1}{1+sT2} \frac{sT3}{1+sT4} \Delta\omega_s \qquad 2.4$$

In this structure, a high-pass filter is used so that its time constant is adjusted in the range of 0.5 to 20 s and T_W is 10 s [104]. The adjustable parameters of PSS are K_i, and time constant T_{1i}–T_{4i}. The lead-lag block in the above structure provides a sufficient phase to compensate for the phase difference between the excitation input and the electric torque. This power system stabilizer can be implemented in both SBDGs and IBDGs. The current challenge in power system stability lies in the inability of CPSS to effectively mitigate both inter-area and intra-area oscillations concurrently due to limited system observability. While other PSSs exhibit effectiveness in dampening power oscillations, other variants are particularly adept at addressing low frequency oscillations. Integrating various types of PSS offers a promising approach to enhancing power system stability by targeting a broader spectrum of oscillation frequencies.

2.7.2.2 PSS-2A

Dual input power system stabilizer 2A (PSS-2A) is a crucial component in modern power systems designed to enhance stability and mitigate oscillations. It functions by adjusting the excitation system of synchronous generators, thereby influencing the generator's electrical output. Specifically, the PSS-2A monitors system conditions and injects a supplementary stabilizing signal into the excitation system to counteract deviations from stable operation. One of the key features of the PSS-2A is its ability to dampen power oscillations effectively, thereby improving the overall stability of the power system. By sensing variations in system frequency and voltage, the PSS-2A can rapidly respond to disturbances and restore equilibrium, ensuring smooth and reliable power transmission. Moreover, the PSS-2A is equipped with advanced control algorithms that enable it to adapt to changing system conditions and optimize its performance accordingly. This adaptive capability ensures robust stabilization across a wide range of operating scenarios, enhancing the resilience of the power grid against disturbances and contingencies. A PSS-2A model serves as the PSS model for the NES-6100 excitation. Fig. 2.20 displays the block diagram for the PSS model of the excitation system. Measurement, isolation, lead/lag correction, proportional amplification, and amplitude limiting units are all part of the PSS adjustment channel. The generator power is represented by Ω, the speed signal is $T_{w1}\backslash T_{w2}\backslash T_{w3}\backslash T_{w4}$ time, the lead/lag link time constant is $T_1\backslash T_2\backslash T_3\backslash T_4$, and gain is K_{s1} [105].

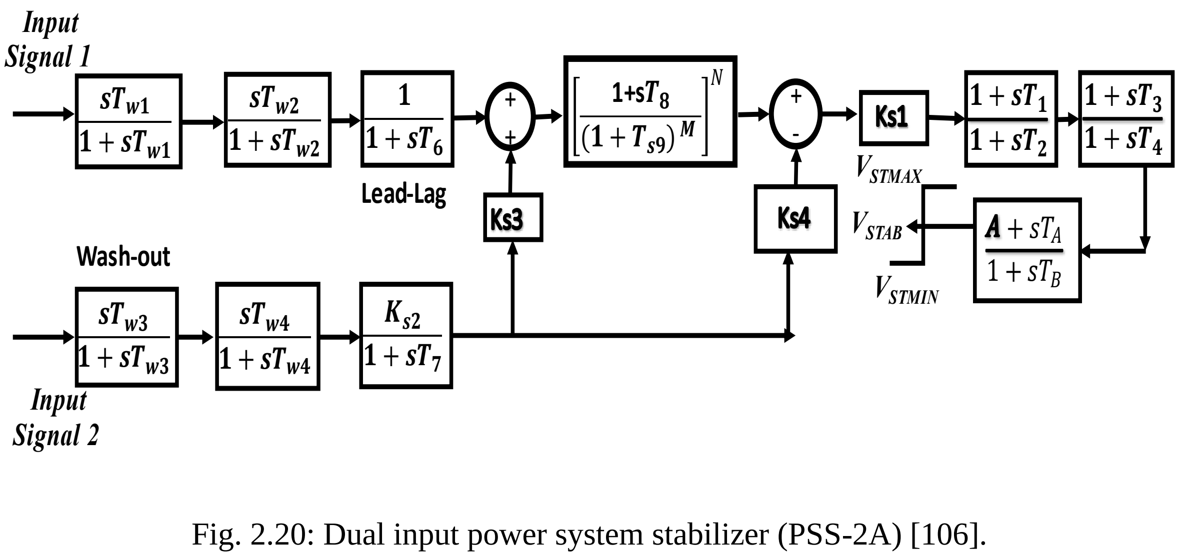

Fig. 2.20: Dual input power system stabilizer (PSS-2A) [106].

Table 2.5: Parameters of PSS-2A [106].

Parameter	Range of Value
$T_{w1}, T_{w2}, T_{w3}, T_{w4}$	1.5-15
$T_2,\ T_4$	0.02-6
$T_1,\ T_3, T_9$	0.02-2
T_6, T_7	>0.02
M	5
N	1
V_{STMAX}, -V_{STMIN}	0.05
K_{s4}	1
K_{s1}, K_{s2}, K_{s3}	10

Table 2.5 presents the key parameters of the PSS-2A power system stabilizer, detailing the specific settings essential for enhancing system stability and damping power system oscillations. The analysis is required to reveal that the choice of parameters and controller performance significantly influence power sharing in AC-microgrids, ensuring continuous power balancing and maximum utilization from RESs generation [46]. Ensuring stability and damping out low-frequency oscillations are crucial for the reliable operation of the interconnected hybrid AC microgrid systems, especially as these systems become more complex and incorporate a diverse set of generation and load characteristics.

2.7.2.3 PSS-2B

A dual input power system stabilizer (PSS-2B) is a control device used in electrical power systems to enhance stability and damping of electromechanical oscillations. It is typically employed in synchronous generators to counteract the effects of disturbances and maintain system stability during transient conditions. The PSS-2B operates by modulating the excitation system of the synchronous generator in response to changes in system frequency and voltage. By adjusting the field excitation, the PSS-2B can influence the generator's electrical output and help dampen undesirable oscillations that can occur in the power system. One of the key features of the PSS-2B is its ability to provide supplementary stabilizing signals to the excitation system based on system frequency and voltage deviations. These signals are designed to reinforce the generator's response to disturbances, thereby improving the overall stability of the power system. The design and tuning of a PSS-2B are critical aspects of its effectiveness. Engineers utilize advanced control algorithms and system modelling techniques to optimize the performance of the stabilizer and ensure compatibility with the specific characteristics of the power system.

Fig. 2.21 displays the IEEE models for the PSS-2B, which is one of the PSS families. The external inputs (speed and electrical power) are the same for both PSS-2A and PSS-2B. Unlike PSS4B, PSS2B just has one speed transducer. By low-pass filtering the rotor speed's raw estimate, or internal frequency, the first method produces a primarily low-frequency component ω_{L-I} [107], whereas the second method derives a predominantly high-frequency component ω_H from Pe. The PSS2B's 3-dB low-frequency cut-off is located at 0.025 Hz, as indicated by their frequency responses. In contrast, the PSS4B's speed transducer's 3-dB cut-off frequency is set at 0.25 Hz. Optional notch filters are available in PSS2B transducers. These filters are sometimes necessary for big nuclear units that have low-frequency torsional modes (less than 15 Hz). A few key basics of PSS-2B in the sector of the compensator transfer function are also shown in Fig. 2.21. In the PSS2B, three traditional lead-lag blocks are used in a single cascade to supply the phase lead at all frequencies of interest [108]. Table 2.5 presents the key parameters of the PSS-2B power system stabilizer, detailing the specific settings essential for enhancing system stability and damping power system oscillations.

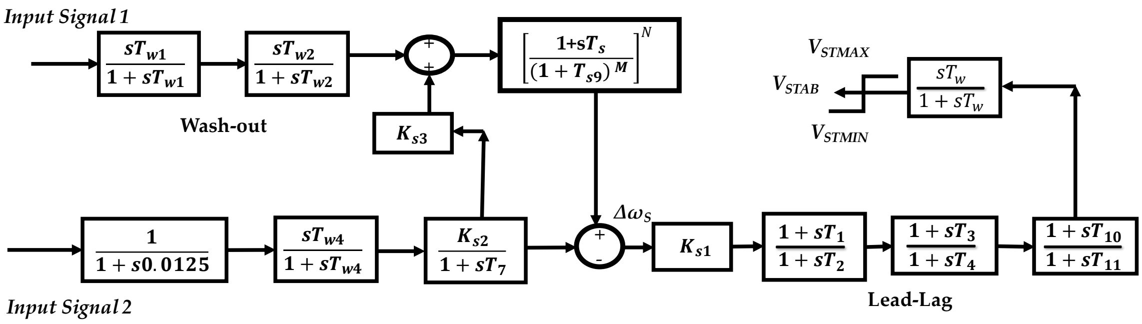

Fig. 2.21: Dual input power system stabilizer (PSS-2B) [108].

Table 2.6: Parameters of PSS-2B [103].

Parameter	Range of Value
K_{s1}	1-50
T_1, T_2, T_3	0.01-1.5
T_4	0.001-1.5
T_{10},T_{11}	0-1
T_{w1}, T_{w2}, T_{w3}	10
V_{STMAX}, $-V_{STMIN}$	0.1
T_7	2H (H=Inertia constant of generator and turbine)
M	5
N	1
T_8	0.5
T_9	0.1
K_{s2},K_{s3}	1

2.7.2.4 Multi-Band Power System Stabilizer (PSS-4B)

When integrating this concept into an interconnected microgrid system, there are also several key benefits such as improved stability, flexibility in addressing various oscillations, improved grid resilience, enhanced integration of renewable resources, support for decentralized operation, and so on. Interconnected microgrid systems have numerous sources and loads, each with its dynamics. Interactions between these components can lead to a variety of oscillation modes. A multi-band PSS can damp multiple oscillation modes simultaneously, ensuring the overall system remains stable [47]. Unlike a single-band PSS that targets a specific frequency, the multi-band PSS can tackle multiple oscillation frequencies. This is especially beneficial in an interconnected microgrid system, where there might be various oscillatory behaviours due to the diversity of sources (like solar, wind, diesel generators) and loads [48]. A multi-band PSS can also help in damping out these oscillations, allowing for higher penetration of renewables without compromising on system stability. Interconnected microgrids are often designed to enhance resilience against disturbances. If one microgrid faces an issue, the others can compensate. A multi-band PSS illustrated in Fig. 2.22(a) supports this resilience by preventing and damping oscillations that could destabilize individual microgrids or their interconnections [49].

As it is stated earlier that interconnected microgrid systems can operate in both grid-connected and islanded modes. Different operational modes might have different oscillation characteristics. A multi-band PSS can adapt to these changing conditions, ensuring stability in both scenarios. With improved stability, each microgrid can be operated closer to its optimal point, ensuring efficient utilization of resources. Instead of implementing multiple single-band PSS devices or other damping controllers to handle various oscillation frequencies, a single multi-band PSS can often suffice, leading to cost savings and reduced complexity. In scenarios where rapid load changes or disturbances occur, a multi-band PSS can help in maintaining transient stability by damping out any resultant oscillations [50].

Hence, a power spectral subtraction method that can effectively handle individual frequency components is deemed more appropriate. The introduction of MB-PSS as a novel dual input stabilizer model was documented in IEEE Std.421.5 [51]. This multi-band low frequency oscillation damper employs three pass filters, namely low, medium, and high pass filters, to effectively mitigate a broad spectrum of oscillations characterized by varying frequencies. This approach aims to enhance the damping performance of all global, intermediate, and local modes within the power system. The Fig. 2.22(b) depicts the input transducers model of the PSS-4B, illustrating the mechanism through which the stabilizer processes input signals and Fig. 2.22(c) provides a graphical representation of the PSS-4B, showcasing its operational characteristics and performance curves.

Recent research has demonstrated that the MB-PSS, an innovative advanced stabilizer, outperforms other PSS varieties in its ability to accommodate all global, inter-area, and local modes. Various varieties of PSSs are primarily developed using a linear model that is centred on a single operating point of the system. The conventional power system stabilizer is typically formulated with a single input, which may correspond to variations in either speed or active power. Previous studies have demonstrated that the use of additional input signals to the PSS can enhance its damping capability [52]. Power system oscillations can consist of sub-signals of varying frequencies, including low, moderate, and high frequencies. So, a multi-band PSS in an interconnected microgrid environment offers a comprehensive solution to the challenges posed by diverse sources, loads, and interconnections. It ensures that the system remains stable and resilient, facilitating the integration of more renewable resources and ensuring optimal performance. Each limb of the MB-PSS can be viewed as a conventional power system stabilizer illustrated in Fig. 2.23, focusing on specific frequency ranges to enhance damping and improve overall system stability.

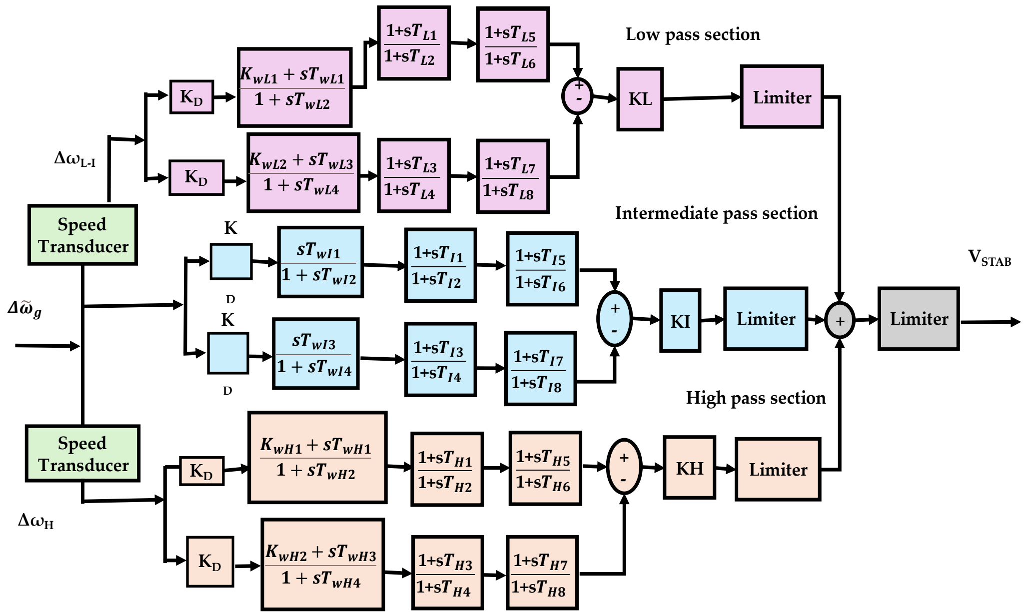

(a)

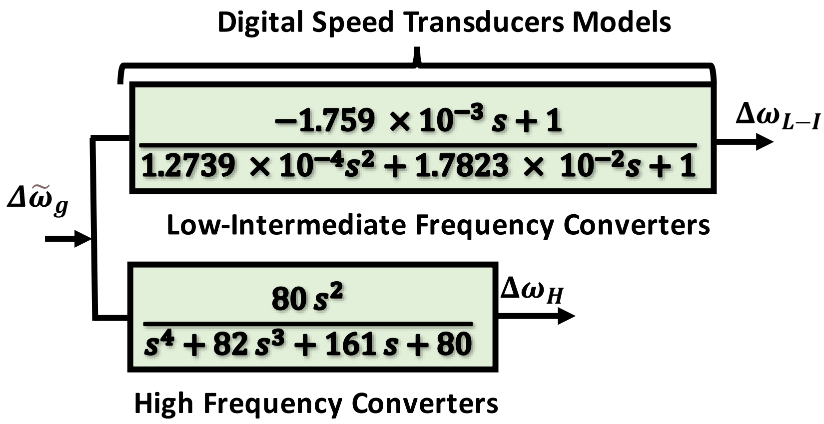

(b)

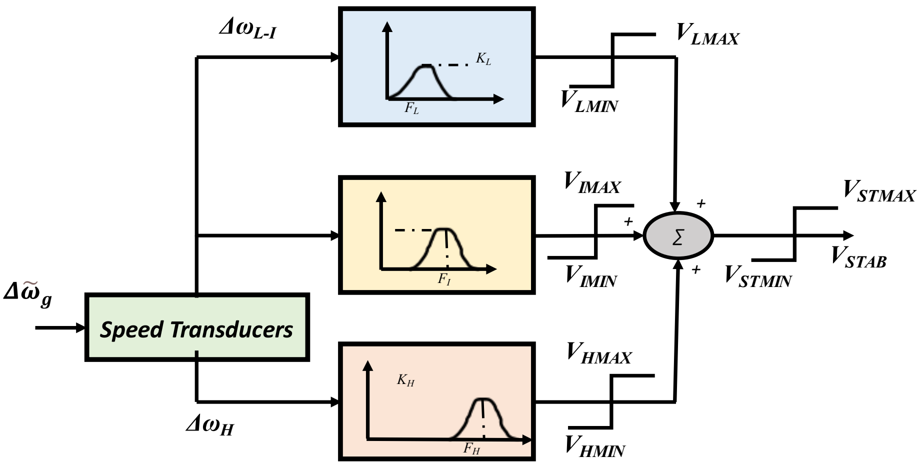

(c)

Fig. 2.22: (a) Block diagram of multi-band power system stabilizer, (b) Input transducers model: PSS-4B, and (c) Graphical representation of PSS-4B.

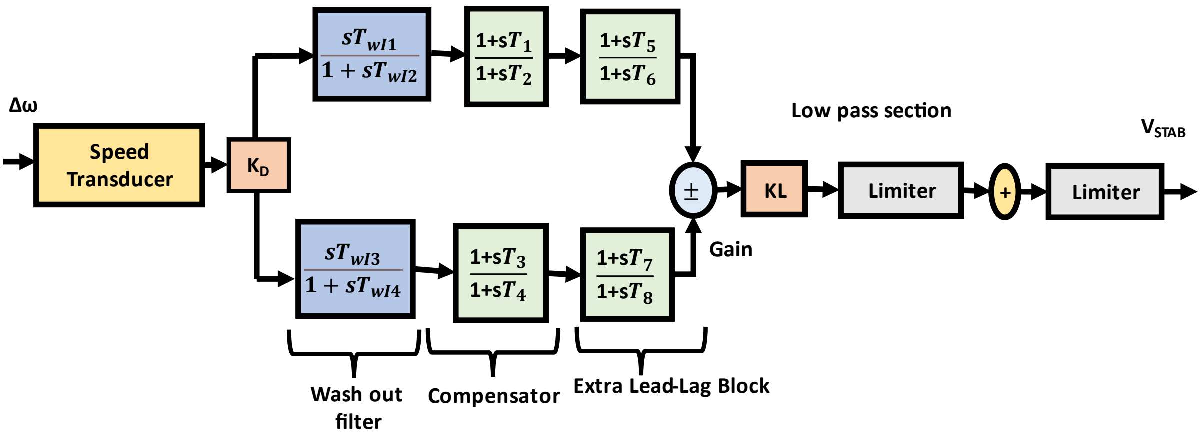

Fig. 2.23: Each limb of MB-PSS viewed as a conventional PSS.

Table 2.7 presents the key parameters of the MB-PSS, outlining essential characteristics and specifications relevant to the study.

Table 2.7: Parameters of MB-PSS [108].

Frequency bands					
Low Frequency (LF)		Intermediate Frequency (IF)		High Frequency (HF)	
T_{L1}	0	T_{I1}	0.25	T_{H1}	0
T_{L2}	0	T_{I2}	0.3	T_{H2}	0
T_{L3}	0	T_{I3}	0.3	T_{H3}	0
T_{L4}	0	T_{I4}	0.36	T_{H4}	0
T_{L5}	0	T_{I5}	0	T_{H5}	0
T_{L6}	0	T_{I6}	0	T_{H6}	0
T_{L7}	0	T_{I7}	0	T_{H7}	0
T_{L8}	0	T_{I8}	0	T_{H8}	0
T_{wL1}	1.667	T_{wI1}	10	T_{wH1}	0.01
T_{wL2}	2	T_{wI2}	10	T_{wH2}	0.012
T_{wL3}	2	T_{wI3}	10	T_{wH3}	0.012
T_{wL4}	2.4	T_{wI4}	10	T_{wH4}	0.014
K_D	100	K_D	140	K_D	140
K_{wL1}	1	K_{wI1}	0	K_{wH1}	1
K_{wL2}	1	K_{wI2}	0	K_{wH2}	1
K_D	100	K_D	140	K_D	140
KL	9.4	KI	47.6	KH	233
VL_{max}	0.075	VI_{max}	0.15	VH_{max}	0.15
VS_{max} = 0.15					

2.7.3 Placement of PSS in Microgrids:

Placement of power system stabilizers in microgrids is a critical aspect to ensure stability and reliable operation of the power system. Microgrids, which are small-scale, localized energy systems, may include distributed energy resources like solar panels, wind turbines, and energy storage systems. The specific placement and tuning of PSSs in a microgrid depend on the unique characteristics of the microgrid and the types of DGs integrated. Therefore, a detailed analysis, possibly involving power system simulation tools, is typically required for effective PSS deployment in microgrids. Here are some considerations for placing PSSs in microgrids:

2.7.3.1 PSS in Synchronous Generator:

While PSSs are more commonly associated with large, interconnected power systems, their application in microgrids with synchronous generators is possible and can contribute to enhancing stability. The decision to implement PSS in a synchronous generator within a microgrid depends on the specific characteristics of the microgrid and the role of synchronous generators in its overall operation. Careful analysis and simulation studies are recommended before deploying PSS in microgrid applications. The PSS is integrated with the generator's automatic voltage regulator (AVR) system which is demonstrated in Fig. 2.24.

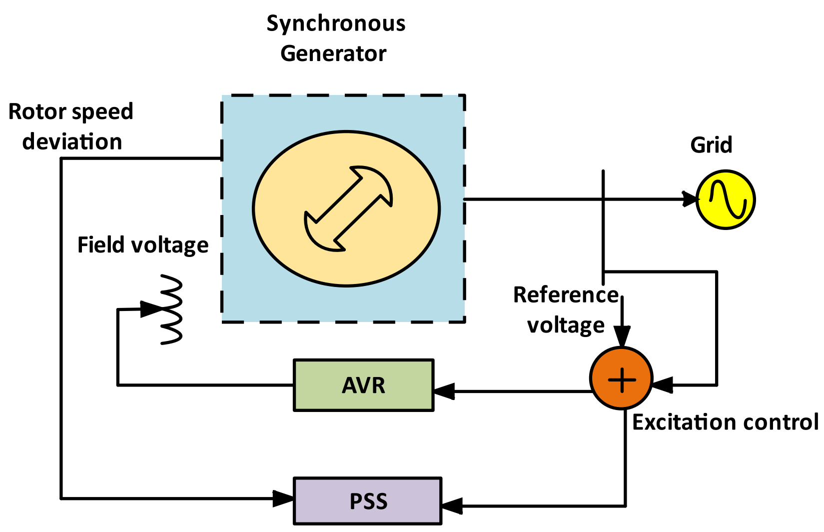

Fig. 2.24: PSS in synchronous generator [53].

2.7.3.2 PSS in ESS Controller:

An ESS-based PSS also offers a promising solution for enhancing the stability of interconnected microgrids, especially with the increasing integration of renewable and inverter-based resources [11]. Incorporating a multi-band PSS within the ESS of an interconnected microgrid environment can provide enhanced control and stabilization capabilities. Some aspects of providing PSS in ESS are as direct oscillation damping through energy storage, voltage regulation and oscillation damping, enhanced renewable integration, extended lifespan of ESS, frequency regulation, and so on. Energy storage systems (like batteries or flywheels) have the capability to rapidly inject or absorb active power. When integrated with a multi-band PSS, the ESS can provide targeted damping to specific oscillatory modes by rapidly adjusting its power output [52]. In addition to active power modulation, ESS can also modulate reactive power. With a multi-band PSS, the reactive power output of ESS can be controlled to damp out oscillations while maintaining the voltage profile of the microgrid [17]. As RESs can introduce variable outputs, the combined action of an ESS and multi-band PSS can counteract the oscillations brought about by renewables, allowing for their smoother integration into the microgrid. Oscillations can lead to frequent charge and discharge cycles, which might degrade the lifespan of certain types of energy storage (like batteries). By damping out these oscillations, the ESS can be operated in a more stable manner, potentially prolonging its operational life. ESS inherently aids in frequency regulation by absorbing or supplying power to counteract deviations from nominal frequency. When coupled with a multi-band PSS, this frequency regulation can be enhanced to target specific low-frequency oscillations. In interconnected microgrid systems, interconnecting tie-lines can experience power oscillations due to mismatches in generation and demand or due to disturbances. By damping these oscillations at the source using ESS integrated with a multi-band PSS, stress on these interconnections can be reduced. This reduces the likelihood of having to curtail renewable sources or ramp up expensive peaked plants to counteract oscillations. A multi-band PSS can ensure that the energy stored in the

ESS is utilized optimally. For instance, it can prioritize using stored energy for damping critical oscillations over less important grid functions. In scenarios where microgrids operate in an islanded mode (disconnected from the main grid), maintaining stability becomes crucial. The integration of a multi-band PSS with ESS can offer advanced control strategies to ensure stability in such modes. Traditionally, mechanical devices like damper windings in generators were used to damp oscillations. With the combined action of an ESS and a multi-band PSS, reliance on such mechanical solutions can be reduced [54]. So, the integration of a multi-band PSS with ESSs in an interconnected microgrid environment offers a synergistic approach to enhance grid stability. A PSS in ESS controller is illustrated in Fig. 2.25.

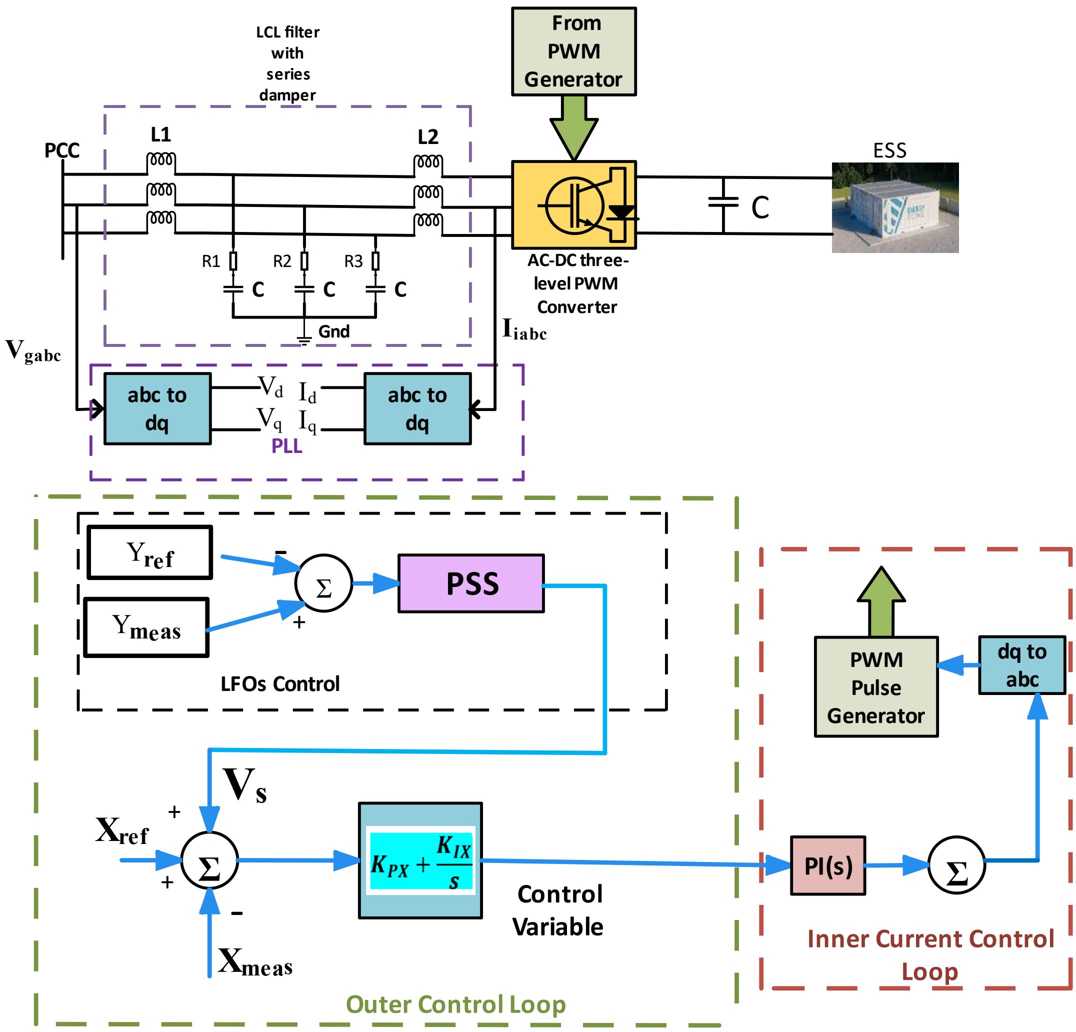

Fig. 2.25: PSS in ESS controller [11].

2.8 SUMMARY

MGs need to be connected, exchange power, and support the voltage and frequency of overloaded MGs in order to reap the full benefits, such as enhanced reliability and the incorporation of renewable energy. The analysis provides an in-depth examination of the characteristics and structures of PSSs within the framework of interconnected microgrid systems. It begins by elucidating the fundamental role of PSS in enhancing the stability of conventional power systems, particularly in mitigating oscillations and improving transient response. It then transitions to discuss the evolving landscape of power systems due to the increasing integration of microgrids, emphasizing the need to adapt PSS designs to accommodate the complexities of interconnected microgrid environments.

Various characteristics and structures of PSS are analyzed, encompassing traditional linear controllers as well as more advanced nonlinear and adaptive control techniques. The chapter explores the suitability of these different approaches in addressing the unique challenges posed by interconnected microgrid systems, such as distributed generation, intermittent renewable sources, and dynamic network configurations. Moreover, the chapter delves into the integration of PSS within interconnected microgrid architectures, considering factors like communication protocols, coordination mechanisms, and interoperability requirements.

The analysis presented on the role and significance of PSS within the context of interconnected microgrid systems. It begins by highlighting the increasing integration of RESs and the resulting need for effective control strategies to manage power oscillations. It discusses traditional damping stabilizers and then delves into the emergence of MB-PSS as promising solutions. Various design methodologies, including decentralized and coordinated control strategies, are examined, along with the incorporation of advanced technologies like artificial intelligence. It begins by elucidating the fundamental concepts of power oscillations and their detrimental effects on grid stability. It then proceeds to discuss the conventional methods employed for power oscillation damping, such as CPSS, PSS-2A, PSS-2B devices. Subsequently, it delves into the emergence of MB-PSS controllers as a promising solution, highlighting their ability to dampen oscillations and enhance system stability.

In conclusion, the chapter underscores the importance of adapting PSS designs to suit the evolving dynamics of interconnected microgrid systems. It highlights the potential of advanced control techniques and emphasizes the need for further research and development to optimize PSS performance in the context of distributed and decentralized energy network.

Chapter 3

DESIGN METHODOLOGY OF AN INTERCONNECTED HYBRID AC MICROGRID SYSTEM AND AN ESS-BASED POWER OSCILLATION DAMPER

This chapter focuses on the methodology and designing aspects of a POD controller tailored specifically for interconnected hybrid AC microgrid systems. By providing an in-depth exploration of the methodologies employed and the design considerations involved, this chapter aims to offer insights into the development process of an interconnected hybrid AC microgrid system and POD controllers that are robust, efficient, and adaptable to the unique characteristics of modern power system.

3.1 INTRODUCTION

The remarkable development of microgrid domains has brought significant advancements, yet several obstacles remain, such as the constraints imposed by DGs, compact capacity issues, and poor inertia. To address these challenges, MGs are linked together to form MG clusters, leveraging cooperation to tackle the problems faced by individual MGs. The integration of RESs and the proliferation of microgrids have reshaped modern power systems, introducing new challenges and opportunities.

This chapter begins with the design methodology of an interconnected hybrid AC microgrid system. By integrating various microgrids into a cohesive system, we aim to enhance the overall capacity, reliability, and efficiency of the power network. The interconnected hybrid AC microgrid system leverages DGs and ESSs to create a flexible and resilient grid capable of meeting diverse energy demands.

However, the interconnectedness and dynamic interactions within this hybrid microgrid system can lead to LFOs. These oscillations are a critical concern, as they can result in inefficiencies, potential equipment damage, and even system-wide instability if not adequately addressed. The occurrence of LFOs necessitates the development of effective solutions to ensure grid stability and reliability.

To mitigate the low-frequency oscillations, the design of a POD becomes paramount. The proposed damping controller is envisioned to enhance the stability of the microgrid by dynamically adjusting to fluctuations and disturbances that cause LFOs. Unlike traditional single-band power oscillation dampers, which target a narrow frequency range, the proposed multi-band power oscillation damper is designed to operate effectively across multiple frequency bands, providing a more comprehensive solution to the complex oscillatory behaviours encountered in interconnected microgrids.

This chapter will detail the conceptual design, theoretical foundations, and implementation strategies for the MB-POD. It begins with an overview of the fundamental principles underlying oscillation damping in electrical networks, followed by a discussion on the specific challenges posed by interconnected microgrid systems. The subsequent sections will elaborate on the architecture of the MB-POD, including the control algorithms and hardware configurations essential for its operation. Additionally, the integration of the MB-POD with existing microgrid control frameworks and its adaptability to various microgrid configurations will be explored.

Through a combination of simulation studies, the effectiveness of the proposed damping controller will be evaluated. This chapter aims to provide a robust framework for the design and deployment of advanced damping solutions that not only enhance the stability and reliability of interconnected microgrid systems but also pave the way for the broader adoption of RESs and innovative microgrid technologies.

3.2 CONFIGURATION OF AN INTERCONNECTED AC MICROGRID SYSTEM

In the context of modern power systems, understanding and mitigating low-frequency oscillations are critical for ensuring grid stability and reliability, particularly in interconnected microgrid configurations. This section delves into the configuration of interconnected microgrid specifically aimed at analysing and addressing low-frequency oscillations. Interconnected microgrid, characterized by their distributed energy resources and collaborative operation, present unique challenges in managing low-frequency oscillations. The configuration process involves several key aspects to effectively analyse and mitigate these oscillations while ensuring seamless integration and operation of the microgrid network.

Additionally, the deployment of synchronized measurement devices across interconnected microgrids enhances the observability of system-wide oscillation phenomena. These devices provide synchronized measurements of voltage, current, and frequency, enabling comprehensive analysis and visualization of oscillation patterns and behaviours across the interconnected network. By configuring interconnected microgrid specifically for analysing low-frequency oscillations, stakeholders can gain valuable insights into system behaviour and dynamics, leading to the development of effective mitigation strategies and enhanced grid resilience.

Figure 3.1 depicts the interconnected microgrid structure, comprising three separate MGs interconnected via interconnecting static switches. Each MG is equipped with its own RESs-based distributed energy resources, loads, converter interfaces, energy storage system, and control system. The coordination of power microgrids within the interconnected MG is managed by the local controller in tandem with the energy storage system of each MGs. Subsequently, the power balance within the interconnected MG system is maintained through the assistance of a distributed control system.

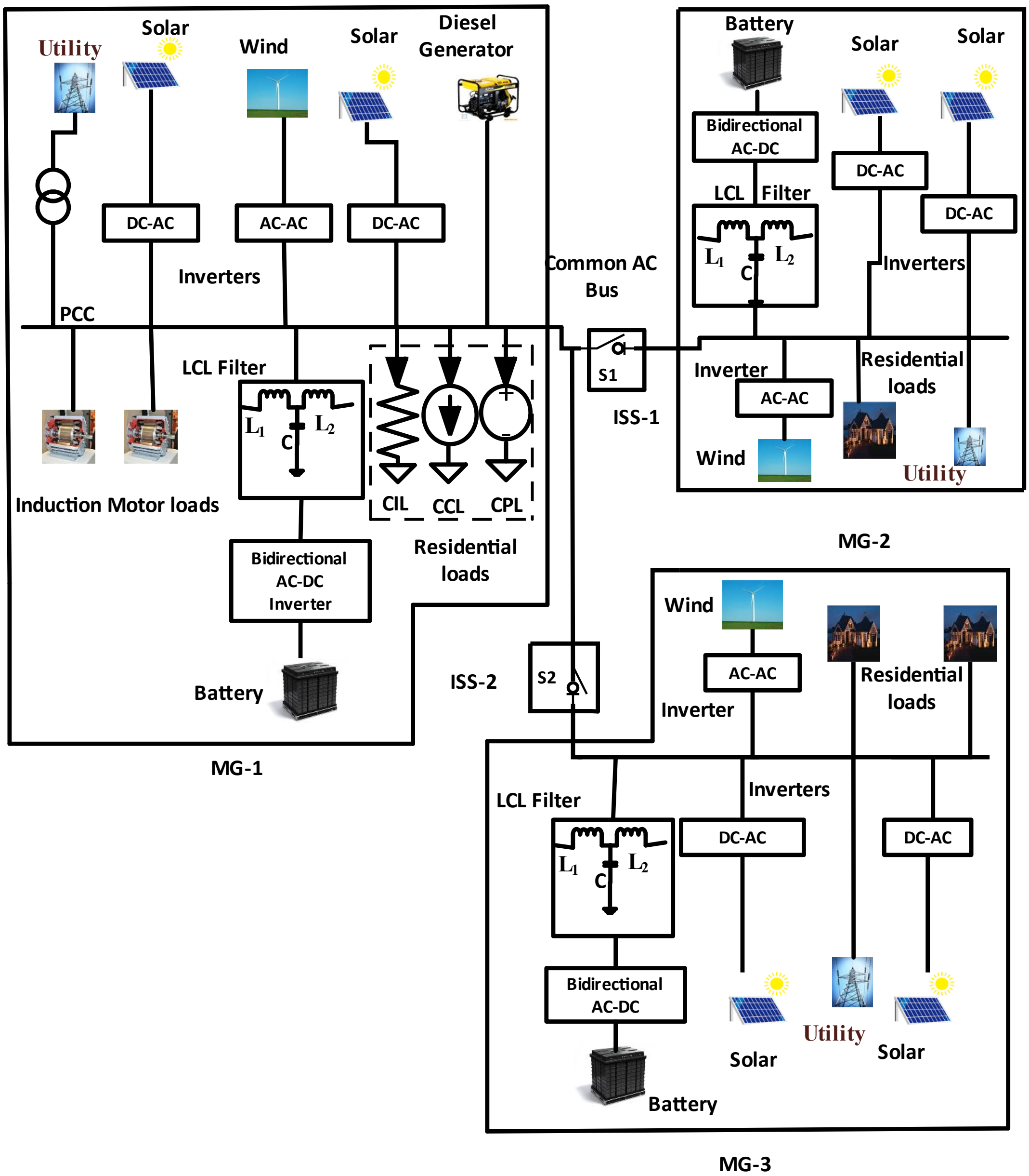

Fig. 3.1: Schematic arrangement of an interconnected hybrid AC microgrid system.

DGs are designed as a current source using power converter interfaces that can inject active power into the system as required. The MG under analysis is rated at the power specified by the DGs. Since RESs are typically preferred as the DGs, where PV and wind generator are considered as the DGs. The behavior of these DGs is dependent on wind speed and solar radiation patterns. The microgrid network illustrated in Fig. 3.2. represents a complete power flow vision system consisting of three microgrids where DG units are equipped with both dynamic and static loads, interconnected transmission lines, and energy storage system.

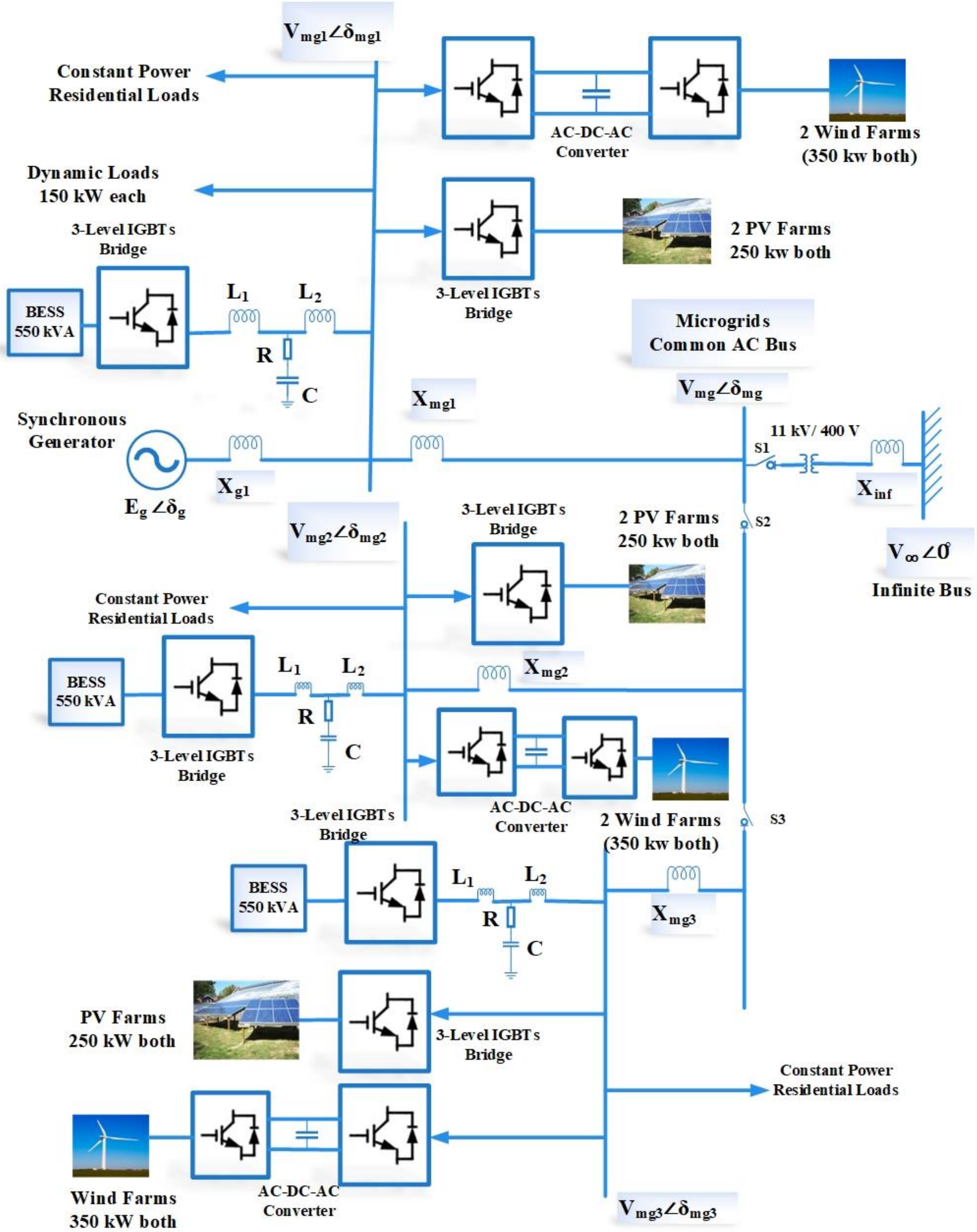

Fig. 3.2: Equivalent network power flow model of AC IMGs system.

3.2.1 PV System:

The PV system is modeled as a DC source, operating with the incremental conductance-based maximum power point tracking (MPPT) algorithm [109], and connected to the DC bus using a boost converter. The PV system model is shown in Fig. 3.3. To achieve the proper DC bus voltage level and maximum power point, the boost converter is controlled according to the signal output from the MPPT.

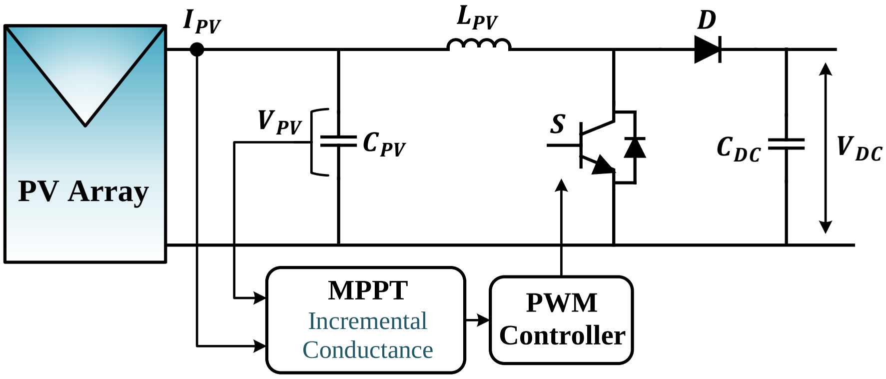

Fig. 3.3: Configuration of PV system.

3.2.2 Wind Generator:

The wind generator is modeled as an AC source and connected to the AC bus using a BTB converter, as shown in Fig. 3.4. The wind generator consists of a variable-speed doubly-fed induction generator (DFIG) with two VSCs connected to the rotor and stator [110]. The rotor-side converter helps in achieving MPPT of the wind turbine using flux-oriented vector control. The d-coordinate is based on the stator flux estimator, and both reactive power and terminal voltage are controlled in the q-coordinate. The grid-side converter regulates DG power generation by controlling the DC-link voltage of the BTB converter. In the grid-side converter control loops, the d-coordinate regulates the DC-link voltage, and the q-coordinate maintains the unity power factor by keeping the reactive current reference zero.

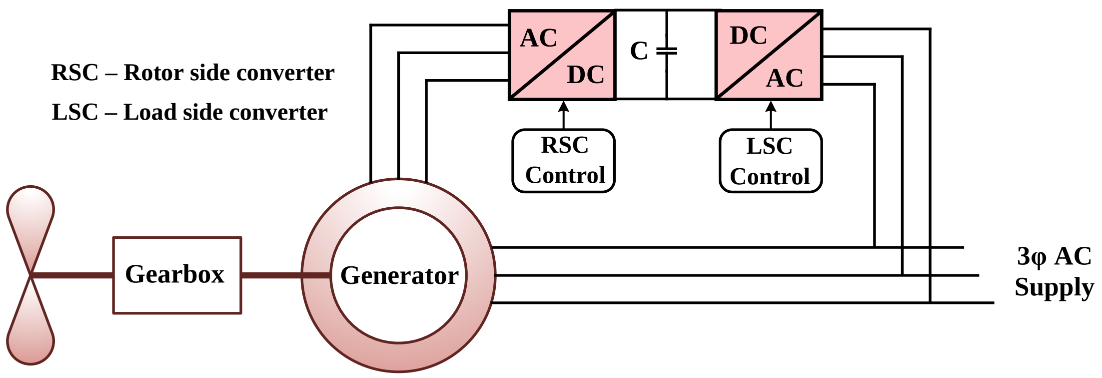

Fig. 3.4: Configuration of doubly-fed induction generator.

3.2.3 Diesel Generator:

Diesel generators are typically used as backup sources in islanded mode and connected to the AC bus as an AC source. In this study, it should only be activated when the power shortage cannot be compensated by other DGs and ESSs in islanded mode and it is unable to respond to an overall power surplus. It does not operate in grid-connected mode.

3.2.4 Energy Storage System:

Voltage-source inverters (VSIs) are employed for the DC-to-AC interface such that the control of the VSIs handles the power exchange between the microgrids and the AC bus. An AC-DC inverter additionally connects the ESSs' to the common AC bus via an inductor-capacitor-inductor (LCL) filter which is made up of L_1 Inductors, C capacitors with R series damper and L_2 inductors located on the grid side [111]. In high-power and low-frequency systems, the LCL filter is used to smooth the output current of the converter by reducing switching current ripple and assuring high steady-state and dynamic performance with lower inductor values [112]. Active and passive damping are two techniques used to reduce resonance and enhance the efficacy of an LCL filter. Here, the technique of passive damping with a series damping resistor has been implemented [113].

Microgrid networks rely heavily on storage technology (batteries, super capacitor, etc.) to mitigate the impact of RESs inconsistent power output and reduce peak power demands. In this work, a lithium-ion battery is explored as a potential energy storage medium because of its high energy density and low self-discharge characteristics [114]. The state of charge (SoC) of battery at time t, can be used to simulate the dynamic behavior of ESS shown in Equation 3.1 [115]:

$$\boldsymbol{SoC_n(t+1) = SoC_n(t) + [\eta_n^{charging}\,\beta_n^{charging}(t) + \frac{\beta_n^{discharging}(t)}{\eta_n^{discharging}}] \cdot P_n^{battery}(t)} \qquad 3.1$$

Here $SoC_n(t)$ represents the state of energy storage of the nth battery at time t. $\boldsymbol{P_n^{battery}(t)}$ indicates the net power exchange between the energy storage and microgrid. $\boldsymbol{\eta_n^{charging}}$ and $\boldsymbol{\eta_n^{discharging}}$ are the charging and discharging efficiencies, respectively. $\boldsymbol{\beta_n^{charging}(t)}$ and $\boldsymbol{\beta_n^{discharging}(t)}$ are logical variables to avoid simultaneous operation of battery charging and discharging power. The nominal voltage and the Ah capacity of the battery bank is 400 V and 700 Ah (280 kWh), respectively. The initial state-of-charge (SoC) of the battery bank is considered as 80% with 500 μF capacitance. A controlling method is implemented within all the ESS of the AC IMGs. Each MGs are having 500kVA battery energy storage system. A common synchronized reference frame PLL is used to synchronize the ESS voltage with the grid voltage and to generate frequency, d-q referenced voltage and current through the input of grid voltage and inverter current [111].

In recent years, renewable energy generation systems (such as photovoltaic and wind power systems) have been connected to the power system by typically applying voltage source converters in response to rising electricity consumption and the imperative need for environmental protection [116]. In order for the MGs to operate successfully with smooth DC-link voltage in ESS and sinusoidal generation current from distributed generators, the converter is essential [117].

3.2.4.1 Energy Storage System Control and Management

The crucial function of ESS, which is dependent on AC-bus controls and frequency tracking in the MG, is a difficult task that necessitates appropriate control and management techniques to guarantee reliable performance. Power electronic converters with extremely low inertia make the entire MG vulnerable during transient conditions because low inertia causes a quick response [118]. In this instance, some inertia is introduced to the ESS controller to handle fluctuations in power flow and avoid abrupt charging or discharging, allowing the ESS in each MG to run independently in grid-connected mode. The ESS controller uses specific algorithms that mimic the behaviour of mechanical inertia. These algorithms adjust the power output of the ESS based on changes in grid frequency or other disturbances, simulating the response of traditional rotating machinery. The control and management parameters of ESS are given in Table 3.1.

Table 3.1: ESS and PWM pulse generator controller parameters data.

ESS Parameters		
Power		500kVA
Rated capacity		700 Ah
Nominal voltage		370V
Initial state-of-charge (SoC)		80%
Capacitance		500µF
ESS Regulator gain (PLL)		
$K_{p_{PLL}}$		180
$K_{i_{PLL}}$		3200
$K_{d_{PLL}}$		1
ESS LCL Filter Parameters		
L_1		5×10^{-4} H
L_2		6.5×10^{-3} H
C		5×10^{-5} F
R		0.05 Ω
ESS PI Controller Parameters		
Inner Current Controller	K_{pc}	10
	K_{ic}	95
Outer Controller (Voltage/Frequency)	K_{pf}	1
	K_{if}	50
	K_{pv}	0.5
	K_{iv}	1

An ESS controller is depicted in Fig. 3.5 where the controller appears to represent a control system schematic for an ESS within a microgrid, incorporating a POD controller. The overall goal of this system is to regulate the power flow, maintain the voltage stability, and dampen any power oscillations that may occur within the microgrid to ensure stable operation.

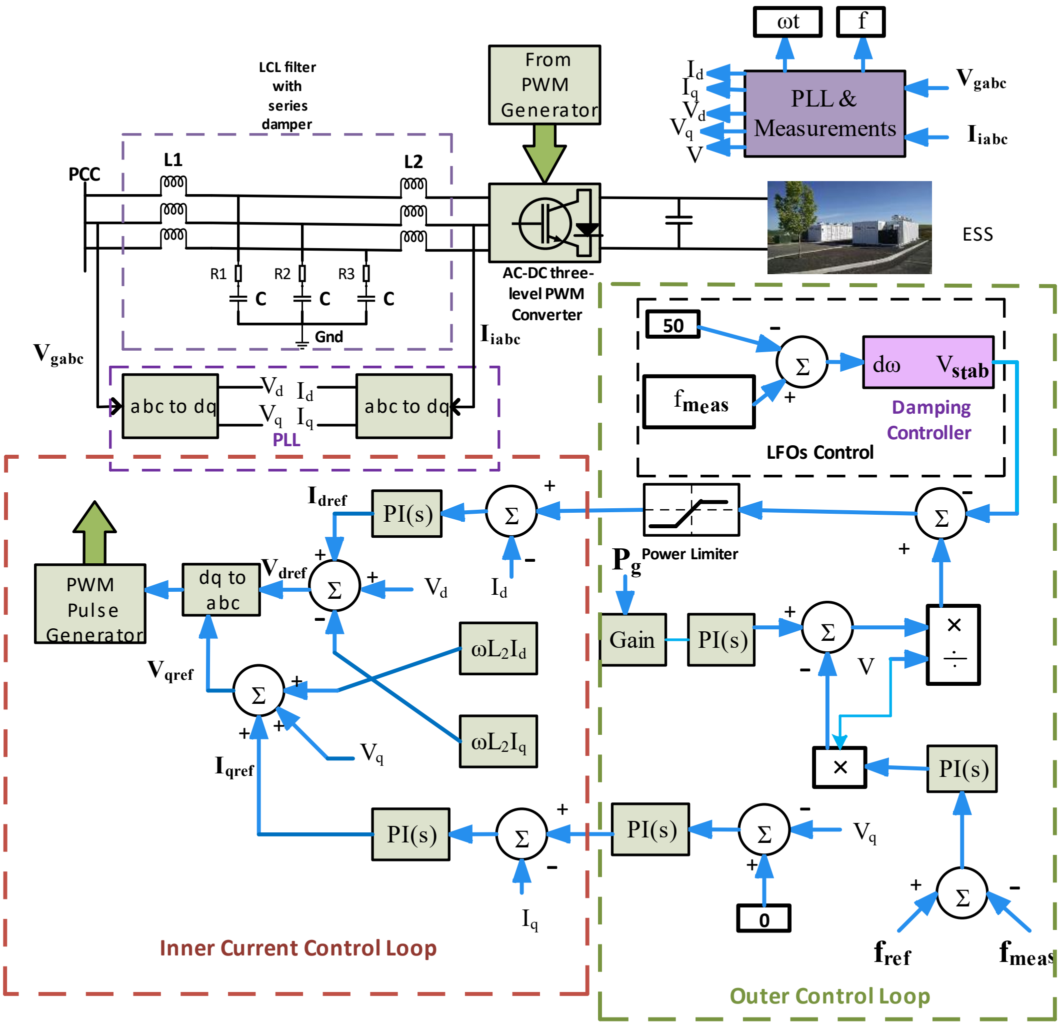

Fig. 3.5: Configuration of energy storage system control.

3.2.4.2 AC-DC Three-Level PWM Converter:

This converts AC to DC using a pulse width modulation (PWM) technique, which is often used for its efficiency in controlling the power flow.

3.2.4.3 LCL Filter with Series Damper:

This filter is connected to the point of common coupling (PCC) and is designed to mitigate the harmonics in the current and voltage waveforms.

3.2.4.4 Inner Current Control Loop:

The inner loop is responsible for the fast dynamic response of the current control. It uses a proportional-integral (PI) controller to ensure the current follows the reference values. The transformation from **abc** to **dq** coordinates (and back) is part of the control strategy to simplify the control of AC signals.

An LCL filter is commonly employed in power electronics, particularly in applications like grid-tied inverters, to attenuate high-frequency switching noise and improve the overall performance of the system. In some cases, series damping is added to the capacitor branch to improve stability and suppress resonance issues [119]. The basic circuit model of an LCL filter with series damping in the capacitor branch can be represented as Fig. 3.6.

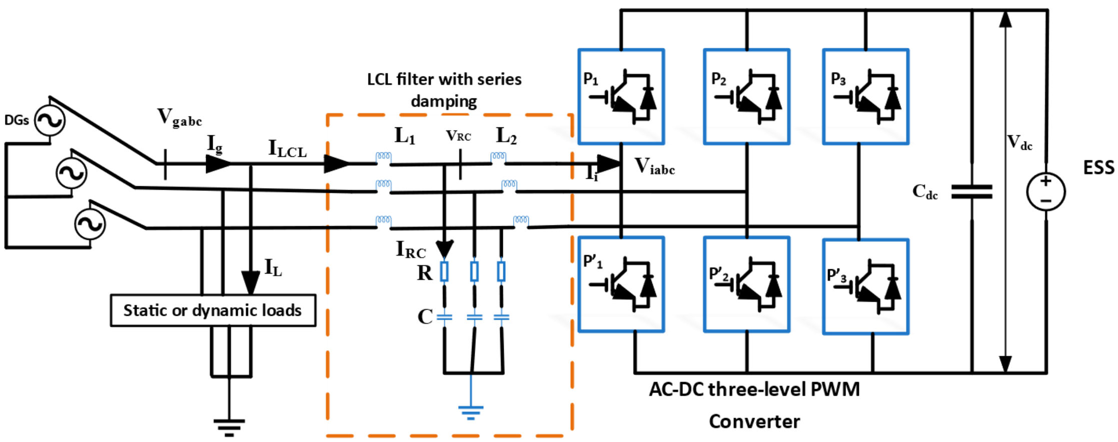

Fig. 3.6: Converter based distributed generations with ESS.

The differential equations describing this LCL filter with damping could be derived from Fig. 3.6 using Kirchhoff's voltage and current laws. Assuming a single-phase representation and using V and I to denote voltages and currents, the equations can be formulated in s-domain as equation 3.2-3.5:

$$V_i(s) - V_{RC}(s) = sL_2 I_i(s) \qquad 3.2$$

$$V_{RC}(s) = I_{RC}(s).\left(R + \frac{1}{sC}\right) \quad 3.3$$

$$I_{RC}(s) = I_g(s) - I_i(s) \quad 3.4$$

$$V_{RC}(s) - V_g(s) = sL_1 I_i(s) \quad 3.5$$

The transfer function of the LCL filter with series damping can be determined by utilizing the model presented in Fig. 3.6 and using equations 3.2-3.5, followed in equation 3.6.

$$\frac{I_g(s)}{V_i(s)} = \frac{\frac{sRC+1}{L_1L_2C}}{s^3 + s^2\frac{(L_1+L_2)R}{L_1L_2} + s\frac{L_1+L_2}{L_1L_2C}} \quad 3.6$$

Where, V_I, V_g and V_{RC} are the voltages at the inverter-side, grid-side and series RC damping node, respectively whereas I_I, I_{RC}, and I_g represent the currents through L_2, RC branch, and L_1, respectively.

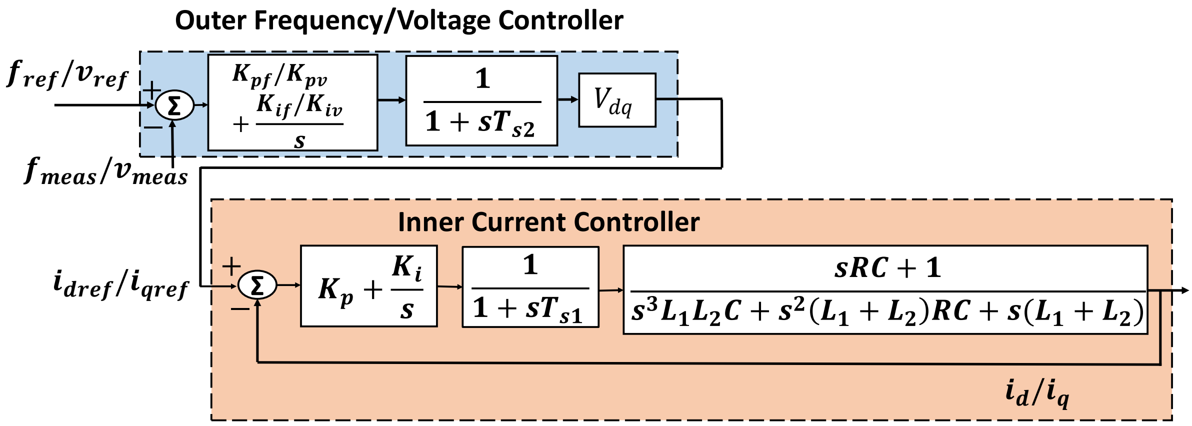

Fig. 3.7: Outer voltage/frequency and inner current controller loop configuration.

The block diagram in Fig. 3.7 depicts the outer voltage/frequency and current controller loop in s-domain where T_{s_1} and T_{s_2} represent the delay caused by the inner and outer controller loop, respectively. The frequency characteristics will be checked by phase and magnitude characteristics by frequency input using the bode diagram. In this investigation, T_{s_1} is selected for 9.46^0 phase margin with 41.4 dB gain margin in the open loop inner current frequency response whereas T_{s_2} is twice the delay constant of inner current controller with 9.17^0 phase margin in the open loop outer voltage controller frequency response as depicted in Fig. 3.8.

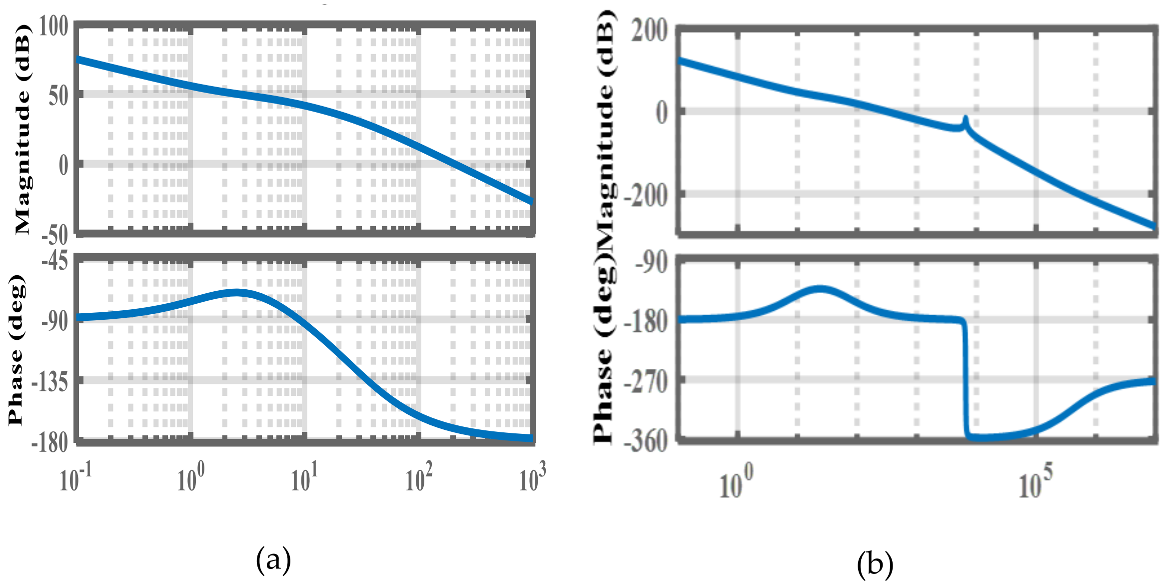

Fig. 3.8: Frequency response characteristics (a) Outer voltage controller (b) Inner current controller.

3.2.4.5 PI Controller Tuning of the Energy Storage System

When a multi-band power oscillation damper is installed in an energy storage system, the stability analysis involving the proportional (Kp) and integral (Ki) gains of the controller becomes crucial. These gains directly influence the dynamic response and stability of the ESS within the power system. By methodically varying Kp and Ki and assessing system stability and performance, the ESS can be finely tuned to enhance the damping of power oscillations and contribute to the overall stability of the power system. This process involves both theoretical analysis and practical testing to ensure reliable operation.

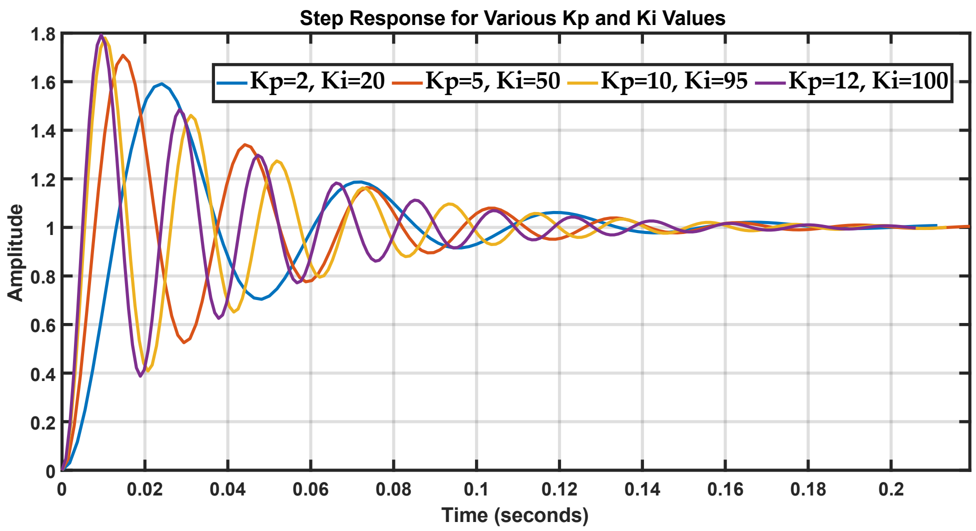

Fig. 3.9: Impact of current PI controller on system performance.

Figure 3.9 illustrates the impact of the current PI controller on system performance, highlighting its influence on stability and efficiency. The blue curve (k_{pc}=2, k_{ic}=20) has the slowest rise and takes longer to reach the steady state but has minimal overshoot. This might be preferred for systems where overshoot must be minimized at the cost of speed. The orange curve (kp=5, ki=50) and the yellow curve (k_{pc} =10, k_{ic}=95) both reach the steady state quicker but with some overshoot. These may be a good balance between speed and overshoot, depending on the acceptable levels for both. The purple curve (k_{pc}=12, k_{ic}=100) has the fastest rise time and quickly reaches the steady state but also exhibits the most significant overshoot, which might indicate a less stable system or one that is too aggressively tuned for certain applications. If the priority is a quick response without regard for overshoot, the purple curve could be seen as the best. If stability and minimal overshoot are more critical, the blue curve might be considered the best. Often, the "best" curve is the one that achieves the desired trade-off between these performance measures while meeting the system's operational requirements.

3.2.4.6 PLL & Measurements:

The PLL is used to synchronize the frequency and phase of the grid with the converter. This section also involves measuring the voltage and current ($\mathbf{V}_{gabc}$, $\mathbf{I}_{iabc}$).

3.2.4.7 Power Limiter:

This ensures that the output power (**Pg**) does not exceed a certain limit to protect the system.

3.2.4.8 LFOs Control:

LFOs control is implemented to dampen power oscillations. The diagram includes a feedback loop that measures frequency deviations (**f_meas**) and adjusts the damping controller accordingly.

3.2.4.9 Outer Control Loop:

This loop is slower than the inner current control loop and is responsible for voltage regulation and frequency control of the microgrid. It also uses PI controllers for voltage ($\mathbf{V_q}$) and frequency ($\mathbf{f_{ref}}$) control.

3.2.4.10 PWM Pulse Generator:

This generates the gating signals for the power switches in the converter based on the control commands from the control loops.

3.2.5 Point of Common Coupling:

This is where the ESS is connected to the wider grid. It's the point where the quality of the electricity must meet certain standards for harmonics, frequency, and voltage levels. This control system is designed to make real-time adjustments to maintain power quality and system stability in a microgrid with an integrated energy storage system.

3.2.6 AC Main Grid:

A balanced 3-phase, 50Hz, 400 V rms line-to-line utility grid coupled with an AC bus is employed in this study to perform the GC mode. In AC grid, each voltage source signifies a phase, with 120° of phase-shift between each phase, in the positive sequence. The PMS used in this study forces the AC grid to act only as a backup system, while the ESS must guarantee the power flow for the DG and load variations.

3.2.7 Loads:

Devices that consume active and reactive power are referred to as loads. Load demand is met by the power generation available in the interconnected MG system at any instant. Both constant impedance loads (CILs), constant power loads (CPLs), constant current loads (CCLs) and dynamic loads, such as induction motors, are used to perform the analysis. Sets of impedance made up of balanced 3-phase resistors and inductors (RL) connected in series or parallel indicate CILs.

3.2.7.1 Static Loads:

Static loads, also known as constant impedance loads, constant power loads or constant current loads which indicates that under various power supply conditions, their electrical properties remain constant and do not influence changes in the dynamic behaviour of the microgrid system.

3.2.7.2 Dynamic Loads:

An electrical load that exhibits varying behavior in response to changes in the microgrid's operating conditions. Unlike static loads, dynamic loads can alter their power consumption and impedance based on factors like voltage, frequency, or load conditions. Induction motors are a common type of dynamic load in microgrids, used in various applications from residential to industrial settings. Their operational characteristics, such as starting, running, and stopping, directly impact the microgrid's performance. Figure 3.10 depicts a microgrid system incorporating both dynamic and static loads, illustrating the interaction and balance between these different types of electrical demands.

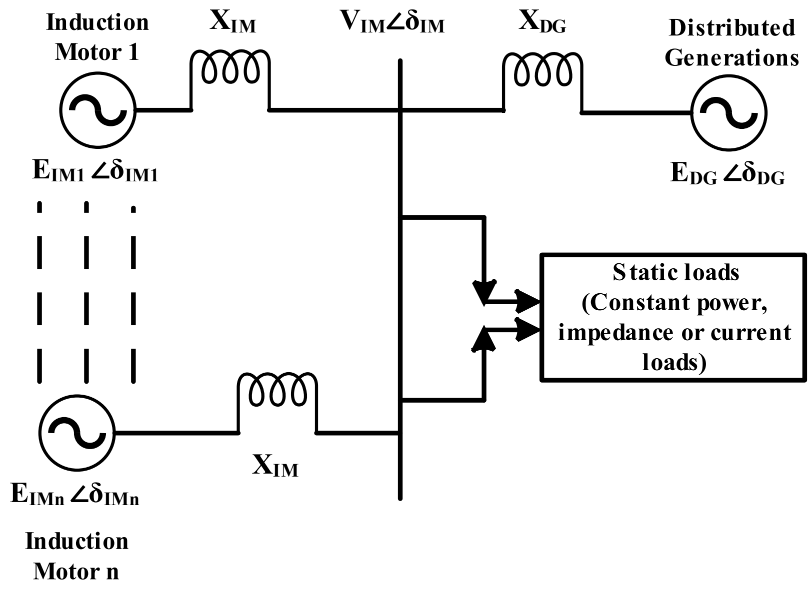

Fig. 3.10: Microgrid system with dynamic and static loads.

3.2.7.3 Mathematical Modelling of an Induction Motor

A fourth-order state-space model of the machine's electrical component and a second-order system of the machine's mechanical component are used to depict them. The arbitrary two-axis dq reference frame is used for all stator and rotor quantities. The fundamental voltage equations of an induction motor in a stationary dq reference frame are given in terms of currents and fluxes for both stator and rotor [120] in equations 3.7-3.12:

$$\varphi_{qs} = L_s i_{qs} + L_m i_{qr} \tag{3.7}$$

$$\varphi_{ds} = L_s i_{ds} + L_m i_{dr} \tag{3.8}$$

$$\varphi_{qr} = L_r i_{qr} + L_m i_{qs} \tag{3.9}$$

$$\varphi_{dr} = L_r i_{qr} + L_m i_{ds} \tag{3.10}$$

$$L_r = L_{lir} + L_m \tag{3.11}$$

$$L_s = L_{lis} + L_m \tag{3.12}$$

Where L stands for an induction motor's inductances with the appropriate subscripts. While the subscripts *lis* and *lir* denote the leakage inductance of the stator and rotor, respectively, the subscripts m, r, and s denote the magnetizing component, rotor, and stator, respectively.

Torque created when electrical power is transformed inside of a machine into mechanical power is referred to as the induced torque. This torque is countered by the torques created by friction and wind resistance within the machine, thus it differs from the torque that can be measured at the motor's terminals [121]. The following equation 3.13 is the formula for determining the induced torque, τ_{ind}:

$$\tau_{ind} = \frac{P_{conv}}{\omega_m} = \frac{P_{ag}}{\omega_{sync}} = \frac{3\, V_{th}^2\, {R_r}/{s}}{\omega_{sync}\left[\left(R_{th} + {R_r}/{s}\right)^2 + \left(R_{th} + {R_r}/{s}\right)^2\right]} \quad (3.13)$$

Where, P_{conv} presents converted power in mechanical form in an induction motor, P_{ag} represents air-gap power; s denotes slip of the rotor, ω_m and ω_{sync} denote rotor speed and synchronous speed, respectively, and subscripts th denotes the thevenin equivalent quantity.

3.2.7.4 Induction Motor Torque-Speed Characteristic Variations

For both small and large IMs, a torque-speed characteristics curve will be drawn. By altering the default IM parameters, comparison research will be conducted using the torque-speed characteristics curve. Fig. 3.11 (iii) and (iv) indicate the torque-speed characteristics for a small IM (5.4 hp IM) for a change in rotor resistance (Rr) and stator resistance (Rs), while Fig. 3.11 (i) and (ii) indicate the torque-speed characteristics for a large IM (215 hp IM). For both forms of IM, it can be seen that torque fluctuates as rotor resistance deviates from set levels. Initial torque is higher when rotor resistance is raised than when it is decreased as the positive primary factor. When the stator resistance changes, however, the situation reverses as a negative secondary factor. able 3.2 addresses stability concerns under various microgrid types, detailing the specific challenges and considerations for maintaining system reliability.

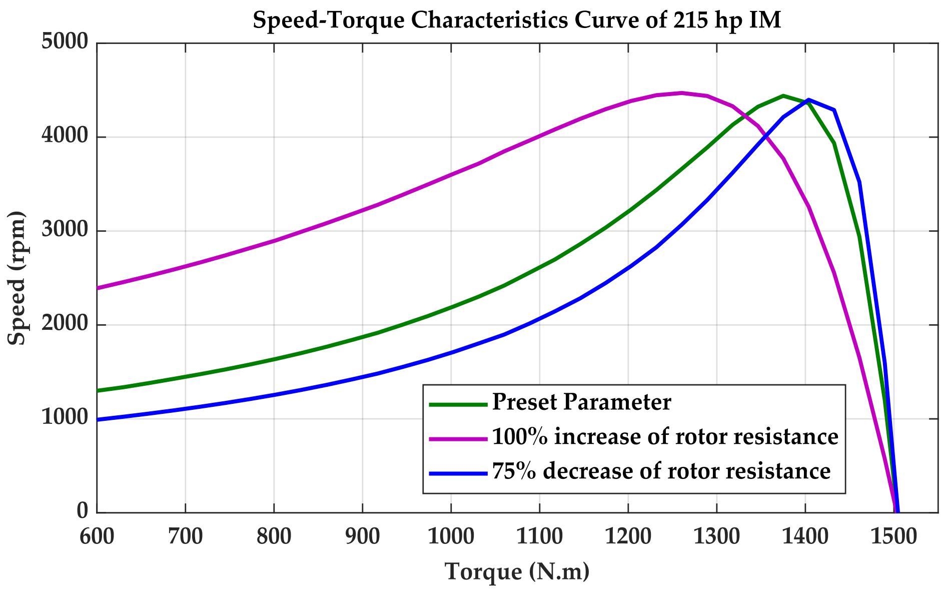

Speed-Torque Characteristics Curve of 215 hp IM
Speed (rpm)
Torque (N.m)
Preset Parameter
100% increase of rotor resistance
75% decrease of rotor resistance

(i)

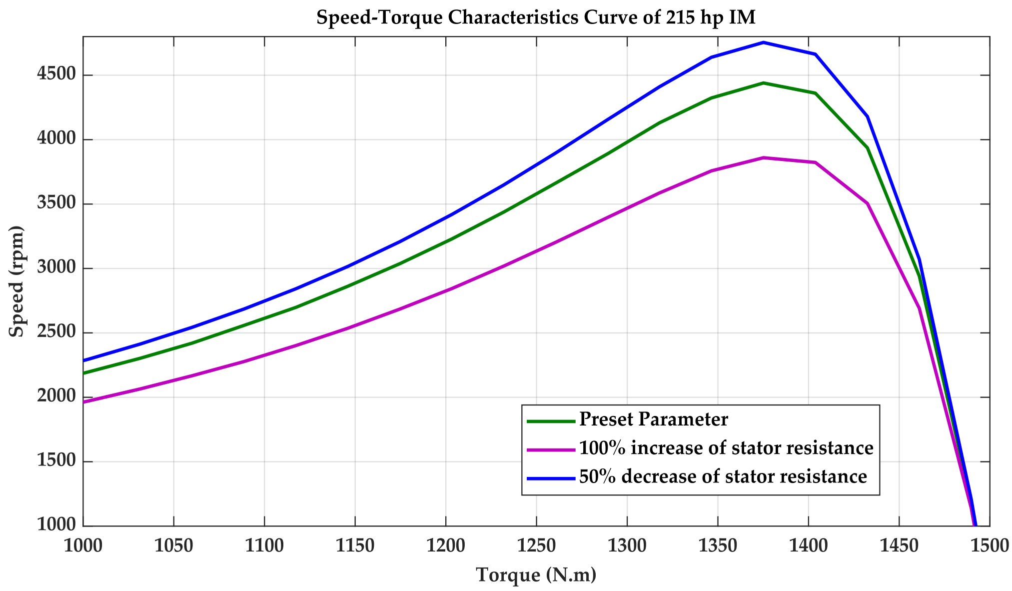

Speed-Torque Characteristics Curve of 215 hp IM
Speed (rpm)
Torque (N.m)
Preset Parameter
100% increase of stator resistance
50% decrease of stator resistance

(ii)

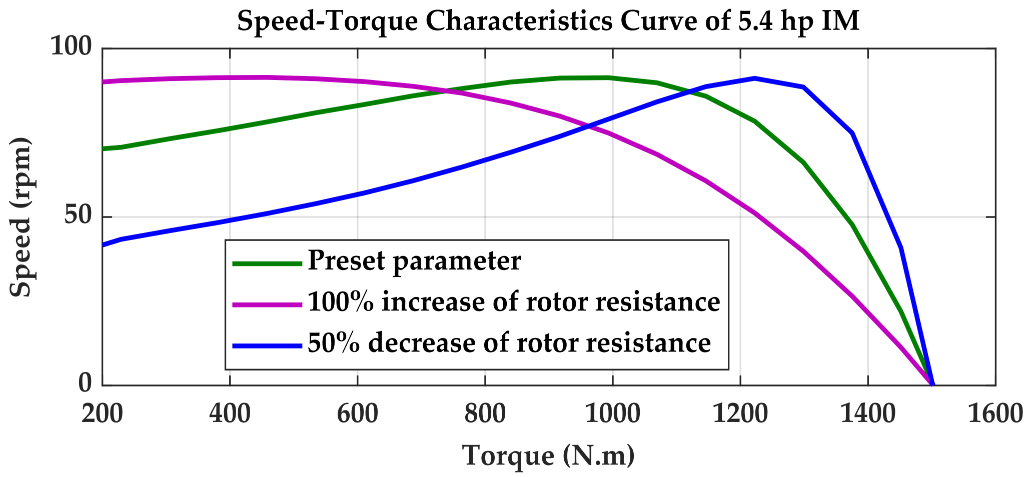

(iii)

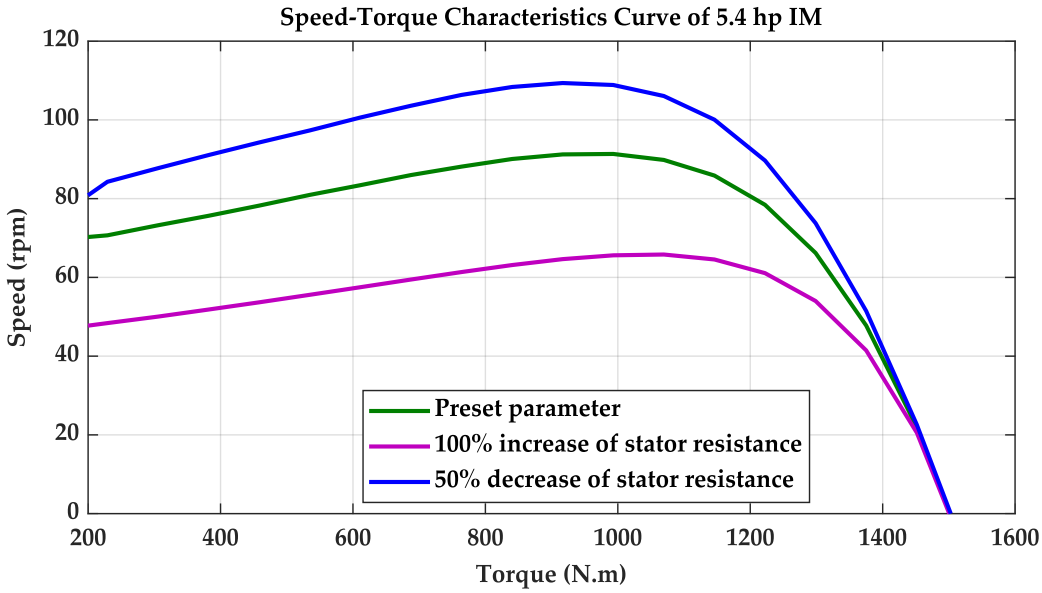

(iv)

Fig. 3.11: Torque-speed characteristics curves, (i) for large IM with deviation of rotor resistance from preset values, (ii) for large IM with deviation of stator resistance from preset values, (iii) for small IM with deviation of rotor resistance from preset values, and (iv) for small IM with deviation of stator resistance from preset values.

Table 3.2 Stability concern under different microgrid types

Microgrid Types	Stability concerns	Remarks
Local Microgrids	Induction motors' load characteristics, especially in islanded microgrids, significantly impact transient stability, and the capacity of motors is inversely related to microgrid stability [122]	Practical relevance, comprehensive analysis on microgrid stability. Full spectrum of induction motor not covered; better analysis requirement to fit into larger microgrid system.
Local Microgrids	Considering the high penetration of power electronics-based DG units and the rising proportion of IM loads, power supply disruptions, faults, and sudden load changes can affect voltage and frequency stability [121]	Detailed analysis posed by IM loads in microgrids; stability is maintained by existing system. Impact of IM loads in islanded microgrids during fault conditions; narrow focus on IM loads.
Medium-voltage local Microgrids	A comprehensive modeling analysis and stabilization method for MV droop-controlled microgrids facing high penetration of dynamic loads like induction motors [75]	Incorporating both dynamic and static loads; effectively linking the frequency dynamics of the microgrid to the dynamics of the motor. Focuses on MV droop-controlled microgrids with induction motor loads; higher order model for distributed generations and induction motors.
Hybrid Microgrids	Focuses on the dynamic behavior of IMs in microgrids, particularly addressing issues such as LFOs [123]	Comprehensive Analysis of IMs in Microgrids; valuable Insights into LFOs; detailed analysis posed by IM loads in microgrids. Limited scope of experimental validation; lower damping controller impact.

3.2.8 Interconnecting Static Switch:

An interconnecting static switch serves as a crucial component in power systems, facilitating the seamless connection or disconnection of electrical circuits. This switch operates in a solid-state manner, offering rapid switching capabilities without mechanical moving parts, thereby ensuring enhanced reliability and efficiency in power transmission and distribution networks. Moreover, the interconnecting static switch contributes to the optimization of power flow management and voltage regulation across interconnected microgrids. Through coordinated control strategies and communication protocols, it enables seamless integration and coordination of distributed energy resources, enhancing grid resilience and stability.

This assumes a crucial role in linking three individual microgrids—MG-1, MG-2, and MG-3—within the power infrastructure. As a solid-state device, this switch offers swift and precise control over the interconnection between microgrids without mechanical components. In the context of connecting multiple microgrids, the interconnecting static switch facilitates efficient energy exchange and coordination among MG-1, MG-2, and MG-3. It enables optimal distribution of power flow, load balancing, and fault isolation, thereby bolstering overall grid stability and reliability across the interconnected network. The static switch empowers operators to dynamically reconfigure the network layout, responding promptly to fluctuations in demand, renewable energy generation, and grid disturbances. By providing a flexible and controllable connection between microgrids, it supports the effective utilization of distributed energy resources and ensures optimal operation of the entire power system.

The microgrid is connected to the other microgrids by electrically through the interconnecting static switch (ISS) devices, which are used to physically link (or disconnect) both systems. Due to their various benefits, which include high speed switching, no mechanical connections, compact size, lightweight, and electronic control, these are used in place of conventional breakers [71]. Their qualities are generally better suited for microgrids. If an unplanned event occurs due to a fault in one of the systems, the shift from grid-connected mode to islanded mode must occur very quickly in order to protect the microgrid and distribution grid components as well as user safety. Since the reconnection is a scheduled process, there is less of a promptness need. However, it will be preferable if the switch closing time is shortened in order to lower the likelihood of synchronization failures and elevated latency. Conventional breakers have a 20–100 ms response time. Static switches are built using thyristors or silicon-controlled resistors (SCRs). Conversely, thyristors react within a quarter or a half of an electrical cycle, and approximately one hundred seconds if they are made of an insulated gate bipolar transistor (IGBT) [124]. At this pace, the transition is undetectable for DG units and loads, achieving smooth characteristics for microgrids and enabling mode switching at any defined instant, not just during emergency or emergent situations. There has been a noticeable increase in dependability and flexibility.

The SCR static switch has been selected as the preferred alternative because it can accommodate high power capacities, is inexpensive, reduces overload, and operates at intervals that meet the requirements for microgrid grid connection. The static switch itself is composed of two anti-parallel SCR units.

This is the static switch's main physical component. It still has to include measurement on both sides, which is accomplished via current and voltage transformers (VT and CT). Digital signal processors (DSPs) that are aggregated can handle the output of relay functions, communication, control, monitoring, and diagnosis [125]. Decisions on internal and external problems, power quality, and synchronization must be made while continuously analyzing the voltage, current, and frequency readings from the microgrid and the main grid. When diagnosing and acting, caution must be taken with regard to security, dependability, and predictability to ensure that there are no unintentional or misleading switch openings or closings, either temporarily or repeatedly [126].

Furthermore, the interconnecting static switch fosters coordinated control and communication among MG-1, MG-2, and MG-3, enabling seamless integration and interoperability. It facilitates the implementation of advanced control strategies such as voltage and frequency regulation, power sharing, and islanding operations, thereby enhancing grid resilience and reliability. Overall, the interconnecting static switch serves as a pivotal component in enabling the seamless connection and operation of three individual microgrids within the broader power network. It promotes a more resilient, flexible, and efficient power system by facilitating efficient energy exchange and coordination among interconnected microgrids.

3.3 ESS-BASED POWER OSCILLATION DAMPER

Low-frequency oscillations are caused by electromechanical oscillatory modes, and a power system stabilizer is an essential part of excitation systems for keeping small-signal stability. In most cases, the system is designed to respond to a single input signal, like a change in velocity or active power (delta-omega PSS and delta-P PSS, respectively) [32]. There are normally three modules that make up a PSS: a gain module, a washout module for filtering out DC components, and a phase correction module for correcting the phase delay that occurs between the exciter input and the electrical torque. However, more input signals can enhance the damping capability. Other stabilizers generate their stabilizing signal from the terminal frequency. There have been numerous studies comparing different PSS models such CPSS, IEEE PSS2B, PSS3B, and PSS4B [33, 34].

3.3.1 Single-Band Power Oscillation Damper

Historically, power system stabilizers have been employed on synchronous generators in order to mitigate the effects of LFOs. Since the ESS responds faster than other sources in the microgrid, a SB-POD based on conventional PSS is installed at the ESS [25]. To dampen the LFOs, this SB-POD supplies an extra stabilizing input to the ESS controller. A network disruption, such as a load shift, DG outage, or a short-circuit failure, would cause voltage/frequency variations in the microgrid, resulting in rotor speed oscillations at induction machine loads. Fig. 3.12 depicts the SB-POD's control architecture, which includes a gain block, a low-pass filter, and a wash-out circuit.

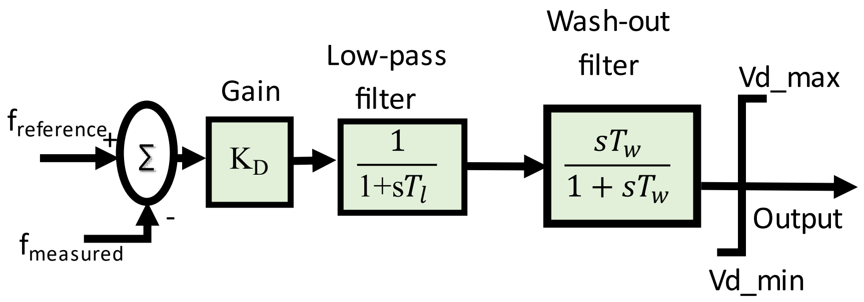

Fig. 3.12: SB-POD’s control architecture.

The SB-POD's transfer function is provided in Equation 3.14,

$$\boldsymbol{H(s) = K_D \left(\frac{1}{1+sT_l}\right)\left(\frac{sT_w}{1 + sT_w}\right)} \qquad 3.14$$

In this equation, K_D, T_l, and T_w represent the gain, low-pass filter time constant, and wash-out filter time constant, respectively.

3.3.2 Multi-Band Power Oscillation Damper

Multi-oscillatory modes of the IMGs system include low-, intermediate-, and high-frequency components. Conventional PSSs, including CPSS, PSSS2B, and PSSS3B, have a single frequency spectrum for the transmission of stabilizing signals. Therefore, a PSS that can independently manage each frequency component is preferable. In this context, IEEE Standard 421.5 introduced the MB-PSS model, a new type of dual input stabilizer, as an innovative option [35]. This PSS employs three distinct pass filter types — low, medium, and high — to cover a broad spectrum of oscillations occurring at various frequencies, allowing for more effective damping of all global, inter-area, and local modes. PSS4B models have been determined to be preferable to single band PSS models. Whereas in the literature [36], proposes a new MB-PSS design in response to the desirable structure of MB-PSS and the nonlinearities and time-varying conditions of power systems. Earlier mentioned in the literature [24], an interconnected hybrid AC microgrids system's small-signal stability is addressed by the introduction of a multi-band power oscillation damper, which is based on the multi-band power system stabilizer. Each band is equipped with a differential band pass filter, an amplifier, and a limiter. The ultimate voltage signal transducer (VST) where VST_{min}/VST_{max} limiter regulates the output intensity of the block signal. The multiple operating frequency band (MB-PSS 4B) capturing structure is depicted in Fig. 2.22(a) & input transducers model in Fig. 2.22(b). It is seen that the rotor speed deviation is measured from a speed transducer and $\Delta\omega_{L-I}$ is calculated. This signal feeds low and intermediate bands. The frequency deviation is transmitted to another speed transducer in order to generate $\Delta\omega_H$ within the high frequency range. The concept of capturing $\Delta\omega_{L-I}$ and $\Delta\omega_H$ is illustrated in Fig. 2.23. The MB-PSS is comprised of a total of 21 tuneable parameters [36]. This parameter adjustment is a significant challenge for MB-PSS design. In this study, the parameters of MB-POD are tuned by a trial-and-error approach. The damper's parameters are listed in the APPENDIX.

The simultaneous functionality of all three frequency bands in the MBPSS exhibits inadequate performance. The low-intermediate band of the MB-PSS offers better time domain performance than the low-intermediate-high band of the MB-PSS, particularly in PSS4B [37]. In the intermediate pass section, the continuous-time transfer function can be expressed in the manner depicted in 3.15.

$$\mathrm{TF1} = \frac{-1.082 \times 10^{-11}\,\mathrm{s}^4 + 6664\,\mathrm{s}^3 + 666.4\,\mathrm{s}^2}{10.8\,\mathrm{s}^4 + 68.16\,\mathrm{s}^3 + 113.3\,\mathrm{s}^2 + 20.66\,\mathrm{s} + 1} \qquad 3.15$$

The continuous-time transfer function for the low pass section is described as follows, as stated in equation 3.16.

$$\mathrm{TF2} = \frac{3302\,s^2 + 1337\,s}{4.8\,s^2 + 4.4\,s + 1} \qquad 3.16$$

The continuous-time transfer function for a low-intermediate pass section in the MB-POD system is represented by the following equation 3.17.

$$TF3 = \frac{3.566 \times 10^4 s^6 + 2.715 \times 10^5 s^5 + 4.978 \times 10^5 s^4 + 2.293 \times 10^5 s^3 + 3.158 \times 10^4 s^2 + 1337 s}{51.84 s^6 + 374.7 s^5 + 854.6 s^4 + 665.9 s^3 + 209 s^2 + 25.06 s + 1} \tag{3.17}$$

The speed deviation is a suitable input signal for the MB-POD, as frequency deviation is proportional to speed deviation. Therefore, the equation must account for the variation in frequency caused by the system's inertia constant. Thus, a new swing equation can be formed such as equated in equation 3.18:

$$\Delta T_m - \Delta T_e = 2H \frac{d}{dt} \Delta \widetilde{\omega_g} \tag{3.18}$$

Where $\Delta \widetilde{\omega}_g = \Delta \omega_g - \Delta \omega_{mg}$

In equation 3.18 which can be called the swing equation of the non-stiff interconnected microgrid system, T_m and T_e represent the mechanical and electrical torque component, respectively. H holds for per unit inertia constant while ω_g and ω_{mg} are the grid and system frequency respectively.

The multi-band power oscillation damping controller represents a sophisticated damping control strategy aimed at enhancing the stability and performance of power systems, particularly in the presence of oscillations induced by various factors such as disturbances or renewable energy integration. Unlike traditional POD controllers, which primarily focus on damping oscillations within a narrow frequency band, the multi-band POD controller operates across three distinct frequency bands, offering enhanced damping capability over a broader spectrum of oscillations.

The multi-band POD controller typically utilizes a combination of linear and nonlinear control techniques, adaptive algorithms, and advanced signal processing methods to achieve optimal damping performance. It leverages real-time measurements from system sensors to continuously adjust damping parameters and adapt to changing operating conditions, ensuring robust and reliable performance under varying load and generation scenarios. One of the key advantages of the multi-band POD controller is its versatility and adaptability to diverse power system configurations, including interconnected microgrid environments, interconnected grids, and systems with high renewable energy penetration. By providing effective damping across multiple frequency bands, this controller contributes to mitigating oscillations, improving transient stability, and enhancing the overall operational efficiency of modern power systems.

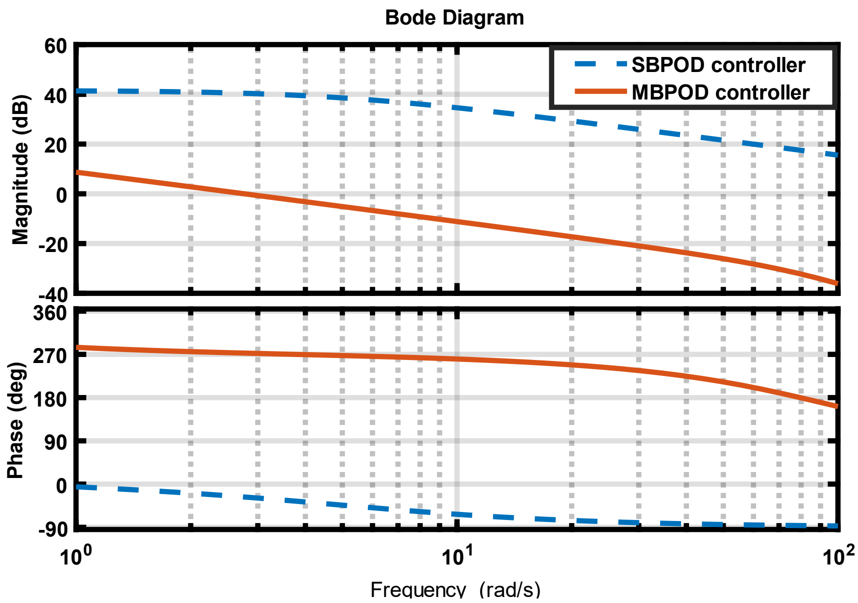

Fig. 3.13: Frequency response characteristics comparison of both POD controllers.

Also, the bode diagrams of single-band damping controller and multi-band power oscillation damper are depicted in Fig. 3.13. These figures clearly show that the bandwidth of MB-POD is wider than single-band controller confirming its superiority performance. The MBPOD offers superior damping performance by providing higher gain and better phase management across multiple frequency bands, enhancing the stability and reliability of interconnected microgrid systems. In low frequencies, the MB-POD performs with a suitable magnitude, while the SB-POD magnitude is very low. The frequency response characteristics depicted in Fig. 3.13 which indicates 11.9^0

phase margin and 9.54^0 phase margin for single-band POD and MB-POD, respectively.

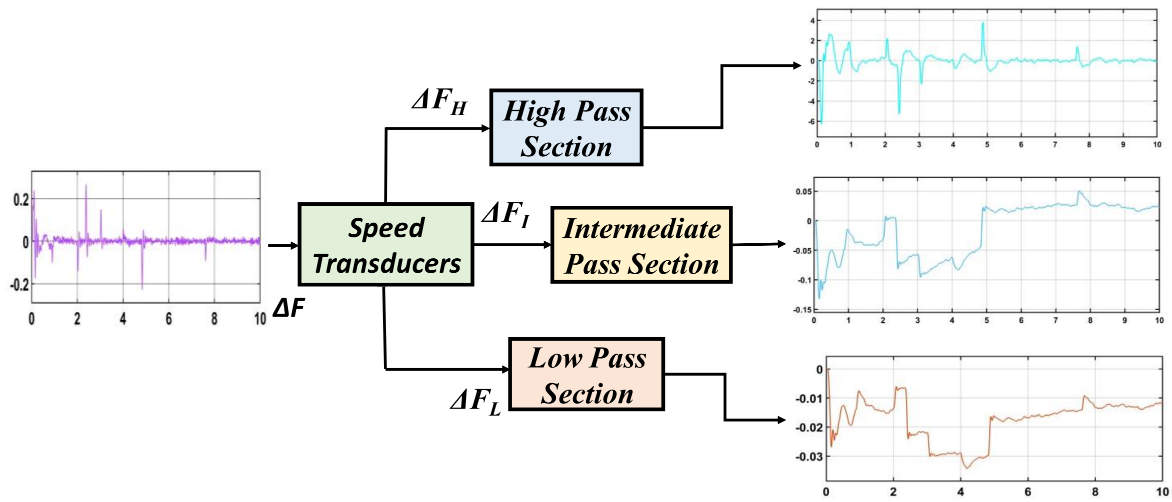

Fig. 3.14: Output signals of MB-POD in each band.

The injected signal from each MB-POD section installed in the ESS is displayed in Fig. 3.14. It illustrates how each section injects its own relative stabilizing signal. As a result, this POD performs better by nature and can inject a stronger signal than SB-POD. The MB-POD can perform much better performance under a wider range of frequencies, and it can inject a stronger stabilizing signal which is seen in Fig. 3.14.

In summary, the multi-band power oscillation damping controller represents a state-of-the-art solution for addressing oscillation-related stability issues in power systems. Its multi-frequency damping capability, coupled with advanced control techniques, makes it a valuable tool for ensuring the reliable and secure operation of complex and dynamic power networks. The description outlines a power system stabilizer model referred to as MB-POD based on PSS4B. This model is designed to mitigate oscillations across multiple frequency bands: low, intermediate, and high.

Here's an interpretation of the given details and their significance in the context of power systems:

3.3.2.1 Multi-Band Differential Filters:

The PSS4B includes three sets of differential filters, each targeting a specific frequency range of power system oscillations. These filters are designed to apply damping control to low-frequency (around 0.3-1.2 rad/s), intermediate-frequency (approximately 1.26 rad/s), and high-frequency (around 625 rad/s) oscillations. Differential filters are used to ensure that the PSS introduces the correct phase lead, essential for effective damping across these different frequency ranges.

3.3.2.2 Filter Structure:

Each filter acts as a bandpass filter, meaning it allows a range of frequencies around a centre frequency to pass through while attenuating frequencies outside of this range. The centre frequency and magnitude of each filter are tuneable, providing flexibility in adapting the PSS to different power system characteristics or operating conditions.

3.3.2.3 Phase Lead Provision:

Each differential filter is capable of providing phase lead in its specified band, which is crucial for adding damping torque in phase with the speed deviation. Phase lead compensates for the inherent phase lag between the excitation system's response and the oscillation frequency, enabling the PSS to effectively counteract oscillatory movements.

The utilization of a multi-band power system stabilizer is to be discussed for damping the low frequency oscillations of an interconnected microgrid system. Each band of the PSS is designed to target a different range of frequencies, which corresponds to different oscillatory modes in the system. The integration of multiple microgrids into a unified interconnected microgrid system offers enhanced reliability, resource sharing, and operational flexibility. However, this complex system architecture introduces significant challenges, particularly in managing and mitigating low-frequency oscillations. These oscillations can arise from dynamic interactions between interconnected microgrids, variability in distributed energy resources, and sudden load changes. To address these challenges effectively, a MBPSS is employed.

3.3.2.4 Frequency Bands Selection:

A tools MATLAB/Simulink is used to model the interconnected microgrid system and perform a frequency response analysis. This analysis helps identify the natural frequencies at which the system tends to oscillate. The frequency ranges are focused on where the system exhibits significant oscillatory behavior. These are often in the range of 0.1 Hz to a few Hz for LFOs in an interconnected microgrid system.

3.3.2.5 Multi-Band Filters Configuration:

In the mentioned Fig. 3.15, it seems that each filter in the PSS is configured as a bandpass filter that can be tuned for a specific frequency range. These ranges are:

- Low-frequency band: 0.1 Hz- 2 Hz
- Intermediate-frequency band: 2 Hz - 5 Hz
- High-frequency band: 5 Hz - 10 Hz

Bandpass filters are characterized by a center frequency, at which they allow signals to pass with maximum gain, and a phase shift that is ideally zero at this center frequency.

3.3.2.6 Phase Lead by Differential Filters:

The differential filters in the PSS are designed to provide phase lead, which is necessary to counteract the inherent delay in the system's response to oscillations. By providing phase lead, these filters help to enhance the damping of oscillations at the targeted frequencies.

3.3.2.7 Design Flexibility:

The authors suggest that having a higher number of degrees of freedom in the design of the PSS allows for more informed decision-making. This flexibility is crucial for resolving trade-offs in a large, interconnected power system where different parts of the system may have different stability needs.

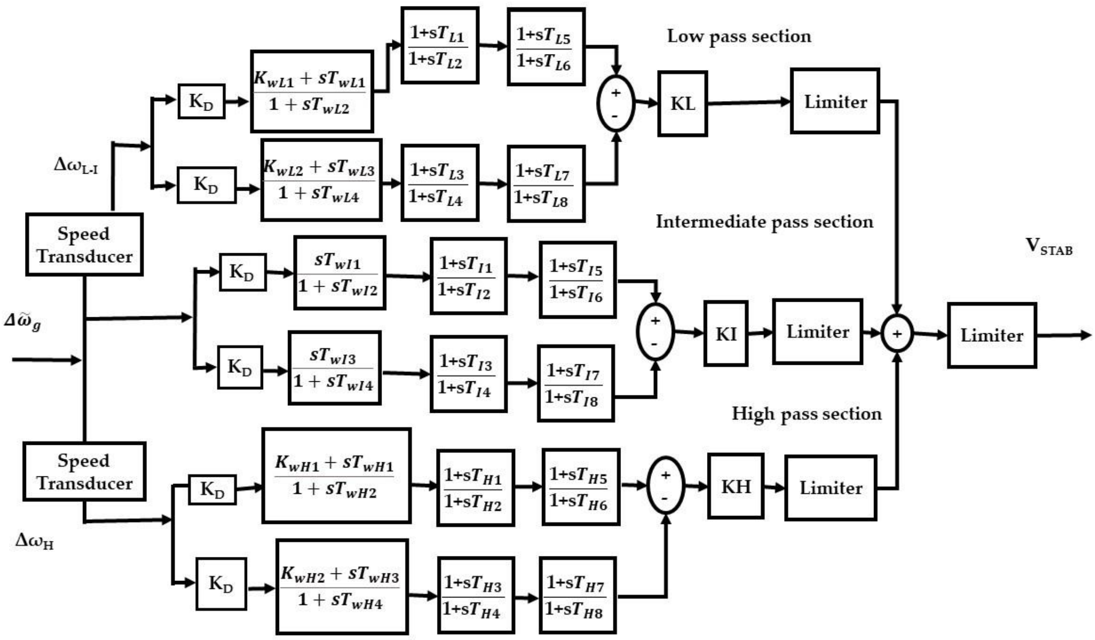

Fig. 3.15: Block diagram of multi-band power oscillation damper.

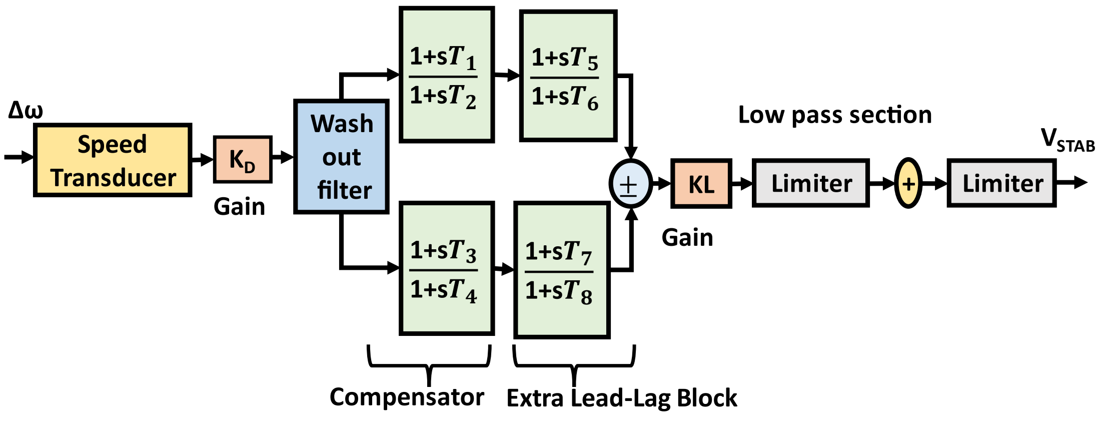

Fig. 3.16: A simple differential filter in each limb of a MB-POD.

3.3.2.8 Differential Filter Transfer Function:

It is simpler to analyze the MB-PSS structure when it is divided into smaller components. Fig. 3.16 shows a basic differential filter diagram of each limb. The transfer function of the differential filter will likely be revisited in the discussion, as it is the mathematical representation of how the filter affects the signals passing through it. Understanding the transfer function is key to tuning the filter's response characteristics to achieve the desired system performance.

The PSS being described is a sophisticated device with adjustable parameters that can be fine-tuned to stabilize specific frequency oscillations within a large power system. The multi-band approach allows for targeted damping, providing a robust solution to improve overall system stability. The differential filters' ability to offer phase lead precisely where needed adds to the PSS's effectiveness in managing complex stability challenges within the grid.

3.3.2.9 Tuning Procedure of Damping Controller Parameters

The value of R mentioned (taken as 1.2) is likely a parameter within the PSS4B that influences the response characteristics of the system. It could be related to the filter settings or a gain factor within the PSS4B, affecting how aggressively the PSS reacts to oscillations within the specified frequency bands. In power systems, stabilizers like the PSS4B are integral to the enhancement of damping, which improves system stability by allowing generators to quickly recover from disturbances and maintain synchrony with the grid. The description indicates that the PSS4B is a sophisticated tool with the flexibility to be fine-tuned to specific system needs, capable of addressing a wide range of oscillatory behaviours within a power system.

$$H(s) = \frac{Output}{Input} = \frac{1+T_1 s}{1+T_2 s} - \frac{1+T_3 s}{1+T_4 s} = \frac{(T_1+T_4-T_2-T_3)s+(T_1T_4-T_2T_3)s^2}{(1+T_2 s)(1+T_4 s)} = \frac{(T_1+T_4-T_2-T_3)s.\left(1+\frac{(T_1T_4-T_2T_3)}{(T_1+T_4-T_2-T_3)}s\right)}{(1+T_2 s)(1+T_4 s)} \quad 3.19$$

The transfer function of equation 3.19 will then be reduced as following equation 3.20:

$$H(s) = \frac{(T_2 - T_4)^2 s}{T_4(1 + T_2 s)(1 + T_4 s)} \quad 3.20$$

Using s=jω above H(s) can be written as equation 3.21:

$$H(s) = \frac{(T_2 - T_4)^2 j\omega}{T_4\left(1 - T_2T_4\omega^2 + j\omega(T_2 + T_4)\right)} \quad 3.21$$

With a center frequency between the two corner frequencies, 1=T_2 and 1=T_4, the structure functions as a band-pass filter. It is possible to select these corner frequencies to provide the desired phase response at a certain frequency. When equivalent gain is added before the differential filter, the phase-response will remain constant even as the magnitude grows. $T_2T_4\omega^2$ = 1 is the condition for the greatest value of the magnitude of H(s), and this value is derived in equation 3.22.

$$|H(s)|_{max} = \frac{(T_2 - T_4)^2}{T_4(T_2 + T_4)} = \frac{\frac{(1-R)^2}{R(1+R)}(R^2 - 2R + 1)}{R(1+R)} \quad 3.22$$

Where R = $\frac{T_2}{T_1} = \frac{T_4}{T_3}$. K is utilized to represent the greatest magnitude of the differential transfer function given in [108] as unity in order to obtain the gain. The differential gain K value is therefore as follows in equation 3.23:

$$\text{K} = \frac{1}{|H(s)|_{\text{m}}} = \frac{R(1+R)}{R^2 - 2R + 1} \quad 3.23$$

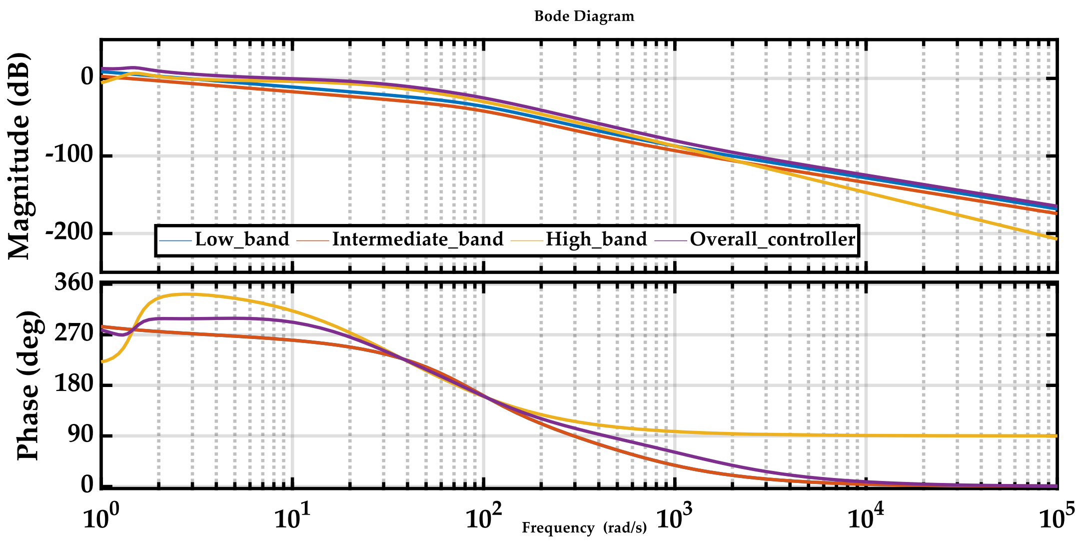

Fig. 3.17: Bode plot of the systems in the MB-POD controller of each frequency section.

Fig. 3.17 is a graphical representation of the frequency response of a system. It's commonly used in control theory and signal processing to show how the output of a system responds to a range of frequencies of the input. It consists of two graphs as magnitude and phase plots. Magnitude graph shows the amplitude gain (or attenuation) of the system in decibels (dB) versus frequency (in radians per second). The gain expresses how much the amplitude of the output signal is increased or decreased compared to the input signal at different frequencies. A value of 0 dB indicates that the output signal is the same amplitude as the input signal. Values below 0 dB indicate attenuation (output is smaller), and values above 0 dB indicate amplification (output is larger). Phase graph shows the phase shift introduced by the system versus frequency. Phase shift is the amount by which the output signal waveform is shifted with respect to the input signal waveform. It is measured in degrees, where 360 degrees corresponds to one full cycle of a sine wave. A positive phase shift means the output lags the input, while a negative phase shift means the output leads the input. This plot compares the frequency responses of multiple bands. This kind of plot is instrumental for designers of electronic filters, control systems, and anywhere system dynamics need to be understood and manipulated across a range of frequencies. A multi-band damping controller may require tuning to ensure that it provides the necessary damping without causing excessive attenuation or phase lag that could affect the performance.

3.3.2.10 Data Setting of MB-POD

Unlisted parameters in the PSS4B configuration default to zero, indicating that any block or parameter not explicitly used or defined within the system is not contributing to the PSS's output. This allows for a more streamlined and efficient design, focusing on the essential components needed for stabilization. Table 3.3 outlines the data settings of the MB-POD, detailing the specific configurations and parameters used in the system.

Table 3.3 Data setting of MB-POD

Frequency bands					
Low Frequency (LF)		Intermediate Frequency (IF)		High Frequency (HF)	
T_{L1}	0	T_{I1}	0	T_{H1}	0
T_{L2}	0	T_{I2}	0	T_{H2}	0
T_{L3}	6.6040	T_{I3}	0.66040	T_{H3}	0.0334
T_{L4}	7.9248	T_{I4}	0.79248	T_{H4}	0.0401
T_{L5}	0	T_{I5}	0	T_{H5}	0
T_{L6}	0	T_{I6}	0	T_{H6}	0
T_{L7}	0	T_{I7}	0	T_{H7}	0
T_{L8}	0	T_{I8}	0	T_{H8}	0
T_{wL1}	5.5033	T_{wI1}	0.55033	T_{wH1}	0.0278
T_{wL2}	6.6040	T_{wI2}	0.66040	T_{wH2}	0.0334
T_{wL3}	0	T_{wI3}	0	T_{wH3}	0
T_{wL4}	0	T_{wI4}	0	T_{wH4}	0
K_{wL1}	1	K_{wI1}	1	K_{wH1}	1
K_{wL2}	1	K_{wI2}	1	K_{wH2}	1
K_D	66	K_D	66	K_D	66
KL	10	KI	5	KH	10
VL_{max}	0.075	VI_{max}	0.15	VH_{max}	0.15
f_l	0.0219 Hz	f_i	0.219 Hz	f_h	4.34 Hz
VS_{max} = 0.15					

Where, $T_{L3} = T_{wL2} = \left(2\pi f_{l\sqrt{R}}\right)^{-1}$, $T_{L4} = T_{L3}*R$, $T_{wL1} = T_{L3}/R$, R = 1.2, $T_{I3} = T_{wI2} = \left(2\pi f_{i\sqrt{R}}\right)^{-1}$, $T_{I4} = T_{I3}*R$, $T_{wI1} = T_{I3}/R$, $T_{I3} = T_{wH2} = \left(2\pi f_{h\sqrt{R}}\right)^{-1}$, $T_{H4} = T_{H3}*R$, $T_{wH1} = T_{H3}/R$

3.4 CONCLUSION

An ESS-controller for a microgrid, which includes a POD controller, uses an AC-DC three-level PWM converter with an LCL filter and series damper at the PCC to reduce harmonics. The system features two main control loops: an inner current control loop with a PI controller for rapid response and an outer loop for voltage and frequency stabilization. A PLL and measurement blocks ensure synchronization with the grid. A power limiter prevents excessive power output, and a damping controller within the LFOs Control section suppresses power oscillations, enhancing stability. The PWM Pulse Generator creates gate signals for the converter.

The stability analysis of the proposed damping controller, integrated within an energy storage system with a multi-band structure, demonstrated improved power oscillation mitigation across multiple frequency bands. Bode analysis identified optimal proportional integral gains for system stability and performance. Time-domain simulations confirmed the controller's robustness under various conditions. This multi-band approach enhances system stability and reliability, addressing the complexities of modern power systems.

Further research is needed to test the controller in diverse power system models and real-world scenarios. The chapter establishes a strong foundation for the proposed damping controller's implementation and suggests avenues for further improvements to support the integration of renewable energy sources and the development of a more sustainable and stable electric grid.

Chapter 4

RESULTS AND PERFORMANCE ANALYSIS OF DAMPING CONTROLLER IN HYBRID AC MICROGRID SYSTEM

This chapter delves into the core attributes that distinguish the MB-POD from its single-band counterparts, including enhanced damping capabilities, robustness against system parameter variations, and flexibility in dealing with a wide spectrum of disturbances in the hybrid AC microgrid systems. The MB-POD's ability to maintain stability across a range of frequencies is particularly beneficial for modern power systems that are subject to varied and unpredictable challenges. We begin with a brief overview of power system oscillations and the need for effective damping mechanisms. We then discuss the operational principles of single-band damping controllers, laying the groundwork to appreciate the advanced features of the MB-POD. Subsequently, we compare the two types of controllers across several dimensions, including performance, complexity, and practical implementation considerations. The objective of this chapter is to provide a comprehensive understanding of the MB-POD's design philosophy and to illustrate its superiority through a systematic comparative analysis. By the end of the chapter, the reader will have a clear insight into the potential of multi-band damping controllers in hybrid AC microgrid system to enhance the stability and efficiency of modern power systems.

4.1 INTRODUCTION

The evolution of power systems, driven by the integration of RESs and the increasing complexity of grid operations, has necessitated the development of advanced control strategies. Among these, damping controllers play a pivotal role in maintaining system stability by mitigating power oscillations, which are a common occurrence in today's dynamic energy landscape. This chapter presents a comparative analysis of the newly proposed multi-band power oscillation damper and its predecessor, the traditional single-band damping controller. Traditionally, single-band damping controllers have been the industry standard, focusing on a specific frequency range to provide system stability. While effective within their operating band, the changing nature of power systems and the emergence of multiple oscillatory modes have exposed the limitations of such controllers. The advent of the MB-POD, which operates across multiple frequency bands, promises enhanced performance and adaptability.

This introduction sets the stage for a detailed examination of the MB-POD, positioning it within the context of evolving power system requirements and laying a foundation for the comparative analysis that follows.

4.2 RESULTS AND PERFORMANCE OF MULTI-BAND DAMPING CONTROLLER FOR DAMPING LOW FREQUENCY OSCILLATIONS IN HYBRID AC MICROGRID SYSTEM

4.2.1 System Modelling and Description

This article discusses two distinct kinds of systems: a hybrid AC microgrid system, a standalone AC microgrid system, and an interconnection of these two AC microgrid systems as transition disturbance. The parts used in all the systems came from MATLAB/Simulink.

4.2.1.1 Hybrid AC microgrid system

A hybrid AC microgrid system consists of two PV systems, one ESS, one diesel generator, one wind generator, and constant power loads, as shown in Fig. 4.1. The power generation capacity of the AC microgrid system is 1000 kW at 400 V AC bus voltage and 50 Hz frequency. As the DGs operate stochastically, a 550 kVA ESS is connected to the system's AC bus to provide backup power. As a backup power system, ESS and diesel generators are generally utilized to outweigh the stochasticity of wind and solar energy. The AC microgrid system is comprised of two PV farms producing 500 kW, a wind generator producing 350 kW, and a diesel engine providing 150 kW. The system is connected to the distribution feeder by a 11kV/400V distribution transformer at the point of common coupling, where voltage and frequency are measured.

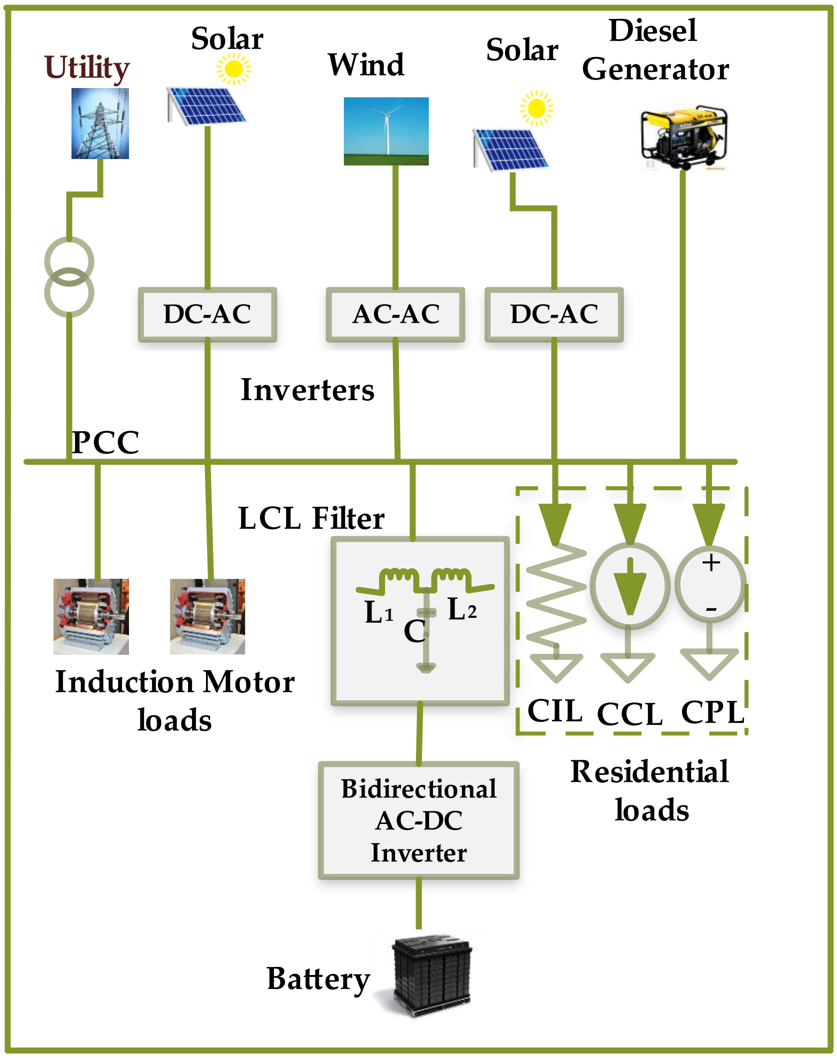

Fig. 4.1: Schematic diagram of a Hybrid AC Microgrid System.

4.2.1.2 Standalone AC microgrid system

Fig. 4.2 depicts a stand-alone AC microgrid with 850 kW of total generation capacity, 500 kW from solar panels and 350 kW from the wind turbine, all connected with a constant impedance load.

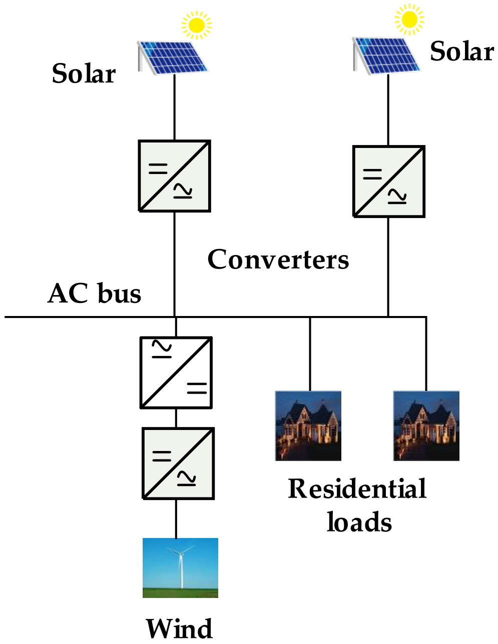

Fig. 4.2: Schematic layout of a standalone AC microgrid system.

4.2.1.3 Local Hybrid AC Microgrid to Interconnected Microgrid Transition

The interconnected AC microgrid system which is consisted of two AC Microgrids named hybrid AC microgrid and AC microgrid system with renewable energy is shown in Fig. 4.3. A stand-alone AC microgrid system is configured in AC microgrid system with renewable energy, whereas a microgrid system with renewable and non-renewable energy sources is configured in hybrid AC microgrid system. Both microgrids share common AC bus but connected with a static switch. They are holding the configuration of their respective systems. The interconnected AC microgrid system's total installed capacity is 1850 kW. At the point of common coupling and the microgrid connectivity point, static switches are situated. It is capable of independently isolating the microgrid from disruptions. This crucial step can eliminate the risk of transient phenomena when connecting microgrids to each other. Here, switches are also employed to comprehend how the EES behaved within the predetermined time.

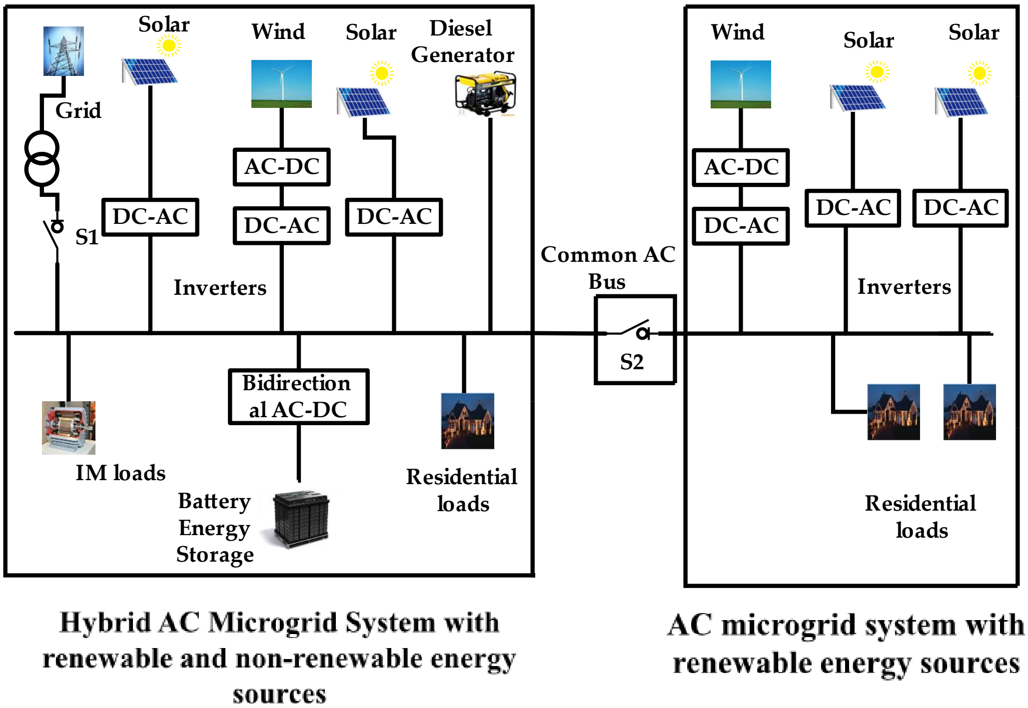

Fig. 4.3: Schematic layout of a local microgrid to interconnected microgrid transition.

4.2.2 Simulation Results

Microgrids are replacing traditional electric power infrastructures. Modern electricity networks include self-managing microgrids. Integrating DGs into microgrids improves stability, dependability, and economic optimality, which has boosted interest in interconnected microgrids research. AC microgrids are interoperable with the utility grid, which enhances the integration of DGs with the utility grid. This integration and load changes in any of the systems cause LFOs. These oscillations may occur locally or between microgrids. This section presents a multi-band damping controller for dampening local and inter-microgrid low frequency oscillatory modes. A hybrid AC microgrid system and an interconnected AC microgrid system have been investigated for both modes. Both systems are designed to operate in a MATLAB/Simulink environment, using the proposed multi-band damping controller as well as the existing single-band damping controller. Performance evaluations of the proposed controller are made using time-domain simulations. The multi-band damping controller is suggested based on simulation results, which show that it considerably improves both systems' oscillatory modes (local and inter-microgrid) in response to rapid load changes and connections to other microgrids, respectively. The performance of the proposed multi-band controller is evaluated using non-linear time-domain simulations. The key objective of this work is to assess AC microgrid systems during local and inter-microgrid oscillatory modes by providing a multi-band damping controller for the synchronous machines and comparing the performances with an existing single-band damping controller through time-domain simulations using MATLAB/SIMULINK. These simulations consider a variety of circumstances and disturbances that are present in both systems. The following possible outcomes were taken into consideration throughout the simulation studies and analyses that were carried out. Figure 4.4 illustrates the methodology for analysing oscillatory modes using a power oscillation damping controller, detailing the steps and techniques employed in the evaluation process.

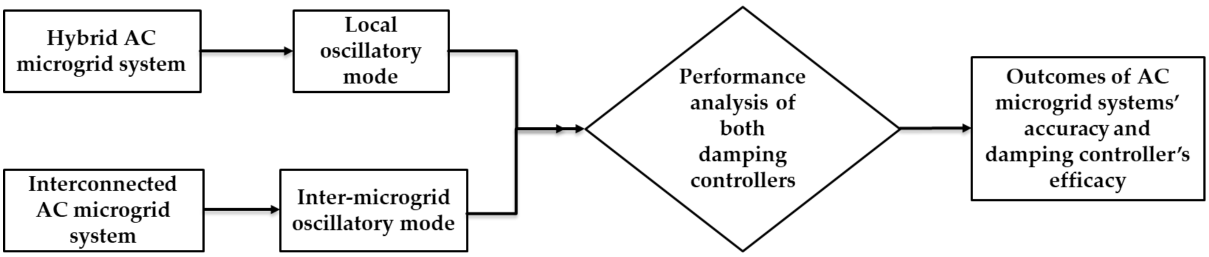

Fig. 4.4: Methodology for analyzing oscillatory modes using a power oscillation damping controller.

4.2.2.1 Hybrid AC Microgrid System with Proposed Multi-Band Damping Controller and the Existing Single-Band Damping Controller (37.5% Induction Motor Loads and 200kW Step Load)

A hybrid AC microgrid system like Fig. 4.1 has been developed to analyse the performance of the proposed damping controller. During the performance evaluation, the system was assumed to be running at 37.5 percent induction motor load with an 80 percent loading condition. The designed system included load-changing operations to compare the controller to the existing one. At time 2s, a 200-kW step load was added, and at time 3s, it was removed. Due to the sudden addition of loads, there was a fluctuation in the AC bus voltage and frequency, which has been graphed in Fig. 4.5(ii) and (iii). Fig. 4.5(i) demonstrates that the multi-band damping controller outperforms the current one by significantly reducing the speed deviation of the diesel generator during load changes and at the end of the simulation. Additionally, the rotor speed of an induction motor illustrated in Fig. 4.5(i) is significantly more stable with the suggested multi-band damping controller than it is with the present single-band damping controller. The proposed damping controller reduces the settling time of induction motor speed oscillations to approximately 2s. Introducing a multi-band dampening controller into this system has also resulted in a 1.5s reduction in the diesel generator's speed oscillation settle time. Consequently, the evaluation of findings reveals that a type of oscillatory mode, known as local mode, is sufficiently adjusted by the proposed damping controller.

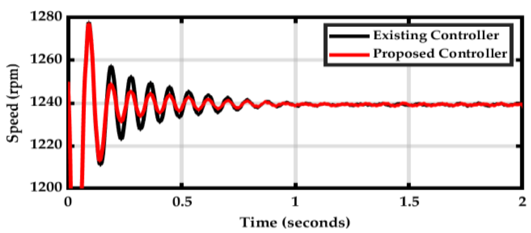

(i)

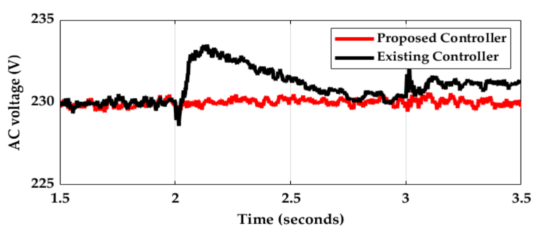

(ii)

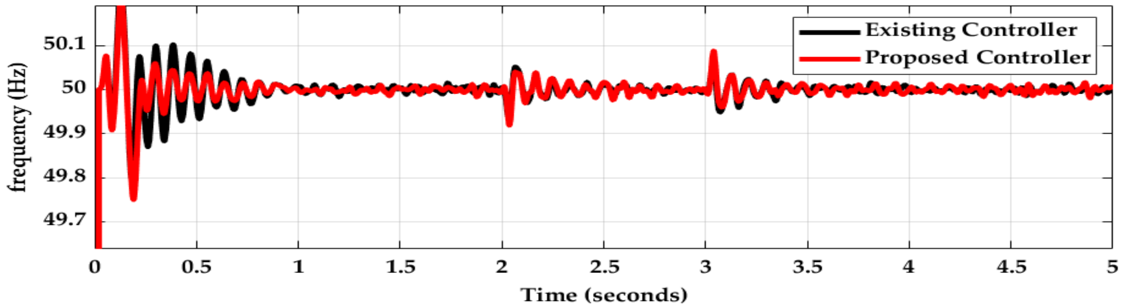

(iii)

Fig. 4.5: Hybrid AC microgrid system (i) IM speed, (ii) AC bus voltage, and (iii) AC bus frequency.

4.2.2.2 Interconnection of Two AC Microgrid with the Proposed Multi-Band Damping Controller and the Existing Single-Band Damping Controller (37.5% Induction Motor Loads and 200kW Step Load in Hybrid AC microgrid, 750kW Constant Power Load in Stand-Alone AC microgrid)

A hybrid AC microgrid system is connected to a standalone AC microgrid system to build an interconnected AC microgrid system, similar to the one in Fig. 4.3, in order to examine the performance of the suggested damping controller for another oscillatory mode can be named as inter-microgrid mode. The system generates a total of 1850 kW from both microgrids, with hybrid AC microgrid contributing 1000 kW and stand-alone AC microgrid contributing 850 kW. Hybrid AC microgrid was operating with 37.5 percent induction motor load having loading condition of 80 percent, but stand-alone AC microgrid was operating with an almost 88 percent constant impedance loading condition. An interconnection of two separate systems has been carried out in order to compare the performance of the proposed multi-band damping controller with the existing single-band one. In hybrid AC microgrid, a 200-kW step load was added at time 2 and withdrawn at time 3. At the same time, stand-alone AC microgrid with a 750-kW constant power load was also getting connected to hybrid AC microgrid concurrently to form an interconnected AC microgrid system. Consequently, there was a fluctuation in the interconnected AC microgrid system's bus voltage and frequency, which has been graphed in Fig. 4.6(iii) and (iv) due to the unexpected addition of loads and another microgrid. Fig. 4.6(ii) shows that by drastically lowering the diesel generator's speed deviation during load changes and connection to another microgrid, the multi-band damping controller surpasses the single-band damping controller. Moreover, compared to the current single-band damping controller, the recommended multi-band damping controller greatly increases the stability of the rotor speed of the induction motor shown in Fig. 4.6(i). After the step load in hybrid AC microgrid is removed, the proposed damping controller reduces the settling period of induction motor speed oscillations to roughly 0.3s. The diesel generator's speed oscillation settle time was also decreased by 0.4s when a multi-band dampening controller was added to this interconnected AC microgrid system. As a result, the examination of the results shows that the suggested damping controller adequately adjusts a form of oscillatory mode known as inter-microgrid mode rather than the existing one.

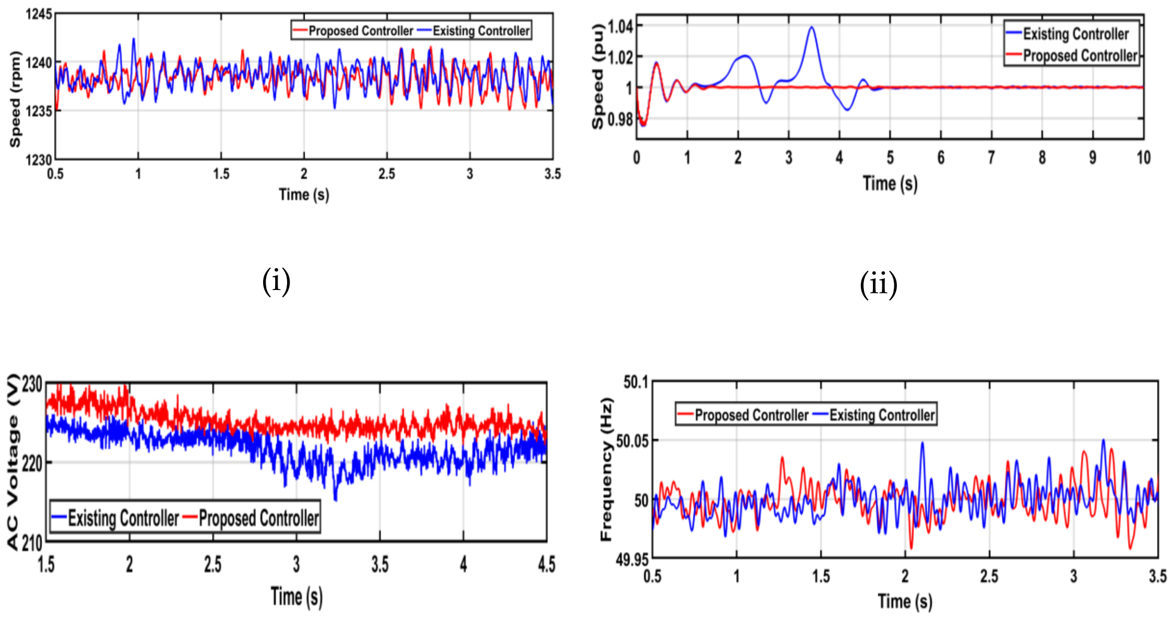

(i) (ii)

(iii) (iv)

Fig. 4.6: Interconnected AC microgrid system (i) IM rotor speed, (ii) Diesel generator speed deviation, (iii) AC bus voltage, and (iv) AC frequency.

4.2.2.3 *Comparative analysis*

The successful operation of an interconnected AC microgrid system demonstrates that system voltage and frequency have been maintained steadily over time. However, a low frequency oscillation developed in the system as a result of asynchronous loads, disturbances, and microgrid connections. To reduce this oscillation, an advanced multi-band damping controller is proposed in this paper. In this study, an advanced multi-band damping controller is suggested for decreasing this oscillation. This is accomplished using a multi-band power system stabilizer acting as a damping controller in an individual AC microgrid system and a system of interconnected AC microgrids that exhibit symmetrical gain behaviour around well-separated centre frequencies for each band. This study compares single-band and multi-band dampening controllers for reducing low-frequency oscillations in an individual and interconnected AC microgrid system. While dampening of local and inter-microgrid modes of oscillation is achieved by the proposed controllers, the symmetrical separation of this controller helps to prevent detrimental impacts on all types of oscillation modes. This paper's major goal is to evaluate the performance of the multi-band damping controller in comparison to the current one under various conditions. The stability analysis and simulation findings show that the damping controller is more successful than the single-band damping controller at reducing oscillations in the power system. As a result, the demonstration of the proposed multi-band damping controller for an individual AC microgrid and the interconnected AC microgrid system in this research ensures its effectiveness. The research study's findings can be summarized as follows:

- The low-frequency local oscillation mode (fluctuations in AC bus voltage and frequency, instability in IM rotor speed, and increased speed deviation of the diesel generator), which is triggered by a sudden load rise in a single AC microgrid system, is significantly dampened by the suggested multi-band damping controller.

- After load changes and the connection of a microgrid, another inter-microgrid oscillation mode with a low frequency emerges. The proposed multi-band damping controller aids greatly in restoring the diesel generator's speed and the rotor speed of the induction motor for the interconnected AC microgrid system.

4.3 RESULTS AND PERFORMANCE ANALYSIS OF MULTI-BAND DAMPING CONTROLLER FOR HYBRID AC MICROGRID SYSTEM ON MULTIPLE DYNAMIC LOADS PENETRATION

MGs have emerged as a promising solution to enhance the reliability and sustainability of modern power distribution systems. In recent years, there has been a growing interest in interconnecting multiple microgrids to create more resilient and efficient energy networks. However, the performance of interconnected microgrid system illustrated in Fig. 4.7 under various dynamic load scenarios configured in Fig. 3.10 remains a critical research area. In this section, problems like LFOs and the dynamic performance of multiple IMs in microgrids instead of a single motor with the same rating under a wide range of operating conditions are looked at. A single microgrid and an interconnected microgrid are two alternative model configurations designed in MATLAB/Simulink that are considered in this study's comparison of non-linear dynamic simulations. The findings show that, compared to a local microgrid system, the performance of an interconnected microgrid system is more susceptible to being impacted by several parallel IM loads. Furthermore, it has been discovered that large IMs have lower LFO damping capabilities than parallel multiple small IMs.

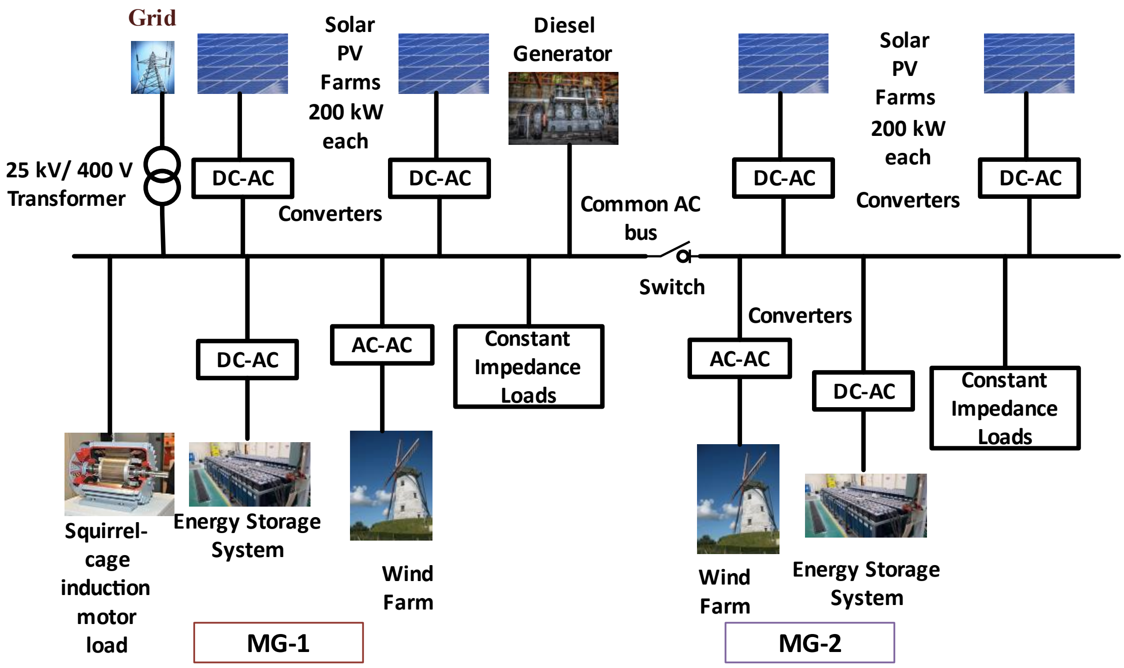

Fig. 4.7: Configuration of an interconnected microgrid system.

4.3.1 Description of the Simulation Platform

4.3.1.1 Hybrid AC microgrid System

Hybrid AC microgrids are small energy systems that can work alone or with the grid. Their ability to combine RESs, energy storage systems, conventional generators, and various loads makes them unique. The hybrid microgrid system is made up of several components, including two PV systems, one ESS, a diesel generator, a wind generator, constant impedance loads, and induction motor loads. This system is illustrated in Fig. 4.7 as MG-1. This system has a power generation capacity of 900 kW, operates at a 400 V AC bus voltage, and has a frequency of 50 Hz. To deal with the variability in power generation from renewable sources like wind and solar, a 200 kVA ESS is connected to the AC bus to provide backup power when needed. Both the ESS and the diesel generator are used as backup power sources to counter the unpredictable nature of wind and solar energy. This microgrid comprises two PV farms generating 200 kW each, a 350-kW wind generator, and a 150-kW diesel generator. The system is linked to the distribution feeder through a 11 kV/400 V distribution transformer at the PCC.

4.3.1.2 Interconnected Microgrids Transition

Interconnected microgrids are a network of two or more neighboring local microgrids that are physically connected and capable of working together seamlessly. The interconnected microgrid system comprises two parts: MG-1 and MG-2, as depicted in Fig. 4.7. MG-2 is designed as another local microgrid system with two PV systems of 200 kW each, a 350-kW wind farm, a 200 kVA energy storage system, and constant impedance loads. Both microgrids share a common AC bus but are connected through a static switch. They each maintain their own unique configurations. The combined installed capacity of the interconnected microgrid system is 1650 kW. There are individual VSIs for each distributed generation and an ESS with a damping control architecture in each microgrid [32]. Frequency measurement employs a phase-locked loop.

To provide a comprehensive analysis of the microgrid's performance under various dynamic conditions, this study aims to conduct an in-depth examination of both local and interconnected microgrids, focusing on their behaviour when induction motors are introduced as dynamic load conditions. Time-domain simulations will be carried out using MATLAB/SIMULINK to capture the nuanced interactions within the microgrid systems. Additionally, the robustness of the proposed microgrid configurations will be demonstrated through non-linear dynamic simulation techniques, which will include the application of step load disturbances, and the implementation of a multi-band damping controller illustrated in Fig. 4.8. This integrated approach will reveal how effectively the microgrid can maintain stability and operational integrity in response to the dynamic characteristics of various induction motor loads.

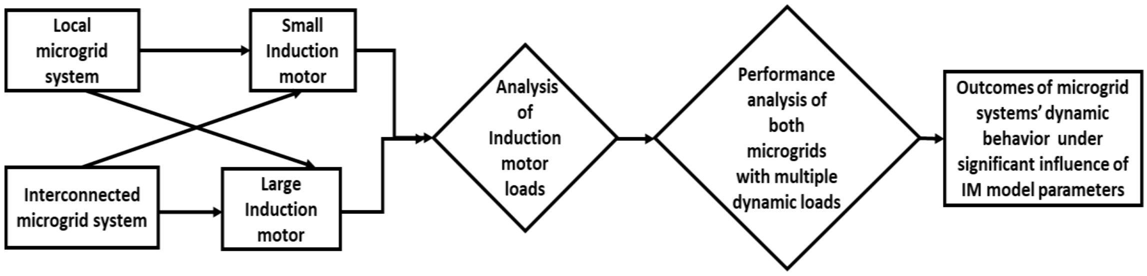

Fig. 4.8: Methodology for analyzing the performance of microgrid systems on multiple dynamic loads penetration.

4.3.2 Simulation results

The performance of the two microgrid systems was evaluated considering LFO characteristics using nonlinear dynamic simulations that considered small and large IM loading patterns with equal power ratings as well as disturbances in the microgrid systems. The simulation and analysis were done while comparing the dynamic performance of 40 parallel 5.4-hp (4 kW) IMs and a 215-hp (160 kW) large IM at the different microgrid systems. The following scenarios are considered for dynamic simulation studies and analysis:

4.3.2.1 Case 1: Hybrid Microgrid System Taking into Consideration 15.09% of IM Loading Patterns under 37.74% of Load Disturbances for Several Small IMs and a Large IM Separately

In this case study, the hybrid microgrid system has been considered among the two types of microgrid configurations stated before. The local microgrid has a 900-kW total generation capacity and is operating at 73.33% loading (with a 500-kW constant impedance load and a 160-kW IM load). At t=2s, a 400-kW step load is added to cause the disturbances. At t=3s, the load is withdrawn, and the performances of the microgrid system are recorded for further analysis. AC microgrid system's point of common coupling voltage and frequency are illustrated in Fig. 4.9 (a) & (b) respectively. Furthermore, when a 400-kW step load is introduced into the microgrid, single IMs loading exhibits a maximum frequency of 49.89 Hz whereas, 49.86 Hz frequency holds for multiple small IMs loading condition. With the increase in IM loading numbers within equal power ratings, 4 volts of system voltage are fluctuating during the starting of the motor. The voltage and frequency oscillations in the microgrid system are caused by load disturbances. Voltage and frequency fluctuations within the microgrid can lead to rotor speed oscillations for several reasons. Firstly, the power consumption of IMs, including both active and reactive power, is affected by variations in the stator voltage and rotor speed. Secondly, fluctuations in frequency directly induce oscillations in the rotor speed of induction motors. Lastly, alterations in rotor speed can, in turn, impact power consumption which is seen in Fig. 4.9 (f) at time t=2s when a step load of 400-kW is injected into the system. The ESS's output power in Fig. 4.9 (d) indicates that when a step load is introduced, it supplies approximately 71 kW of active power for a single large IM, whereas it provides only 41 kW for multiple smaller IMs. Diesel generators are typically rated to handle brief overloads, but if the combined inrush current of all the motors exceeds the generator's capacity, it can lead to a speed deviation which is visible in Fig. 4.9 (c). For a single large IM, the diesel generator speed deviation is lower than the multiple small IMs. As a result, a type of LFOs introduced in [32] is getting more severe for multiple small IMs in a hybrid microgrid system. Table 4.1 provides a performance comparison, highlighting the key metrics and outcomes for evaluating the effectiveness and efficiency of various systems or methodologies under consideration.

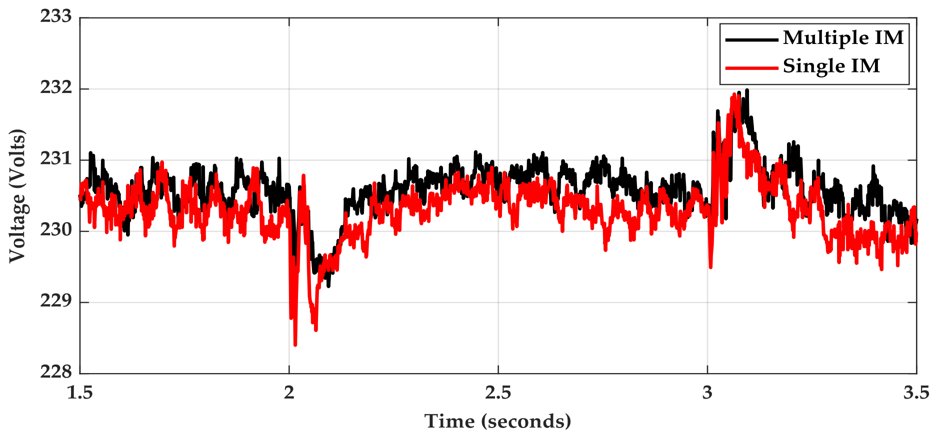

(a)

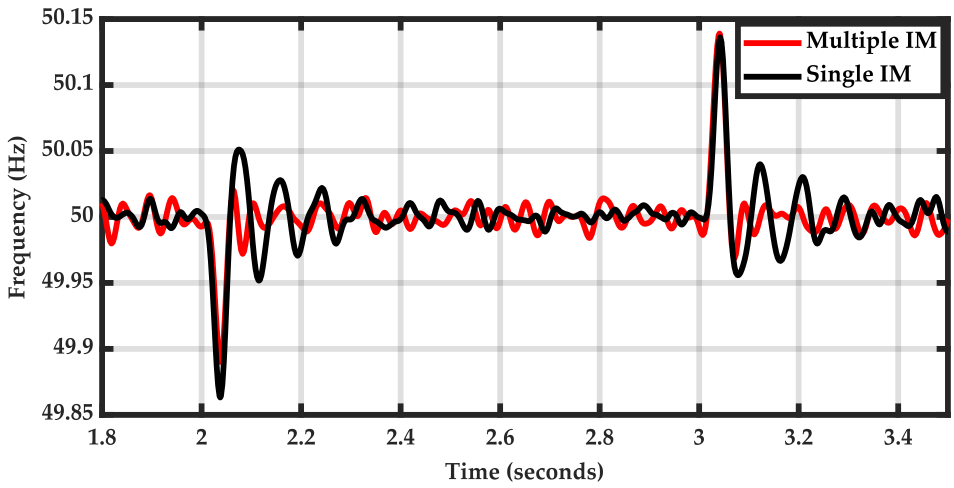

Multiple IM
Single IM
Frequency (Hz)
Time (seconds)
50.15
50.1
50.05
50
49.95
49.9
49.85
1.8
2
2.2
2.4
2.6
2.8
3
3.2
3.4

(b)

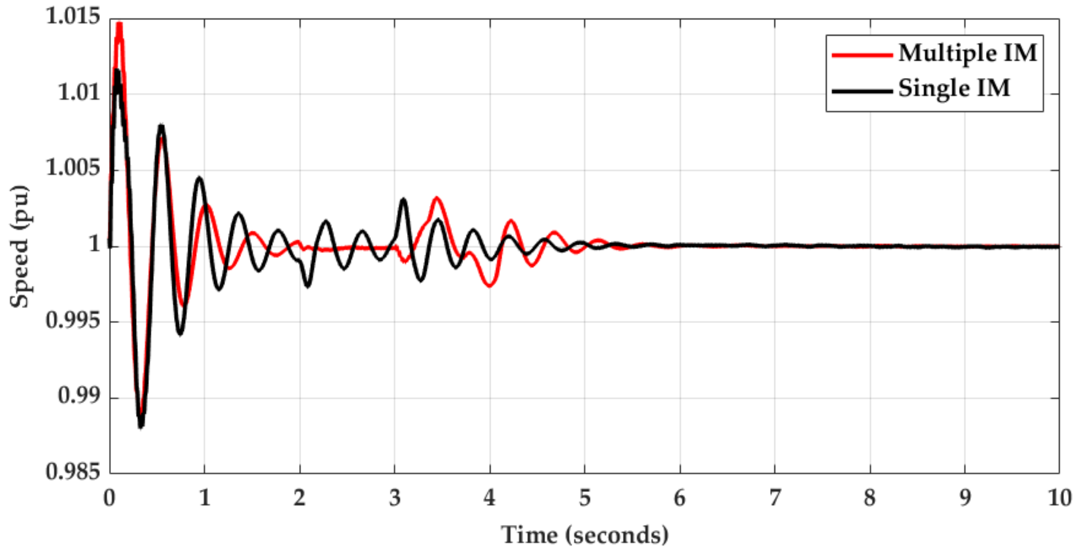

Multiple IM
Single IM
Speed (pu)
Time (seconds)
1.015
1.01
1.005
1
0.995
0.99
0.985
0
1
2
3
4
5
6
7
8
9
10

(c)

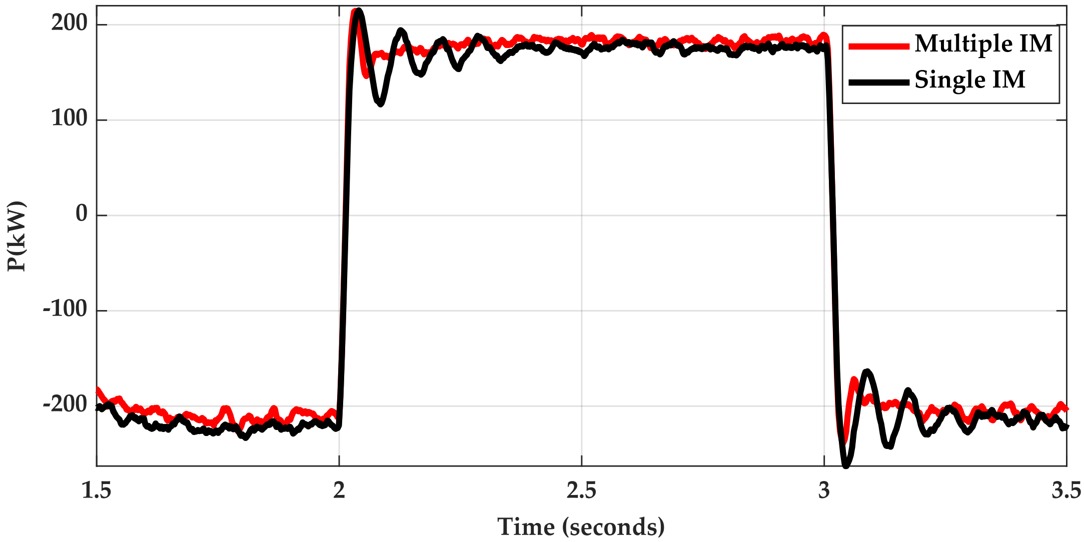

200
100
0
-100
-200
P(kW)
1.5
2
2.5
3
3.5
Time (seconds)
Multiple IM
Single IM

(d)

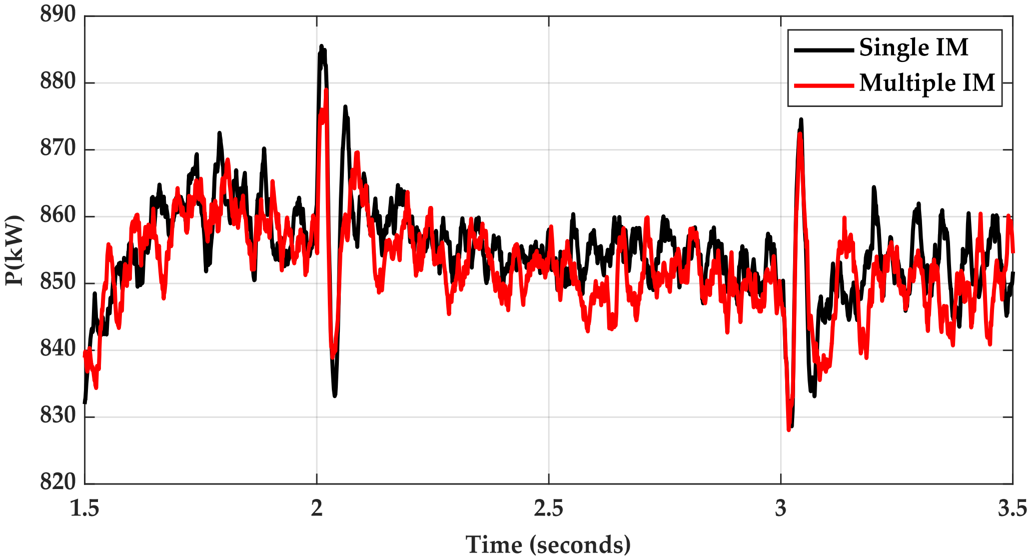

890
880
870
860
850
840
830
820
P(kW)
1.5
2
2.5
3
3.5
Time (seconds)
Single IM
Multiple IM

(e)

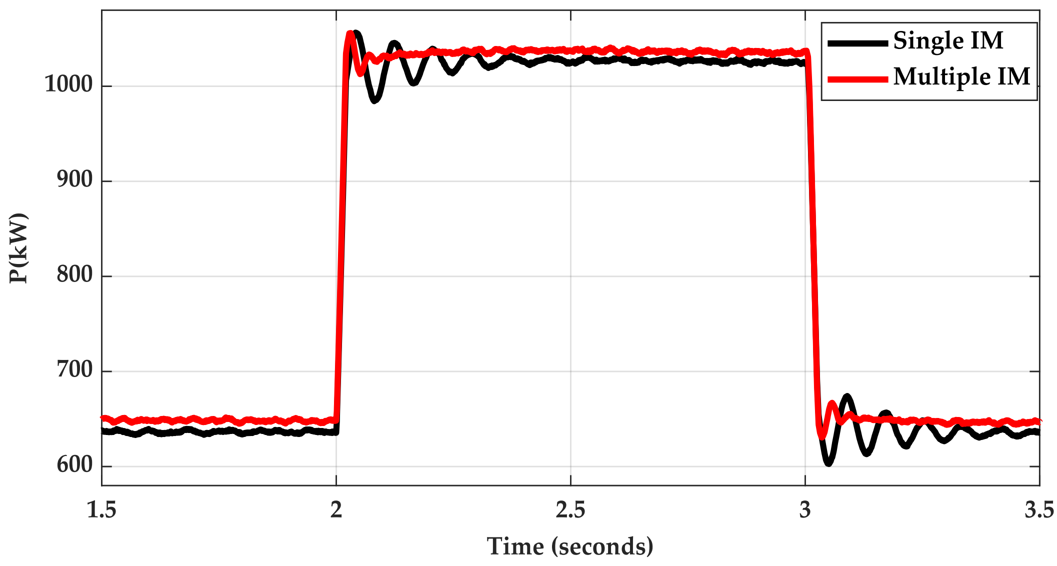

(f)

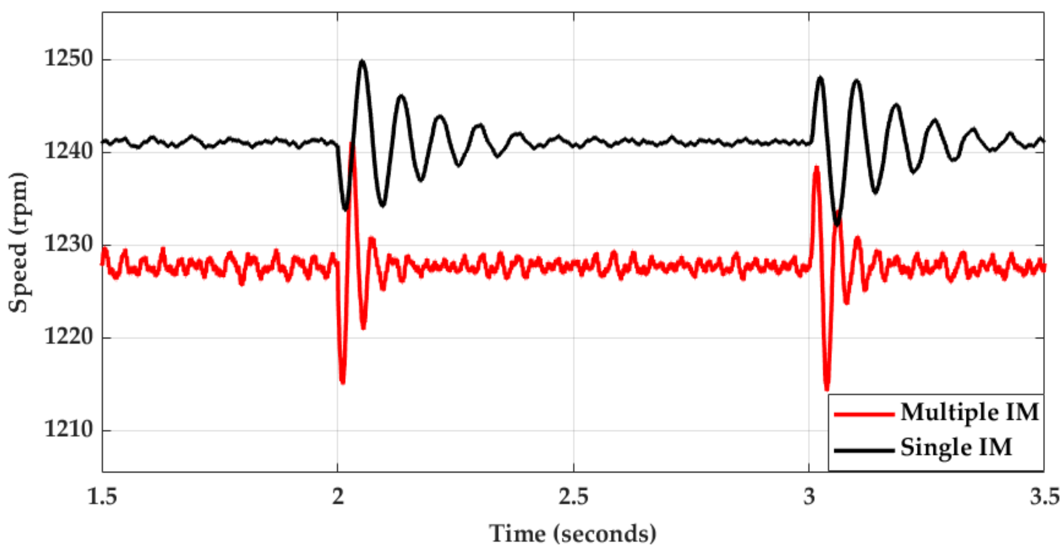

(g)

Fig. 4.9: Hybrid microgrid system with 15.09% of IM loading patterns under 37.74% of load disturbances for both several small IMs and a large IM condition, (a) AC system voltage, (b) AC system frequency, (c) Diesel generator speed, (d) ESS power sharing, (e) Power generation from microgrid, (f) Total load curve in microgrid, and (g) Induction motor speed.

Table 4.1 Performance comparison

Parameters	Multiple IM	Single IM
Maximum frequency range	49.86 Hz	49.89 Hz
Induction motor speed oscillation settling time	Third peak	Sixth peak
Power curves smoothened	First peak	Fifth peak
Diesel generator speed deviation (Starting)	0.0237 (pu)	0.026 (pu)

4.3.2.2 Case 2: Interconnected Microgrid System Taking Account of Both Several Parallel Small IMs and a Large IM Penetration Separately, with 15.09% of IM Loading under 37.74% of Load Disturbances in MG-1 and 53.33% of Lading Condition under 26.32% of Load Disturbances in MG-2

When the extra 200 kW constant impedance load is linked to the MG-2, it draws power from the MG-2. This decrease in power supplied from the MG-2 to the MG-1 causes a shortage of power in the MG-1. This power imbalance can cause voltage and frequency oscillations in the microgrid system. When step loads are introduced in both microgrids, it is seen in Fig. 4.10 (a) that the single IMs experience a comparatively smaller frequency deviation than multiple small IMs. As a result of this sudden change in load, the voltage of the common AC bus of the interconnected system starts to fluctuate as illustrated in Fig. 4.10 (b). To compensate for the power imbalance, the ESS connected to the PCC in the MG-1 is utilized, as shown in Fig. 4.10 (d-j). The rotor speed settled after about the sixth peak in the single IM case, but after the third peak in the multiple IM case and the settled duration is shorter in this case for this configuration of microgrid system illustrated in Fig. 4.10 (k).

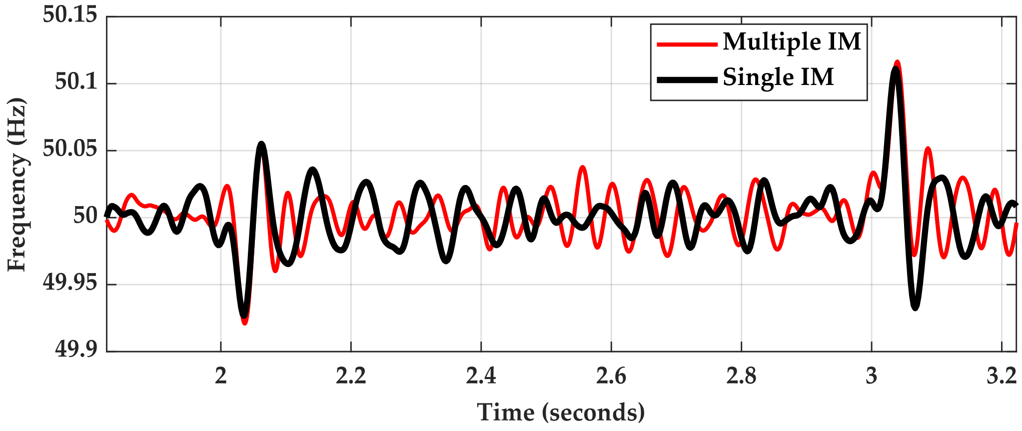

50.15
50.1
50.05
50
49.95
49.9
Frequency (Hz)
2
2.2
2.4
2.6
2.8
3
3.2
Time (seconds)
Multiple IM
Single IM

(a)

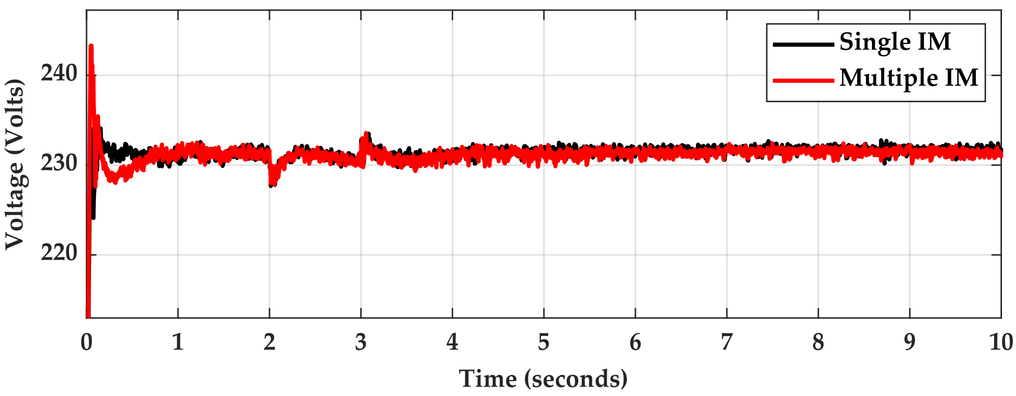

240
230
220
Voltage (Volts)
0
1
2
3
4
5
6
7
8
9
10
Time (seconds)
Single IM
Multiple IM

(b)

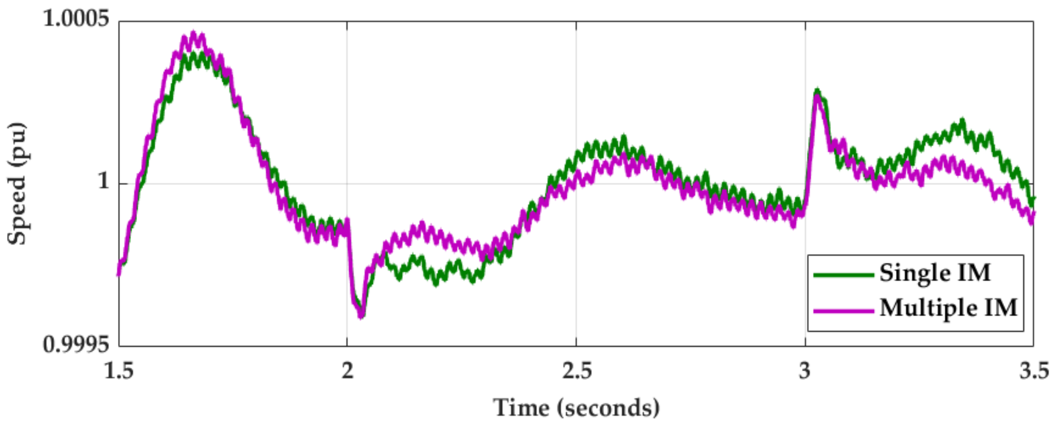

1.0005
1
0.9995
Speed (pu)
1.5
2
2.5
3
3.5
Time (seconds)
Single IM
Multiple IM

(c)

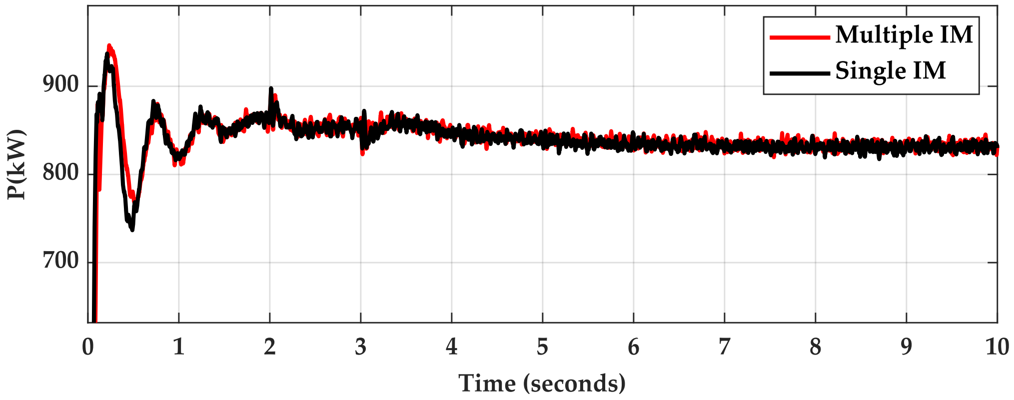
Multiple IM
Single IM
900
800
700
P(kW)
0
1
2
3
4
5
6
7
8
9
10
Time (seconds)

(d)

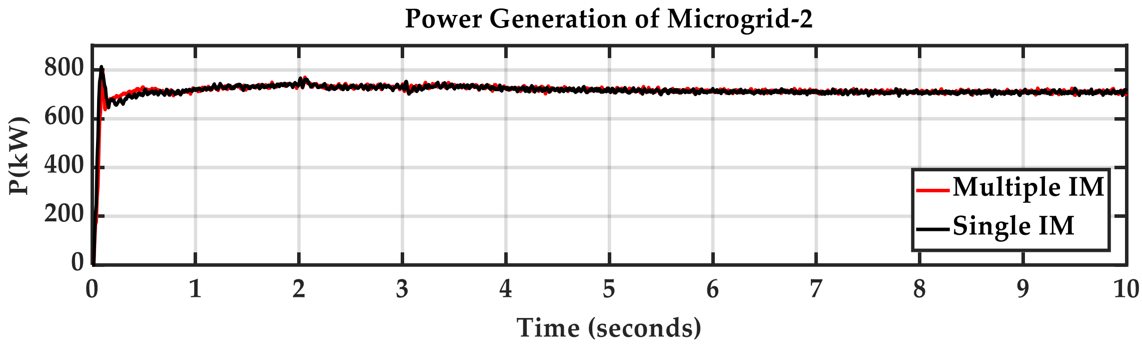
Power Generation of Microgrid-2
800
600
400
200
0
P(kW)
Multiple IM
Single IM
0
1
2
3
4
5
6
7
8
9
10
Time (seconds)

(e)

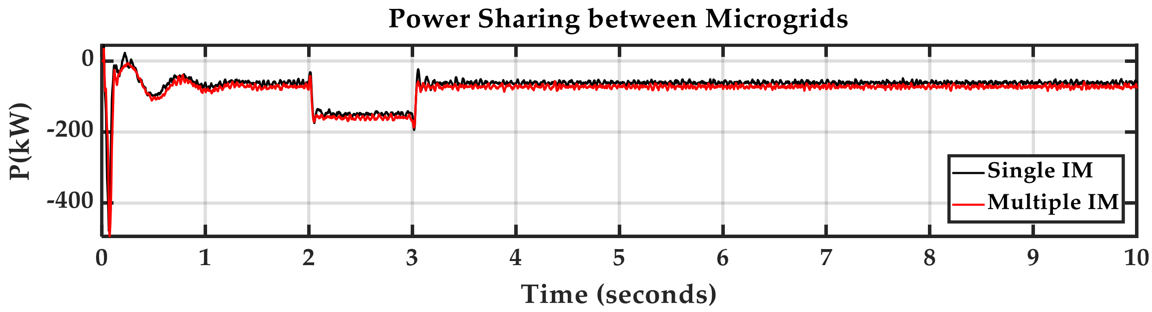
Power Sharing between Microgrids
0
-200
-400
P(kW)
Single IM
Multiple IM
0
1
2
3
4
5
6
7
8
9
10
Time (seconds)

(f)

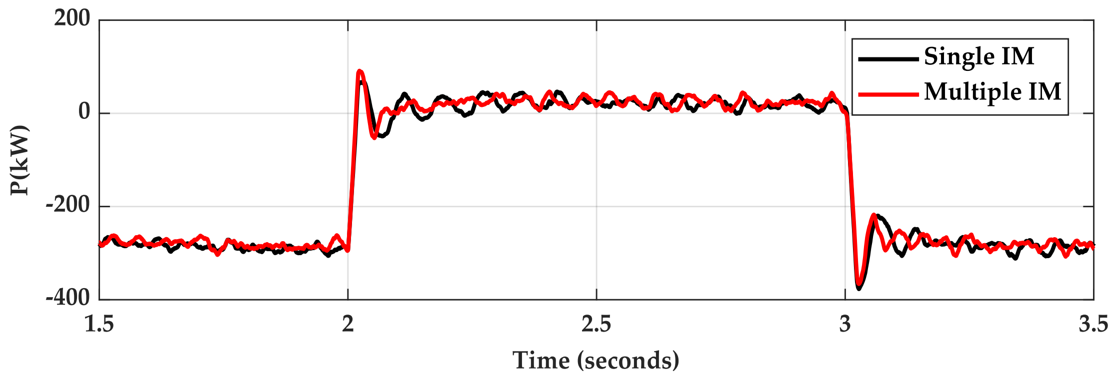
200
0
-200
-400
P(kW)
1.5
2
2.5
3
3.5
Time (seconds)
Single IM
Multiple IM

(g)

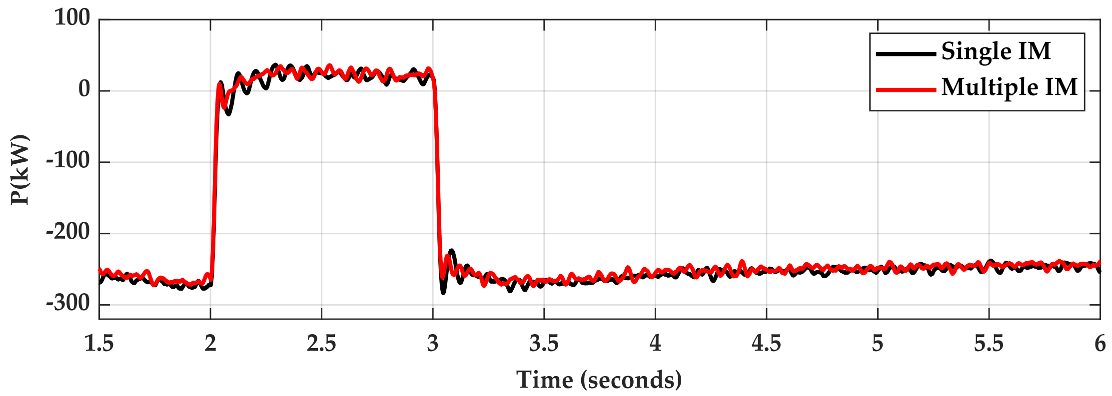
100
0
-100
-200
-300
P(kW)
1.5
2
2.5
3
3.5
4
4.5
5
5.5
6
Time (seconds)
Single IM
Multiple IM

(h)

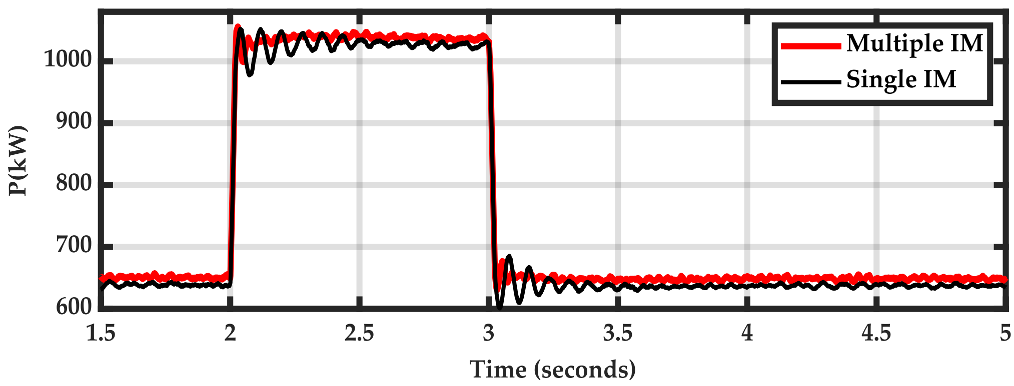
1000
900
800
700
600
P(kW)
1.5
2
2.5
3
3.5
4
4.5
5
Time (seconds)
Multiple IM
Single IM

(i)

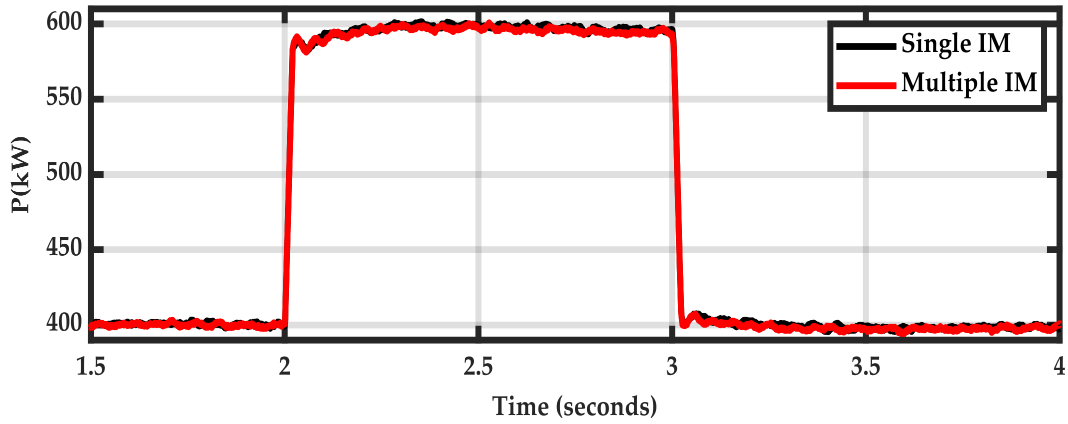

(j)

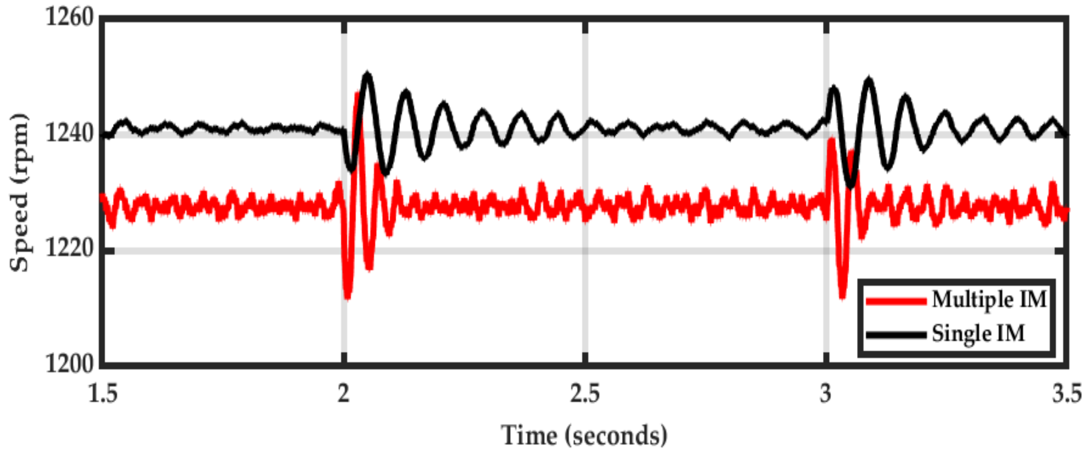

(k)

Fig. 4.10: An interconnected microgrid system with 15.09% of IM loading under 37.74% of load disturbances in MG-1 and 53.33% of loading condition under 26.32% of load disturbances in MG-2 for both several small IMs and a large IM condition, (a) AC system frequency, (b) AC system voltage, (c) Diesel generator speed, (d)Power generation of MG-1, (e) Power generation of MG-2, (f) Power sharing between microgrids, (g) ESS power of MG-1, (h) ESS power of MG-2, (i) Load power of MG-1, (j) Load power of MG-2, and (k) Induction motor speed.

4.3.2.3 A Comparative Study on Case 1 and Case 2 (between Hybrid and Interconnected Microgrids)

The Fig. 4.11 appears to be showing the speed response of induction motors in a microgrid system under different load conditions and cases, plotted over time. The speed is measured in revolutions per minute (rpm), and the time is in seconds. The graph illustrates the dynamic behavior of the induction motors when subjected to certain disturbances or load changes, which are common in microgrid applications. The variations in speed over time reflect how the motors' control systems respond to maintain their target operation speed. The responses show oscillations which may be due to the transient effects of the load application or removal. All the curves exhibit some degree of oscillatory behavior, which could be due to the application of a step load or another type of disturbance. Each curve eventually stabilizes, although the time it takes, and the stability level vary. This is indicative of the damping characteristics of the system and the effectiveness of any controllers in place. Comparing the 'Multiple IM' curves with 'Single IM' curves for both cases shows that having multiple induction motors in the system affects the speed response, suggesting interactions between the motors and the microgrid. There's a noticeable difference in the response between case 1 and case 2, implying that the load conditions or control settings in these two cases are different.

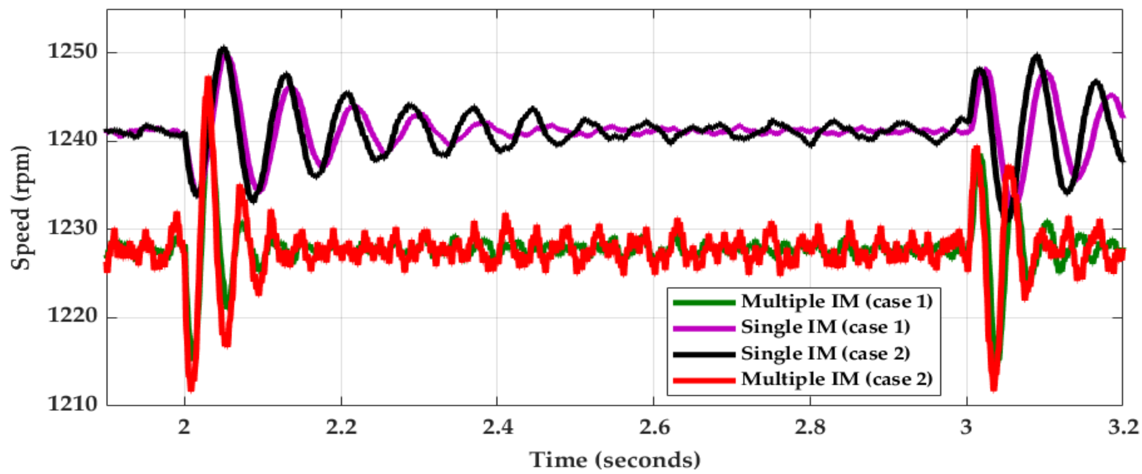

Fig. 4.11: Induction motor speed for case 1 and case 2.

4.3.2.4 Test mode 1: Interconnected Microgrid System Taking Account of Several Parallel Small IMs and a Large IM Penetration Separately, with 15.09% of IM Loading under 37.74% of Load Disturbances in MG-1 and 21.05% of IM Loading under 26.32% of Load Disturbances in MG-2

In this part, IM loading in both microgrids is introduced to better understand the dynamic behavior of both forms of IM. It is significant to notice that although the scenario has 26.32% load disturbances. The IM rotor speed and the system frequency are depicted in Fig. 4.12 (a) and (b), respectively. Additionally, Fig. 4.12 (c) and (d) show, respectively, the PCC voltage and the power sharing between microgrids. It is found that having numerous parallel working IMs increases non-linearity in the system dynamics. Furthermore, increasing dynamic loads (i.e., IMs) causes greater rotor speed oscillations and frequency deviations in the interconnected microgrid, necessitating higher damping torque. But the diesel generator's speed oscillation settle time is reduced by 0.2 seconds when a single IM is installed instead of the many IMs shown in Fig. 4.12 (e).

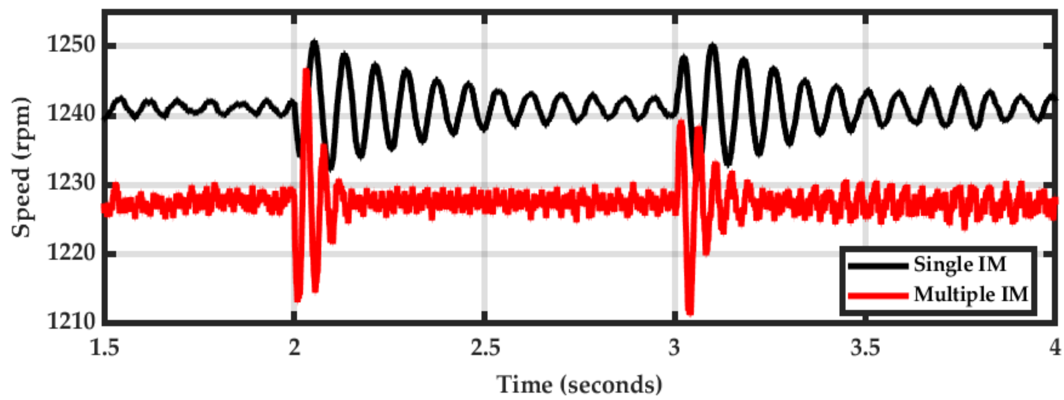

(a)

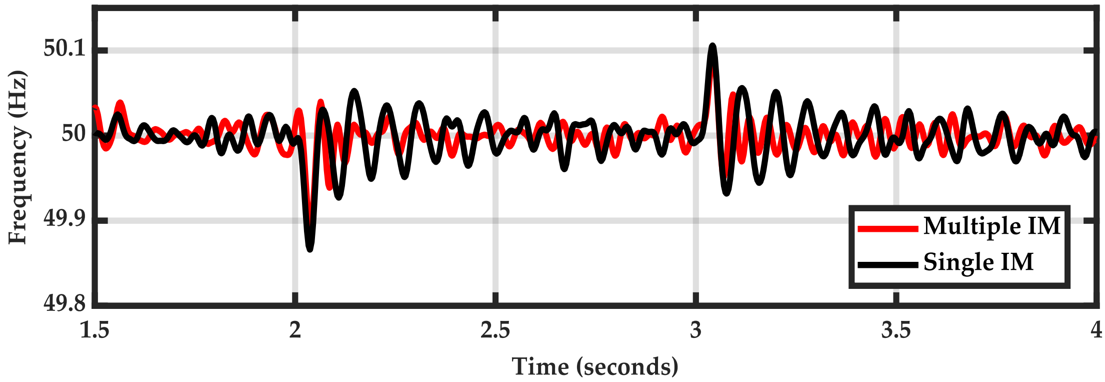
50.1
50
49.9
49.8
Frequency (Hz)
1.5
2
2.5
3
3.5
4
Time (seconds)
Multiple IM
Single IM

(b)

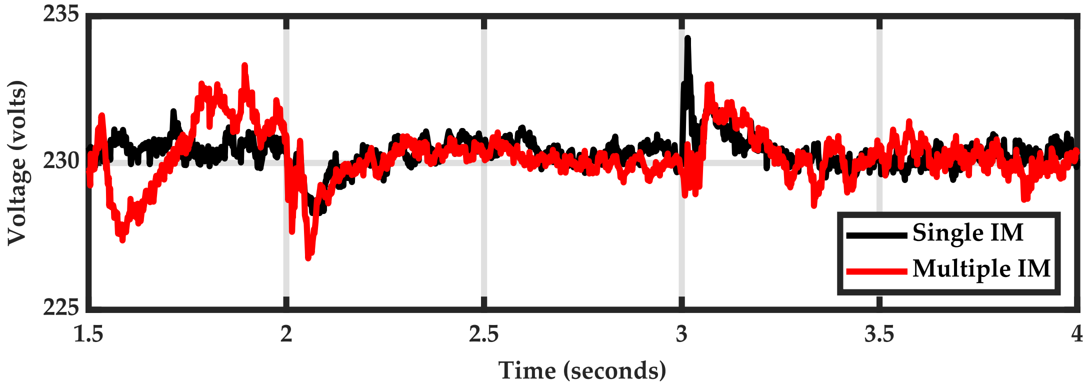
235
230
225
Voltage (volts)
1.5
2
2.5
3
3.5
4
Time (seconds)
Single IM
Multiple IM

(c)

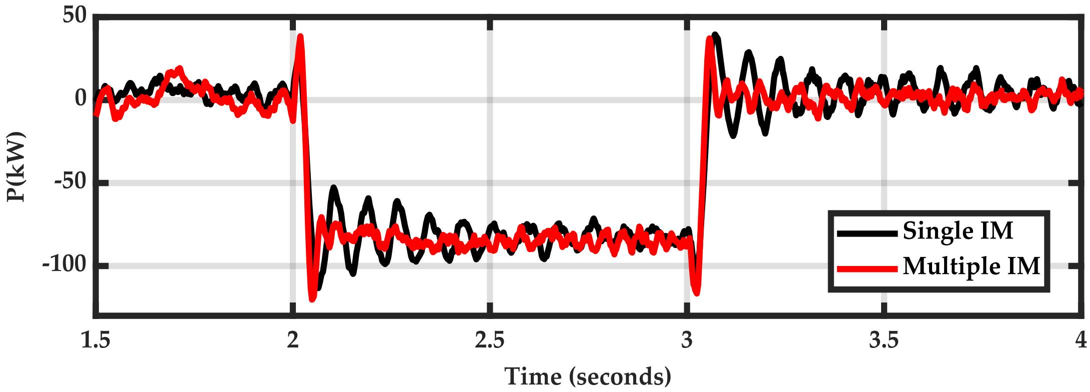
50
0
-50
-100
P(kW)
1.5
2
2.5
3
3.5
4
Time (seconds)
Single IM
Multiple IM

(d)

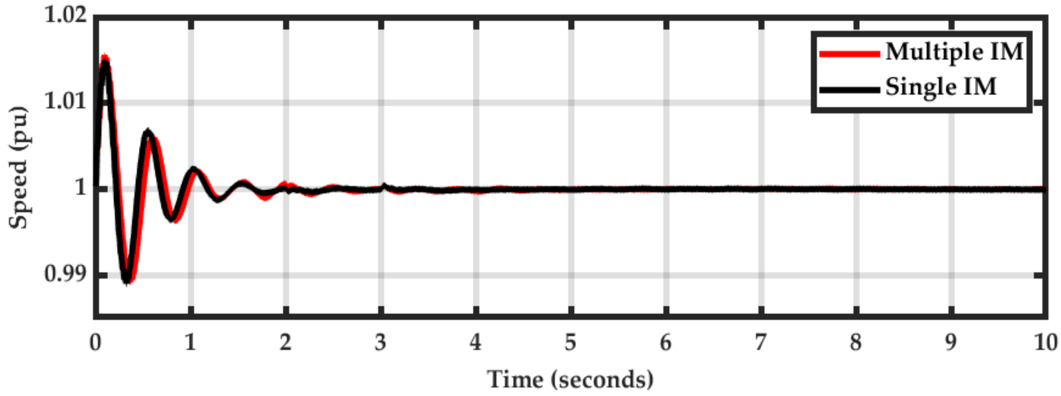

(e)

Fig. 4.12: An interconnected microgrid system with 15.09% of IM loading under 37.74% of load disturbances in MG-1 and 21.05% IM loading under 26.32% of load disturbances in MG-2 for both several small IMs and a large IM condition, (a) Induction motor speed, (b) AC system frequency, (c) PCC voltage, (d) Power sharing between microgrids, and (e) Diesel generator speed.

4.3.2.5 Test mode 2: Interconnected Microgrid System Taking Account of Both Several Parallel Small IMs and a Large IM Penetration in MG-1 with 22.22% of Each Type of IM Loading under 32.78% of Load Disturbances and 33.33% Multiple Parallel IM Load Penetration under 26.32% of Load Disturbances in MG-2

In this test scenario, MG-1 is subjected to both forms of IM loading, whereas MG-2 is subjected to multiple small IM loading categories. Fig. 4.13 (a) and (b) illustrate the rotor speeds of the small and big IMs with and without disturbances when both types of IMs are coupled in MG-1. Small IM exhibits a 30% greater speed deviation than without interruptions, but large IM shows a 25% greater speed deviation. As a result, it is revealed that multiple parallel operating IMs show more non-linearity than a large IM.

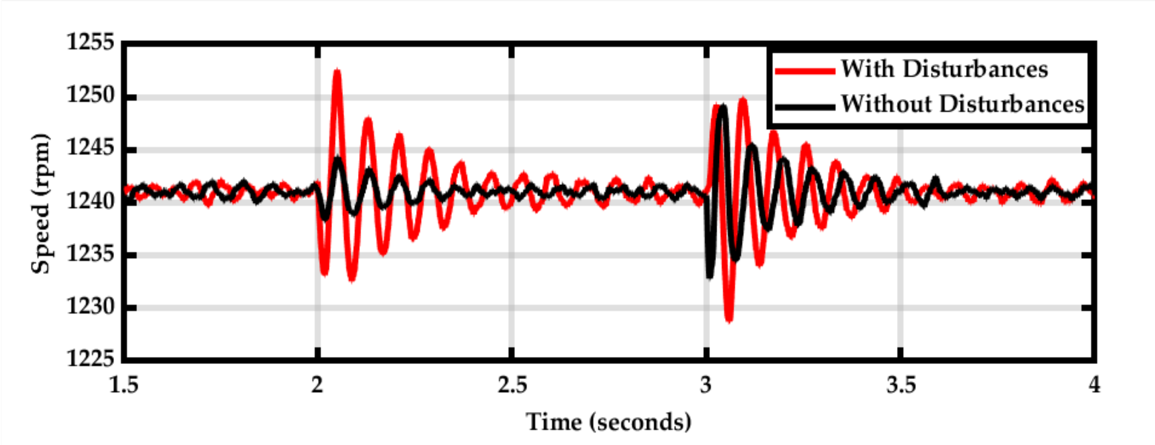

(a)

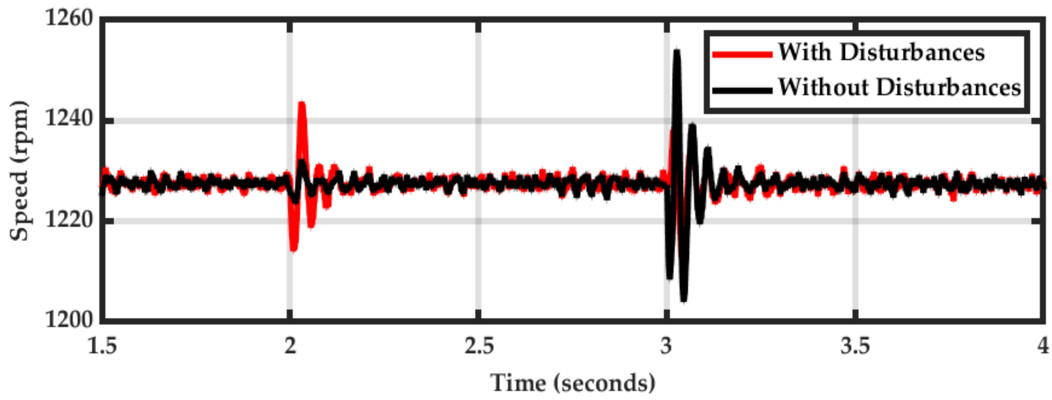

(b)

Fig. 4.13: Induction motor speed of MG-1 with and without disturbances, (a) Rotor speed of multiple small IM and (b) Rotor speed of large IM.

4.3.3 Comparative Analysis

These cases delved into the dynamic effects of introducing both small and large IM loads in microgrids. The findings of these simulations underscore the significant influence of IM model parameters, with rotor resistance emerging as the positive primary factor and stator resistance emerging as the negative secondary factor affecting its dynamic performance. Additionally, non-linear dynamic simulations of a large single induction motor or several small parallel induction motors with sudden load step changes for two microgrid configurations are used to examine the dynamic performance of IMs. It is obvious that the sudden load fluctuations have a major impact on the IM rotor speed, system frequency, and power sharing from energy storage systems.

4.4 CONLCUSION

Firstly, microgrids are gaining momentum as flexible and sustainable alternatives to traditional power distribution systems. Their ability to operate independently or in conjunction with the main grid, incorporating various distributed energy resources, enhances reliability and sustainability. The interconnectedness of multiple microgrids creates more resilient and efficient networks, capable of sharing resources and supporting dynamic loads.

The comparative analysis focused on the impact of dynamic loads, particularly multiple induction motors, on the stability and performance of both local and interconnected microgrid systems. The analysis emphasized that the performance of interconnected microgrid systems is more sensitive to the dynamics of multiple parallel induction motor loads, which can introduce low-frequency oscillations and affect overall system stability.

The implementation of a multi-band damping controller was proposed to sustain transient disturbances and improve stability. This controller was proven to be effective in dampening low-frequency oscillations in the microgrid systems under various load conditions, demonstrating an advantage over traditional single-band controllers.

In conclusion, the advancement of microgrid technologies, coupled with effective control mechanisms like the multi-band damping controller, paves the way for more robust and stable microgrid operations. These findings highlight the potential for significant enhancements in the performance of microgrid systems, ensuring they can meet future energy demands while accommodating the dynamic nature of various load types.

Chapter 5

RESULTS AND PERFORMANCE ANALYSIS OF PROPOSED POWER OSCILLATION DAMPING CONTROLLER IN THE INTERCONNECTED HYBRID AC MICROGRID SYSTEM

In the realm of modern power systems, maintaining stability and enhancing performance in interconnected networks is paramount. The proliferation of renewable energy sources and the subsequent development of hybrid ac microgrid systems have introduced complexities that challenge traditional power oscillation damping techniques. This chapter delves into the results and performance analysis of a proposed power oscillation damping (pod) controller specifically designed for interconnected hybrid ac microgrids. By addressing the dynamic interactions and inherent oscillatory behaviours within these sophisticated networks, the proposed pod controller aims to enhance system stability, improve reliability, and ensure efficient power distribution. The ensuing analysis provides insights into the controller's efficacy, showcasing its potential to mitigate oscillations and maintain robust performance in diverse operational scenarios.

5.1 INTRODUCTION

AC microgrids are increasingly used in power systems to accommodate DGs but managing multiple units within a single microgrid can be challenging. IMGs can help in system outages or power deficiencies, enhancing stability and mitigating load shedding. AC IMG architectures offer resiliency, efficiency, and distributed energy management. However, microgrid integration can lead to oscillatory modes and load disturbances, affecting stability and operational efficacy. The paper introduces an ESS-based POD designed to mitigate LFOs that addresses a significant concern regarding the stability and efficiency of interconnected microgrid systems. The study highlights the deficiencies in conventional power oscillation damping methods and proposes a novel MB-POD specifically designed for an interconnected hybrid AC microgrid system. The proposed MB-POD is compared to the existing SB-POD using time-domain simulations in a MATLAB/Simulink environment. The simulations and case studies demonstrate the effectiveness of the MB-POD in damping multiple oscillatory modes, improving system stability, and reducing transient response time. The findings suggest that the MB-POD offers substantial improvements over the SB-POD in enhancing the resilience and adaptability of interconnected hybrid AC microgrid system.

5.2 RESULTS AND PERFORMANCE OF MULTI-BAND POWER OSCILLATION DAMPING CONTROLLER IN AN INTERCONNECTED HYBRID AC MICROGRID SYSTEM

Typical microgrid oscillations include voltage and frequency. The microgrid may experience these variations as loads fluctuate. These variances are normally monitored and controlled within a small range to guarantee steady and reliable power supply to connected devices and equipment. If power demand spikes in the microgrid, voltage may dip before stabilizing. When a major power source, such as solar panels or wind turbines, fluctuates owing to environmental circumstances, the microgrid's frequency may oscillate slightly [127]. When two or more microgrids are connected, their controllers and load dynamics produce system oscillations that must be considered for the optimal microgrid design because IMGs have fundamentally different and low-inertia DGs. Variations reduce IMGs' stability and operation. IMGs are huge power systems with several converter-interfaced or synchronously interfaced dispersed generators and load sources, each with its structure and features. These systems are vulnerable to frequency fluctuations caused by even minor disruptions such as load shifts, dynamic load insertion, power sharing, IMG system architecture modifications, etc.

In this section, the modelling of typical AC IMGs shown in Fig. 3.1 is presented which has been developed in MATLAB/Simulink. The parameters used to regulate the various DGs were taken away from [32]. As IMGs, MG-1, MG-2, and MG-3 work together. One AC bus serves MG-1, MG-2, and MG-3. To maintain generality, the dynamic performance of MG-1 is being researched as the study MG. The second and third microgrids are external. Each microgrid has local loads, renewable and non-RESs, and a PCC to the upper-level distribution system. As a low voltage weak distribution microgrid, each cable connecting each DG to the AC sub-grid PCC has a reactance to resistance (X /R) ratio of 0.4. Each participating microgrid shares a 400V rms line-to-line AC bus with a 50 Hz system frequency.

The DC-to-AC interface uses VSIs to govern power exchange between microgrids and the AC bus. An AC-DC inverter connects the ESSs to the AC bus via an LCL filter with L_1 Inductors, C capacitors with R series damper, and grid-side L_2 inductors. Here, the technique of passive damping with a series damping resistor has been implemented [113]. Microgrid networks rely heavily on their storage technology (batteries, supercapacitor, etc.) to mitigate the impact of DG's inconsistent power output and reduce peak power demands. In this work, a lithium-ion battery is explored as a potential energy storage medium because of its high energy density and low self-discharge characteristics [114]. The battery bank has 2000 V and 700 Ah (1400 kWh) nominal voltage and capacity respectively. With 500 μF capacitance, the battery bank has an initial SoC of 80%. All AC IMGs' ESS uses a controlling technique. Each MG has 500kVA battery storage. By utilizing grid voltage and inverter current input, a common synchronized reference frame PLL is employed to generate frequency, d-q referenced voltage, and current [128]. They all have different kinds of loads, like an induction motor load, a CPL, a CCL, and a CIL.

This phenomenon of induction motors being less reliable in conventional large, interconnected power systems is called electromechanical oscillations, or LFOs; oscillatory modes in IMGs are characterized according to that result [129]. These oscillatory modes are classified as: local microgrid oscillatory modes that result from DGs in the same microgrid oscillating against one another and inter-microgrid oscillatory modes in which DGs in one microgrid oscillate in opposition to DGs in another microgrid. Another local/inter-microgrid oscillation mode caused by the swing of nearest synchronous-based DGs and inverter-based DGs that affects the stability of the AC IMGs system has also been found in the literature [130]. LFOs are more likely to occur in a local microgrid with many parallel induction motor loads than with a single large load with an equivalent rating. The presence of oscillating rotor flux components in induction motors poses challenges in the management of microgrid stability and performance. When integrated into another microgrid, as a consequence of intra-microgrid oscillations, these fluctuations have the potential to induce voltage and frequency oscillations. Furthermore, a distinct oscillation mode emerges when examining large AC IMG systems, incorporating induction motor loads of diverse sizes across all microgrids [131]. Thus, for different configurations of the system and types of load disturbance in an IMG, Table 5.1 displays a wide range of oscillatory modes generated by the LFOs.

5.2.1 MATLAB/Simulink Platform

The MATLAB/Simulink environment is a suitable platform for developing simulation models of MG systems, control strategies for power electronic converters, and other physical aspects of MG-based systems utilizing “Simscape Electrical” system. Interconnected microgrids, which are networks of small-scale power generation and distribution systems, can exhibit oscillatory modes within a specific frequency range. These oscillations typically arise due to the dynamic interactions between the microgrids and the power electronics within them. The frequency range of these oscillatory modes depends on several factors, including the topology of the microgrid network, the control strategies employed, and the types of DGs connected to the microgrids. Common oscillation frequencies in microgrids can fall within the range of a few hertz to several tens of hertz. The MATLAB/Simulink microgrid model has been used to form an AC IMGs system to validate and analyse the comparative performance of the two types of PODs in different cases. The low frequency oscillations with MOMs are studied to see how well they can be dampened by the suggested POD placed in ESS by non-linear time-domain simulations considering small-signal stability. The oscillatory modes of the IMG system were analyzed using a linearization model implemented in MATLAB Simulink, specifically focusing on the ESS-based proposed POD controller's input and output points. This approach enabled the identification of critical frequencies and damping ratios, essential for designing effective damping strategies to mitigate power oscillations. These characteristics are typically represented by the real and imaginary parts of the eigenvalues obtained from the system's linearized state-space model. The imaginary part of the eigenvalue corresponds to the oscillation frequency, while the real part indicates the damping. Thus, for different configurations of the system and types of load disturbance in an IMG, Table 5.1 displays a wide range of oscillatory modes generated by the LFOs. The identified oscillatory modes were classified based on their frequency and damping characteristics.

Table 5.1 Range of Oscillatory Modes

Mode	Oscillatory type	Eigen Values	Oscillation Frequency (Hz)	Damping
Mode 1	Local microgrid	-0.6995 ± 0.543783i	0.086545	0.8
Mode 2	Inter-microgrid	-0.556969± 0.403137i	0.064161	0.819
Mode 3	Local/Inter-microgrid	-0.5041± 0.3001i	0.04770	0.86
Mode 4	Intra-microgrid	-0.456969 ±0.251058i	0.03995	0.877

In the following case studied electromechanical oscillatory modes are defined in accordance with the considerations of several disturbances. Finally, the MB-POD's overall superiority will be established by comparing its performance to that of the SB-POD in successfully damping numerous modes of LFOs under a variety of disturbances. The Appendix A contains component specifications for AC IMGs system and detailed setting parameters of both PODs' can be found in Appendix A. Table 5.2 outlines the status of dynamic and static loading according to different operational modes, detailing how each type of load affects system performance under varying conditions.

Table 5.2 Status of dynamic and static loading according to modes.

Mode	**Disturbances Status**	**Status of dynamic and static loading**
Mode 1	Local microgrid Oscillatory mode (32.9 % of static load disturbances at MG-1, 33.33 % at MG-2, and 38.46% at MG-3)	MG-1: 2×215 hp IM, 300 kW CPL, 200 CIL MG-2: 250 kW CIL, 150 kW CCL MG-3: 200 kW CCL, 200 kW CPL
Mode 2	Inter-microgrid Oscillatory mode (32.9 % of static load disturbances at MG-1, 33.33 % at MG-2, and 38.46% at MG-3)	MG-1: 2×215 hp IM, 300 kW CPL, 200 CIL MG-2: 250 kW CIL, 150 kW CCL MG-3: 200 kW CCL, 200 kW CPL
Mode 3	Local/inter-microgrid Oscillatory mode (32.9 % of static load disturbances at MG-1, 26.32 % at MG-2, and 32.89% at MG-3)	MG-1: 2×215 hp IM, 300 kW CPL, 200 CIL MG-2: 250 kW CIL, 150 kW CCL, 215 hp IM MG-3: 200 kW CCL, 200 kW CPL, 215 hp IM
Mode 4	Intra-microgrid Oscillatory mode (32.9 % of static load disturbances at MG-1, 33.33 % at MG-2, and 38.46% at MG-3)	MG-1: 80×5.4 hp IM 300 kW CPL, 200 CIL MG-2: 250 kW CIL, 150 kW CCL MG-3: 200 kW CCL, 200 kW CPL

5.2.1.1 Mode 1: Local microgrid oscillatory mode

Aforementioned four types of oscillatory modes in Table 5.1, this mode is considered as local microgrid mode where only static loads are injected as load disturbances. MG-1 has a total generation capacity of 900 kW (400 kW solar, 350 kW wind, and 150 kW diesel), while MG-2 and MG-3 have a capacity of 750 kW (400 kW solar, 350 kW wind). The loading status is detailed in Table 5.2 for every oscillatory mode. The IM and static loads on MG-1 are 39.02% and 60.98%, respectively. Both MG-2 and MG-3 are currently running at full static loads. While 400 kW of CCL load is applied to the MG-1, 200 kW of CPL load is added to the MG-2, and 250 kW of CIL load is added at time t = 2.0 s, and subsequently withdrawn at time t = 3.0 s, the performance of the proposed multi-band POD controller is recorded.

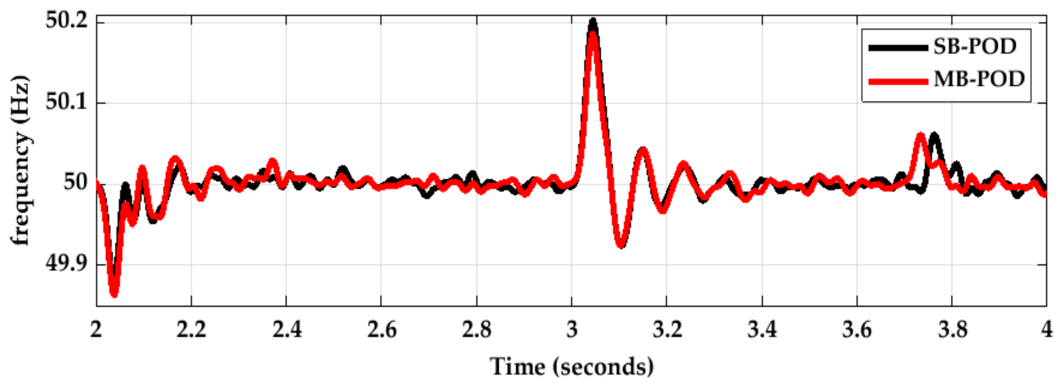

(a)

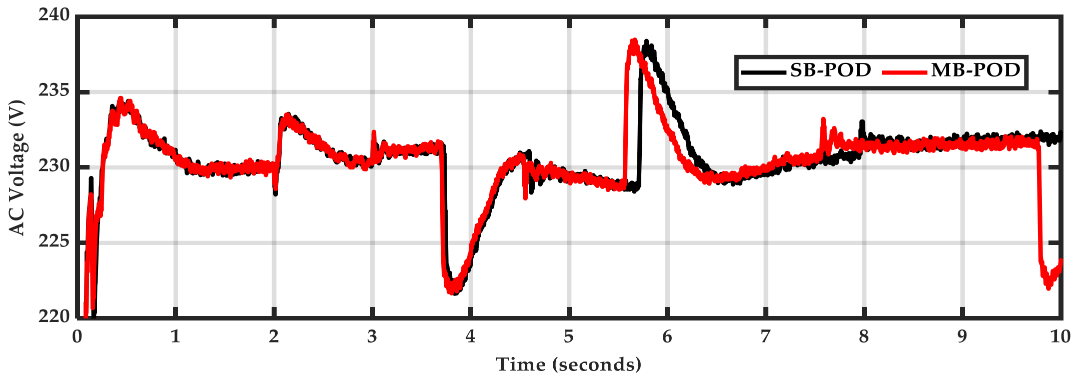

(b)

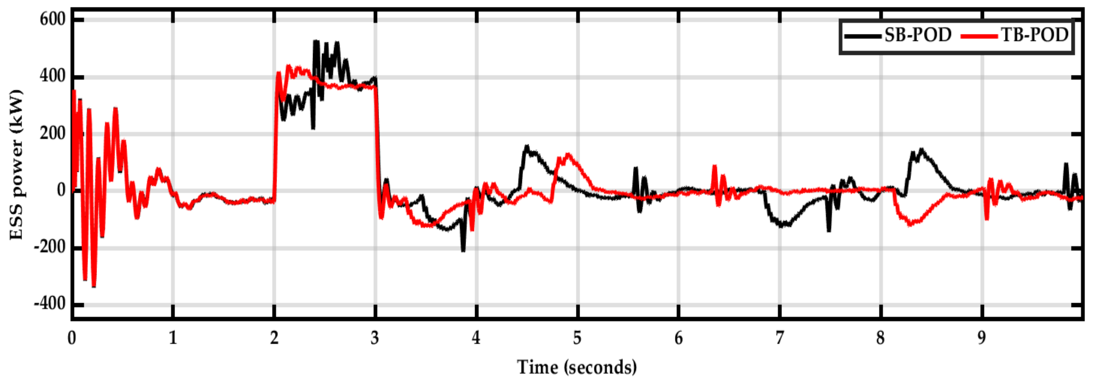

(c)

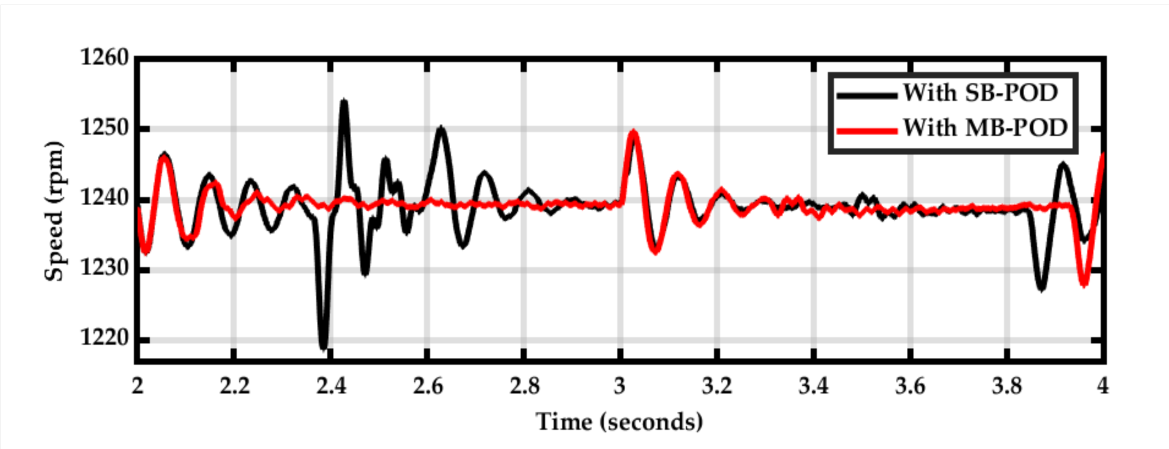

(d)

Fig. 5.1: MG-1 local microgrid oscillatory mode (32.9 % of static load disturbance), (a) System frequency, (b) System AC voltage, (c) ESS power, and (d) IM rotor speed.

The occurrence of load disturbances has resulted in voltage and frequency oscillations within the MG-1 system. The bus voltage and frequency of the MG-1 system are illustrated in Fig. 5.1 (a) and (b) correspondingly. In the given circumstance, the SB-POD exhibits a maximum frequency variation of 50.27 Hz, whereas the MB-POD has a maximum frequency deviation of 50.2 Hz. The voltage and frequency oscillations have led to power oscillations within the MG-1 system. The rotor speed of the IM also demonstrates significant oscillations in the absence of the proposed MB-POD controller. However, the implementation of the MB-POD controller has resulted in a considerable decrease in rotor speed oscillations, as depicted in Fig. 5.1 (d). When an additional demand of 400 kW is connected to the MG-1, the ESS is responsible for supplying the necessary load power to maintain stability in the system's voltage and frequency. After the successful implementation of the MB-POD controller, it can be observed that the power curve of the ESS shown in Fig. 5.1 (c) has been effectively smoothed. This situation corresponds to a local oscillatory mode.

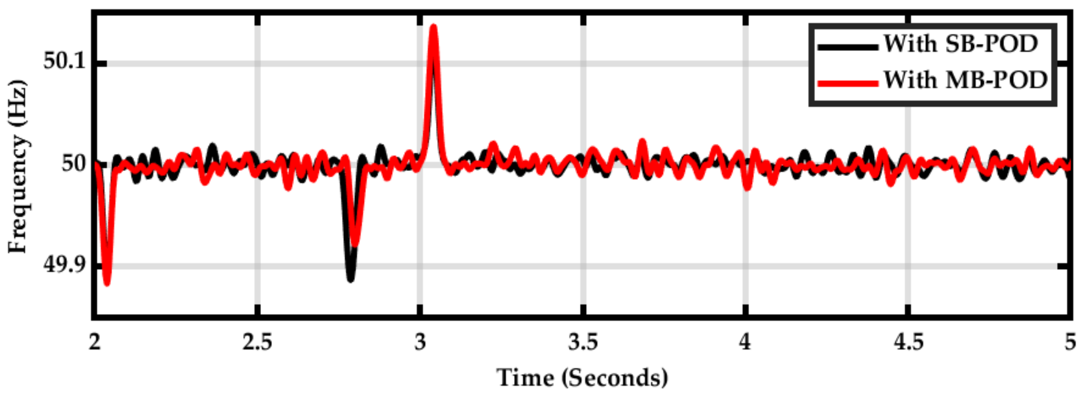

(a)

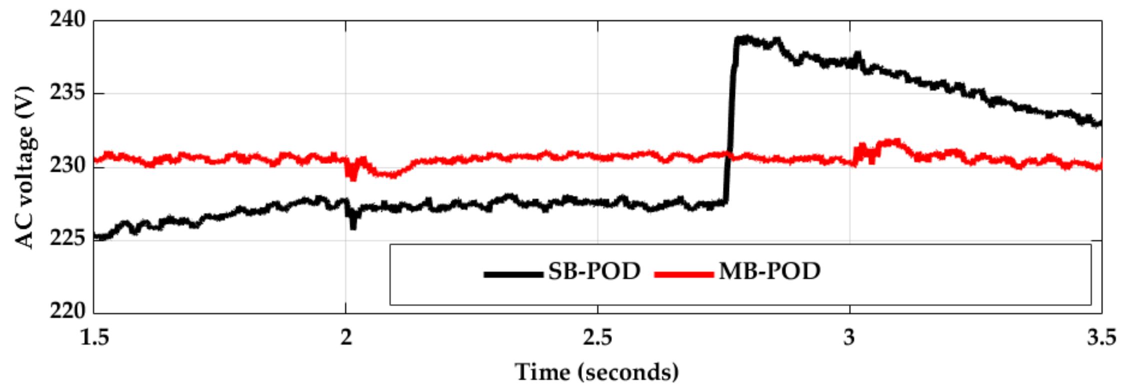

(b)

Fig. 5.2: MG-2 local microgrid oscillatory mode (33.33 % of static load disturbance), (a) System frequency, and (b) System AC voltage

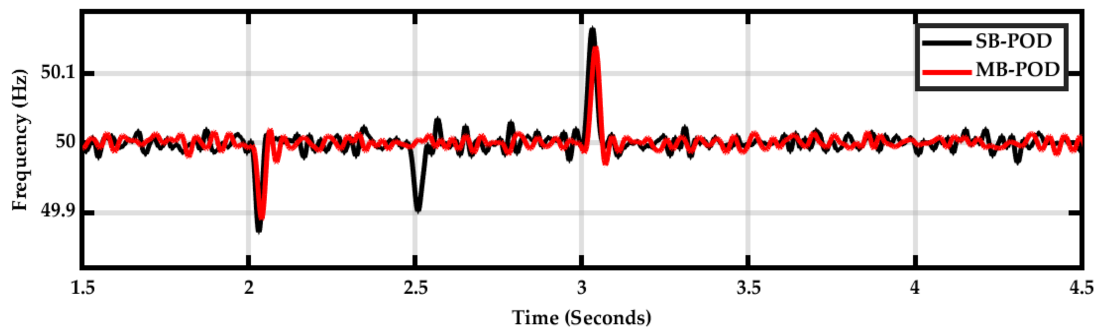

(a)

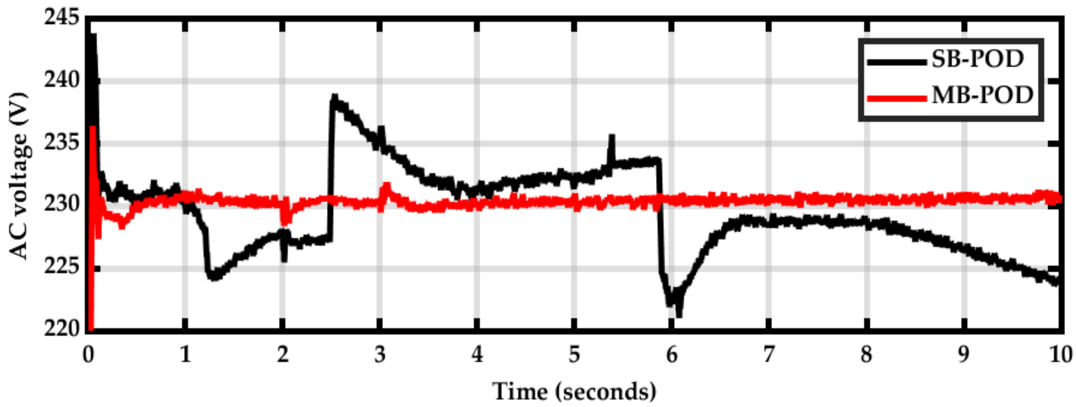

(b)

Fig. 5.3: MG-3 local microgrid oscillatory mode (38.46 % of static load disturbance), (a) System frequency, and (b) System AC voltage.

Voltage and frequency fluctuations in a microgrid without IM loads can still occur due to various factors. Although IM loads are a common source of voltage and frequency variations, other factors can also affect the microgrid's stability. MG-2 and MG-3 do not have IM loads. In MG-1, sudden load changes of 200 kW occurred at t=2s and were removed at t=3s, whereas in MG-2, load changes of 250 kW occurred. Fig. 5.2 (a), (b), and Fig. 5.3 (a), (b) depict that a proposed MB-POD exists in MG-1 marginally dampens voltage and frequency oscillation for MG-2 and MG-3, which is still present. This oscillation holds local microgrid oscillatory type.

5.2.1.2 Mode 2: Inter-microgrid oscillatory mode

Based on mode 1, an AC IMG system is established by considering the generation capacity and loading condition of three microgrids. Load disturbances are also introduced in the same way to analyze an oscillatory type known as inter-microgrid oscillatory mode. The performance of the suggested MB-POD is documented in this scenario. The AC IMG system's bus voltage and diesel generator speed of MG-1 are illustrated in Fig. 5.4 (a) & (b) respectively, whereas Fig. 5.4 (c) and (d) depict the MG-1 power sharing and IM speed, respectively. Fig. 5.4 (b) indicates that the speed deviation of the diesel generator has improved significantly after the implementation of the proposed MB-POD controller. The voltage and frequency of an AC IMG system may oscillate if any of the microgrids experiences a sudden change in demand. Here, load disturbances are present in every microgrid. These voltage and frequency oscillations may cause rotor speed oscillation of dynamic loads. From Fig. 5.4 (a) and (o), it is seen that the load disturbance has brought about voltage and frequency oscillations in the AC IMG system. These voltage and frequency oscillations have resulted in power oscillations in AC IMG system. The IM rotor speed also exhibits significant oscillations (without the proposed MB-POD controller); however, rotor speed oscillations have decreased significantly after the MB-POD controller was implemented shown in Fig. 5.4 (d). When 400 kW of additional demand is connected to the MG-1, 200 kw in MG-2, and 250 kW in MG-3, the ESS provides the additional load power to keep the AC IMG system's voltage and frequency stable. Following the implementation of the proposed MB-POD controller, the power curves of all ESSs depicted in Fig. 5.4 (e), (h) & (l) have been smoothed. Moreover, the power sharing curves shown in Fig. 5.4 (c) & (i) are also affected by load disturbance, which the proposed MB-POD controller has also substantially improved. The direct-on-line start IM has a significant beginning transient, resulting in a significant speed deviation during the starting instant. According to Fig. 5.4 (d), the proposed MB-POD controller has considerably reduced the speed oscillations of the IM during the IM's startup. Fig. 5.4 (f), (j), and (m) depict the load curve for all microgrids, whereas Fig. 5.4 (g), (k), and (n) depict the power generation curve for all microgrids. There is a common enhancement across all graphs because of the proposed MB-POD. The performance of the proposed MB-POD controller, the attenuation between the first and fifth maxima of IM rotor speed oscillations is considered. Without the POD controller, the rotor speed oscillations were attenuated by 77.78%, compared to 88.24% with the POD controller. Without the POD controller, the rotor speed oscillation settling time is 2.73 s, but it has been improved to 2.54 s with the proposed POD controller, resulting in a 0.19 s reduction in the settling time. The MB-POD controller has reduced the rotor speed oscillations by 16.67% at the moment of start. In Fig. 5.4 (o), frequency deviation has been attenuated 0.04 Hz which is defined as inter-microgrid oscillatory mode where DGs of one MG is oscillating against DGs of another MG. Therefore, these results provide additional evidence that the proposed MB-POD controller is efficacious for attenuating this type of oscillatory mode. Table 5.3 presents a performance comparison, summarizing the effectiveness and efficiency of different systems or components based on various performance metrics.

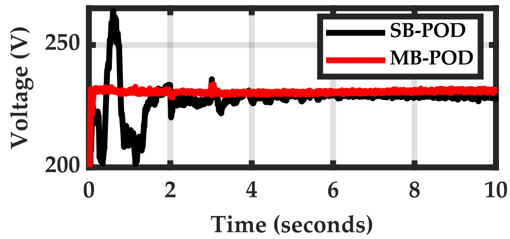
SB-POD
MB-POD
Voltage (V)
250
200
0
2
4
6
8
10
Time (seconds)

(a)

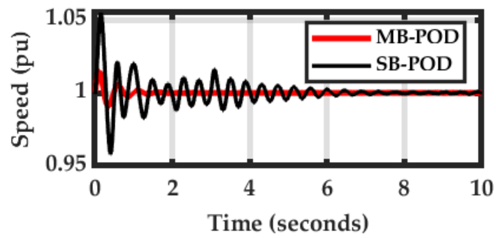
MB-POD
SB-POD
Speed (pu)
1.05
1
0.95
0
2
4
6
8
10
Time (seconds)

(b)

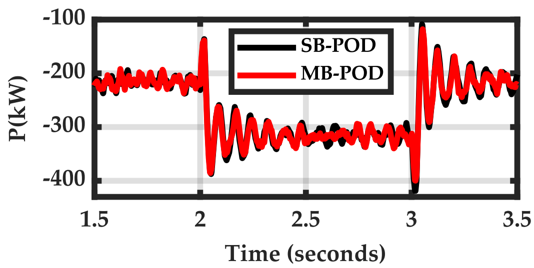
SB-POD
MB-POD
P(kW)
-100
-200
-300
-400
1.5
2
2.5
3
3.5
Time (seconds)

(c)

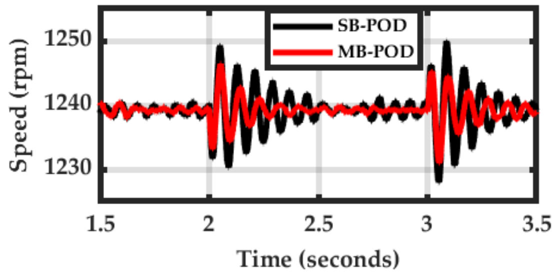
SB-POD
MB-POD
Speed (rpm)
1250
1240
1230
1.5
2
2.5
3
3.5
Time (seconds)

(d)

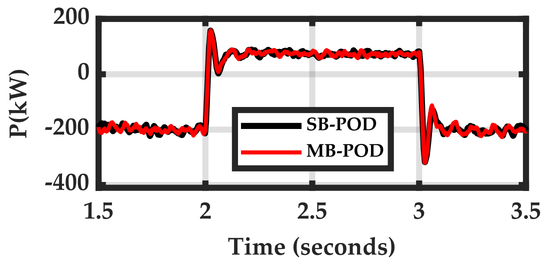
SB-POD
MB-POD
P(kW)
200
0
-200
-400
1.5
2
2.5
3
3.5
Time (seconds)

(e)

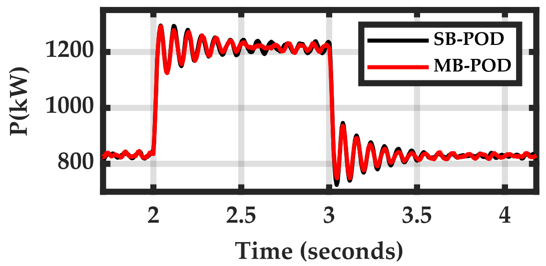
SB-POD
MB-POD
P(kW)
1200
1000
800
2
2.5
3
3.5
4
Time (seconds)

(f)

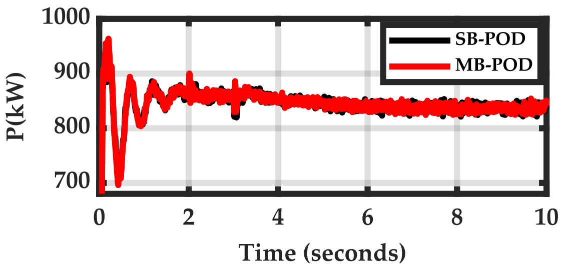
SB-POD
MB-POD
P(kW)
1000
900
800
700
0
2
4
6
8
10
Time (seconds)

(g)

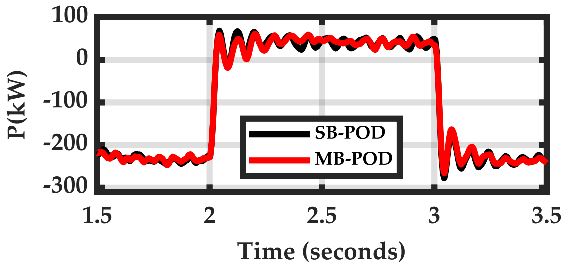
SB-POD
MB-POD
P(kW)
100
0
-100
-200
-300
1.5
2
2.5
3
3.5
Time (seconds)

(h)

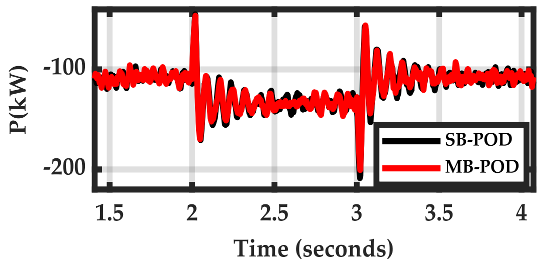
P(kW)
-100
-200
1.5
2
2.5
3
3.5
4
Time (seconds)
SB-POD
MB-POD

(i)

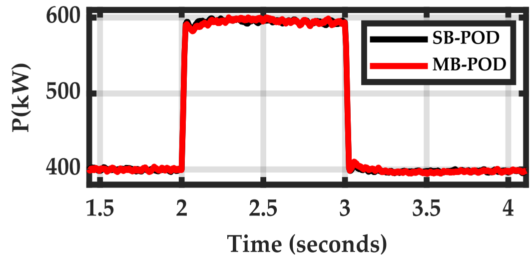
P(kW)
600
500
400
1.5
2
2.5
3
3.5
4
Time (seconds)
SB-POD
MB-POD

(j)

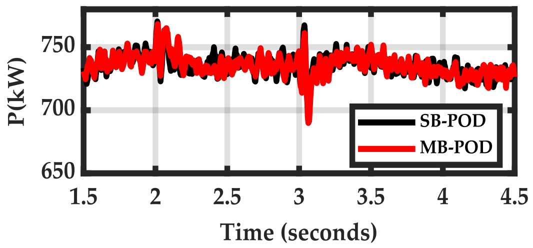
P(kW)
750
700
650
1.5
2
2.5
3
3.5
4
4.5
Time (seconds)
SB-POD
MB-POD

(k)

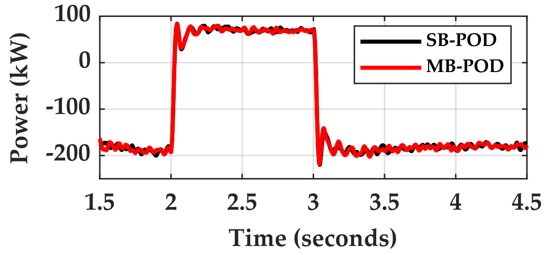
Power (kW)
100
0
-100
-200
1.5
2
2.5
3
3.5
4
4.5
Time (seconds)
SB-POD
MB-POD

(l)

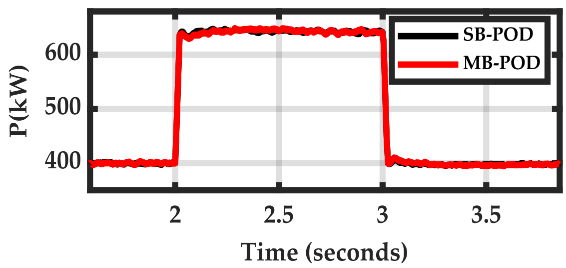
P(kW)
600
500
400
2
2.5
3
3.5
Time (seconds)
SB-POD
MB-POD

(m)

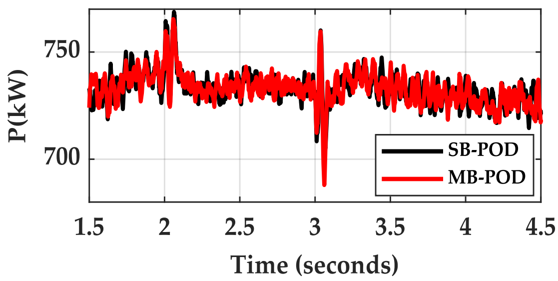
P(kW)
750
700
1.5
2
2.5
3
3.5
4
4.5
Time (seconds)
SB-POD
MB-POD

(n)

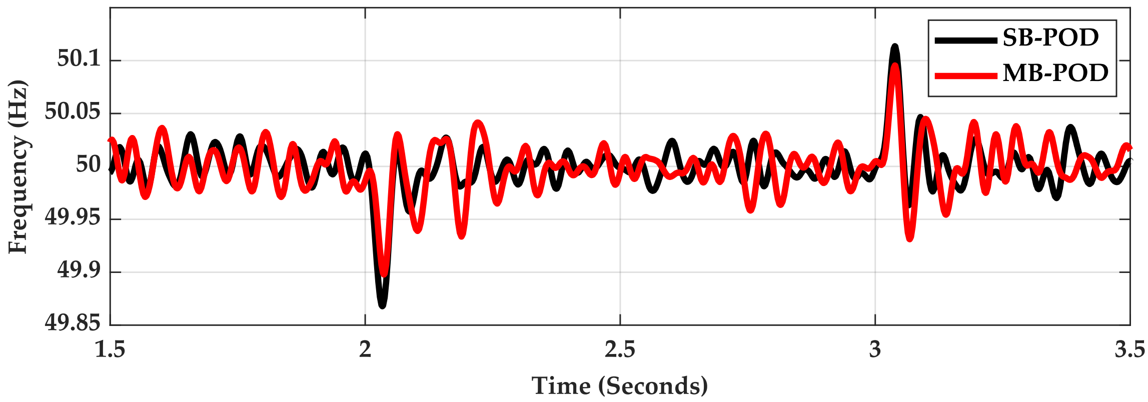

(o)

Fig. 5.4: AC IMG system with inter-microgrid Oscillatory type (mode-2) (32.9 % of static load disturbances at MG-1, 33.33 % at MG-2, and 38.46% at MG-3), (a) AC bus voltage, (b) Diesel generator speed of MG-1, (c) MG-1 power sharing, (d) IM speed of MG-1, (e) MG-1 ESS power, (f) MG-1 load curve, (g) MG-1 power generation, (h) MG-2 ESS power, (i) MG-2 power sharing, (j) MG-2 load curve, (k) MG-2 power generation, (l) MG-3 ESS power, (m) MG-3 load curve, (n) MG-3 power generation, and (o) AC system frequency.

Table 5.3 Performance Comparison

Performance parameters	**MB-POD**	**SB-POD**
Maximum frequency range	**50.09 Hz**	50.15 Hz
Induction motor speed Oscillation settling time	**Third peak**	Sixth peak
Power curves smoothened	**First peak**	Fifth peak

Diesel generator speed deviation (Starting)	**0.0237 (pu)**	0.026 (pu)

5.2.1.3 Mode 3: Local/inter-microgrid oscillatory mode

In this scenario, the MG-1 is connected to the same IM loading configuration used for mode-1 and mode-2. To further evaluate the efficacy of the proposed MB-POD controller, a 215 hp IM load is connected to both the MG-2 and MG-3. The load disturbances for all three microgrids are identical to mode 1. The graphs illustrate a comparative analysis of the performance of a multi-band power oscillation damper and a single-band power oscillation damper in stabilizing various parameters in an interconnected microgrid system. The Fig. 5.5(a) shows that the MB-POD stabilizes the diesel generator speed in per unit more effectively, with quicker damping and lower oscillation amplitudes than the SB-POD. The graph in Fig. 5.5(b), depicting induction motor speed in revolutions per minute, further highlights the superior performance of the MB-POD, showing fewer and smaller oscillations compared to the SB-POD. The voltage response, as shown in Fig. 5.5(c), indicates that the MB-POD achieves faster and more consistent voltage stabilization, while the SB-POD experiences larger and more prolonged fluctuations. Finally, the frequency response in Fig. 5.5(d) demonstrates that the MB-POD maintains the frequency closer to its nominal value with less deviation and quicker stabilization than the SB-POD, which exhibits significant frequency deviations and longer oscillation periods. Overall, these graphs collectively demonstrate that the MB-POD offers superior damping capabilities, ensuring enhanced stability and reliability of the interconnected microgrid system by effectively mitigating low-frequency oscillations across various operational parameters.

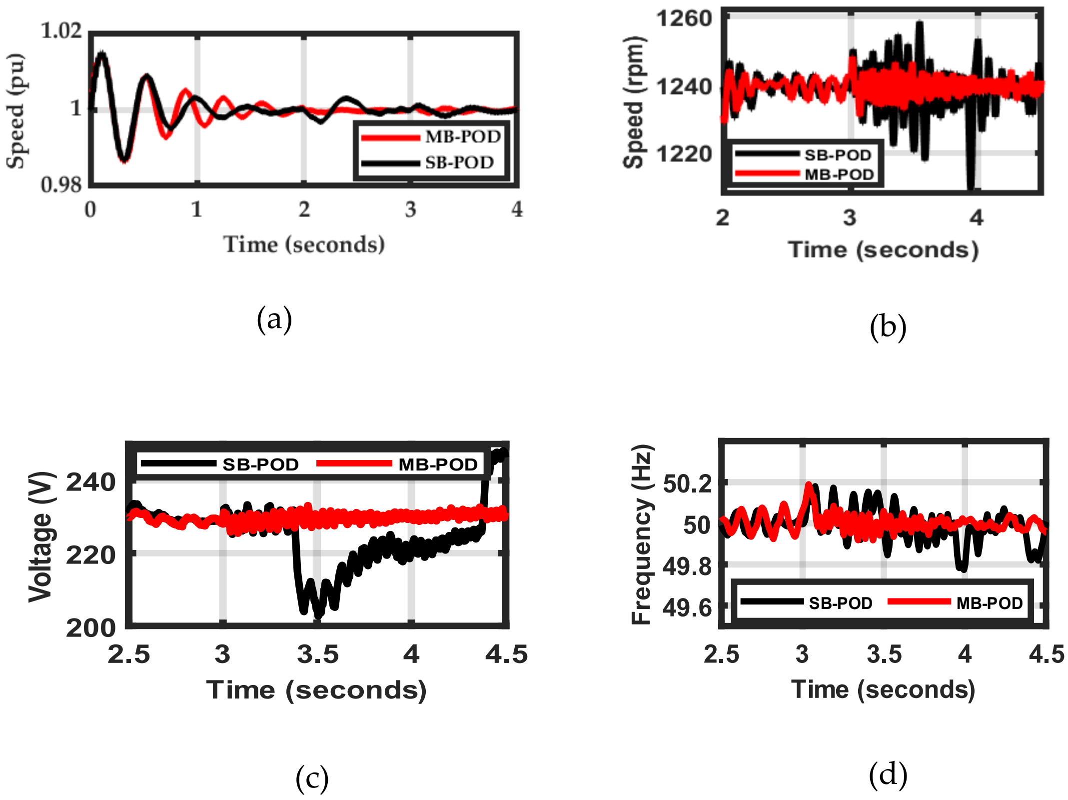

Fig. 5.5: Local/inter-microgrid Oscillatory mode (32.9 % of static load disturbances at MG-1, 26.32 % at MG-2, and 32.89% at MG-3), (a) Diesel generator speed of MG-1, (b) IM speed of MG-1, (c) AC bus voltage, and (d) AC system frequency.

5.2.1.4 Mode 4: Intra-microgrid oscillatory mode

This section presents an analysis of the robustness of the proposed MB-POD in an AC IMG system under comparable loading and generation conditions as mode 4. In this experimental setup, all three MGs are interconnected. The purpose of this design is to inject load disturbances and record simulated data. The efficacy of the proposed MB-POD scheme is assessed by examining the connection (at t = 2s) and disconnection (at t = 3s) of a 400-kW load in MG-1, a 200-kW load in MG-2, and a 250-kW load in MG-3. These loads are subject to rapid variations in the form of CCL, CIL, and CPL, respectively. Fig. 5.6 (a) and (b) depict the corresponding responses of the speed of the diesel generator and the voltage of the AC bus. Fig. 5.6 (c) and (d) illustrate the rotor speed of the small IM and the frequency of the AC system. In this case, an oscillatory mode known as intra-microgrid oscillation is being seen, characterized by a comparable frequency oscillation. The proposed MB-POD demonstrates effective dampening of this oscillation. Table 5.4 provides a performance comparison of various systems or components, while Table 5.5 offers a detailed analysis of performance comparisons specifically involving damping controllers in an interconnected hybrid AC microgrid system.

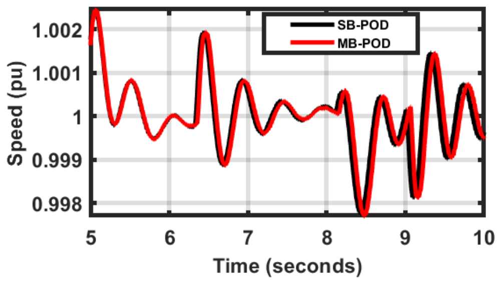

(a)

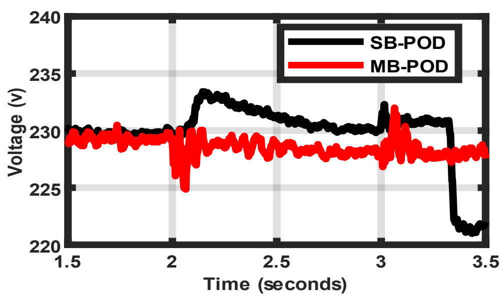

(b)

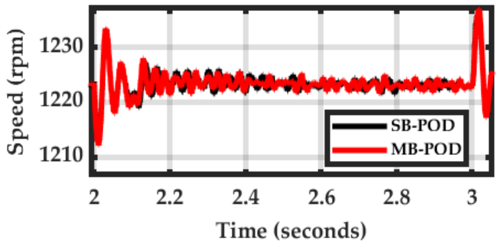

(c)

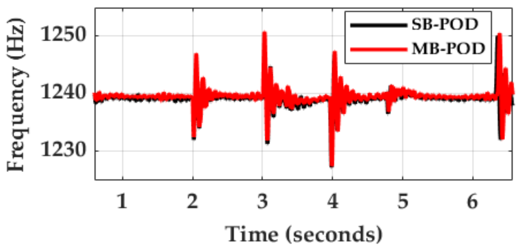

(d)

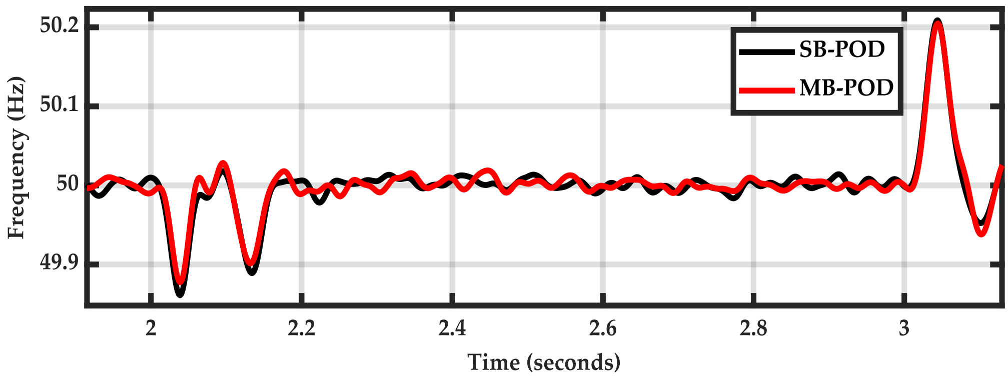

(e)

Fig. 5.6: Intra-microgrid Oscillatory mode (32.9 % of static load disturbances at MG-1, 33.33 % at MG-2, and 38.46% at MG-3), (a) Diesel generator speed of MG-1, (b) AC bus voltage, (c) Small IM speed in MG-1, (d) Large IM speed, and (e) AC IMG system frequency.

Table 5.4 Performance Comparison

Performance Parameters	**Multiple IM**	**Single IM**
Maximum frequency	49.9 Hz	49.86 Hz
Induction motor speed oscillation settling time	Third peak	Ninth peak

Table 5.5 Performance Comparison Analysis with the Damping Controllers for Interconnected Hybrid AC Microgrid System

References	Grid-connected	Hybrid DGs	IMG	Damping Controller	Performance on LFOs		Placement of PODs'
					Single Microgrid	Interconnected Microgrid	
[33]	×	✓	×	SB-POD	Better but for only single frequency band	N/A	ESS
[132]	✓	✓	✓	SB-POD	Better but for only single frequency band	Better but for only single frequency band	SG
Proposed	✓	✓	✓	MB-POD	Better damping quality with multiple frequency band (10-20%)	Better damping quality with multiple frequency band (4-6%)	ESS

5.3 PERFORMANCE COMPARISON ANALYSIS

Table 5.5 compares the performance and configuration of single microgrid and interconnected microgrid systems based on the presence or absence of hybrid DGs, IMG, and damping controllers. It uses symbols to indicate these aspects, where one symbol suggests adequacy, and another indicates inadequacy. The table also evaluates the effectiveness of power oscillation damping controllers, specifically SB-POD and MB-POD in mitigating LFOs and the placement of PODs. The single microgrid setup shows improved damping but only within a single frequency band, while the interconnected microgrid system, equipped with MB-POD, offers better damping quality across multiple frequency bands. Overall, the table highlights that the MB-POD in single and interconnected microgrid provides superior performance than SB-POD in managing oscillations over a broader frequency range.

5.4 CONCLUSION

The efficacy of the MB-POD in mitigating several oscillatory modes, enhancing system stability, and decreasing transient response time is evinced by the simulations and case studies. Compared to single-band dampers, interconnected hybrid AC microgrid system with an ESS-based multi-band power oscillation damper reduces oscillations by 4-6%. Due to the increasingly scattered structure of energy systems, conventional damping oscillation approaches generally fail to manage interconnected microgrid designs. The MB-POD exhibits remarkable adaptability and sensitivity under varying load levels, effectively stabilizing the system in numerous scenarios where the damping ratio has been adjusted from 9.1% in mode-1 to mode-4. A higher damping ratio indicates faster decay of oscillations, leading to improved stability. So, MB-POD is more susceptible for IMGs. When two types of induction motor loads are present, big motor loading conditions are more likely to be upset than numerous parallel conditions. Compared to SB-POD, the induction motor speed oscillation settling time has been lowered by 60% which indicate MB-POD's rapid capacity to dampen oscillations and improve interconnected AC microgrid stability and reliability. The MB-POD is a major advance, yet it faces obstacles. Its characteristics should be tuned for more complicated disturbances and its operational sustainability studied in the future.

Chapter 6

CONCLUSIONS

6.1 GENERAL

A focus on an interconnected AC microgrid system is presented, along with an in-depth exploration of the integration of RESs into power systems, emphasizing the need for robust control strategies to maintain stability amid the dynamics introduced by DGs. It thoroughly examines the effectiveness of a MB-POD in enhancing the damping capabilities of AC IMGs system, particularly in mitigating LFOs which are a significant concern for system stability.

6.2 KEY FINDINGS

- The proposed multi-band damping controller significantly reduces low-frequency oscillations caused by inductive loads and disturbances in both individual and interconnected AC microgrid systems, demonstrating superior performance compared to single-band controllers. It effectively stabilizes AC bus voltage, frequency, and rotor speeds of induction motors and diesel generators under various load conditions.
- Under conditions of 15.09% IM loading and 37.74% load disturbances, the hybrid microgrid system with multiple IMs demonstrates improved performance, achieving faster stabilization with lower frequency deviation (49.86 Hz vs. 49.89 Hz), quicker settling of motor speed oscillations by the third peak compared to

the sixth, smoother power curves by the first peak instead of the fifth, and reduced initial diesel generator speed deviation (0.0237 pu vs. 0.026 pu) compared to a single IM system.

- In an interconnected microgrid system with varying IM loading and disturbances, the multiple small IMs configuration outperforms the single large IM setup. Despite causing greater initial frequency deviation, the multiple IMs configuration achieves faster stabilization, with rotor speeds settling by the third peak compared to the sixth peak for the single IM. The use of the ESS helps mitigate power imbalances, stabilizing voltage and frequency oscillations more effectively in the multiple IMs setup under these specific loading and disturbance conditions.
- The simulations highlight that both small and large IM loads significantly influence microgrid dynamics. Rotor resistance positively impacts IM performance, while stator resistance has a negative effect. Non-linear dynamic simulations reveal that sudden load changes notably affect IM rotor speed, system frequency, and power sharing from energy storage systems, emphasizing the importance of IM model parameters and configurations in maintaining stable microgrid operations.
- The MB-POD controller significantly outperforms the SB-POD controller, achieving a maximum frequency of 50.09 Hz compared to 50.15 Hz, induction motor speed oscillation settling by the third peak versus the sixth peak, and smoother power curves by the first peak instead of the fifth. Additionally, the MB-POD controller results in a lower diesel generator speed deviation (0.0237 pu vs. 0.026 pu) under both local and inter-microgrid oscillatory modes.

- Under both local/inter-microgrid and intra-microgrid oscillatory modes, the multiple IM configuration achieves faster stabilization, with induction motor speed oscillation settling by the third peak compared to the ninth peak for a single IM. The maximum frequency deviation is slightly higher at 49.9 Hz with multiple IMs versus 49.86 Hz with a single IM, highlighting the superior dynamic response of multiple IMs in managing load disturbances.

6.3 LIMITATION OF THE STUDY

- The simulations, while extensive, may not encompass all conceivable real-world operational scenarios and disturbances that microgrids might encounter.
- The intermittent nature of RESs, such as solar and wind, presents challenges in modelling and prediction that may not be fully accounted for in the study.
- Designing a multi-band power oscillation damper for an interconnected microgrid system can be complex due to the need for precise tuning and control to effectively dampen low-frequency oscillations across various bands.

6.4 RECOMMENDATION FOR FURTHER STUDY

Future studies should aim to corroborate the simulation results with real-world field tests to validate the MB-POD’s performance under practical operating conditions. Exploration into more advanced control techniques, including artificial intelligence and machine learning algorithms, could offer further enhancements to microgrid stability. Future research could focus on deploying the MB-POD in a wider variety of microgrid configurations to test its effectiveness across a broader spectrum of conditions.

With the increasing digitalization of power systems, the cybersecurity aspect of the control systems, particularly for the MB-POD, should be a focus to ensure operational integrity against potential cyber-attacks. A detailed economic analysis considering the cost-benefit aspects of implementing the MB-POD on a larger scale would provide valuable insights for stakeholders.

It is needed to investigate adaptive and AI-driven control algorithms to enhance real-time tuning and control of MB-PODs in dynamic interconnected microgrid environments.

Bibliography

[1] S.-E. Razavi, E. Rahimi, M. S. Javadi, A. E. Nezhad, M. Lotfi, M. Shafie-khah, *et al.*, "Impact of distributed generation on protection and voltage regulation of distribution systems: A review," *Renewable and Sustainable Energy Reviews,* vol. 105, pp. 157-167, 2019.

[2] M. H. Saeed, W. Fangzong, B. A. Kalwar, and S. Iqbal, "A review on microgrids' challenges & perspectives," *IEEE Access,* vol. 9, pp. 166502-166517, 2021.

[3] D. Saha, N. Bazmohammadi, J. C. Vasquez, and J. M. Guerrero, "Multiple microgrids: A review of architectures and operation and control strategies," *Energies,* vol. 16, p. 600, 2023.

[4] Z. Xu, P. Yang, C. Zheng, Y. Zhang, J. Peng, and Z. Zeng, "Analysis on the organization and Development of multi-microgrids," *Renewable and Sustainable energy reviews,* vol. 81, pp. 2204-2216, 2018.

[5] J. Singh, S. Prakash Singh, K. Shanker Verma, A. Iqbal, and B. Kumar, "Recent control techniques and management of AC microgrids: A critical review on issues, strategies, and future trends," *International Transactions on Electrical Energy Systems,* vol. 31, p. e13035, 2021.

[6] I. P. Nikolakakos, H. H. Zeineldin, M. S. El-Moursi, and N. D. Hatziargyriou, "Stability evaluation of interconnected multi-inverter microgrids through critical clusters," *IEEE Transactions on Power Systems,* vol. 31, pp. 3060-3072, 2015.

[7] Z. Shuai, Y. Sun, Z. J. Shen, W. Tian, C. Tu, Y. Li, *et al.*, "Microgrid stability: Classification and a review," *Renewable and Sustainable Energy Reviews,* vol. 58, pp. 167-179, 2016.

[8] L. Mariam, M. Basu, and M. F. Conlon, "Microgrid: Architecture, policy and future trends," *Renewable and Sustainable Energy Reviews,* vol. 64, pp. 477-489, 2016.

[9] M. J. Hossain, M. A. Mahmud, F. Milano, S. Bacha, and A. Hably, "Design of robust distributed control for interconnected microgrids," *IEEE Transactions on Smart Grid,* vol. 7, pp. 2724-2735, 2015.

[10] B. Chen, J. Wang, X. Lu, C. Chen, and S. Zhao, "Networked microgrids for grid resilience, robustness, and efficiency: A review," *IEEE Transactions on Smart Grid,* vol. 12, pp. 18-32, 2020.

[11] P. Sharma, H. D. Mathur, P. Mishra, and R. C. Bansal, "A critical and comparative review of energy management strategies for microgrids," *Applied Energy,* vol. 327, p. 120028, 2022.

[12] E. Bullich-Massagué, F. Díaz-González, M. Aragüés-Peñalba, F. Girbau-Llistuella, P. Olivella-Rosell, and A. Sumper, "Microgrid clustering architectures," *Applied energy,* vol. 212, pp. 340-361, 2018.

[13] J. Lai, X. Lu, Z. Dong, and S. Cheng, "Resilient distributed multiagent control for AC microgrid networks subject to disturbances," *IEEE Transactions on Systems, Man, and Cybernetics: Systems,* vol. 52, pp. 43-53, 2021.

[14] B. Fan, S. Guo, J. Peng, Q. Yang, W. Liu, and L. Liu, "A consensus-based algorithm for power sharing and voltage regulation in DC microgrids," *IEEE Transactions on Industrial Informatics,* vol. 16, pp. 3987-3996, 2019.

[15] M. Zolfaghari, M. Abedi, and G. B. Gharehpetian, "Power flow control of interconnected AC–DC microgrids in grid-connected hybrid microgrids using modified UIPC," *IEEE Transactions on Smart Grid*, vol. 10, pp. 6298-6307, 2019.

[16] J. Lai, X. Lu, X. Yu, and A. Monti, "Cluster-oriented distributed cooperative control for multiple AC microgrids," *IEEE Transactions on Industrial Informatics,* vol. 15, pp. 5906-5918, 2019.

[17] M. Goyal and A. Ghosh, "Microgrids interconnection to support mutually during any contingency," *Sustainable Energy, Grids and Networks,* vol. 6, pp. 100-108, 2016.

[18] Y. Han, X. Ning, L. Li, P. Yang, and F. Blaabjerg, "Droop coefficient correction control for power sharing and voltage restoration in hierarchical controlled DC microgrids," *International Journal of Electrical Power & Energy Systems,* vol. 133, p. 107277, 2021.

[19] D. Das, M. J. Hossain, S. Mishra, and B. Singh, "Bidirectional power sharing of modular DABs to improve voltage stability in DC microgrids," *IEEE Transactions on Industry Applications,* vol. 58, pp. 2369-2377, 2022.

[20] M. Z. Kreishan and A. F. Zobaa, "Optimal allocation and operation of droop-controlled islanded microgrids: A review," *energies*, vol. 14, p. 4653, 2021.

[21] Q. Xu, Y. Xu, Z. Xu, L. Xie, and F. Blaabjerg, "A hierarchically coordinated operation and control scheme for DC microgrid clusters under uncertainty," *IEEE Transactions on Sustainable Energy,* vol. 12, pp. 273-283, 2020.

[22] Y. Shan, J. Hu, and B. Shen, "Distributed Secondary Frequency Control for AC Microgrids Using Load Power Forecasting Based on Artificial Neural Network," *IEEE Transactions on Industrial Informatics*, 2023.

[23] M. M. A. Abdelaziz, M. F. Shaaban, H. E. Farag, and E. F. El-Saadany, "A multistage centralized control scheme for islanded microgrids with PEVs," *IEEE Transactions on Sustainable Energy,* vol. 5, pp. 927-937, 2014.

[24] L. Meng, Q. Shafiee, G. F. Trecate, H. Karimi, D. Fulwani, X. Lu, *et al.*, "Review on control of DC microgrids and multiple microgrid clusters," *IEEE journal of emerging and selected topics in power electronics,* vol. 5, pp. 928-948, 2017.

[25] M. Batool, F. Shahnia, and S. M. Islam, "Multi-level supervisory emergency control for operation of remote area microgrid clusters," *Journal of Modern Power Systems and Clean Energy,* vol. 7, pp. 1210-1228, 2019.

[26] Z. H. A. Al-Tameemi, T. T. Lie, G. Foo, and F. Blaabjerg, "Control strategies of DC microgrids cluster: A comprehensive review," *Energies,* vol. 14, p. 7569, 2021.

[27] M. E. T. Souza and L. C. G. Freitas, "Grid-Connected and Seamless Transition Modes for Microgrids: An Overview of Control Methods, Operation Elements and General Requirements," *IEEE Access,* 2022.

[28] X. Zhang, C. Lu, S. Liu, and X. Wang, "A review on wide-area damping control to restrain inter-area low frequency oscillation for large-scale power systems with increasing renewable generation," *Renewable and Sustainable Energy Reviews,* vol. 57, pp. 45-58, 2016.

[29] A. Sesetti, H. K. Nunna, S. Doolla, and A. K. Rathore, "Multi-agent based energy trading platform for energy storage systems in distribution systems with inter-connected microgrids," in *2018 IEEE Industry Applications Society Annual Meeting (IAS),* 2018, pp. 1-8.

[30] P. J. dos Santos Neto, T. A. dos Santos Barros, J. P. C. Silveira, E. Ruppert Filho, J. C. Vasquez, and J. M. Guerrero, "Power management strategy based on virtual

inertia for DC microgrids," *IEEE Transactions on Power Electronics,* vol. 35, pp. 12472-12485, 2020.

[31] A. Nocoń and S. Paszek, "A Comprehensive Review of Power System Stabilizers," *Energies,* vol. 16, p. 1945, 2023.

[32] T. J. Rumky, T. Ahmed, M. Ahmed, and S. Mekhilef, "Tri-Band Damping Controller for Low Frequency Oscillations in AC Microgrid System," in *2023 IEEE IAS Global Conference on Renewable Energy and Hydrogen Technologies (GlobConHT),* 2023, pp. 1-6.

[33] M. Ahmed, A. Vahidnia, M. Datta, and L. Meegahapola, "An adaptive power oscillation damping controller for a hybrid AC/DC microgrid," *IEEE Access,* vol. 8, pp. 69482-69495, 2020.

[34] B. Hartono, Y. Budiyanto, and R. Setiabudy, "Review of microgrid technology," in *2013 international conference on QiR,* 2013, pp. 127-132.

[35] A. K. Marvasti, Y. Fu, S. DorMohammadi, and M. Rais-Rohani, "Optimal operation of active distribution grids: A system of systems framework," *IEEE Transactions on Smart Grid,* vol. 5, pp. 1228-1237, 2014.

[36] J. Yang and C. Su, "Robust optimization of microgrid based on renewable distributed power generation and load demand uncertainty," *Energy,* vol. 223, p. 120043, 2021.

[37] L. F. Fuentes-Cortés and A. Flores-Tlacuahuac, "Integration of distributed generation technologies on sustainable buildings," *Applied Energy,* vol. 224, pp. 582-601, 2018.

[38] E. Jamil, S. Hameed, and B. Jamil, "Power quality improvement of distribution system with photovoltaic and permanent magnet synchronous generator based renewable energy farm using static synchronous compensator," *Sustainable energy technologies and assessments,* vol. 35, pp. 98-116, 2019.

[39] D. A. Gadanayak, "Protection algorithms of microgrids with inverter interfaced distributed generation units—A review," *Electric Power Systems Research,* vol. 192, p. 106986, 2021.

[40] A. Z. A. Shaqsi, K. Sopian, and A. Al-Hinai, "Review of energy storage services, applications, limitations, and benefits," *Energy Reports,* vol. 6, pp. 288-306, 2020.

[41] L. M. Andersen, L. G. Hansen, C. L. Jensen, and F. A. Wolak, "Can incentives to increase electricity use reduce the cost of integrating renewable resources," National Bureau of Economic Research2019.

[42] Y. Yoldaş, A. Önen, S. Muyeen, A. V. Vasilakos, and I. Alan, "Enhancing smart grid with microgrids: Challenges and opportunities," *Renewable and Sustainable Energy Reviews,* vol. 72, pp. 205-214, 2017.

[43] O. Egbue, D. Naidu, and P. Peterson, "The role of microgrids in enhancing macrogrid resilience," in *2016 International Conference on Smart Grid and Clean Energy Technologies (ICSGCE),* 2016, pp. 125-129.

[44] V. K. Sood and H. Abdelgawad, "Microgrids architectures," in *Distributed Energy Resources in Microgrids,* ed: Elsevier, 2019, pp. 1-31.

[45] P.-H. Huang, M. S. El Moursi, and S. A. Hasen, "Novel fault ride-through scheme and control strategy for doubly fed induction generator-based wind turbine," *IEEE transactions on energy conversion,* vol. 30, pp. 635-645, 2014.

[46] J. Marqusee, S. Ericson, and D. Jenket, "Impact of emergency diesel generator reliability on microgrids and building-tied systems," *Applied energy,* vol. 285, p. 116437, 2021.

[47] M. Abbasi, E. Abbasi, L. Li, R. P. Aguilera, D. Lu, and F. Wang, "Review on the microgrid concept, structures, components, communication systems, and control methods," *Energies*, vol. 16, p. 484, 2023.
[48] W. Cao, Y. Ma, F. Wang, L. M. Tolbert, and Y. Xue, "Low-frequency stability analysis of inverter-based islanded multiple-bus AC microgrids based on terminal characteristics," *IEEE Transactions on Smart Grid*, vol. 11, pp. 3662-3676, 2020.
[49] M. A. Hoummadi, M. Bouderbala, H. Alami Aroussi, B. Bossoufi, N. El Ouanjli, and M. Karim, "Survey of Sustainable Energy Sources for Microgrid Energy Management: A Review," *Energies*, vol. 16, p. 3077, 2023.
[50] A. Muhtadi, D. Pandit, N. Nguyen, and J. Mitra, "Distributed energy resources based microgrid: Review of architecture, control, and reliability," *IEEE Transactions on Industry Applications*, vol. 57, pp. 2223-2235, 2021.
[51] L. Ahmethodzic and M. Music, "Comprehensive review of trends in microgrid control," *Renewable Energy Focus*, vol. 38, pp. 84-96, 2021.
[52] M. Naderi, Y. Khayat, Q. Shafiee, F. Blaabjerg, and H. Bevrani, "Dynamic modeling, stability analysis and control of interconnected microgrids: A review," *Applied Energy*, vol. 334, p. 120647, 2023.
[53] X. Zhou, L. Zhou, Y. Chen, J. M. Guerrero, A. Luo, W. Wu, *et al.*, "A microgrid cluster structure and its autonomous coordination control strategy," *International Journal of Electrical Power & Energy Systems*, vol. 100, pp. 69-80, 2018.
[54] Z. Rostami, S. N. Ravadanegh, N. T. Kalantari, J. M. Guerrero, and J. C. Vasquez, "Dynamic modeling of multiple microgrid clusters using regional demand response programs," *Energies*, vol. 13, p. 4050, 2020.
[55] C. Li, T. Dragicevic, N. L. D. Aldana, A. C. L. Hernández, Y. Guan, T. B. Rasmussen, *et al.*, "Grid architecture for future distribution system—A cyber-physical system perspective," in *IECON 2017-43rd Annual Conference of the IEEE Industrial Electronics Society*, 2017, pp. 5235-5239.
[56] H. Karimi, R. Bahmani, S. Jadid, and A. Makui, "Dynamic transactive energy in multi-microgrid systems considering independence performance index: A multi-objective optimization framework," *International Journal of Electrical Power & Energy Systems*, vol. 126, p. 106563, 2021.
[57] H. F. Sindi, S. Alghamdi, M. Rawa, A. I. Omar, and A. H. Elmetwaly, "Robust control of adaptive power quality compensator in Multi-Microgrids for power quality enhancement using puzzle optimization algorithm," *Ain Shams Engineering Journal*, vol. 14, p. 102047, 2023.
[58] M.-C. Pham, Q.-T. Tran, A. Hably, and S. Bacha, "Application of energy routers for frequency support in an AC/DC multi-microgrid system," in *2021 IEEE International Conference on Environment and Electrical Engineering and 2021 IEEE Industrial and Commercial Power Systems Europe (EEEIC/I&CPS Europe)*, 2021, pp. 1-6.
[59] K. Cabana-Jiménez, J. E. Candelo-Becerra, and V. Sousa Santos, "Comprehensive analysis of microgrids configurations and topologies," *Sustainability*, vol. 14, p. 1056, 2022.
[60] M. Baruwa and M. Fazeli, "Impact of virtual synchronous machines on low-frequency oscillations in power systems," *IEEE Transactions on Power Systems*, vol. 36, pp. 1934-1946, 2020.
[61] T. J. Rumky, T. Ahmed, M. Ahmed, S. Ahmad, and M. Rahman, "Performance of Microgrid Systems on Multiple Dynamic Loads Penetration," in *2023 10th IEEE International Conference on Power Systems (ICPS)*, 2023, pp. 1-6.

[62] E. Zhao, E. Liu, L. Li, Y. Han, P. Yang, and C. Wang, "Hierarchical Control Strategy Based on Droop Coefficient Calibration and Bus Voltage Compensation for DC Microgrid Cluster," in *2021 IEEE 2nd China International Youth Conference on Electrical Engineering (CIYCEE)*, 2021, pp. 1-7.
[63] M.-A. Nasr, S. Nikkhah, G. B. Gharehpetian, E. Nasr-Azadani, and S. H. Hosseinian, "A multi-objective voltage stability constrained energy management system for isolated microgrids," *International Journal of Electrical Power & Energy Systems*, vol. 117, p. 105646, 2020.
[64] M. A. Hassan, "Dynamic stability of an autonomous microgrid considering active load impact with a new dedicated synchronization scheme," *IEEE Transactions on Power Systems*, vol. 33, pp. 4994-5005, 2018.
[65] S. S. Khorramabadi and A. Bakhshai, "Critic-based self-tuning PI structure for active and reactive power control of VSCs in microgrid systems," *IEEE Transactions on smart grid*, vol. 6, pp. 92-103, 2014.
[66] H. Moussa, A. Shahin, J.-P. Martin, B. Nahid-Mobarakeh, S. Pierfederici, and N. Moubayed, "Harmonic power sharing with voltage distortion compensation of droop controlled islanded microgrids," *IEEE Transactions on Smart Grid*, vol. 9, pp. 5335-5347, 2017.
[67] M. Bajaj and A. K. Singh, "Grid integrated renewable DG systems: A review of power quality challenges and state-of-the-art mitigation techniques," *International Journal of Energy Research*, vol. 44, pp. 26-69, 2020.
[68] Y. Naderi, S. H. Hosseini, S. G. Zadeh, B. Mohammadi-Ivatloo, J. C. Vasquez, and J. M. Guerrero, "An overview of power quality enhancement techniques applied to distributed generation in electrical distribution networks," *Renewable and Sustainable Energy Reviews*, vol. 93, pp. 201-214, 2018.
[69] S. B. Rao, Y. P. Kumar, M. Amir, and F. Ahmad, "An adaptive neuro-fuzzy control strategy for improved power quality in multi-microgrid clusters," *IEEE Access*, vol. 10, pp. 128007-128021, 2022.
[70] A. Q. Al-Shetwi, M. Hannan, K. P. Jern, M. Mansur, and T. M. I. Mahlia, "Grid-connected renewable energy sources: Review of the recent integration requirements and control methods," *Journal of Cleaner Production*, vol. 253, p. 119831, 2020.
[71] Z. Hossain, S. Ahmad, U. K. Jhuma, S. Mekhilef, M. Mubin, H. Mokhlis, *et al.*, "A Flexible Interconnection and Power Sharing Strategy For Two Autonomous Microgrid Systems," in *2021 IEEE 6th International Conference on Computing, Communication and Automation (ICCCA)*, 2021, pp. 472-477.
[72] G. Rogers, "The nature of power system oscillations," in *Power System Oscillations*, ed: Springer, 2000, pp. 7-30.
[73] M. Saadatmand, G. B. Gharehpetian, A. Moghassemi, J. M. Guerrero, P. Siano, and H. H. Alhelou, "Damping of low-frequency oscillations in power systems by large-scale PV farms: A comprehensive review of control methods," *IEEE Access*, vol. 9, pp. 72183-72206, 2021.
[74] A. A. Anderson and R. Podmore, "Why not connect? Untapped power markets and FACTS for interconnecting islanded microgrids," in *2016 IEEE Global Humanitarian Technology Conference (GHTC)*, 2016, pp. 379-386.
[75] A. Kahrobaeian and Y. A.-R. I. Mohamed, "Analysis and mitigation of low-frequency instabilities in autonomous medium-voltage converter-based microgrids with dynamic loads," *IEEE Transactions on Industrial Electronics*, vol. 61, pp. 1643-1658, 2013.

[76] R. H. Amin Khodabakhshian, Majid Moazzami, "Multi-band power system stabilizer design by using CPCE algorithm for multi-machine power system," vol. 101, August 2013.
[77] M. Farrokhabadi, C. A. Canizares, J. W. Simpson-Porco, E. Nasr, L. Fan, P. A. Mendoza-Araya, *et al.*, "Microgrid stability definitions, analysis, and examples," *IEEE Transactions on Power Systems*, vol. 35, pp. 13-29, 2019.
[78] R. Singh and M. Kirar, "Transient stability analysis and improvement in microgrid," in *2016 International Conference on Electrical Power and Energy Systems (ICEPES)*, 2016, pp. 239-245.
[79] J. Solano, J. M. Rey, J. D. Bastidas-Rodríguez, and A. I. Hernández, "Stability issues in microgrids," *Microgrids Design and Implementation*, pp. 287-310, 2019.
[80] H. Ali, G. Magdy, and D. Xu, "A new optimal robust controller for frequency stability of interconnected hybrid microgrids considering non-inertia sources and uncertainties," *International Journal of Electrical Power & Energy Systems*, vol. 128, p. 106651, 2021.
[81] G. K. Suman, J. M. Guerrero, and O. P. Roy, "Robust Frequency Control in Interconnected Microgrids: An H $ _2 $/H $ _ {\infty} $ Control Approach," *IEEE Systems Journal*, vol. 16, pp. 2044-2055, 2021.
[82] M. Khamies, G. Magdy, M. E. Hussein, F. A. Banakhr, and S. Kamel, "An efficient control strategy for enhancing frequency stability of multi-area power system considering high wind energy penetration," *IEEE Access*, vol. 8, pp. 140062-140078, 2020.
[83] X. Feng, A. Shekhar, F. Yang, R. E. Hebner, and P. Bauer, "Comparison of hierarchical control and distributed control for microgrid," *Electric Power Components and Systems*, vol. 45, pp. 1043-1056, 2017.
[84] F. Bandeiras, E. Pinheiro, M. Gomes, P. Coelho, and J. Fernandes, "Review of the cooperation and operation of microgrid clusters," *Renewable and Sustainable Energy Reviews*, vol. 133, p. 110311, 2020.
[85] A. Ouammi, H. Dagdougui, L. Dessaint, and R. Sacile, "Coordinated model predictive-based power flows control in a cooperative network of smart microgrids," *IEEE Transactions on Smart grid*, vol. 6, pp. 2233-2244, 2015.
[86] M. Islam, F. Yang, and M. Amin, "Control and optimisation of networked microgrids: A review," *IET Renewable Power Generation*, vol. 15, pp. 1133-1148, 2021.
[87] A. Arabpour and H. Hojabri, "An improved centralized/decentralized accurate reactive power sharing method in AC microgrids," *International Journal of Electrical Power & Energy Systems*, vol. 148, p. 108908, 2023.
[88] K. Jithin, R. Harikumar, N. Mayadevi, and V. Mini, "A centralized control algorithm for power management in interconnected dc microgrids," in *Proceedings of Symposium on Power Electronic and Renewable Energy Systems Control: PERESC 2020*, 2021, pp. 451-461.
[89] X. Hou, K. Sun, N. Zhang, F. Teng, X. Zhang, and T. C. Green, "Priority-driven self-optimizing power control scheme for interlinking converters of hybrid AC/DC microgrid clusters in decentralized manner," *IEEE Transactions on Power Electronics*, vol. 37, pp. 5970-5983, 2021.
[90] Y. Wang, A. O. Rousis, D. Qiu, and G. Strbac, "A stochastic distributed control approach for load restoration of networked microgrids with mobile energy storage systems," *International Journal of Electrical Power & Energy Systems*, vol. 148, p. 108999, 2023.

[91] X.-K. Liu, J. Cai, L. Xing, and Y.-W. Wang, "Distributed Event-Triggered Current Sharing Control for Islanded DC Microgrids With Quantized State," *IEEE Transactions on Sustainable Energy,* 2023.
[92] C. Samende, F. Gao, S. M. Bhagavathy, and M. McCulloch, "Decentralized voltage control for efficient power exchange in interconnected DC clusters," *IEEE Transactions on Sustainable Energy,* vol. 12, pp. 103-115, 2020.
[93] J. Zhou, H. Zhang, Q. Sun, D. Ma, and B. Huang, "Event-based distributed active power sharing control for interconnected AC and DC microgrids," *IEEE Transactions on Smart Grid,* vol. 9, pp. 6815-6828, 2017.
[94] L. Che, M. Shahidehpour, A. Alabdulwahab, and Y. Al-Turki, "Hierarchical coordination of a community microgrid with AC and DC microgrids," *IEEE Transactions on smart grid,* vol. 6, pp. 3042-3051, 2015.
[95] X. Hou, Y. Sun, J. Lu, X. Zhang, L. H. Koh, M. Su, *et al.*, "Distributed hierarchical control of AC microgrid operating in grid-connected, islanded and their transition modes," *Ieee Access,* vol. 6, pp. 77388-77401, 2018.
[96] M. A. H. Sadi and M. H. Ali, "Combined operation of SVC and optimal reclosing of circuit breakers for power system transient stability enhancement," *Electric Power Systems Research,* vol. 106, pp. 241-248, 2014.
[97] A. Sabo, N. I. A. Wahab, M. L. Othman, M. Z. A. B. M. Jaffar, H. Acikgoz, H. Nafisi, *et al.*, "Artificial intelligence-based power system stabilizers for frequency stability enhancement in multi-machine power systems," *IEEE Access,* vol. 9, pp. 166095-166116, 2021.
[98] D. A. L. Roca, P. Mercado, and G. Suvire, "System frequency response model considering the influence of power system stabilizers," *IEEE Latin America Transactions,* vol. 20, pp. 912-920, 2022.
[99] M. Saranya, A. Rajapandiyan, K. Fathima, S. Hema, S. GeethaPriya, and S. Saravanan, "A power system stabilizer for multi-machine power based on hybrid BF0A-PSO," *International Journal of Electrical and Computer Engineering,* vol. 5, p. 213, 2015.
[100] M. Eslami, H. Shareef, and A. Mohamed, "Power system stabilizer design based on optimization techniques," in *2011 Fourth International Conference on Modeling, Simulation and Applied Optimization*, 2011, pp. 1-7.
[101] J. Sugiura and S. Jones, "Simulation and Measurement of High-Frequency Torsional Oscillation (HFTO)/High-Frequency Axial Oscillation (HFAO) and Downhole HFTO Mitigation: Knowledge Gains Continue Using Embedded High-Frequency Drilling Dynamics Sensors," *SPE Drilling & Completion,* vol. 35, pp. 553-575, 2020.
[102] P. Kundur, "Power system stability," *Power system stability and control,* vol. 10, pp. 7-1, 2007.
[103] J. J. Kim and J. H. Park, "A novel structure of a power system stabilizer for microgrids," *Energies,* vol. 14, p. 905, 2021.
[104] R. Devarapalli, N. K. Sinha, and F. P. García Márquez, "A review on the computational methods of power system stabilizer for damping power network oscillations," *Archives of Computational Methods in Engineering,* vol. 29, pp. 3713-3739, 2022.
[105] S. Lu, W. Zhang, T. Wang, Y. Cai, X. Sui, H. Li, *et al.*, "Parameter tuning and simulation analysis of PSS function in excitation system with suppression of low frequency Oscillation," in *2019 IEEE 8th International Conference on Advanced Power System Automation and Protection (APAP),* 2019, pp. 474-479.

[106] https://www.powerworld.com/WebHelp/Content/TransientModels_HTML/Stabilizer%20PSS2A.htm.
[107] H. Vu and J. Agee, "Comparison of power system stabilizers for damping local mode oscillations," *IEEE transactions on energy conversion*, vol. 8, pp. 533-538, 1993.
[108] I. Kamwa, R. Grondin, and G. Trudel, "IEEE PSS2B versus PSS4B: the limits of performance of modern power system stabilizers," *IEEE transactions on power systems*, vol. 20, pp. 903-915, 2005.
[109] N. Karami, N. Moubayed, and R. Outbib, "General review and classification of different MPPT Techniques," *Renewable and Sustainable Energy Reviews*, vol. 68, pp. 1-18, 2017.
[110] L. Xu, L. Yao, and C. Sasse, "Grid integration of large DFIG-based wind farms using VSC transmission," *IEEE Transactions on power systems*, vol. 22, pp. 976-984, 2007.
[111] D. Datta, S. K. Sarker, and M. R. I. Sheikh, "Designing a unified damping and cross-coupling rejection controller for LCL filtered PV-based islanded microgrids," *Engineering Science Technology, an International Journal*, vol. 35, p. 101244, 2022.
[112] H. Zhang, J. Xian, J. Shi, S. Wu, and Z. Ma, "High performance decoupling current control by linear extended state observer for three-phase grid-connected inverter with an LCL filter," *IEEE Access*, vol. 8, pp. 13119-13127, 2020.
[113] C. C. Gomes, A. F. Cupertino, and H. A. Pereira, "Damping techniques for grid-connected voltage source converters based on LCL filter: An overview," *Renewable Sustainable Energy Reviews*, vol. 81, pp. 116-135, 2018.
[114] A. Berrueta, I. San Martín, P. Sanchis, and A. Ursúa, "Lithium-Ion Batteries as Distributed Energy Storage Systems for Microgrids; 2019," ed.
[115] H. C. Nazaripouya, Yu-Wei & Akhil, Abbas, "ENERGY STORAGE IN MICROGRIDS: CHALLENGES, APPLICATIONS AND RESEARCH NEED," *International Journal of Energy and Smart Grid*, vol. 3, pp. 60-70, 2019.
[116] L. Guan and J. Yao, "Dynamic stability improvement scheme for dual-sequence PLLs in VSC based renewable energy generation system during asymmetrical LVRT," *International Journal of Electrical Power Energy Systems*, vol. 145, p. 108683, 2023.
[117] M. N. Tasnim, T. Ahmed, M. A. Dorothi, S. Ahmad, G. Shafiullah, S. Ferdous, *et al.*, "Voltage-Oriented Control-Based Three-Phase, Three-Leg Bidirectional AC–DC Converter with Improved Power Quality for Microgrids," *Energies*, vol. 16, p. 6188, 2023.
[118] W. Wu, Y. Chen, A. Luo, L. Zhou, X. Zhou, L. Yang, *et al.*, "A virtual inertia control strategy for DC microgrids analogized with virtual synchronous machines," *IEEE Transactions on Industrial Electronics*, vol. 64, pp. 6005-6016, 2016.
[119] M. Büyük, A. Tan, K. Ç. Bayindir, and M. Tümay, "Analysis and comparison of passive damping methods for shunt active power filter with output LCL filter," in *2015 Intl Aegean Conference on Electrical Machines & Power Electronics (ACEMP), 2015 Intl Conference on Optimization of Electrical & Electronic Equipment (OPTIM) & 2015 Intl Symposium on Advanced Electromechanical Motion Systems (ELECTROMOTION)*, 2015, pp. 434-440.

[120] P. Dattaray, P. Wall, V. Terzija, D. Chakravorty, P. Mohapatra, and J. Yu, "Impact of load dynamics on torsional interactions," in *2016 Power Systems Computation Conference (PSCC)*, 2016, pp. 1-7.

[121] N. Afrin, F. Yang, J. Lu, and M. Islam, "Impact of induction motor load on the dynamic voltage stability of microgrid," in *2018 Australian & New Zealand Control Conference (ANZCC)*, 2018, pp. 397-402.

[122] D. Wu, H. Wu, and H. Dong, "Influence of induction motor starting on microgrid," in *2018 IEEE PES Asia-Pacific Power and Energy Engineering Conference (APPEEC)*, 2018, pp. 376-381.

[123] M. Ahmed, A. Vahidnia, L. Meegahapola, and M. Datta, "Impact of multiple motor loads on dynamic performance and stability of microgrids," in *2019 IEEE International Conference on Industrial Technology (ICIT)*, 2019, pp. 1704-1709.

[124] B. Kroposki, C. Pink, J. Lynch, V. John, S. M. Daniel, E. Benedict, *et al.*, "Development of a high-speed static switch for distributed energy and microgrid applications," in *2007 Power Conversion Conference-Nagoya*, 2007, pp. 1418-1423.

[125] B. Kroposki, R. Lasseter, T. Ise, S. Morozumi, S. Papathanassiou, and N. Hatziargyriou, "Making microgrids work," *IEEE power and energy magazine*, vol. 6, pp. 40-53, 2008.

[126] D. Klapp and H. T. Vollkommer, "Application of an intelligent static switch to the point of common coupling to satisfy IEEE 1547 compliance," in *2007 IEEE Power Engineering Society General Meeting*, 2007, pp. 1-4.

[127] L. a. L. Shi, Kwang and Wu, Feng, "Robust ESS-Based Stabilizer Design for Damping Inter-Area Oscillations in Multimachine Power Systems," *IEEE Transactions on Power Systems,* vol. 31, pp. 1-12, 2015.

[128] A. C. Kathiresan, J. PandiaRajan, A. Sivaprakash, T. Sudhakar Babu, and M. R. Islam, "An adaptive feed-forward phase locked loop for grid synchronization of renewable energy systems under wide frequency deviations," *Sustainability,* vol. 12, p. 7048, 2020.

[129] P. Kundur, *Power System Stability and Control*, 14th ed.: Tata McGraw Hill Education Private Limited, 1994.

[130] A. Aderibole, H. H. Zeineldin, and M. Al Hosani, "A Critical Assessment of Oscillatory Modes in Multi-Microgrids Comprising of Synchronous and Inverter-Based Distributed Generation," *IEEE Transactions on Smart Grid*, vol. 10, pp. 3320-3330, 2019.

[131] T. A. Tajrin Jahan Rumky , Moudud Ahmed ,Shameem Ahmad and M. M. Rahman "Performance of Microgrid Systems on Multiple Dynamic Loads Penetration," 2023.

[132] A. Aderibole, H. H. Zeineldin, and M. Al Hosani, "A critical assessment of oscillatory modes in multi-microgrids comprising of synchronous and inverter-based distributed generation," *IEEE Transactions on Smart Grid,* vol. 10, pp. 3320-3330, 2018.

Apendices

Appendix A : Parameters of Power Oscillation Damping Controllers'

Table 6.1: Parameters of the MB-POD (Detailed settings)

Frequency bands					
Low Frequency (LF)		Intermediate Frequency (IF)		High Frequency (HF)	
T_{L1}	0	T_{I1}	0	T_{H1}	0
T_{L2}	0	T_{I2}	0	T_{H2}	0
T_{L3}	6.6040	T_{I3}	0.66040	T_{H3}	0.0334
T_{L4}	7.9248	T_{I4}	0.79248	T_{H4}	0.0401
T_{L5}	0	T_{I5}	0	T_{H5}	0
T_{L6}	0	T_{I6}	0	T_{H6}	0
T_{L7}	0	T_{I7}	0	T_{H7}	0
T_{L8}	0	T_{I8}	0	T_{H8}	0
T_{wL1}	5.5033	T_{wI1}	0.55033	T_{wH1}	0.0278
T_{wL2}	6.6040	T_{wI2}	0.66040	T_{wH2}	0.0334
T_{wL3}	0	T_{wI3}	0	T_{wH3}	0
T_{wL4}	0	T_{wI4}	0	T_{wH4}	0

K_{wL1}	1	K_{wI1}	1	K_{wH1}	1
K_{wL2}	1	K_{wI2}	1	K_{wH2}	1
K_D	66	K_D	66	K_D	66
K_L	10	K_I	5	K_H	10
VL_{max}	0.075	VI_{max}	0.15	VH_{max}	0.15
f_l	0.0219 Hz	f_i	0.219 Hz	f_h	4.34 Hz
VS_{max} = 0.15					

Where, $T_{L3} = T_{wL2} = \left(2\pi f_{l\sqrt{R}}\right)^{-1}$, $T_{L4} = T_{L3}*R$, $T_{wL1} = T_{L3}/R$, R = 1.2, $T_{I3} = T_{wI2} = \left(2\pi f_{i\sqrt{R}}\right)^{-1}$, $T_{I4} = T_{I3}*R$, $T_{wI1} = T_{I3}/R$, $T_{I3} = T_{wH2} = \left(2\pi f_{h\sqrt{R}}\right)^{-1}$, $T_{H4} = T_{H3}*R$, $T_{wH1} = T_{H3}/R$

Table 6.2: Parameters of modified SB-POD

Parameters Name	**Value**
Low-pass filter time constant, T_l	0.2
Wash-out filter time constant, T_w	10
Gain, K_D	120

Appendix B : Parameters Of Microgrid Systems'

Table 6.3: Parameters of three interconnected microgrids

MG-1 **(Total generation: 900kW)**
PV Farms' Parameters

Power	200 kW
Parallel string	88
Module per string	7
Open-circuit voltage	85.3V
Short-circuit current	6.09A
Voltage at MPPT	72.9V
Current at MPPT	5.69A
Diesel Generator	
Power	150kW
Pole pairs	2
Inertia co-efficient, H	3.2s
Friction factor	0.08 pu
Rotor speed deviation	0.05%
w_{ref}	1.0 pu
Stator resistance, R_s	2.8544×10^{-3} pu
ESS Parameters	
Power	500kVA
Rated capacity	700 Ah
Nominal voltage	400V
Initial state-of-charge (SoC)	80%
Capacitance	500µF
ESS Regulator gain (PLL)	

$K_{p_{PLL}}$	180
$K_{i_{PLL}}$	3200
$K_{d_{PLL}}$	1
ESS LCL Filter Parameters	
L_1	6×10^{-3} H
L_2	5×10^{-4} H
C	5×10^{-5} F
R	0.05 Ω
Induction Motors Parameters	
Load	150 kW
Rotor type	Squirrel-cage
Stator inductance, L_s	0.00019 H
Stator resistance, R_s	0.018181 Ω
Rotor inductance, L_s	0.00019 H
Rotor resistance, R_s	0.009956 Ω
Mutual Inductance, L_m	0.00945 H
Inertia, J	3.1 kgm^2
Friction factor, F	0.1 Nms
Pole pairs, p	2
DFIG Parameters	
Generator Data	
Power	350 kW

Rotor-type	Wound		
Stator resistance, R_s	0.023 pu		
Stator inductance, L_{ls}	0.18 pu		
Rotor resistance, R_r	0.016 pu		
Rotor inductance, L_{lr}	0.16 pu		
Magnetizing inductance, L_m	2.9 pu		
Inertia constant, H	0.685 s		
Friction factor, F	0.01 pu		
Pole pairs, p	3		
ESS PI Controller Parameters			
Inner Current Controller	K_p	10	
	K_i	95	
Outer Controller (Voltage/Frequency)	K_{pf}	1	
	K_{if}	50	
	K_{pv}	0.5	
	K_{iv}	1	
MG-2 & MG-3 (Total generation: 750kW each)			
PV Farms' Parameters, DFIG Parameters, and ESS Parameters			
Same as MG-1			

- **IM parameters**

Both of the microgrids distributed generations parameters and ESS control parameters are taken from and IM parameters are chosen from [32]

- 5.4-hp (4 kW) IM parameters:

  R_r = 1.395 Ω, R_s = 1.405 Ω, H = 0.0131 kgm^2, L_r = 0.005839 H, L_s = 0.005839 H, P = 2, and L_m = 0.00769 H.

- 215-hp (160 kW) IM parameters:

  R_r = 0.007728 Ω, R_s = 0.01379 Ω, H = 2.9 kgm^2, L_r = 0.000152 H, L_s = 0.000152 H, P = 2, and L_m = 0.00769 H.

Appendix C : MATLAB/ Simulink Model of Control Strategies

Energy Storage System Control:

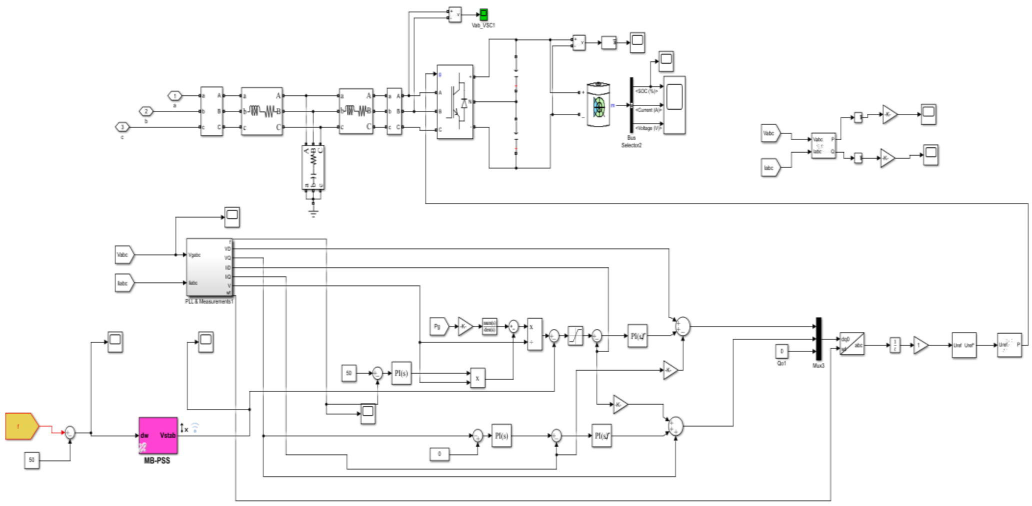

Fig. 1: Block Diagram of overall ESS with POD controller.

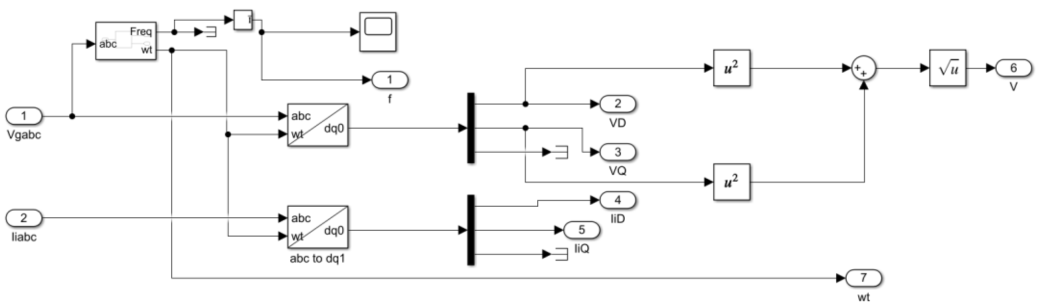

Fig. 2: Block Diagram of PLL and measurements.

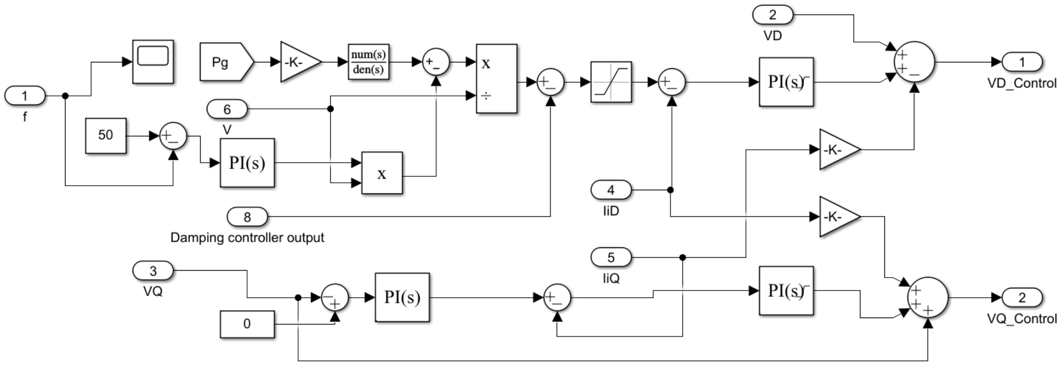

Fig. 3: Block Diagram of Voltage/Frequency and Current Control Loop.

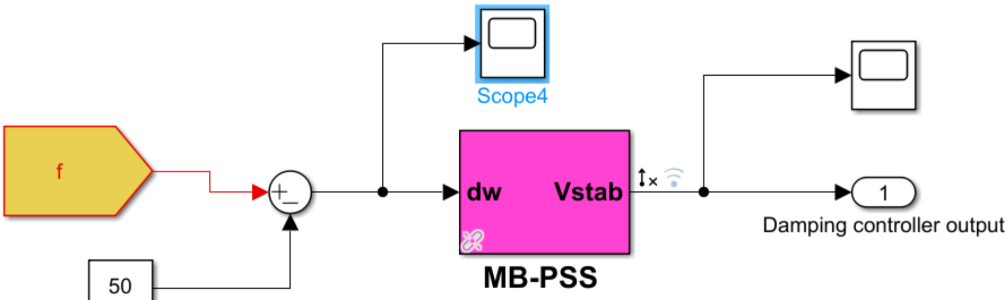

Fig. 4: Block Diagram of Damping Controller Loop.

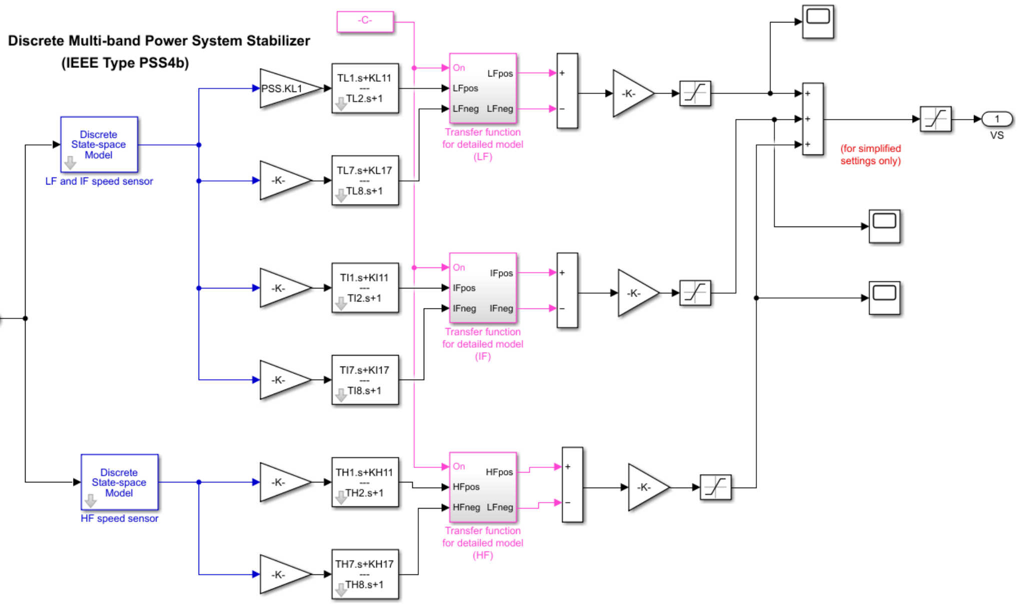

Fig. 5: Block Diagram of Multi-Band Power Oscillation Damper.

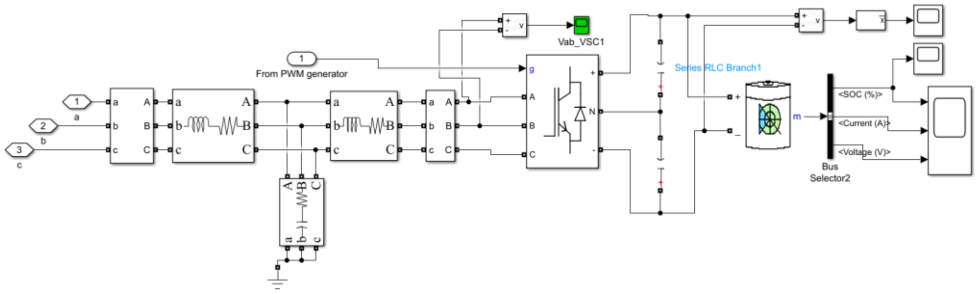

Fig. 6: Block Diagram of Energy Storage System with LCL Filter.

Appendix D : Matlab/Simulink Model of The Microgrid Models

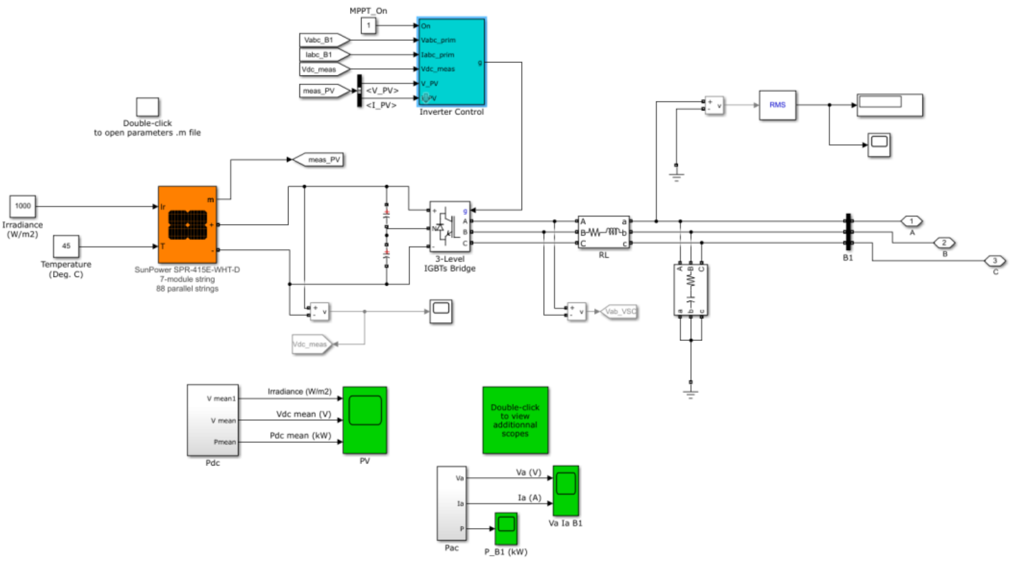

Fig. 9: Block Diagram of PV.

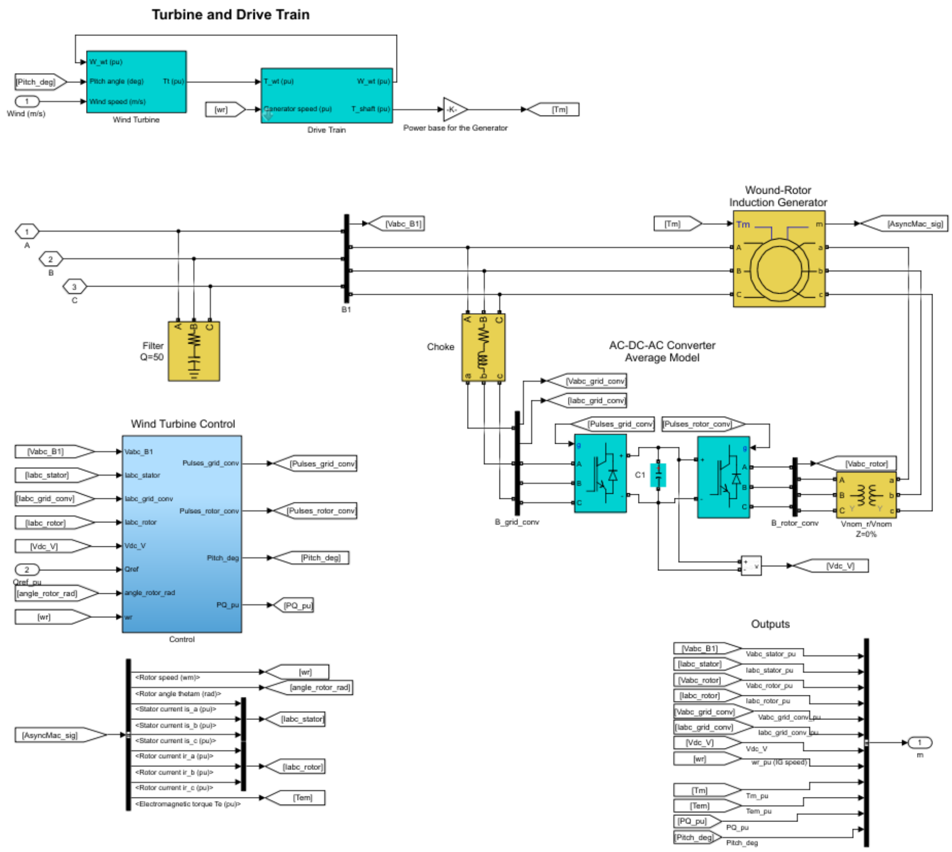

Fig. 10: Block Diagram of Wind Generator.

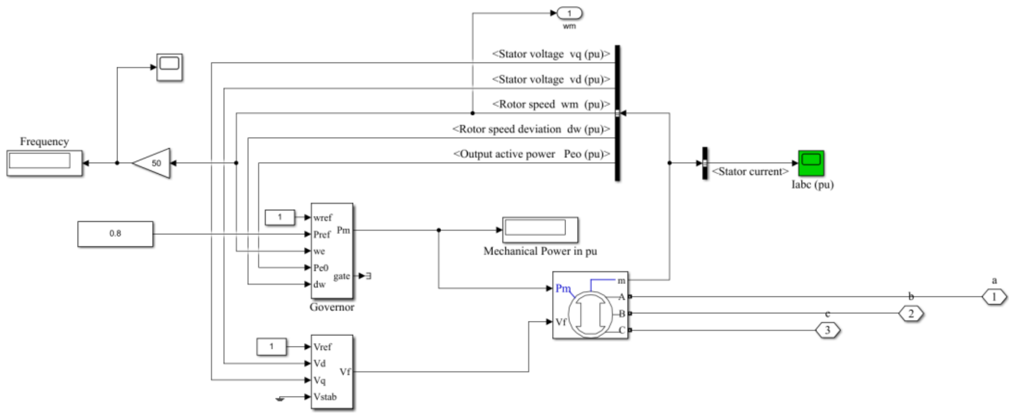

Fig. 11: Block Diagram of Diesel Generator.

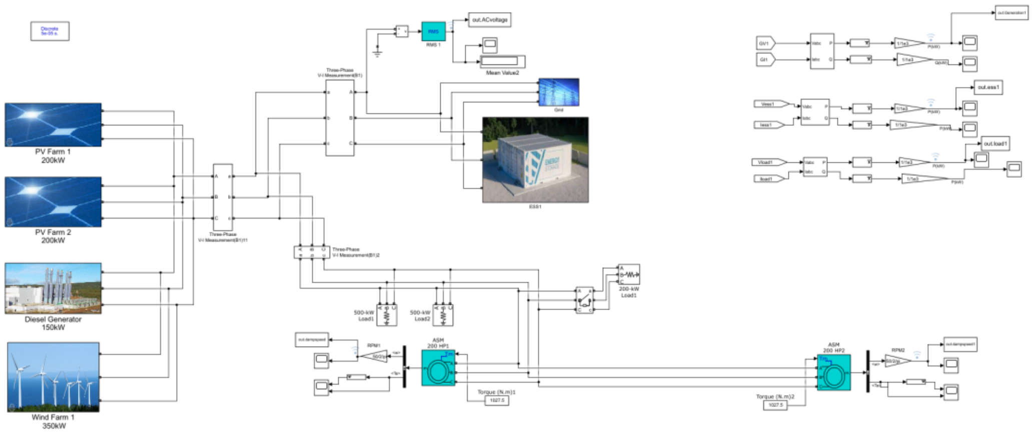

Fig. 12: Block Diagram of Local Microgrid System (MG-1).

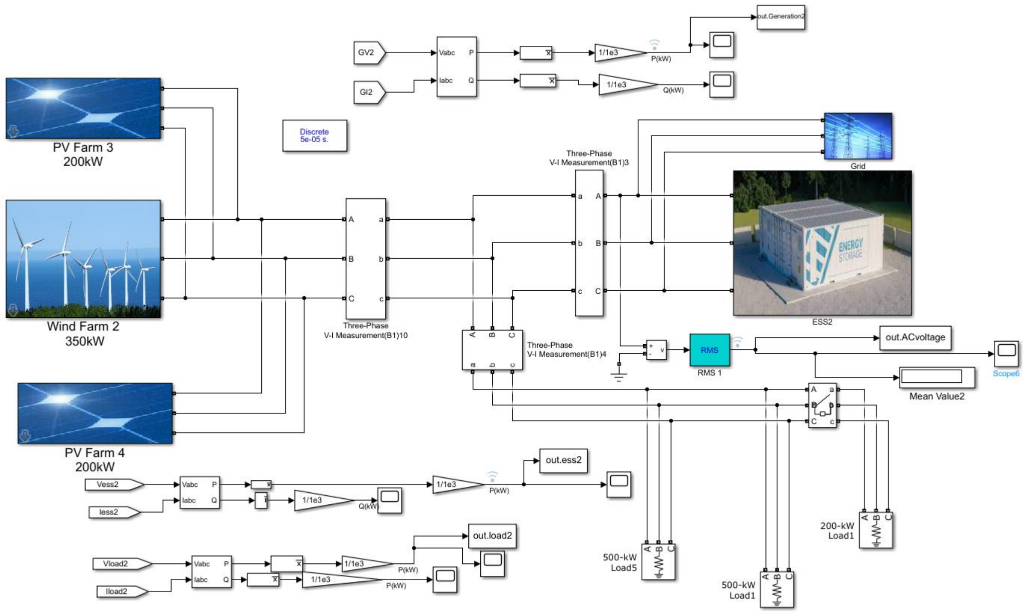

Fig. 13: Block Diagram of Local Microgrid System (MG-2).

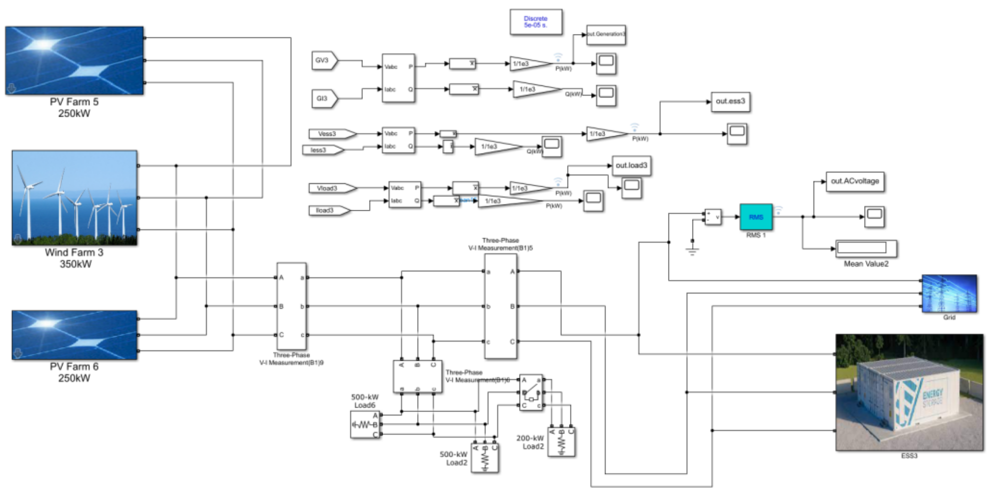

Fig. 14: Block Diagram of Local Microgrid System (MG-3).

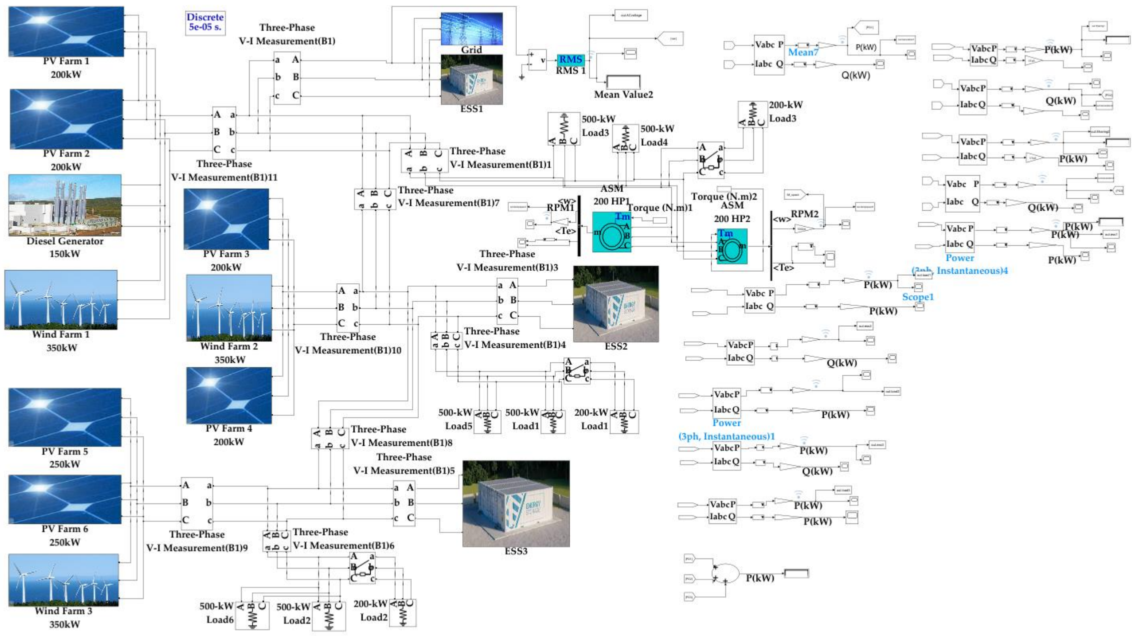

Fig. 13: Block Diagram of an Interconnected AC Microgrid System.